Concept Design of a Thermo-Chemical Heat Pump Using Calcium Chloride-NH_3 and Magnesium Chloride-NH_3 Working Pairs

by

Oluyemi Jegede

A thesis submitted in partial fulfilment of the requirements for the degree of Doctor of Philosophy

University of Warwick, Department of Engineering

May 2017

Contents

List of Figures

List of Tables

Acknowledgement

I want to express my deepest gratitude to my supervisor, Professor Robert Critoph, for his steadfast support and inspiration throughout the course of this PhD work. Throughout the process, he was ever ready to impart his immense knowledge and guide me at short notice –I couldn't have had a better supervisor.

In addition, I want to extend my sincere appreciation to all the staff (Dr Steve Metcalf, Dr Zacharie Tamainot-Telto, Dr Roger Thorpe, Dr Roger Moss and Dr Angeles Rivero Pacho) of the Sustainable Thermal Energy Technologies Group for their invaluable help and insight in designing experiments and simulation. Also, I want to thank Dr Michel Van der Pal of the ECN for his very useful insights into the behaviour of salt-ammonia reactions. Further, I want to thank all the technicians of the School of Engineering who helped to bring my experimental rig designs to life-Joel Whittle, Iain Brown, Robert Edwards, and the rest of the team.

I also want to extend my appreciation to my friends, they made sure to encourage me when things went tough and I was struggling with motivation. To my girlfriend-Teniola King, who stayed up with me through those sleepless nights. This is to say thank you, I love you very much.

Finally, I must express the highest of gratitude to my parents-Femi and Eniola Jegede, who never wavered in their belief that education is the ultimate enabler for uplifting society. I want to express my most sincere thanks for the huge financial sacrifice they have made to put me through world class education from a very young age. I owe it to them to do the best that I can to positively impact my country, Nigeria and the wider world. I will do so, so help me God.

Declaration

I declare that the work in this thesis has been composed by me and no portion of the work has been submitted in support of an application for another degree or qualification of this or any other university or other institute of learning. The work has been my own except where indicated and all quotations have been distinguished by quotations marks and the sources of information have been acknowledged.

Parts of this thesis have been published by the author. These publications are listed in the next section.

Contributions to Knowledge

Peer Reviewed Journal Paper

- Oluyemi O. Jegede, Robert E. Critoph, *Extraction Of Heat Transfer Parameters In Active Carbon–Ammonia Large Temperature Jump Experiments*, Applied Thermal Engineering, Volume 95, 25 February 2016, Pages 499-505, ISSN 1359-4311

Peer Reviewed Conference Paper

- Oluyemi O. Jegede, Robert E. Critoph, (2016), *Modelling And Testing Of Large Temperature Jump $CaCl_2$-NH_3 Synthesis And Decomposition Reactions*, Heat Powered Cycles, Nottingham, UK.

Poster Presentation

- Oluyemi O. Jegede, Robert E. Critoph, (2015), *Modelling And Testing Of Large Temperature Jump $CaCl_2$-NH_3 Synthesis And Decomposition Reactions*, Sorption Friends Conference, Milazzo, Italy

Abstract

This work presents the design of a double effect thermochemical heat pump based on the calcium chloride-ammonia and magnesium chloride-ammonia working pairs. The work began with a comprehensive theoretical and literature review of the similar systems which exist in the literature.

Once the literature review was done, a large temperature jump experimental rig was built in order to be able to determine the behaviour of the relevant working pairs. Even though the focus of the work is thermochemical reactions, the activated carbon-ammonia pair was first used to validate the large temperature jump rig. The reason for this is that the activated carbon-ammonia pair is better understood compare to the thermochemical reactions.

The experiments on the activated carbon- ammonia pair yielded some useful results. The results obtained show that two heat transfer properties (thermal conductivity, k and heat transfer coefficient, h) with physical meaning can be extracted from large temperature jump data. Furthermore, the change in thermal conductivity with the packing density of the adsorbent was investigated. The general trend was one of increasing thermal conductivity as the packing density was increased, the thermal conductivity increased from $0.2 Wm^{-1}K^{-1}$ to $0.4 Wm^{-1}K^{-1}$ as the packing density was increased from $530 kgm^{-3}$ to $705 kgm^{-3}$.

When the calcium chloride-ammonia and magnesium chloride-ammonia working pairs were investigated in the large temperature jump setup, the kinetic parameters for each respective reaction were obtained. This enabled the development of a dynamic model of a representative thermochemical heat pump based on the aforementioned working pairs. The dynamic model helped to investigate the performance of the heat pump under various operating conditions. The coefficient of performance (COP) and the specific heating power ranged from 1.21 to 1.40 and 40W/litre to 400W/litre respectively depending on the operating conditions.

Nomenclature

Symbols

A	cross-sectional area (m^2) or kinetic parameter (s^{-1})
B	porosity (%)
C_p	specific heat capacity ($J\ kg^{-1}\ K^{-1}$)
C	stiffness constant
Ca	intercept of ammonia saturation line in Clapeyron diagram (K^{-1})
d	diameter (m)
E	slope of ammonia saturation line on clapeyron diagram (K)
F	force/load (N)
f	factor of safety
G	Gibb's free energy ($J\ mol^{-1}$)
H	heat of reaction per unit mole ($J\ mol^{-1}$)
$\hat{H}$	heat of reaction per unit mass (Jkg^{-1})
h	heat transfer coefficient ($Wm^{-2}\ K^{-1}$)
he	enthalpy (J)
$\hat{he}$	specific enthalpy ($J\ kg^{-1}$)
K	concentration in Gibb's equation (bar) or Dubinin equation (-)
kc	spring rate ($N\ m^{-1}$)
k	thermal conductivity ($Wm^{-1}\ K^{-1}$)
L	latent heat ($J\ kg^{-1}$)
l	length of channel (m)
m	mass (kg)
M	molar mass ($kg\ mol^{-1}$)
n `	no of discrete sample layers (-)
N	no of moles reacted (mol)
Nu	Nusselt number (-)
Pr	Prandtl number (-)
P	pressure (bar)
R	gas constant ($JK^{-1}mol^{-1}$)

Re	Reynold's number (-)
r	radius (m)
S	entropy (J mol^{-1} K^{-1})
Sa	shape factor (m)
T	temperature (K)
t	time (s)
u	diffusion velocity (m s^{-1})
v	volumetric flow rate (m^3 s^{-1})
V	volume (m^3)
x	concentration (-)
X	advancement of reaction (-)
Y	advancement of reaction (-)
Q	heat energy (J)
$\hat{Q}$	heat energy per unit mass (Jkg^{-1})
W	thermal resistance (m^2 K W^{-1})
yo	pseudo-order of reaction (-)

Greek Symbols

β	affinity coefficient
Δ	change
ε	isothermal compression work (J)
π	pi
ς	pore diameter distribution
ϑ	rate constant
σ	stress (Pa)
Ω	surface area (m^2)
δ	thickness (m)
φ	uncertainty
μ	dynamic viscosity (Pa. s)

Subscripts

0	limiting
a	adsorbent

ads	adsorbed
base	base
b	bolt
bulk	bulk
bolt	bolt
bottom	bottom
bv	buffer volume
ch	channel
con	condensation
dec	desorption or decomposition
ev	evaporation
eq	equilibrium
f*inal*	final
*ht*f	heat transfer fluid
i	current
in	inner/inlet
initial	initial
max	maximum
min	minimum
no	Nusselt number correlation constant
NH_3	ammonia
out	outer/outlet
pw	pipework
p	against static stress exceeding proof stress
r.c	reference calorimeter
rec	recovery
sample	test sample
s	against joint separation
sat	saturation
sim	simulated
*stand**ard*	standard
syn	synthesis

sys	system
tc	test cell
t	tension
top	top
w	wall
yield	yield

Superscripts

0	standard conditions

Abbreviations

$BaCl_2$	Barium Chloride
$CaCl_2$	Calcium Chloride
ENG	expanded graphite
$MgCl_2$	Magnesium Chloride
PEEK	polyether ether ketone

Parameters

COP	coefficient of performance (-)
SHP	specific heating power (Wl^{-1})

Chapter 1 : Introduction

1.1 Motivation

In recent decades, synthetic refrigerants such as chlorofluorocarbons (CFC) and halons which are found in conventional vapour compression systems have been pinpointed as contributors to the depletion of the stratospheric ozone layer and also contributors of greenhouse effects which lead to global warming. Their global warming potentials are thousands of times greater than that of carbon dioxide[1]. The extent of their contribution to global warming led to the agreement of the Montreal Protocol in 1987 by all United Nations (UN) members to phase them out. This has led to the research and development of systems based on alternative less environmentally damaging refrigerants such as ammonia and water.

One of the aforementioned alternative systems is adsorption systems which are based thermal compression rather than mechanical compression of the refrigerant using certain materials called adsorbents. Some of these adsorbents (activated carbon, silica etc) typically form weak physical bonds with refrigerants, others (calcium chloride, magnesium chloride etc) form stronger energy intensive chemical bonds. Adsorption systems operate on a cycle which can be applied in both refrigeration and heat pumping applications but the focus in this work is on a heat pumping application.

1.2 Why Sorption Systems?

Sorption systems have significant advantages over vapour compression systems which justify the attention which has been devoted to their research and development recently. These advantages are highlighted in bullet points below.

- Sorption systems can offer a more efficient utilisation of primary energy compared to electricity based vapour compression system. Critoph [2] explained that the coefficient of performance (cooling power divided by input power) for a conventional vapour compression cycles may be up to 300%. However, the conversion of fuel (oil, gas, coal or nuclear) to electricity at a power station and the following transmission and distribution of the power may only be 25% efficient. This means that the overall efficiency of the entire process in the case of conventional vapour compression cycles may not exceed 75%. For a gas based heat driven heat pumps, the overall efficiency of

conversion from the point of primary energy would typically be slightly greater than 100%. This is relatively better than the vapour compression case.

- Adsorption systems can produce heat at higher temperature levels than vapour compression systems[2]. According to Critoph [2], sorption systems can operate at temperature levels up to several hundreds of degrees, the refrigerants and compressors used in conventional systems simply cannot withstand these temperatures.
- Adsorption systems require less maintenance because they don't have any moving parts and are thus more reliable. This reduced requirement for maintenance also means that they have a longer lifespan than vapour compression systems.

1.3 Aims and Objectives

The main aim of this work is to design in concept, a double effect thermochemical heat pump based on the calcium chloride-ammonia and the magnesium chloride-ammonia pairs. The objectives which are integral to the achievement of the stated aim are given below.

- To study the underlying theory behind adsorption systems
- To conduct a literature review of the state of the art systems in the area of thermochemical systems.
- To study the heat transfer and kinetic behaviour of the relevant reactions-calcium chloride-ammonia and magnesium chloride-ammonia.
- To design and develop a Matlab model to simulate a representative double effect thermochemical heat pump based on the chosen reactions

1.4 Thesis Outline

This thesis is divided into 7 chapters. Chapter 1 (this chapter) presents a background and the context of the project. It also makes a case for the choice of sorption systems as an alternative to vapour compression systems. Finally, the aim and objectives of the project are listed using bullet points.

Chapter 2 provides explanations of some of the underlying theory of adsorption systems. This is with a view to understand the basic principles behind the operation of

adsorption systems. Some of the concepts which are discussed range from adsorption equations of state to the thermodynamics of the entire adsorption cycle.

Chapter 3 contains a literature review of the state of the art in the area of thermochemical heat pumps. The focus is on multiple stage/effect systems. Furthermore, other advanced cycles such as the thermal wave cycle are discussed.

In Chapter 4, the design and fabrication of a large temperature jump setup is detailed and the results of initial experiments on active carbon are also detailed. Active carbon was used in the initial stages of experiments in the large temperature jump setup because it is a well-understood adsorbent.

Chapter 5 presents a detailed procedure for the preparation of experimental samples of Calcium Chloride ($CaCl_2$) and Magnesium Chloride ($MgCl_2$). In addition, the results of Anter thermal conductivity tests and large temperature jump experiments on the two salts samples are presented, providing a better way for understanding the heat transfer and kinetic characteristics of the samples.

The results from Chapter 5, form the basis of the dynamic model which is described in Chapter 6. Chapter 6 shows the results from this dynamic model based on a combination of different working conditions.

Chapter 7 presents a conclusion on the project, highlighting the major points from the different chapters of this thesis and the major contributions of the work to knowledge.

1.5 References

1. Stephan, K., Krauss, R.,, *Regulated CFCs and Their Alternatives*, in *Solid Sorption Refrigeration Symposium*. 1992: Paris.
2. Critoph, R.E.C., *Chapter 10 - Adsorption Refrigerators and Heat Pumps*, in *Carbon Materials for Advanced Technologies*, T.D. Burchell, Editor. 1999, Elsevier Science Ltd: Oxford. p. 303-340.

Chapter 2 : Underlying Theory of Adsorption Machines

2.1 Introduction

This chapter of the thesis presents the theory which forms the basis of adsorption machines. It begins with an explanation of the workings of a basic adsorption machine (heat pump or chiller) on a macro level. Thereafter, the concepts of physical adsorption and chemical adsorption are explained, highlighting the fundamental differences between them. Then, the common equilibrium models used in describing physical adsorption are discussed. Furthermore, the mechanism behind chemical adsorption is also discussed before focusing on the reaction kinetic model which is subsequently relevant to this work. Finally, the thermodynamics of a basic adsorption cycle is detailed by considering the different stages of the cycle.

2.2 The Process of Heat Pumping/Refrigeration

In principle, the typical adsorption heat pump operates at three temperature levels: a high temperature heat source (Q2) to drive the process, a low temperature heat source (Q0) and a medium temperature heat sink (Q1) as shown in Figure 2-1. For a heat pump, the heat rejected to the heat sink can be used to provide space heating or warm water for domestic use usually within the range of 20◦C to 70◦C [1]. The low temperature heat source is typically air from a dry cooler or solar collector.

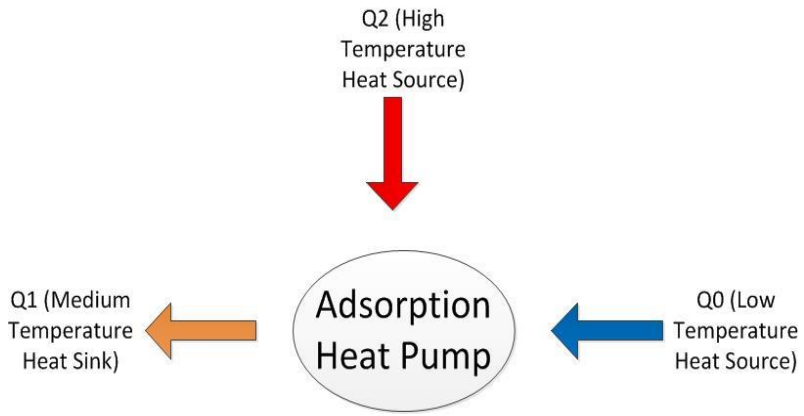

Figure 2-1: Adsorption heat pump system

In the case of cooling or refrigeration, the configuration is the same but the low temperature heat source is the cold space i.e the low temperature heat is obtained from the space to be cooled. The heat could be provided from temperature levels as low as -40◦C (industrial application) or as high as 18◦C (air conditioning). The medium

temperature heat waste is usually rejected to the environment or some sort of cooling system. The temperature of the rejected heat can range from 23◦C to 40◦C or even higher in certain cases [1].

The driving heat temperature for both applications will vary based on temperature lift. Higher temperature lifts will require driving heat of higher temperatures [1]. For increased performance, more complex configurations have been introduced. These include multiple bed cascades and the thermal wave. It is clear that adsorption heat pumps and refrigerators can operate interchangeably for heating or cooling. Also, they can be used in the rare case that heating and cooling is needed at the same time.

2.3 The Concept of Adsorption

The concept of the adsorption of fluid on the surface of solid substances is one that has been around for some time. Faraday [2], as far back as 1823 discovered this behaviour between silver chloride and ammonia. He observed that the ammonia combined with the silver chloride when cooled and it was released at higher temperatures. Essentially, it is the adhesion of atoms or molecules of a gas onto the surface of a solid when they are at low temperature. In this work, these solid substances are called adsorbents in the case of physical adsorption, or salts when a chemical reaction is involved, while the sorbent fluids that adhere onto them are refrigerants. The adsorption cycle in its most basic form as described by Metcalf et al [3] consists of a system of two linked vessels. There is a free flow of refrigerant (ammonia) between the two vessels and one contains an adsorbent.

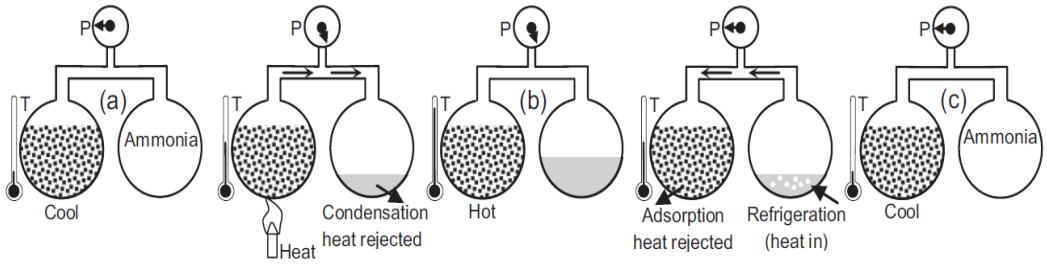

Figure 2-2: Schematic showing simplified adsorption cycle [2]

The vessel carrying the adsorbent is called the generator and the other vessel doubles as a condenser and an evaporator. At the beginning of the cycle at (a), the adsorbent is cool and so it contains a high concentration of refrigerant. The generator is then heated and this causes the adsorbent to release refrigerant causing the pressure in the

system to rise. As a result of this increase in pressure, the desorbed gas condenses in the right hand vessel (condenser) rejecting heat. When the generator is cooled again the adsorbent adsorbs refrigerant and the pressure in the system reduces. As a result, the refrigerant boils in the right hand vessel, removing heat from the vessel's surroundings and creating a refrigeration effect. Afterwards, the system is back to its original state at (c) and the cycle is complete and ready to begin again.

2.4 Physical sorption and Chemical sorption: The Fundamental Differences

2.4.1 Mechanism

There are differences between the mechanisms with which physical adsorption and chemical sorption occur. Physical adsorption is driven by van der Waals forces. Relatively, the bonding force between the fluid molecules and the solid surface is rather weak. It is usually likened to the condensation of the refrigerant on the surface of the solid [4] as the adsorption heat is similar to condensation heat in scale. No new substance is formed in the process and multilayer adsorption is possible.

Chemical adsorption is not the same. In this case, a chemical reaction occurs and new substances are formed in the process. The forces involved in chemical adsorption can include complexation (metal chlorides and ammonia), hydrogenation (metal hydrides and hydrogen) or oxidation (metal oxides and oxygen). Here only monolayer adsorption occurs because the refrigerant selectively reacts with the solid and when all the reaction sites on the solid are covered, the sorption process ceases. Because of stronger bonds, the heat of reaction in chemical adsorption is higher and chemical adsorption has the advantage of larger concentration change during adsorption/desorption. This is important for improved performance. However, agglomeration and swelling during chemical adsorption can hamper mass transfer performance.

2.4.2 Equilibrium Models

Physical and chemical adsorption processes also vary in terms of equilibrium. For physical adsorption, equilibrium condition is a function of adsorbent temperature (T) and gas pressure (P).

$$x_{\infty} = f(P,T) \tag{2.1}$$

Chemical adsorption is different. Here, equilibrium is described by only one property rather than two in the case of physical adsorption. As such, each reaction between the adsorbent and the refrigerant can only occur at one unique independent condition as shown in equation(2.2).

$$P = f(T) \tag{2.2}$$

Therefore, once this condition is reached and the reaction has occurred, any increase in pressure would not initiate more adsorption or desorption.

2.5 Physical Adsorption Equations

2.5.1 The Polanyi Adsorption Potential Theory

Wang et al [5] describes the original Polanyi theory. Polanyi's theory assumed that each site on the adsorbent possessed an adsorption potential. The adsorption centre is the point with the greatest potential while all the sites with the same potential are collectively called an equi-potential surface and the point where the distance is farthest ($r_{\max}$) to the adsorption centre has a potential of zero. Polanyi proposed that the adsorbed refrigerant is compressed such that it creates a force between the site and the space around it. As such the adsorptive potential at a point can be given as the isothermal compression work of the adsorbed gas. The isothermal compression work, ε is given by Equation (2.3).

$$\varepsilon = RT \ln\left(\frac{P_{sat}}{P}\right) \tag{2.3}$$

Over the years, Polanyi's theory underwent different modifications. Major highlights of these modifications are the Dubinin theories, the Dubinin-Raduskivech and Dubinin-Asthakov equations.

2.5.2 The Dubinin Equations

The Dubinin-Raduskivech [5] work tested a particular adsorbent and found that it had the same adsorptive behaviour regardless of the refrigerant used and proposed the following for that adsorbent.

$$\varepsilon_l = \frac{\varepsilon}{\beta} \tag{2.4}$$

β, the affinity coefficient is related only to the refrigerant and it shows the molar volume ratio of the refrigerant to benzene under the same temperature. Dubinin et al also tested activated carbon with micropores in the range $18-20\times10^{-10}$ m and found that they obeyed Gaussian distribution. Adsorbents with this micropore range were classed as one group and tests showed that the following relationship between the volume of adsorbate adsorbed, V_{ads} and the maximum adsorbable volume, $V_{\max}$ exists.

$$V_{ads} = V_{\max} \exp\left[-B\left(\frac{\varepsilon}{\beta}\right)^2 \right] \tag{2.5}$$

B relates to the porosity of the adsorbent- a more porous adsorbent will have a lower value. If ε is substituted in Equation (2.5), the Equation (2.6) is obtained.

$$V_{ads} = V_{\max} \exp\left[-B\left(\frac{RT}{\beta}\ln\frac{P_{sat}}{P}\right)^2 \right] \tag{2.6}$$

Equation (2.6) is the Dubinin-Astakhov (D-A) equation in its original formulation [4]; different P values correspond with different V_{ads} values and when $P = P_{sat}$, then the volume adsorbed, V_{ads} would be equal to the maximum adsorbable, V_0. It is usually assumed that the density of the adsorbed phase of the refrigerant can be compared to that of a saturated liquid at the same temperature and that the relationship between saturation pressure and temperature can be represented by the Clausius-Clapeyron equation.

$$\ln P = Ca - \frac{E}{T_{sat}} \tag{2.7}$$

If Equation(2.7) is substituted in Equation(2.6), Equation (2.8) is obtained. The index of 2 is changed to ζ to expand the application of the equation to other working pairs. ζ represents the pore diameter distribution of the adsorbent. When ζ is 2 then it means that a majority of the pore diameters are within the range of $18-20\times10^{-10}$ m. If ζ is less than 2 then a majority of the pores have diameters larger than $18-20\times10^{-10}$ m and if ζ is greater than 2 then pore diameters less than $18-20\times10^{-10}$ m are dominant.

$$V_{ads} = V_{\max} \exp\left[-B\left(\frac{RE}{\beta}\left(\frac{T}{T_{sat}} - 1 \right) \right)^{\varsigma} \right] \tag{2.8}$$

The concentration per unit mass of refrigerant adsorbed or in a saturated phase can be expressed in terms of the density of adsorbed phase and volume adsorbed.

$$x_{ads} = \rho V_{ads} \tag{2.9}$$

As a result, equation (2.8) becomes equation (2.10). The terms $B\left(\frac{RE}{\beta} \right)$ are lumped up into a constant K which reflects the working pair being used.

$$x_{ads} = x_{\max} \exp\left[-K\left(\frac{T}{T_{sat}} - 1 \right)^{\varsigma} \right] \tag{2.10}$$

The Dubinnin equations have been used extensively for the analysis of microporous surfaces and they have been found to be suitable for a large range of temperatures and pressures.

2.6 Thermochemical Reactions

Chemical heat pumps operate based on a reversible chemical reaction between a gas and a solid [6]. This reaction is represented by Equation (2.11) below

$$\text{Salt+nGas} \leftrightarrow \text{Salt.n.(Gas)+nHeat of reaction} \tag{2.11}$$

The synthesis (adsorption) between the working pairs occurs on the left while the decomposition (desorption) of the working pairs is on the right hand side. The equilibrium here is mono-variant [6] i.e the system can be described by one parameter (pressure) and given the pressure, the temperature can be specified. The Gibb's free energy of the system, which is basically the amount of obtainable reaction-initiating work, is given as Equation (2.12)

$$\Delta G^0 = (n)(\Delta H^0 - T\Delta S^0) \tag{2.12}$$

At equilibrium, the Gibb's free energy is 0 and can be given as in [5] below:

$$\Delta G = \Delta G^0 + RT \ln K = 0 \tag{2.13}$$

Combining equations (2.12) and (2.13) gives the Van't Hoff equation:

$$\ln(K) = n\left(-\frac{\Delta H^0}{RT} + \frac{\Delta S^0}{R}\right) \tag{2.14}$$

Wang [5] expressed K using the concentration of the reactants, products and gas pressure. The Van't Hoff Equation was expressed as:

$$\ln(P) = -\frac{\Delta H^0}{RT} + \frac{\Delta S^0}{R} \tag{2.15}$$

The Van't Hoff equation is an equilibrium relationship between the pressure and temperature of the reacting refrigerant and the salt [7]. It relates the temperature to the equilibrium pressure of the decomposition and synthesis reactions between salt and gas. Both enthalpy and entropy change are regarded as constants as they are not dependent on temperature.

2.7 Kinetics of Thermochemical Reactions

The general form of kinetic models as used in [5, 8, 9] is:

$$\frac{dx}{dt} = f(P,T).f(X) \tag{2.16}$$

The rate of the reaction, dx/dt is a function of two things. They are the degree of completion of the reaction ($f(X)$) and the distance of the system from equilibrium ($f(P,T)$). There are many models of these reactions including shrinking core models, cracking core models, grain-pellet models and changing voidage models. The shrinking core models are considered to be the most accurate of these models, this has been shown by various literature [8, 10-13]. The model which is used in this work is a shrinking core model called the Mazet Model. It is introduced here in Equation (2.17) and is better described in Chapter 5.

$$\frac{dX}{dt} = (1-X)^{yo} A \frac{P - P_{eq}}{P_{eq}} \tag{2.17}$$

X is the advancement of the reaction while A is a kinetic parameter which describes the rate of the reaction. yo is the pseudo order of the reaction and $\frac{P - P_{eq}}{P_{eq}}$ represents the difference between the distance of the system from equilibrium.

2.8 Thermodynamic Analysis of a Basic Physical Adsorption Cycle

It is important to study the thermodynamics of the adsorption cycle so as to determine estimate values for its performance. Figure 2-3 shows a basic ideal adsorption cycle.

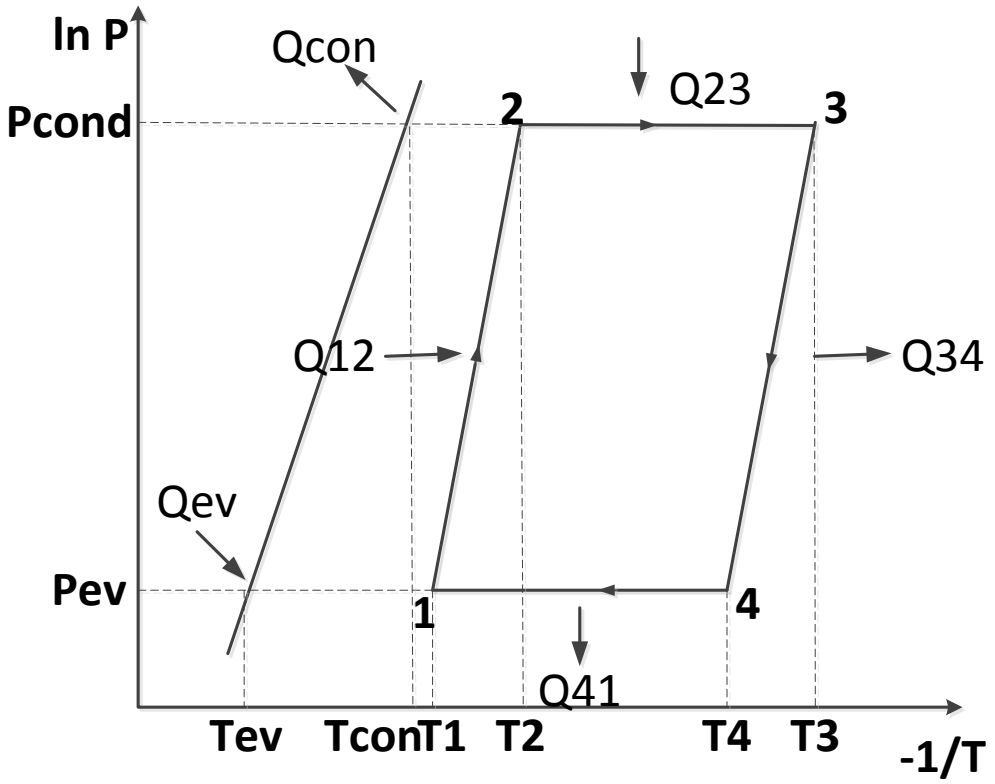

Figure 2-3: An ideal adsorption cycle

2.8.1 Process 1 to 2

As in Figure 2-3, process 1 to 2 is the isosteric heating. During this stage, there is no actual desorption taking place. Therefore, the refrigerant concentration of the adsorbent remains constant at maximum throughout this process. The heating at this stage amounts to a sensible heating of the adsorbent bed and its constituents. The heat input per unit mass is given as in Equation (2.18).

$$\hat{Q}_{12} = \int_{T1}^{T2} \left(C_{p,a} + x_{\max} C_{p,NH_3} \right) dT \qquad (2.18)$$

$C_{p,a}$ and C_{p,NH_3} are the specific heat capacities of the adsorbent and the adsorbed refrigerant respectively. The specific heat of the refrigerant is approximated as that of saturated liquid at the same temperature [4]. The heating in this stage increases the pressure in the system until the saturation temperature (T_{sat}) is equal to the condensation temperature (T_{con}).

2.8.2 Process 2 to 3

Process 2 to 3 is where the desorption occurs at the pressure (P_{con}) of the condenser. During desorption, the concentration of the refrigerant in the adsorbent reduces from its maximum value at point 2 to a minimum at point 3. The energy used up during this process is split into two parts. The first is the sensible heating and increase in internal energy of the adsorbent bed constituents. The other is dedicated to the transition of the refrigerant from liquid to gas phase. The heat input per unit mass of adsorbent for process 2 to 3 can be represented by Equation (2.19).

$$\hat{Q}_{23} = \int_{T2}^{T3} \left(C_{p,a} + xC_{p,NH_3} \right) dT + \int_{x_{\min}}^{x_{\max}} \hat{H}\, dx \tag{2.19}$$

There is no pressure increase during this stage due to the condensation of gaseous refrigerant in the condenser. $\hat{H}$ is the desorption heat per unit mass of the adsorbent bed. Critoph [4] expressed $\hat{H}$ as a multiple of the latent heat.

$$\hat{H} = L\frac{T_a}{T_{sat}} \tag{2.20}$$

2.8.3 Process 3 to 4

During process 3 to 4, isosteric cooling occurs. This process precedes the adsorption of gas back into the adsorbent bed. Therefore, the refrigerant concentration ratio and gas mass remains constant at its minimum. During this process energy is lost from the bed. The heat leaving the bed is given by Equation (2.21).

$$\hat{Q}_{34} = \int_{T4}^{T3} \left(C_{p,a} + x_{\min} C_{p,NH_3} \right) dT \tag{2.21}$$

2.8.4 Process 4 to 1

It is during this process that adsorption occurs. The adsorbent cools down until it reaches equilibrium with the surroundings. During adsorption the concentration increases from a minimum point to a maximum point and the process generates heat of adsorption. The heat loss from the system has two parts: the sensible heat of the adsorbent and adsorbate, the heat of adsorption and the change in enthalpy as the refrigerant is cooled from T_{ev} to T_{sat} .

$$\hat{Q}_{41} = \int_{T1}^{T4} \left(C_{p,a} + xC_{p,NH_3} \right) dT + \int_{x_{\min}}^{x_{\max}} \left(\hat{H} - [\hat{he}_{T_{sat}} - \hat{he}_{T_{ev}}] \right) dx \qquad (2.22)$$

2.8.5 Performance

The coefficient of performance (COP) is one of the parameters used to evaluate a cycle. It is essentially, the ratio of the cooling or heating produced to the heat energy consumed. The COP of a basic cycle is given by Equation (2.23).

$$COP_{cooling} = \frac{\hat{Q}_{ev}}{\hat{Q}_{12} + \hat{Q}_{23}}, COP_{heatpump} = \frac{\hat{Q}_{con}}{\hat{Q}_{12} + \hat{Q}_{23}} \qquad (2.23)$$

This allows for comparison between two or more cycles or operating conditions. To this end, it is important to evaluate the heat removed from the space being cooled (cooling) and the heat released during condensation in the condenser. The cooling can be determined by the difference in enthalpy of the refrigerant in its gas phase when it leaves the evaporator and liquid condensed phase.

$$\hat{Q}_{ev} = \int_{x_{\min}}^{x_{\max}} (\hat{he}_{g,Tev} - \hat{he}_{f,Tcon}) dx \qquad (2.24)$$

The heat rejected at condensation is usually a combination of the condensation heat and the sensible heat lost to the process of cooling the gas down to condensation temperature.

$$\hat{Q}_{con} = \int_{x_{\min}}^{x_{\max}} (\hat{he}_{g,T_3} - \hat{he}_{f,Tcon}) dx \qquad (2.25)$$

2.9 Summary

In this chapter, some of the basic concepts that pertain to this work have been explained. This lays a foundation of clear understanding for the next chapter which is a review of the different adsorption systems which have been researched in the past. The work in this chapter is also useful understanding for the rest of the thesis beyond the literature review.

References

1. Kühn, A. and F. Ziegler, *Cycle Basics Of Thermally Driven Heat Pumps*, In *Thermally Driven Heat Pumps For Heating And Cooling*. 2013, Universitätsverlag der TU Berlin: Berlin. p. 5-17.
2. Faraday, M., *On the Condensation of Several Gases into Liquids.* Philosophical Transactions of the Royal Society of London, 1823. **113**: p. 189-198.
3. Metcalf, S.J., R.E. Critoph, and Z. Tamainot-Telto, *Optimal Cycle Selection In Carbon-Ammonia Adsorption Cycles.* International Journal of Refrigeration, 2012. **35**(3): p. 571-580.
4. Critoph, R.E.C., *Chapter 10 - Adsorption Refrigerators and Heat Pumps*, in *Carbon Materials for Advanced Technologies*, T.D. Burchell, Editor. 1999, Elsevier Science Ltd: Oxford. p. 303-340.
5. Wang, R., Wang, L., Wu, J.,, *Adsorption Refrigeration Technology*. 2014, Singapore: Wiley.
6. Yu, Y.Q., et al., *Energy Upgrading By Solid–Gas Reaction Heat Transformer: A Critical Review.* Renewable and Sustainable Energy Reviews, 2008. **12**(5): p. 1302-1324.
7. Atkins, P. and J. de Paula, *Atkins' Physical Chemistry*. 2010: OUP Oxford.
8. Mazet, N., M. Amouroux, and B. Spinner, *Analysis And Experimental Study Of The Transformation Of A Non-Isothermal Solid/Gas Reacting Medium.* Chemical Engineering Communications, 1991. **99**(1): p. 155-174.
9. Wang, L., et al., *Adsorption Performances And Refrigeration Application Of Adsorption Working Pair Of Cacl2−NH3.* Science in China Series E: Technological Sciences, 2004. **47**(2): p. 173-185.

10. Ishida, M. and C.Y. Wen, *Comparison Of Zone-Reaction Model And Unreacted-Core Shrinking Model In Solid—Gas Reactions—I Isothermal Analysis.* Chemical Engineering Science, 1971. **26**(7): p. 1031-1041.
11. Ishida, M., C.Y. Wen, and T. Shirai, *Comparison Of Zone-Reaction Model And Unreacted-Core Shrinking Model In Solid—Gas Reactions—II Non-Isothermal Analysis.* Chemical Engineering Science, 1971. **26**(7): p. 1043-1048.
12. Levenspiel, O., *The Coming-Of-Age Of Chemical Reaction Engineering.* Chemical Engineering Science, 1980. **35**(9): p. 1821-1839.
13. Mazet, N. and M. Amouroux, *Analysis Of Heat Transfer In A Non-Isothermal Solid-Gas Reacting Medium.* Chemical Engineering Communications, 1991. **99**(1): p. 175-200.

Chapter 3 : Literature Review

3.1 Introduction

This literature review focuses on adsorption systems which can be found in the literature. Since adsorbent-refrigerant pairs are at the heart of adsorbent systems, the chapter begins with considering common adsorbent-refrigerant working pairs which have been used in adsorbent systems. Further, thermochemical systems and their classifications are discussed and finally different heat recovery based cycles are highlighted. They include multiple salt cascaded systems such as the system which is the focus of this work, mass recovery cycles and thermal wave cycles.

3.2 Common Working Pairs in the Literature

3.2.1 Zeolite-Water

Zeolite is a hydrophilic adsorbent. This means it has a high affinity for polar substances such as water. Zeolites have been used for a wide range of adsorption applications. These range from industrial adsorption chillers to locomotive air conditioners as in Myat et al in [1]. Zeolites can be used at relatively high temperature compared to other physical adsorbents. Zeolites can be used at temperatures up to 500◦C without damaging their adsorption and regenerative capacities [2]. Wang et al [3] designed and modelled a novel zeolite-water adsorption system that makes use of waste heat from internal combustion engine of the locomotive at 450◦C. Table 3-1 below gives further details about some thermo-physical properties of natural Zeolite.

Table 3-1: Thermo-physical properties of natural Zeolite[1]

Appearance	Ivory white
Porosity (%)	45–50
Average pore diameter (A)	4
pH	7–8
Bulk density (kgm^{-3})	650–850
Melting temperature (°C)	1300
Mezopore surface area (m^2g^{-1})	29
Micropore surface area (m^2g^{-1})	11
Thermal conductivity ($Wm^{-1}K^{-1}$)	0.155

There are about two hundred types of Zeolites, a quarter of which are naturally occurring. Manufactured Zeolites are more expensive than natural Zeolites, however,

they perform better in terms of heat and mass transfer [4]. The adsorption capability of zeolites is affected by the ratio of its constituents, Silicon and Aluminium, more Aluminium is tantamount to higher adsorption ability [4]. Zeolites are often tagged with water as a working pair due to their inherent affinity for polar adsorbates. Adsorption capacities of nearly 12% have been found in the zeolite-water pair with hysterisis becoming increasingly apparent at higher temperature[5].

The zeolite-water pair has been explored in a good number of studies/designs ranging from refrigeration [1-3] to floor heating. Dawoud [6] incorporated a gas condensing boiler with a zeolite-water adsorption heat pump for floor heating application (35/28◦C and 55/45◦C). This type of setup is called the mixed-operation mode and both systems work in series to cover the heating demand. Zeolites have also been used in composite adsorbents. Tso et al [7] utilised a novel composite adsorbent made up of zeolite and calcium chloride in a heat pump application. As a result, a much lower desorption temperature was possible and a performance improvement was obtained.

Although, water is the most common refrigerant used with zeolites, zeolites have been tried out with other refrigerants such as carbon dioxide (CO_2) and Nitrogen (N_2), they are part of a list of new adsorption pairs with huge potential. Ridha et al [8] tested the capacity of Nitrogen to be adsorbed by Zeolite for natural gas drying. The conducted tests found an adsorption capacity of about 0.04g/g at a pressure of 100kPa and 0◦C. The associated isoteric heat was a relatively low, 12.2kJ/mol. However, carbon dioxide exhibited better adsorption properties with Zeolite. Adsorption capacity reached up to 0.27g/g at 100kPa and 0◦C [1]. Observed isoteric heat was approximately 42kJ/mol.

3.2.2 Active Carbon-Ammonia

Activated carbon can be manufactured from a variety of sources. These sources can range from fossil fuels and coal to bone and coconut shell. Activated carbon manufacture is generally done by pyrolising and carbonising these source materials at very high temperatures, typically between 700◦C and 800◦C [9]. Activated carbon is produced in various forms, some are granular, and some powder and others are in fibre from. Experiments suggest that the fibres have a better mass and heat transfer performance compared to granules and powder. Powdered activated carbon is generally used in the adsorption of liquids while activated carbon in granulated, pellet

or fibre form is used for the adsorption of gases [2]. This is due to larger specific surface area[4]. Another advantage of the active-carbon pair is its suitability with operating temperatures above 200◦C[10].

Taimainot-Telto and Critoph [11], examined the adsorption refrigeration system using monolithic carbon-ammonia pair. The experiments conducted found maximum specific cooling power (SCP) of about 60W/kg and a maximum coefficient of performance (COP) of 0.12 with generator temperatures between 90◦C and 120◦C. The authors attributed the low COP of 0.12 to the relatively low generating temperature range. Overall, the monolithic carbon gave a 90% higher SCP compared to granular carbon. The generator used by Taimainot-Telto and Critoph in [11] consists of a shell with fins between which the monolithic carbon discs were inserted.

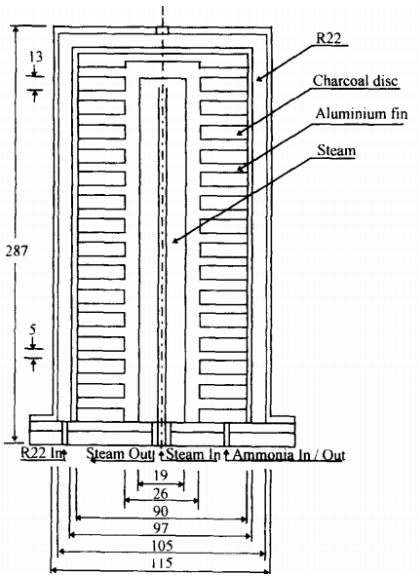

Figure 3-1: Generator used by Taimainot-Telto and Critoph in [11]

Critoph and Metcalf[12] utilised a plate type generator and a higher driving temperature of 200◦C and attained a higher SCP and COP of 2000W/kg and 0.35 respectively.

Activated carbon has also been paired with methanol for refrigeration, particularly in solar powered systems [34]. The major advantage attached to this pair is large adsorption quantity. The activated carbon-methanol pair is known to reach a maximum adsorption quantity of 0.45g/g.

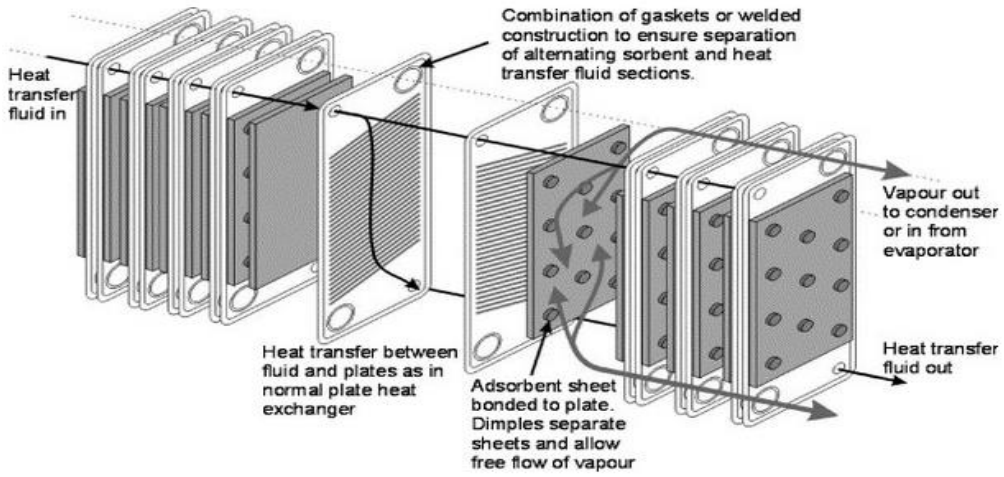

Figure 3-2: Plate type generator used by Critoph and Metcalf in[12]

3.2.3 Silica gel-Water

Silica gel is a tough and hard granular form of silicon dioxide made synthetically from sodium silicate. They are two typical types of silica gel and they are distinguished by pore diameter. Type A have diameters between 2nm and 3nm while type B possess a diameter of 0.7nm [4]. Type A Silica gel can be used in all conditions while type B Silica gel is only suitable at below 50% relative humidity. Adsorption of refrigerant on Silica gel is mainly influenced by the hydroxyl attached to its structure. This hydroxyl group is polar and is capable of forming bonds with polar oxides such as water. So, adsorption is bound to increase as polarity increases [4]. Silica gel is known to have high adsorption ability and they are commonly paired with water. However, this pair carries a disadvantage in its unsuitability for evaporation temperatures below 0◦C. Its adsorption quantity with water is about 0.2g/g.

There are many silica-water systems in the literature. They have been particularly successful in the production of chilled water using low grade heat. Wang et al [13, 14] designed, modelled and tested an adsorption chiller that produces chilled water at 15.7◦C with generating temperature as low as 60◦C and obtained reasonable performance (COP of 0.3). However, the performance improved with increasing generating temperature. The low operating temperature range of silica-water systems make them suitable for solar applications [15, 16]. Silica-water systems have also been sold commercially.

Chemical Adsorbents/Salts Based Systems

Various chemical salts have been proposed for use in thermochemical heat pumps. They can be based on a varying array of chemical materials ranging from sulphur dioxide to alkaline earth and alkaline metals. Alkaline earth metals are six element elements (Beryllium, Barium, Calcium, Strontium, Radium and Magnesium) in group 2 of the periodic table which occur naturally. Many combinations have been proposed for salt based systems in the literature and Wongsuwan [17] offers a detailed classification.

The literature on all these types of heat pumps is extensive but this project focuses on solid-gas reaction between alkaline salts, alkaline earth salts and ammonia (NH_3). Veselovskaya et al [18] tested a composite of $BaCl_2$ and vermiculite in a lab scale adsorption chiller. The composite was developed by dry impregnation of vermiculite with $BaCl_2$ at a 45% salt weight and 1-2mm grain size. The ensuing reaction between the composite and ammonia (NH_3) gas was a one stage type reaction where 8 moles of ammonia reacts with 1 mole of Barium Chloride.

The same author, Veselovskaya in [19] suggest that the introduction of a matrix with $BaCl_2$ does not affect the equilibrium properties between the equilibrium of the salt with ammonia gas. The resulting data was analysed to determine the heat produced in the generator, the coefficient of performance (COP) and the specific cooling performance (SCP). Overall, it was concluded that the sorption composite $BaCl_2$/Vermiculite can be used in an adsorption chiller with low potential heat source (80◦-90◦) with a COP of up to 0.54 and a SCP ranging from 300 to 680W/Kg.

Grekova et al [20] tested the sorption characteristics of ammonia on a composite of $BaCl_2$ and $BaBr_2$ (both Barium halides) using vermiculite as the host matrix. The experiments performed on these composites were geared towards adsorption cooling. Upon adsorption the complex $BaCl_xBr_{2-x}.8NH_3$ was formed. A decrease in equilibrium pressure was observed with samples of higher $BaBr_2$ molar content. The associated enthalpy of sorption obtained was ΔH=-35±3kJmol^{-1}. This value was found to be independent of ammonia uptake.

Salt composites operating at a higher temperature have also been investigated. Aidoun et al [21] is based on a solid-gas reaction between cobalt chloride ($CoCl_2$) impregnated into carbon fibres and ammonia. Heat input of 2000W was applied to the salt composite at 200◦C. A small scale laboratory rig was used to test the performance of this combination and it was found that the mass transfer rate reduced drastically with an increase in number of process cycles. This is unfavourable since mass transfer rate is one of the most important mechanisms in the working of a chemical heat pump. The desorption of ammonia from the salt composite was measured directly by continuously measuring the weight of the reactor. Overall, the material was found to perform well with a power density of about 280 kW m^{-3} putting it in competition with the best known materials.

3.3 Heat Recovery Cycles

The limitations of temperature lift and system efficiency of heat pumps based on basic cycles make a case for advanced cycles. Many cycles have been tried. They range from multi-salt cascades to multi-stage cycles and thermal waves [22]. Even though this work focuses on multi-salt cascades in subsequent chapters, various types of advanced cycles are discussed in this literature review.

3.3.1 Heat Regeneration Cycles

Heat regeneration cycles are usually made of two or more adsorbent beds and the heat produced from one bed undergoing adsorption is used to preheat the heat transfer fluid for desorption in the other bed in order to improve performance. A typical regenerative cycle was used by Tchernev [23] to recover 80% of the heat released in one of the adsorption beds. Douss et al [24] details a similar two bed adsorption cycle. The Clapeyron diagram for the cycle is shown in Figure 3-3 below.

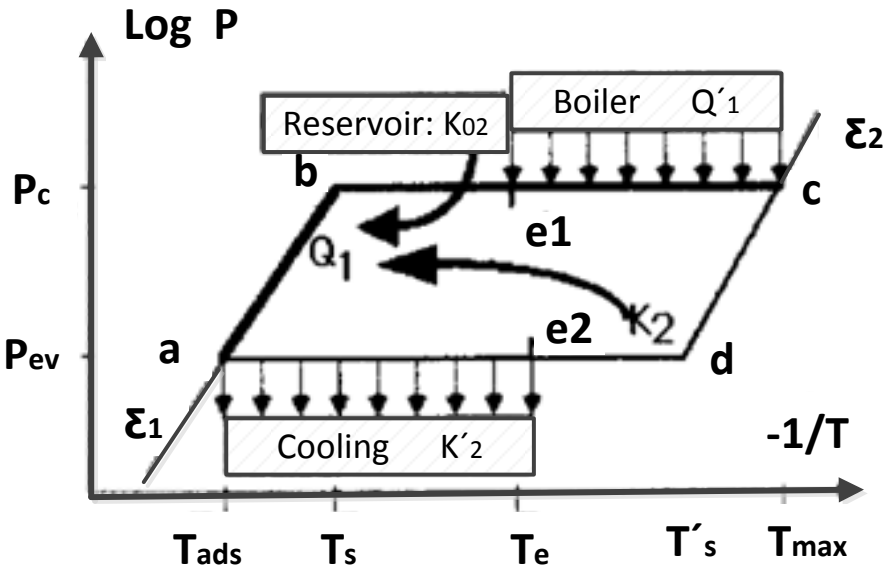

Figure 3-3: Clapeyron diagram for a two-adsorber cycle[24]

Adsorber 1 is represented by the thicker (abc) line in the cycle while the thinner (cda) line is for adsorbent 2. The heat recovered from the adsorption (adsorber 2) bed is used in raising the temperature of the desorption (adsorber 1) bed from T_{ads} to T_{e1} so that the boiler is only used to complete the temperature rise to T_{max}. Therefore, the heat input to adsorber 1 (Q_1) is made up of heat provided by adsorber 2 (K_2) and heat from the boiler (K_{02}). After, there is external cooling (K_2') and heating (Q_1') to get adsorber 2 down to T_{ads} and get adsorber 1 up to T_{max}. Subsequently, the scenario is reversed and the adsorber 1 will be in adsorption. The heat input to adsorber 2 is made up of the heat from the boiler (K_{01}) and recovered heat from adsorber 1. To complete the cycle, external cooling and heating is carried by the heat exchanger and boiler on adsorber 1 and adsorber 2 respectively. At this stage, the heat input to adsorber 2 is Q_2' while the heat output from adsorber 1 is K_1'. If the heat of evaporation is Q_{ev1} for adsorber 1 and Q_{ev2} for adsorber 2, the cooling COP is

$$COP_{cooling} = \frac{Q_{ev1} + Q_{ev2}}{Q_1' + Q_2' + K_{01} + K_{02}} \tag{3.1}$$

And the heat pumping COP is

$$COP_{heatpump} = \frac{Q_{c1} + Q_{c2} + K_1^{'} + K_2^{'}}{Q_1^{'} + Q_2^{'} + K_{01} + K_{02}} \quad (3.2)$$

3.3.2 Multiple Salts Cycles and Other Advanced Cycles

Cascaded cycles have been proposed with the aim of increased efficiency of sorption systems. Like other heat recovery cycles, they are commonly based on the principle of energy reutilisation. With cascaded cycles, two or more types of salts are used and the synthesis heat produced by one reactant is used for another's decomposition [22].

3.3.2.1 Multiple Stage Multiple Effect Cascaded Cycles

Neveu and Castaing [25] used two solid-gas reactors, a condenser and an evaporator for continuous refrigeration. Basically, heat recovered from one of the salts at high temperature was used to drive the desorption process in the other at a lower temperature. This type of system is commonly termed 'double effect'. The first effect comes from the external heat source and the second effect is derived from the recovered heat.

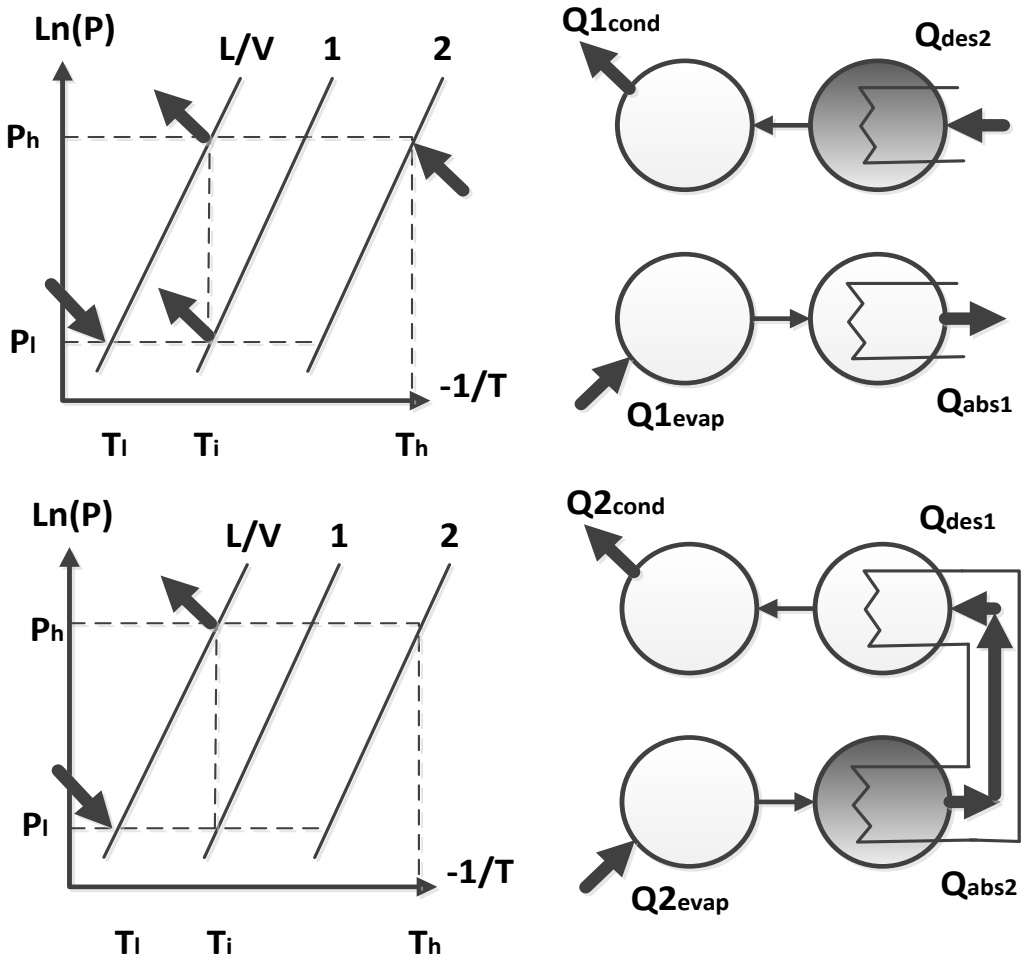

Figure 3-4: The two main phases of Neveu and Castaing[25] proposed cascade system

As shown in Figure 3-4 above, the system works in two phases. Phase 1 on the left features one reactor at high temperature in the decomposition stage while the other medium temperature reactor is undergoing adsorption of gas from the evaporator. On the right (phase 2) of Figure 3-4, the reaction heat from the high temperature reactor is transferred to the medium temperature reactor for its regeneration. The supposed advantage of this system lies in its enhanced energy efficiency. In phase 1, there is condensation heat subsequent to high temperature decomposition reaction while there is an output of condensation heat subsequent to the medium temperature decomposition reaction in phase 2 following internal heat recovery. Furthermore, the heat of reaction from the synthesis reaction of the medium temperature salt can be utilised. Therefore, three lots of heat output are available for utilisation at the expense of one external heat input.

The Neveu and Castaing cycle is bound by a few temperature related constraints. Considering the cycle below in Figure 3-5.

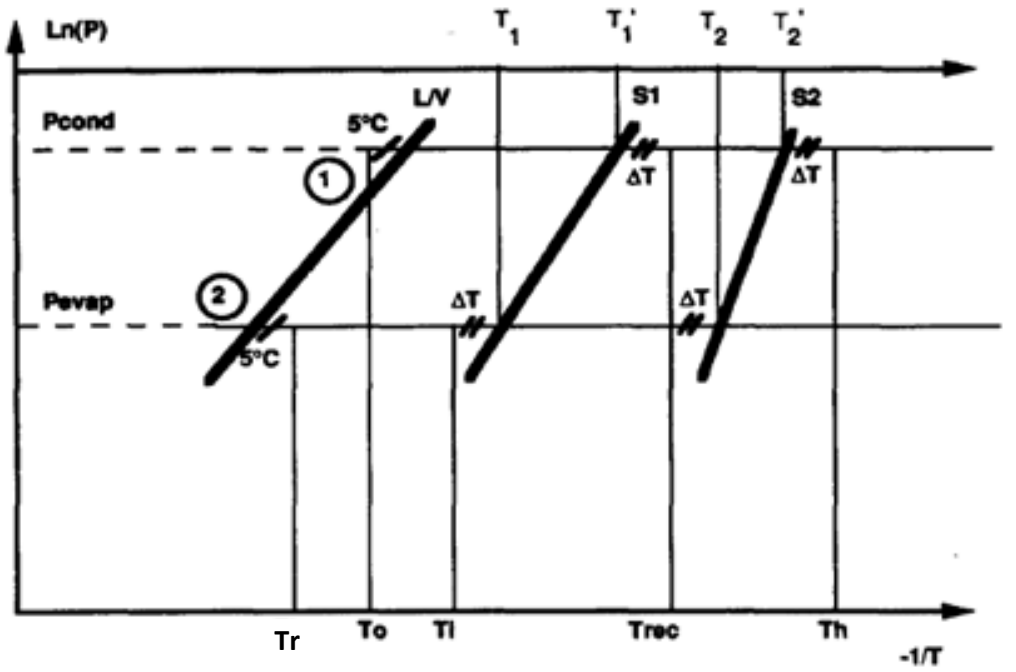

Figure 3-5: The double effect cycle described by Neveu and Castaing

Here, ΔT denotes the deviation from thermal equilibrium, T_0 is the heat sink temperature, T_r is the refrigeration temperature and T_h is the temperature at which salt 2 (s2) is heated. The associated constraints are as follows:

1. For any salt which is used, the heat sink/condensation temperature (T_0) must be equal or less than the required refrigeration temperature (T_r).
2. The heat recovery stage can only go ahead if and only if ΔT is positive. Otherwise heat will be lost by salt 1 and gained by salt 2 instead of the reverse.

Goetz et al [26] proposed a similar two salt cycle (shown in Figure 3-6) for a thermal transformer which has two inputs at medium temperature, transforms some to a high temperature and dumps the rest to ambient. In this case, the condensation and evaporation processes above are replaced by synthesis and decomposition reactions respectively.

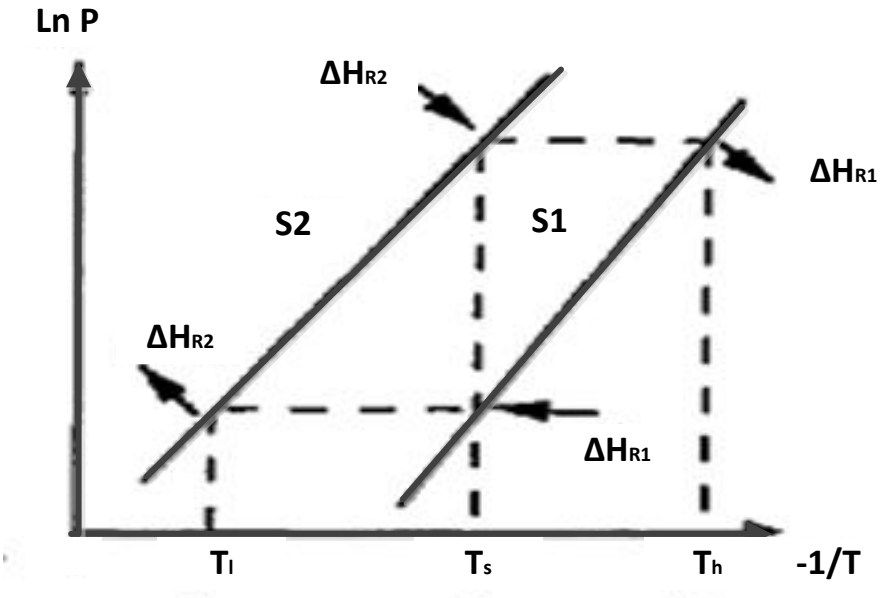

Figure 3-6: Clapeyron's diagram showing the operation of two salt cycle[26]

Multiple salt configurations have also been investigated for metal hydride systems. Suda et al [27] proposed a double stage cycle with three different metal hydrides operating under three different pressure levels. The three different salts are placed three pairs of solid-gas reactors, each pair with a distinct salt as in below in Figure 3-7.

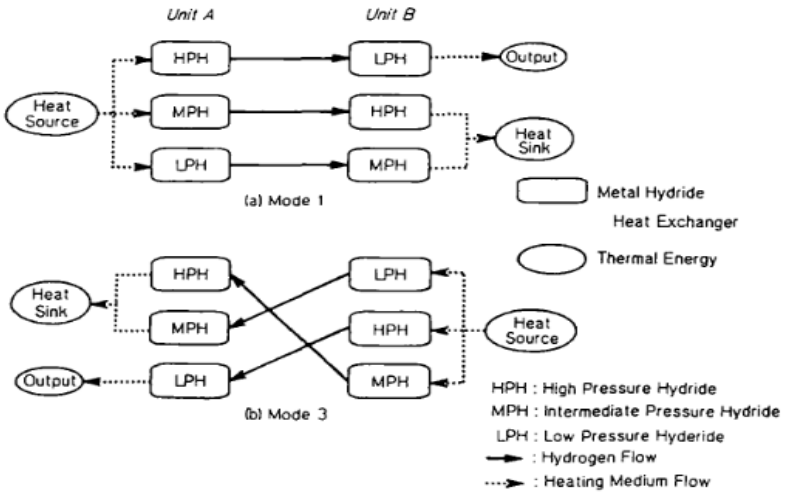

Figure 3-7: Flow pattern of a double stage metal hydride heat pump [27]

Each reactor in each unit acts as both a donor (mode 1) and a receiver (mode 3) of hydrogen. As the heat source is applied simultaneously on the left of mode 1, thermal output at the highest temperature is utilised at LPH in mode 1, unit B while the heat

output (heat sink) from HPH and MPH is supplied back into the system in the reverse direction. This makes for a thermal output on both sides and thus continuous operation because the units are working out of phase.

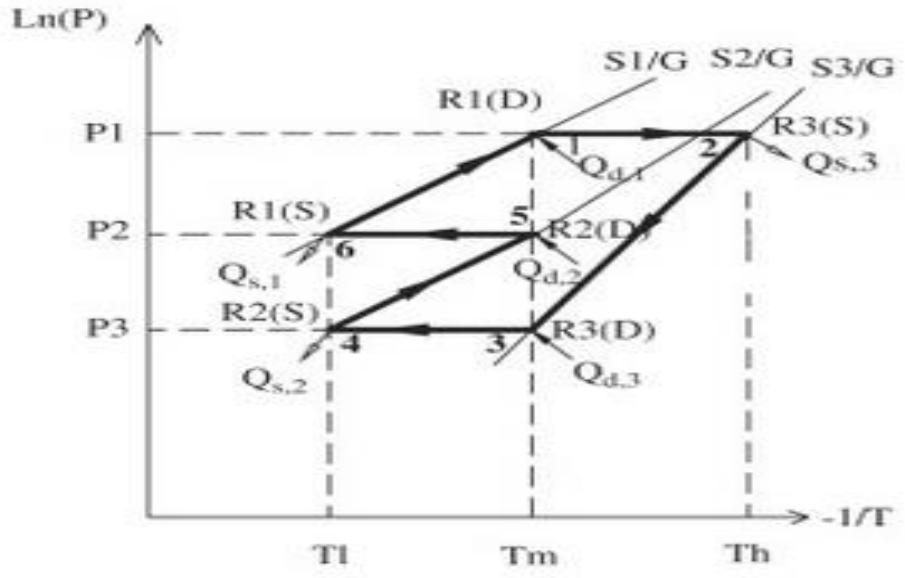

Figure 3-8: Clapeyron's diagram showing the operation of the Suda et al cycle[27]

In the cycle shown in Figure 3-8, S stands for synthesis, D stands for decomposition while R stands for reaction. Therefore, the Suda et al cycle will typically possess only one generating period (point 1 to point 2 in Figure 3-8) and two recovery periods (point 3 to point 4 and point 5 to point 6 in Figure 3-8). Sun [28] researched the possibility of a similar three-salt cycle to the Suda et al cycle but with two generating periods (see Figure 3-9) hence a double effect. Sun's paper also presents the same components (three different metal hydrides in six reactors) in three different applications (heat pumping, heat amplification and refrigeration), described as follows.

- Heat pumping/transformation when medium/low grade heat is upgraded to useful heat.
- Heat amplifier (i.e. a heat pump) when high grade waste heat and ambient heat is used to create large amounts of heat at intermediate temperature.
- Refrigeration when high grade waste heat and an atmospheric heat sink is used to generate cooling.

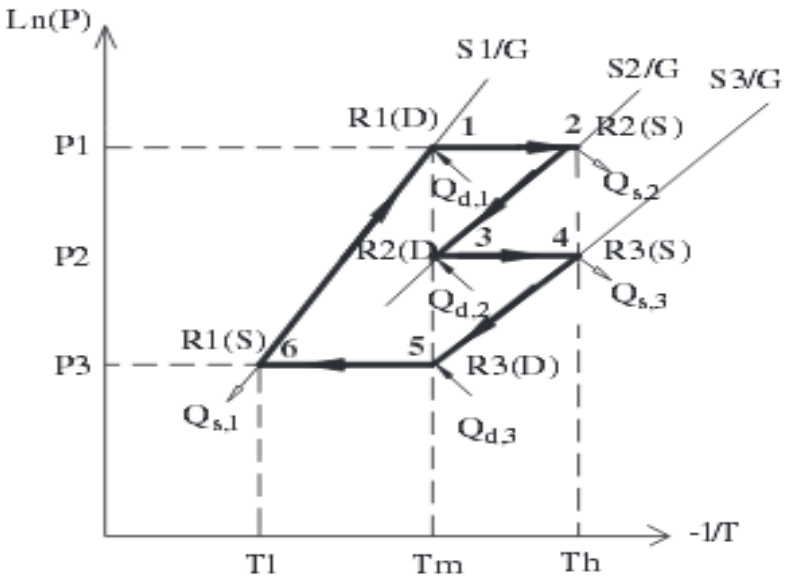

Figure 3-9: Clapeyron's diagram showing the operation of Sun's three-salt double effect cycle for heat transformation[28]

Spinner et al [29] studied the use of different transport fluids in the same system. A $MnCl_2/H_2O$ and $NiCl_2/NH_3$ refrigeration system were studied. The log pressure-temperature diagram in Figure 3-10 below shows the operation of the system in which heat is supplied from a heat source for regeneration of the $MnCl_2/H_2O$ sub-system at 130◦C. The heat of synthesis from this reaction is recovered to decompose the $NiCl_2/NH_3$ sub-system. The heat of condensation from $NiCl_2/NH_3$ is discarded to the atmosphere at 20◦C and the ensuing ammonia (NH_3) is evaporated at -30◦C and goes to the $NiCl_2/NH_3$ reactor where it reacts to produce the heat that is then retrieved to decompose the $MnCl_2/H_2O$ again.

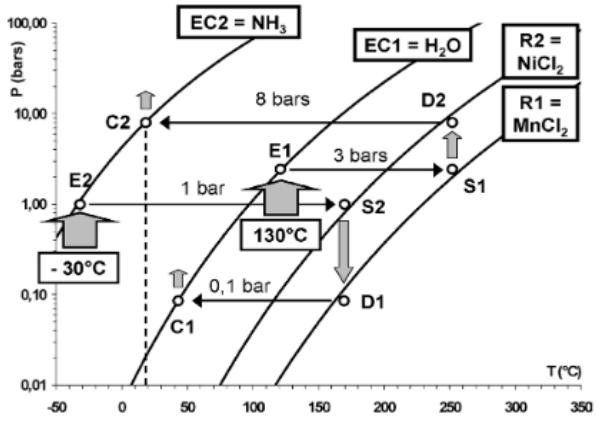

Figure 3-10: The operation of a two-gas, two-salt cascade system[29]

Li [30] presented a solid-gas triple effect system using three reactive salts with ammonia which employ two internal recovery processes. One reactor is filled with a high temperature salt and the other two are filled with a medium temperature salt and low temperature salt respectively. In the first phase of its operation as seen in Figure 3-11, a heat input is applied on the high temperature salt (SG reactor 1) from an external heat source. The refrigerant that is desorbed moves to the condenser where it condenses and heat is released into the sink and the condensed refrigerant is transferred to the evaporator. Simultaneously, the medium temperature salt (SG reactor 2) adsorbs gas that is evaporated from the evaporator and this forms the first cooling stage. The heat of adsorption produced in the medium temperature reactor is recovered for use in the low temperature salt (SG reactor 3) where refrigerant is desorbed into another condenser.

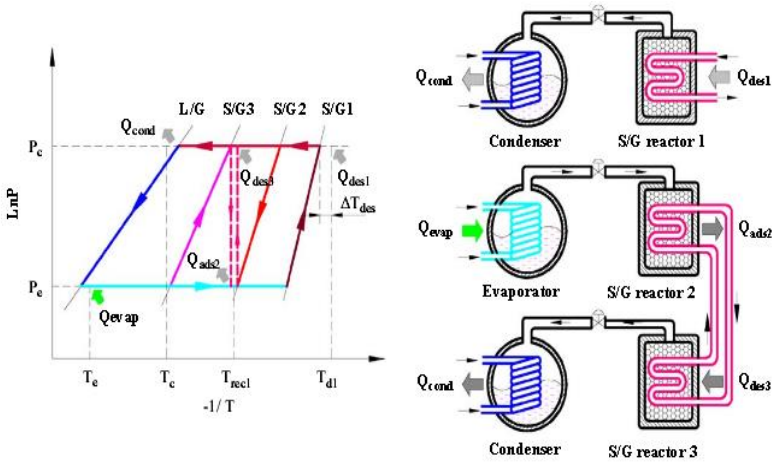

Figure 3-11: Schematic and Clapeyron diagram for the first phase of the triple effect refrigeration system described by Li[30]

The second phase of the Li system features a reversal of the roles of the condenser and evaporator. The low temperature reactor evaporates refrigerant from the evaporator to create a second cooling stage. At the same time, refrigerant is evaporated from another evaporator into the high temperature salt and this is the third stage of cooling. The heat produced in the HTS is used to regenerate the medium temperature salt in the second internal heat recovery process. Overall, three lots of cooling are derived from only one heat input and this in theory should improve the efficiency of refrigeration.

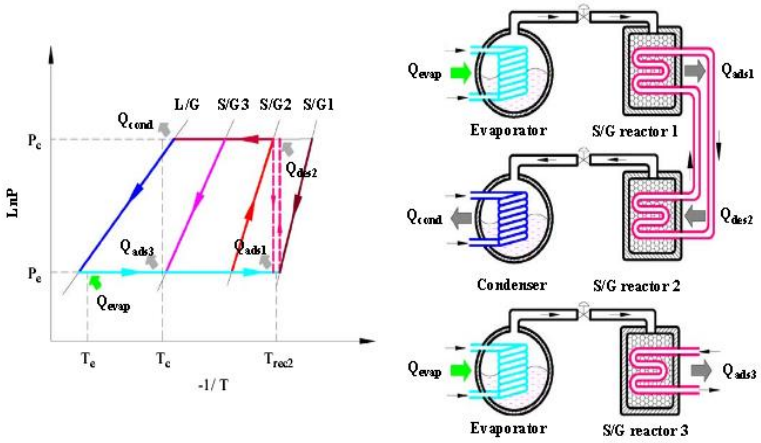

Figure 3-12: Schematics and Clapeyron diagram for the second phase of the triple effect refrigeration system described by Li[30]

Li [30] however also identified that the performance of the system depended on the reaction enthalpy of the salt utilised. This was evident in a single effect comparison between $MnCl_2$ and $NiCl_2$ as reactants. $MnCl_2$ had a higher COP as seen in Figure 3-13 since it has a higher enthalpy of reaction.

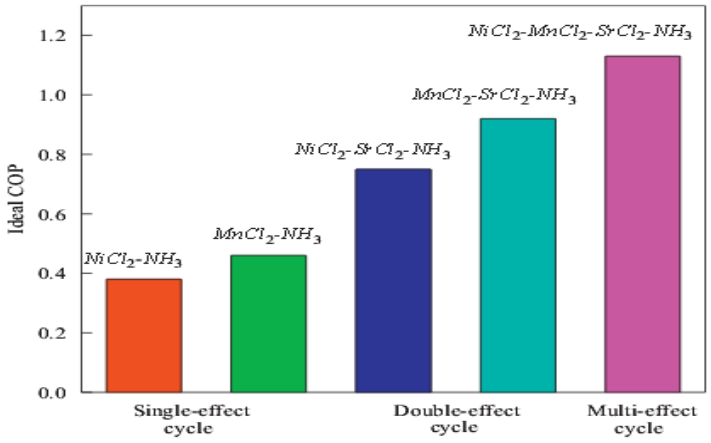

Figure 3-13: COP comparison between $NiCl_2$ and $MnCl_2$ for single and multiple effect systems[30]

There are however problems associated with the use of ammonia as the refrigerating fluid in these systems. Mauran [31] researched the problem of the changing molar volumes of reactants as they undergo synthesis leading to swelling and agglomeration. This is generally considered an obstacle although Spinner [32] identified the use of this problem as a positive property by some researchers by using these molar volume

increases to improve the contact coefficients between the salts and the binder translating into an improvement in heat transfer coefficients.

Further, Spinner [32] discussed the occurrence of a reduced rate of reaction across certain zones in ammoniates. Efforts have been made to understand the evolution of these zones as a function of pressure and temperature but to no avail. Another highlighted problem is the position of the equilibrium line of the salt used. It is important to avoid selecting salts whose equilibrium lines are close to the ammonia saturation line.

The swelling and agglomeration of ammoniate grains during synthesis translates into obstacles also [32]. It means that upon swelling, there is a major decrease in the permeability of the bed leading to reduced mass transfer. The original texture of the grains does not return upon a subsequent decomposition reaction since ammoniates still contain a few molecules of ammonia after decomposition (e.g. $CaCl_2$ 4-2 NH_3). This problem could also limit the transformation and effectiveness of the synthesis process. The potential solution is the development of binders capable of accommodating the swelling without reducing the permeability of the system. Several methods however have been proposed to solve the swelling and agglomeration problem although not all were very successful. Some of them are:

- Rockenfeller [33] patented a method based on maintaining the solid reactants at their optimum reaction densities by restricting volumetric expansion. This method produces poor heat and mass transfer characteristics.
- Spinner [32] contains details about the Doi and Ikeuchi reactor with crystallisation on the exchanger walls to offer constant contact with the wall and continuous optimum contact within the grains as well. This system yielded low heat transfer coeffcients.
- Spinner [32] also discusses a proposed implementation of ammoniates infused in expanded natural graphite. This method has been shown to be valid for different chlorides such as $MnCl_2$ $MgCl_2$ and $NiCl_2$. Other matrices such as vermiculite have been used in the literature.

These solutions and many others have been proposed over the years. They are usually limited by one or more the reaction dynamics which could be mass transfer or heat transfer.

Cascades have also been applied with physical adsorption systems. Meunier [34] investigated the cascading of the zeolite-water and the carbon-methanol pairs. One of Meunier's case studies considered the cogeneration of chilled water at 2◦C and hot water at 70◦C. The system is made up of two zeolite-water reactors, two active carbon reactors, two condensers, two evaporators and a heat storage unit. Basically, the active carbon is regenerated to 100◦C partly from the condensation heat of water at 65◦C and the heat of adsorption of zeolite which is typically between 60◦C and 75◦C.

A combined double way cycle is proposed in [35]. Here, the system mainly consists of a high temperature reactor, a low temperature reactor, a condenser and an evaporator. As seen in part 'a' of Figure 3-14, in the first phase of the cycle, the high temperature salt receives an external heat input (Q_{des1}) at a high temperature (T_d). This initiates a desorption process in the high temperature salt. Refrigerant is desorbed into the condenser where heat is rejected into the environment at T_c. The liquid refrigerant flows into the evaporator where it creates the first cooling effect.

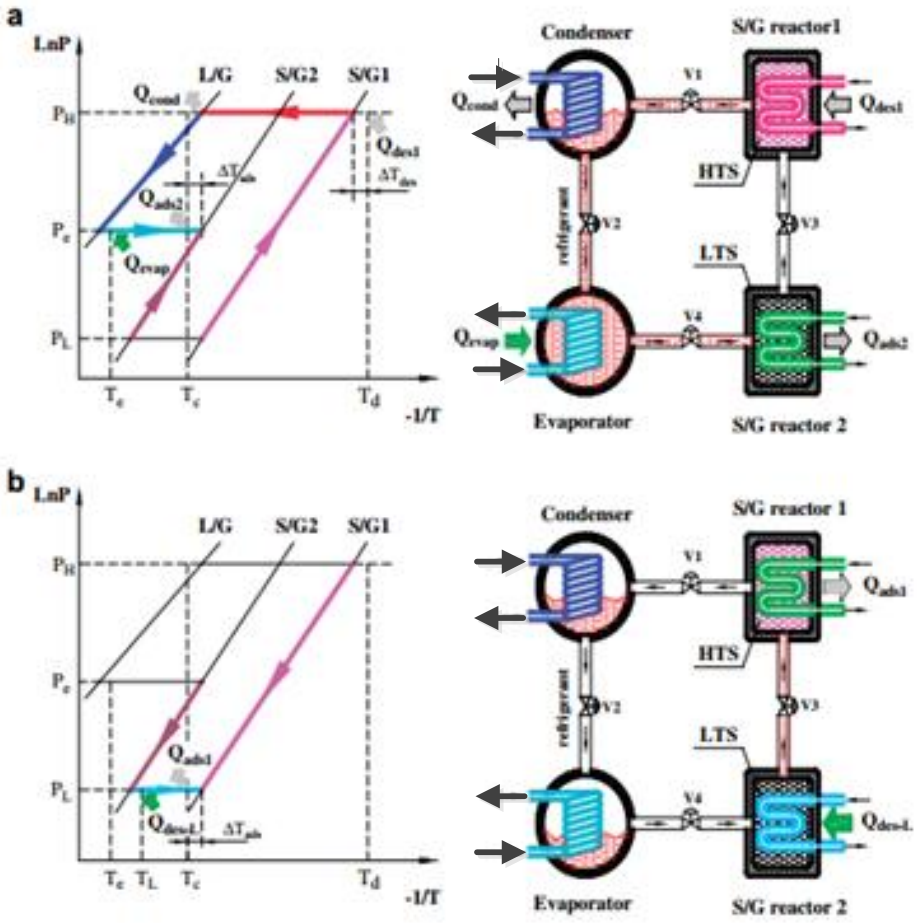

Figure 3-14: Schematic diagram of combined double-way sorption refrigeration cycle[35]. a) Phase 1 b) Phase 2

Simultaneously, the low temperature salt in the low temperature reactor is cooled by a heat sink to allow the adsorption of evaporated gas from the evaporator. Because the heat of desorption of the low temperature salt is taken from the heat sink, this creates another cooling effect in the evaporator. In the second phase of the cycle, the initial working modes are reversed. Reactor 1 (HTS) performs adsorption while reactor 2 (LTS) performs desorption.

Li [35] suggests that this cycle offers better performance parameters than the conventional adsorption cycle for the same amount of adsorbed refrigerant and heat input. This is because the reaction enthalpy for the desorption in the LTS is far greater than the vaporization enthalpy of the refrigerant. Also, two cooling effects are obtained from one heat input.

Goetz et al [36] detailed a double resorption cooling system which consists of four solid-gas reactors made up of three different salts. Heat is recovered during the second of the two phases as seen in Figure 3-15 below. The system works in a similar fashion as the aforementioned cascaded systems.

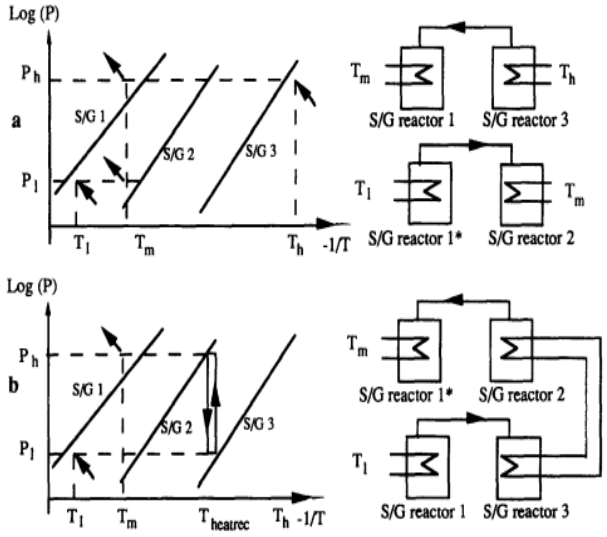

Figure 3-15: Working mode of Goetz et al double resorption cycle[36] a) Phase 1 b) Phase 2

There are many other similar cascaded salt systems which are detailed in literature. Since, they are similar in concept to the afore-discussed systems, they are summarised below.

1. Wang et al [37] detailed a two stage triple effect system made up of four adsorbent beds utilising two types of adsorbents, zeolite and activated carbon.
2. Douss et al [38] developed a cascading cycle using zeolite-water pair in the high temperature range and and intermittent active-carbon-methanol pair for the low temperature stage. The active carbon adsorber was fired by heat recovered from the zeolite-water adsorption.
3. Rockenfeller et al [39] proposed a thermochemical system with multiple stages using three different reactors (high medium and low temperatures).
4. Meunier [40] investigated the relationship between the number of cascades used and theoretical efficiency using second law analysis. The impact of cascade numbers on the heat transfer is also discussed.

3.3.2.2 Mass Recovery Cycles

Mass recovery cycles make use of a pressure difference between two interconnected beds rather than a temperature difference as in heat recovery cycles. The performance of the machine is improved by way of synthesis or decomposition of more refrigerant per cycle. At the end of the individual decomposition or synthesis phase, the beds are connected together so that refrigerant from the pressurised decomposition bed is transferred to the low pressure synthesis bed. The sudden drop in pressure in the decomposition bed initiates further decomposition and the introduction of refrigerant into the synthesis bed aids the overall synthesis stage. Figure 3-16 shows the schematic of a mass recovery system.

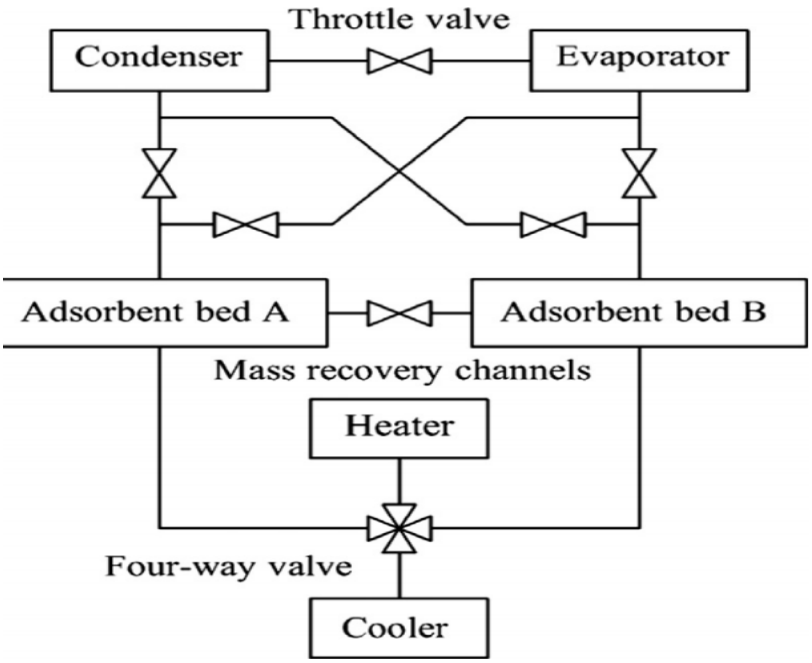

Figure 3-16: Schematic of mass recovery cycle[41]

Vasiliev et al [42] details a double effect resorption system where $BaCl_2$ and $NiCl_2$ are combined with Busofit (activated carbon) in a two and four reactor set up. Internal heat recovery is enabled by mass transfer between the reactors. A schematic of the two reactor set up is shown in Figure 3-17.

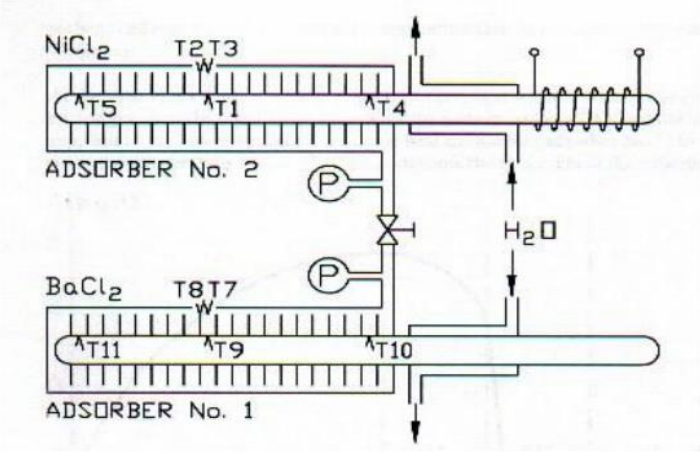

Figure 3-17: Schematic of the two-adsorber set-up [43]

The low temperature salt composite made up of $BaCl_2$ and Busofit is installed in the low temperature reactor (Adsorber 1) while the other composite made up of $NiCl_2$ and Busofit is installed in the high temperature reactor (Adsorber 2) as the high temperature salt composite. When heat at low temperature is supplied to Adsorber 1, ammonia is desorbed at high pressure and it immediately goes into adsorber 2 where it is adsorbed on the high temperature composite thereby producing heat that increases the temperature of the high temperature salt from 50°C to 220°C.

In the four-adsorber scenario, the opportunity for continuous operation is presented. Two sides of the heat pump are operated in an out-of-phase manner.

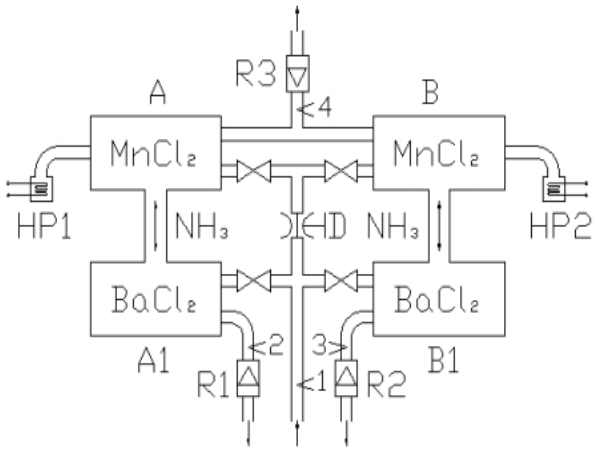

Figure 3-18: Schematic of the four-adsorber set-up[43]

In this set-up, the set-up shown in Figure 3-18 is operated in two main phases which corresponds to two levels of pressure. Reactors A and B hold high temperature salt,

$MnCl_2$ infused in Busofit just as in the two-adsorber set-up while the reactors A1 and B1 hold the low temperature counterparts. The system is limited in performance by low thermal conductivity of the salt and the swelling that occurs as a result of the solid-gas reaction.

3.3.2.3 Thermal Wave

The thermal wave cycle is another heat regeneration technique used to improve the performance of adsorption systems. The basic thermal wave cycle used in adsorption systems was first proposed by Shelton[44, 45], a two-bed system was detailed. The heat recovery is done through one heating/cooling fluid circuit with a reversible pump as shown in Figure 3-19.

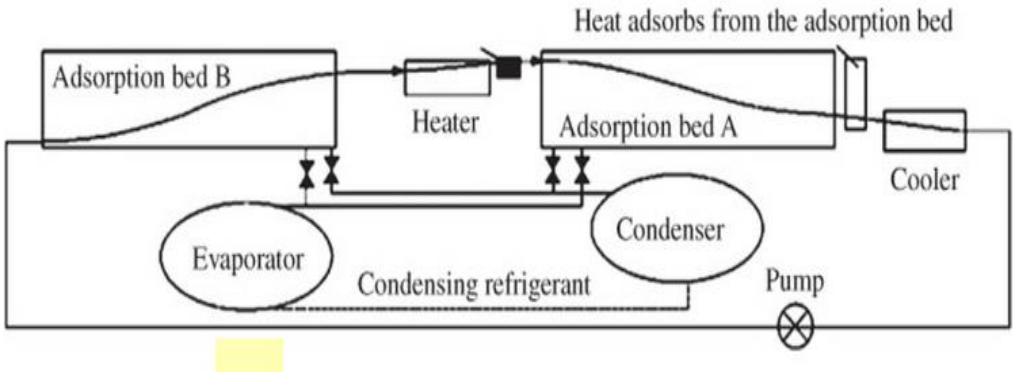

Figure 3-19: The temperature distribution and heat transfer process in ideal thermal wave cycle [37]

At the beginning of the cycle, adsorbent bed B is hot (minimum adsorbate concentration) and adsorbent A is cold (maximum adsorbate concentration). The pump transfers fluid from the cooler into adsorbent bed B, recovering heat from it. This heated fluid flows into the heater where it is further heated up to the temperature required to desorb the adsorbate concentrated in adsorbent bed A into the condenser. Here, the fluid loses heat to the adsorbent bed A and is then passed through the cooler. Simultaneously, the heat transfer fluid is flowing from the cooler to adsorbent bed B where adsorbate is adsorbed from the evaporator. As a result, a thermal wave front is formed in the beds. The pump is then subsequently reversed and the thermal wave front is formed in the opposite direction. It is important to point out that this works when the heat capacity flow rate of the fluid is small compared to the thermal mass of

the bed. Otherwise there will be no wave. Thermal wave cycle designs with more than two beds also exist in literature. Rivero-Pacho [46] developed a four-bed system based on the cycle proposed by Jones in [47].

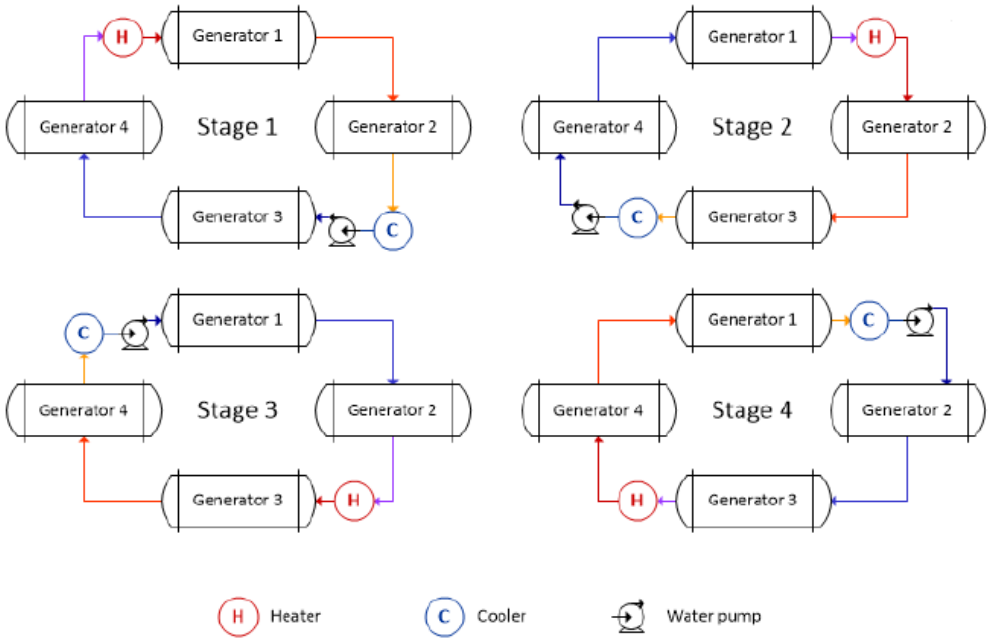

Figure 3-20: Four beds thermal wave cycle[46]

Figure 3-20 is a virtual representation of the stages of the aforementioned cycle. In stage 1 of the cycle, the heater (H) heats the hot fluid which then flows through generator 1 causing desorption of adsorbate. The same fluid leaves generator 1 at a slightly lower temperature and enters generator 2, creating a preheating effect. The fluid is then passed into the cooler (C) where the fluid is made cold for adsorption generator 3. It leaves generator 3 slightly warmer and then precools generator 4. In subsequent stages, the the configuration is changed such that a bed which was preheated/precooled in a previous stage is heated or cooled in the current stage. For example, generator 2 which was preheated in stage 1 is heated in stage 2 and generator 4 which was precooled in stage 1 is cooled in stage 2.

Based on earlier thermal wave cycles [44, 45], Critoph [48] proposed the forced convection thermal wave cycle in which forced convection is carried out between the refrigerant gas and the adsorbent, the adsorbent is directly heated and cooled by the refrigerant gas (Figure 3-21).

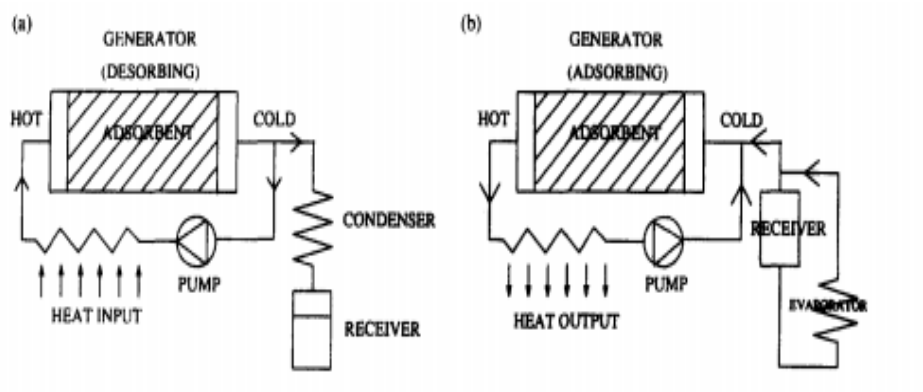

Figure 3-21: Forced convection cycle in desorption phase (a) and adsorption phase (b)[48]

In the desorption phase, the gas around the heat exchanger is heated and flows into the adsorbent bed afterwards. There, it provides the heat needed for the desorption of refrigerant from the generator through convective heat transfer between the hot gas and the cold bed. The gas used in the heat transfer process and the desorbed gas flow out of the generator. A part of the gas flows into the pump where it is heated ready to provide heat for desorption again. The other part flows into the condenser where it condenses. In the adsorption phase, the gas flows in the opposite direction. The pump conveys low temperature gas into the generator where it is adsorbed and adsorption heat is released. This adsorption heat can be recovered if two beds are used. Essentially, the heat released from the adsorption bed is used as input heat for the gas going into the desorption bed. With time, a thermal wave front similar to that which was proposed by Shelton et al [44] is formed in the bed(s).

3.4 Summary

In this chapter, various systems were described with the aim to set the scene for the rest of the thesis. Although the chapter began with a discussion on the common types of adsorbent-refrigerant working pairs, most of the chapter focussed on systems which made use of internal heat recovery.

3.5 References

1. Myat, A., et al., *Experimental Investigation On The Optimal Performance Of Zeolite–Water Adsorption Chiller.* Applied Energy, 2013. **102**(0): p. 582-590.

2. Srivastava, N.C. and I.W. Eames, *A Review Of Adsorbents And Adsorbates In Solid–Vapour Adsorption Heat Pump Systems.* Applied Thermal Engineering, 1998. **18**(9–10): p. 707-714.
3. Wang, D.C., Z.Z. Xia, and J.Y. Wu, *Design And Performance Prediction Of A Novel Zeolite–Water Adsorption Air Conditioner.* Energy Conversion and Management, 2006. **47**(5): p. 590-610.
4. Wang, L.W., R.Z. Wang, and R.G. Oliveira, *A Review On Adsorption Working Pairs For Refrigeration.* Renewable and Sustainable Energy Reviews, 2009. **13**(3): p. 518-534.
5. Solmuş, İ., et al., *Adsorption Properties Of A Natural Zeolite–Water Pair For Use In Adsorption Cooling Cycles.* Applied Energy, 2010. **87**(6): p. 2062-2067.
6. Dawoud, B., *On The Development Of An Innovative Gas-Fired Heating Appliance Based On A Zeolite-Water Adsorption Heat Pump; System Description And Seasonal Gas Utilization Efficiency.* Applied Thermal Engineering, 2014. **72**(2): p. 323-330.
7. Tso, C.Y., et al., *Experimental Performance Analysis On An Adsorption Cooling System Using Zeolite 13X/Cacl2 Adsorbent With Various Operation Sequences.* International Journal of Heat and Mass Transfer, 2015. **85**: p. 343-355.
8. Ridha, F.N., Y. Yang, and P.A. Webley, *Adsorption Characteristics Of A Fully Exchanged Potassium Chabazite Zeolite Prepared From Decomposition Of Zeolite Y.* Microporous and Mesoporous Materials, 2009. **117**(1–2): p. 497-507.
9. Askalany, A.A., et al., *An Overview On Adsorption Pairs For Cooling.* Renewable and Sustainable Energy Reviews, 2013. **19**: p. 565-572.
10. Tamainot-Telto, Z., et al., *Carbon–Ammonia Pairs For Adsorption Refrigeration Applications: Ice Making, Air Conditioning And Heat Pumping.* International Journal of Refrigeration, 2009. **32**(6): p. 1212-1229.
11. Tamainot-Telto, Z. and R.E. Critoph, *Adsorption Refrigerator Using Monolithic Carbon-Ammonia Pair.* International Journal of Refrigeration, 1997. **20**(2): p. 146-155.

12. Critoph, R.E. and S.J. Metcalf, *Specific Cooling Power Intensification Limits In Ammonia–Carbon Adsorption Refrigeration Systems.* Applied Thermal Engineering, 2004. **24**(5–6): p. 661-678.
13. Wang, D.C., et al., *Study Of A Novel Silica Gel–Water Adsorption Chiller. Part II. Experimental Study.* International Journal of Refrigeration, 2005. **28**(7): p. 1084-1091.
14. Wang, D.C., et al., *Study Of A Novel Silica Gel–Water Adsorption Chiller. Part I. Design And Performance Prediction.* International Journal of Refrigeration, 2005. **28**(7): p. 1073-1083.
15. Luo, H.L., et al., *An Efficient Solar-Powered Adsorption Chiller And Its Application In Low-Temperature Grain Storage.* Solar Energy, 2007. **81**(5): p. 607-613.
16. Tangkengsirisin, V., A. Kanzawa, and T. Watanabe, *A Solar-Powered Adsorption Cooling System Using A Silica Gel–Water Mixture.* Energy, 1998. **23**(5): P. 347-353.
17. Wongsuwan, W., Et Al., *A Review Of Chemical Heat Pump technology and applications.* Applied Thermal Engineering, 2001. **21**(15): p. 1489-1519.
18. Veselovskaya, J.V., et al., *Novel Ammonia Sorbents "Porous Matrix Modified By Active Salt" For Adsorptive Heat Transformation: 3. Testing Of "Bacl2/Vermiculite" Composite In A Lab-Scale Adsorption Chiller.* Applied Thermal Engineering, 2010. **30**(10): p. 1188-1192.
19. Veselovskaya, J.V., M.M. Tokarev, and Y.I. Aristov, *Novel Ammonia Sorbents "Porous Matrix Modified By Active Salt" For Adsorptive Heat Transformation: 1. Barium Chloride In Various Matrices.* Applied Thermal Engineering, 2010. **30**(6–7): p. 584-589.
20. Grekova, A.D., et al., *Ammonia Sorption On The Composites "(Bacl2&Babr2) Inside Vermiculite Pores".* Colloids and Surfaces A: Physicochemical and Engineering Aspects, 2014. **448**(0): p. 169-174.
21. Aidoun, Z. and M. Ternan, *Salt Impregnated Carbon Fibres As The Reactive Medium In A Chemical Heat Pump: The NH3–Cocl2 System.* Applied Thermal Engineering, 2002. **22**(10): p. 1163-1173.
22. Yu, Y.Q., et al., *Energy Upgrading By Solid–Gas Reaction Heat Transformer: A Critical Review*. Renewable and Sustainable Energy Reviews, 2008. **12**(5): p. 1302-1324.

23. Tchernev, D.I., *Regenerative Zeolite Heat Pump*, in *Studies in Surface Science and Catalysis*, P.A. Jacobs and R.A.v. Santen, Editors. 1989, Elsevier. p. 519-526.
24. Douss, N., F.E. Meunier, and L.M. Sun, *Predictive Model And Experimental Results For A Two-Adsorber Solid Adsorption Heat Pump.* Industrial & Engineering Chemistry Research, 1988. **27**(2): p. 310-316.
25. Neveu, P. and J. Castaing, *Solid-Gas Chemical Heat Pumps: Field Of Application And Performance Of The Internal Heat Of Reaction Recovery Process.* Heat Recovery Systems and CHP, 1993. **13**(3): p. 233-251.
26. Goetz, V., F. Elie, and B. Spinner, *The Structure And Performance Of Single Effect Solid-Gas Chemical Heat Pumps.* Heat Recovery Systems and CHP, 1993. **13**(1): p. 79-96.
27. Suda, S., et al., *Development Of A Double-Stage Heat Pump: Experimental And Analytical Surveys.* Journal of the Less Common Metals, 1991. **172–174, Part 3**(0): p. 1092-1110.
28. Sun, D.-W., *Thermodynamic Analysis Of The Operation Of Two-Stage Metal-Hydride Heat Pumps.* Applied Energy, 1996. **54**(1): p. 29-47.
29. Spinner, B., et al., *New Cascades For Thermo-Chemical Refrigeration.* International Journal of Thermal Sciences, 2005. **44**(12): p. 1110-1114.
30. Li, T.X., et al., *A Conceptual Design And Performance Analysis Of A Triple-Effect Solid–Gas Thermochemical Sorption Refrigeration System With Internal Heat Recovery.* Chemical Engineering Science, 2009. **64**(14): p. 3376-3384.
31. Mauran, S., Bodiot, D., Crozat, G., *Optimisation Des Densités Énergétiques De Systèmes De Stockage Chimique Basés Sur Des Réactions Solide-Gaz Renversables.* Applied Physics Reviews, 1983. **18**(1983): p. 107-112.
32. Spinner, B., *Ammonia-Based Thermochemical Transformers.* Heat Recovery Systems and CHP, 1993. **13**(4): p. 301-307.
33. Rockenfeller, U., *Method And Apparatus For Achieving High Reaction Rates In Solid-Gas Reactor Systems*. 1995, Google Patents.
34. Meunier, F., *Theoretical Performances Of Solid Adsorbent Cascading Cycles Using The Zeolite-Water And Active Carbon-Methanol Pairs: Four Case Studies.* Journal of Heat Recovery Systems, 1986. **6**(6): p. 491-498.

35. Li, T.X., et al., *A Combined Double-Way Chemisorption Refrigeration Cycle Based On Adsorption And Resorption Processes.* International Journal of Refrigeration, 2009. **32**(1): p. 47-57.
36. Goetz, V., B. Spinner, and E. Lepinasse, *A Solid-Gas Thermochemical Cooling System Using Bacl2 And Nicl2.* Energy, 1997. **22**(1): p. 49-58.
37. Wang, R., Wang, L., Wu, J.,, *Adsorption Refrigeration Technology*. 2014, Singapore: Wiley.
38. Douss, N. and F. Meunier, *Experimental Study Of Cascading Adsorption Cycles.* Chemical Engineering Science, 1989. **44**(2): p. 225-235.
39. Rockenfeller, U., et al., *Advanced Heat Pump Staging For Complex Compound Chemisorption Systems*, In *Solid Soprtion Refrigeration*. 1992: Paris.
40. Meunier, F., *Second Law Analysis Of A Solid Adsorption Heat Pump Operating On Reversible Cascade Cycles: Application To The Zeolite-Water Pair.* Journal of Heat Recovery Systems, 1985. **5**(2): p. 133-141.
41. Li, X.H., et al., *A Review On Development Of Adsorption Cooling—Novel Beds And Advanced Cycles.* Energy Conversion and Management, 2015. **94**: p. 221-232.
42. Vasiliev, L.L., et al., *Resorption Heat Pump.* Applied Thermal Engineering, 2004. **24**(13): p. 1893-1903.
43. Vasiliev, L.L., Mishkinis, D.A., Antukh, A.A., Kulakov, A.G., Vasiliev Jr, L.L., *Resorption Heat Pump*, In *V Minsk International Seminar "Heat Pipes, Heat Pumps, Refrigerators"*. 2003: Minsk, Belarus. p. 450-459.
44. Shelton, S.V., W.J. Wepfer, and D.J. Miles, *Ramp Wave Analysis Of The Solid/Vapor Heat Pump.* Journal of Energy Resources Technology, 1990. **112**(1): p. 69-78.
45. Shelton, S.V., *Solid Adsorbent Heat Pump System*. 1986.
46. Rivero-Pacho, A.M., *Thermodynamic And Heat Transfer Analysis Of A Carbon – Ammonia Adsorption Heat Pump*, in *Engineering*. 2014, University of Warwick.
47. Jones, J.A., *Special Issue Solid Sorption Refrigeration And Heat Pumps Sorption Refrigeration Research at JPL/NASA.* Heat Recovery Systems and CHP, 1993. **13**(4): p. 363-371.

48. Critoph, R.E., *Forced Convection Enhancement Of Adsorption Cycles.* Heat Recovery Systems and CHP, 1994. **14**(4): p. 343-350.

Chapter 4 : The Large Temperature Jump Setup and Initial Tests Using Active Carbon

4.1 Introduction

There is a need to measure the performance of adsorbent materials. This is mostly done by measuring the quantity of refrigerant uptake or release and how long this process takes under certain conditions in order to understand the dynamics of the process. These measurements are vital because they directly affect the performance of adsorption machines. They can be performed through gravimetric, volumetric, calorimetric or chromatographic methods. Volumetric and gravimetric methods [1] are used to measure the adsorption rate while calorimetry [2] is used for thermodynamic studies of working pairs. The large temperature jump method is adopted for this work. It is a volumetric method that determines the changes in refrigerant content of an adsorbent using the pressure change in a vessel of known volume. The choice of the large temperature jump for this work is based on its simplicity and ability to replicate the isobaric stages of an adsorption cycle. The uptake of refrigerant on the sample is determined through changes in pressure within a known volume of gas. This is simpler compared to gravimetric methods where a sophisticated weighing cell is required to study the change in the weight of the sample. The possible limitation of taking such a simplistic approach is the potential for errors in the calculation of refrigerant uptake based on the pressure change in the system.

The underlying process here is depicted in Figure 4-1. It involves keeping a sorbent sample at an equilibrium temperature in a test cell, which is then followed by a large step temperature change though the sudden introduction of heat (Q). This induces the sorption process at constant volume and under quasi-isobaric pressure, allowing the emulation of points 2 to 3 (desorption) or points 4 to 1 (adsorption) of the ideal adsorption cycle which is shown in Figure 2-3 of Chapter 2. The simulations that match the experimental pressure rise most closely are those using the heat transfer parameters assumed to be closest to reality and may be used for modelling a full size system. Thus, large temperature jump experiments are a relatively easy means of understanding the behaviour of various adsorbents/beds before spending time and effort testing them in full size adsorption heat pumps. The analysis of data obtained

from large temperature jump experiments in this work was performed differently compared to what was done in literature. The large temperature jump data was analysed with the aim of obtaining certain heat transfer characteristics (thermal conductivity and heat transfer coefficient) of activated carbon samples. The distinction between this work and literature is explained in detail in sections 4.4.1 and 4.4.2

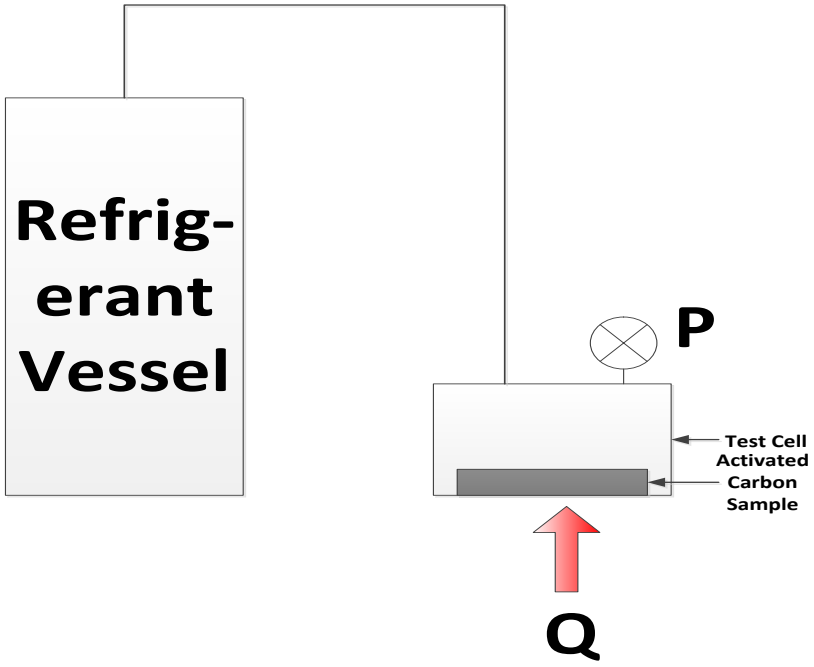

Figure 4-1: The concept of the large temperature jump setup

This chapter outlines the details of the large temperature rig used on this project. It also outlines the experimental procedure involved with large temperature jump testing and the first set of results obtained from the rig. These tests were conducted using active carbon as the sample and results were analysed with the aim of obtaining heat transfer parameters (k (thermal conductivity and h (heat transfer coefficient)) relating to the sample. The change in these heat transfer parameters with the bulk density of the active carbon sample was also investigated. The decision not to start experiments with salts at this point was based on the need to validate the designed rig. Active carbon is well researched and its behaviour is understood. Nevertheless, the work here is useful beyond the validation of the rig as it obtains more heat transfer information from large temperature jump tests which could ultimately help design better packed adsorbent beds for adsorption machines since poor heat transfer has been widely identified as one of the major problems in packed adsorbent beds [3, 4].

The approach presented in this work deduces one dimensional heat transfer characteristics of the bed by fitting a relatively simple numerical model to the measured pressure evolution over the sample while varying the thermal conductivity (k) and contact heat transfer coefficient (h) values. The heat transfer coefficient referred to in this work accounts for only convection and does not include any radiation effects. The k and h value combinations which produced the least root mean square error when compared to experimental measurement were taken as best fit. It is important to note that the approach presented here is only valid for cases where high pressure (1.4 - 2 bar) ammonia is used as adsorbate. In this Chapter, the temporal evolution of the pressure over the sample depends primarily on the heat transfer parameters (k and h) separated in this work and the influence of mass transfer resistance can be ignored. For a given cooling power, the gas velocities for ammonia are much lower compared to those of lower density gases such as water. Thus the pressure drop across the packed bed based on Ergun equation [5] is very low and the assumption of constant pressure throughout the bed is valid. Tamainot-Telto et al [6] also found that pressure drop across a monolithic carbon-ammonia generator bed is insignificant.

4.2 The Large Temperature Jump Rig

The rig setup can be divided into three parts for simplification. They are listed below.

1. The pressurised ammonia circuit- depicted in blue colour in Figure 4-2
2. Temperature control (Water heat exchanger loop and controlled isothermal container) - depicted in red colour in Figure 4-2
3. Instrumentation- depicted in green colour in Figure 4-2

The aforementioned parts of the rig all integrate to facilitate the operation of the large temperature jump rig, which is shown in Figure 4-2 and Figure 4-3. Their design and fabrication is described in subsequent sub sections.

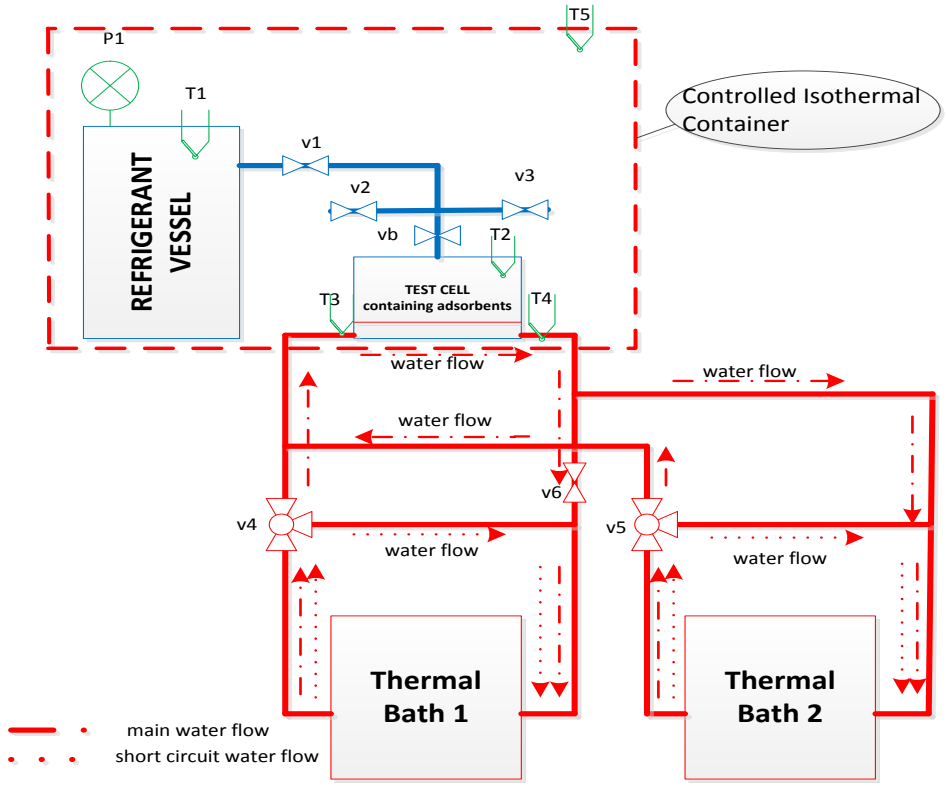

Figure 4-2: Colour coded schematic of large temperature jump rig

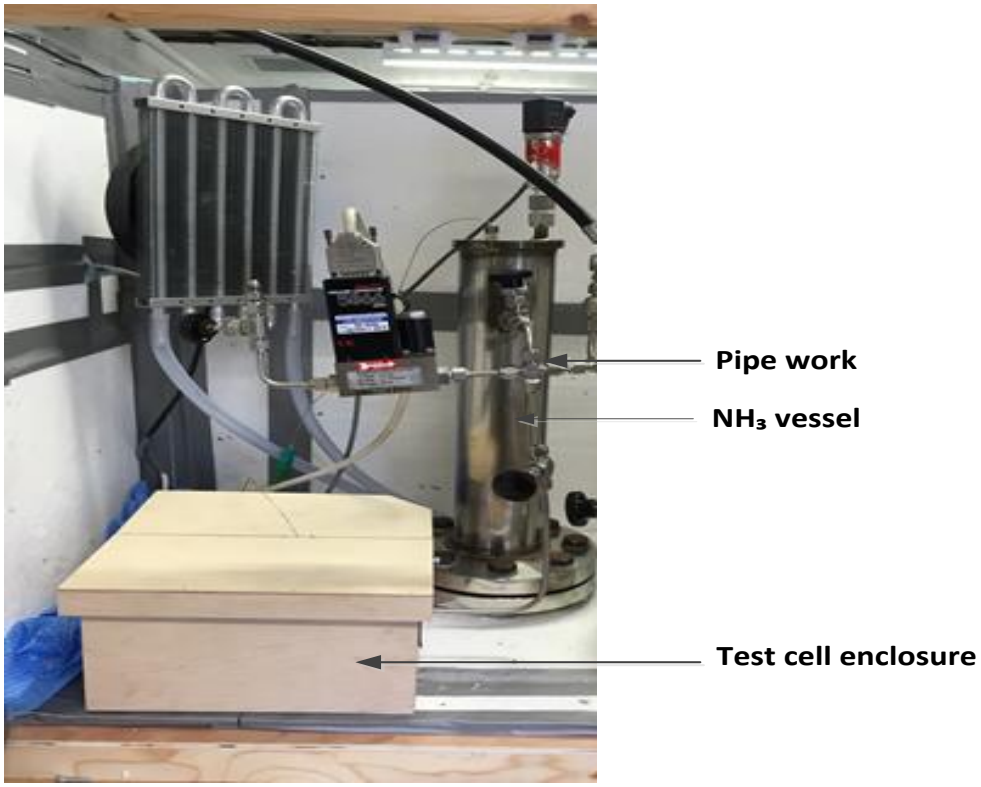

Figure 4-3: Picture of large temperature setup in isothermal container

4.2.1 Pressurised ammonia circuit

This is the part of the system where the pressure change in the known volume is monitored. It is made up of a gas vessel/reservoir, a test cell and a network of pipework to link the two and allow for vacuuming and introduction of refrigerant gas. The sub-sections below discuss these components of the pressurised ammonia circuit.

4.2.1.1 The Test Cell

The main use of the test cell is to hold the sample during tests, allow for free flow of refrigerant and the taking of temperature measurements of the gas it contains. The Solid Works 3D model of the test cell is shown in Figure 4-4. The Solid Works drawings can be found in Appendix 1 and Appendix 2 of this thesis. The test cell was designed in the form of a cylinder in order to be able to withstand higher pressures if they become necessary during experiments. It has a diameter of 80mm and a depth of 70mm, allowing for the testing of a wide range of sample sizes.

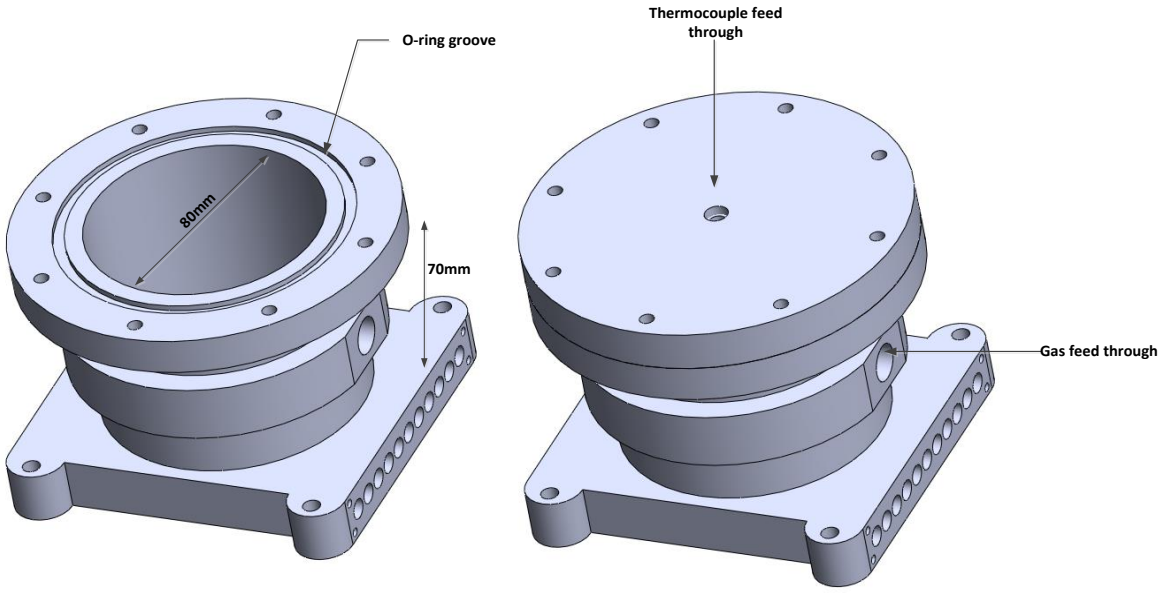

Figure 4-4: Solid Works 3D Model of the test cell and cover

The test cell features a hole on the side for refrigerant gas access. This access hole is supplied by ¼" Swagelok pipework. The test cell is covered on top as shown in Figure 4-4. The cover features a feed-through for a thermocouple in its middle and 8 holes through which it is fastened to the test cell by means of 6mm screws. Nitrile rubber O-rings that are in line with BS4518 were used to keep the test cell leak proof.

The test cell was fabricated in the University of Warwick School of Engineering workshops. Aluminium 6082 was used in the fabrication due to its ease of machining, compatibility with ammonia and high thermal conductivity compared to stainless steel. However, the choice of Aluminium is not without its drawbacks as stainless steel is mechanically stronger than Aluminium. Therefore adequate analysis was essential in order to ascertain the mechanical integrity of this test cell design with regards to the experiments to be carried out.

This analysis was approached from two perspectives. First, by considering stresses in the test cell as a result of its cylindrical shape and second by considering the stresses in the bolts joining the test cell to its cover. The cell was designed with a wall thickness of 5mm. Therefore considering hoop stress in the cylinder, the maximum amount of pressure that can be present in the pressure vessel (test cell) is given by Equation (4.1)

$$P_{\max} = \frac{2\sigma_{yield}\delta}{d_{in}} \tag{4.1}$$

Based on a yield stress (σ_{yield}) of 250MPa, an inner diameter (d) of 80mm and a wall thickness (δ) of 5mm, the maximum pressure ($P_{\max}$) is 312.5bar. The maximum pressure in the experiment will not go beyond 30 bar and this indicates a factor of safety of 10 at worst with regards to the hoop stress.

A tension loaded connection consisting of eight M8 screws was used between the test cell and the cover. The holes in the cover were unthreaded while the holes in the test cell were threaded. The schematic of the cross section of one of the fully loaded connections is shown in Figure 4-5.

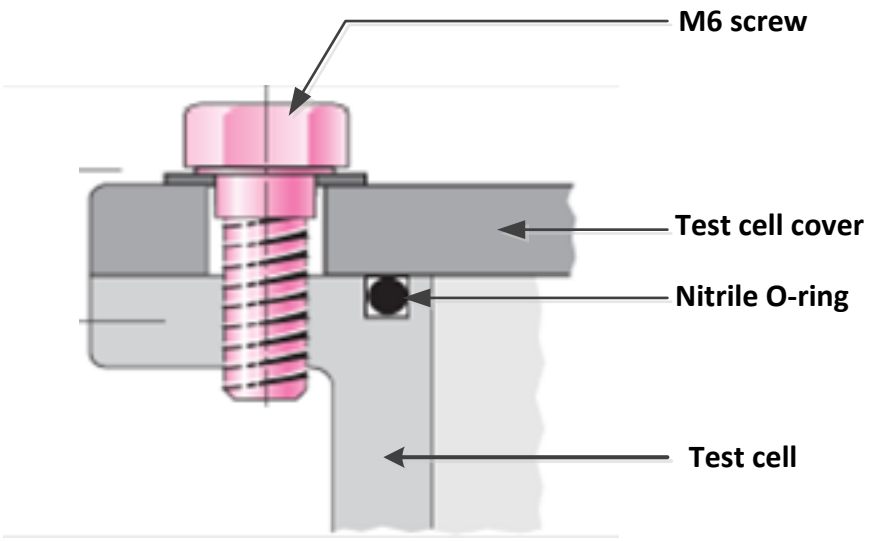

Figure 4-5: Sample sectional view of a fully loaded test cell-cover connection [7]

The tensile load per bolt used is calculated based on the pressure in the cylinder. The pressure in the cylinder is exerted on the end plates and it is reacted to equally by the eight restraining bolts on the test cell. Therefore, the load, F_b on each bolt is therefore given by Equation (4.2).

$$F_b = \frac{P(\pi r_b^{\,2})}{8} \tag{4.2}$$

The stiffness constant, C of the joint is calculated from the spring rate of the bolt (kc_b) and that of the test cell (kc_{tc}) as in Equation (4.3)

$$C = \frac{kc_b}{kc_b + kc_{tc}} \tag{4.3}$$

Table 4-1 below presents various pressure scenarios and their corresponding factors of safety, following the same procedure used by Budynas et al in [7]. The two most important columns in Table 4-1 are the fifth and sixth columns. They show the factors of safety against two failure modes which was considered. The traditional factor of safety (f_p) is worked out in the fifth column of Table 4-1. This is a ratio of the maximum bolt stress to the proof strength of the bolt. The sixth column shows the factor of safety (f_s) against separation of the joint. This guards against failure which may occur due to excessive force from the pressure causing the joint to separate and

the bolt to bear the entire load. The formula for both factors of safety are given by Equation (4.4) and Equation (4.5) respectively. The tensile stress area of the screw used was A_b =20.1mm² and the minimum proof stress was σ_p =310MPa.

$$f_p = \frac{\sigma_p A_b}{CP + F_b} \tag{4.4}$$

$$f_s = \frac{F_b}{P(1-C)} \tag{4.5}$$

Table 4-1: Factors of safety for test cell (modelled after Budynas et al [7])

P (bar)	Load per Bolt, F_b (kN)	Pre-Load, (kN)	SC of joint, C	F.O.S.p.s, fp	F.O.S.s, fs
5	0.314	4.83	0.18	1.28	18.76
10	0.628	4.83	0.18	1.26	9.38
15	0.942	4.83	0.18	1.25	6.25
20	1.256	4.83	0.18	1.23	4.69
25	1.57	4.83	0.18	1.22	3.75
30	1.884	4.83	0.18	1.21	3.13

The Pre-Load was calculated as shown in Equation (4.6) using 85% of the yield stress of the bolt.

$$\text{Pre-Load} = 0.75 A_{bolt}\, 0.85 \sigma_{yield} \tag{4.6}$$

4.2.1.2 Gas Vessel and Ammonia Pipework

The gas vessel (shown in Figure 4-6) which was used was not designed originally for this project but was an existing vessel used on a previous project. It was pressure tested up to 20 bar when it was initially made. It wasn't important in this work to carry out further pressure tests on the vessel because the working pressure here does not exceed 10bar. However, higher pressure tests will be required if pressures higher than 20bar are to be used in the vessel in the future.

The gas pipework was built with ¼" high pressure Swagelok stainless steel tubes. The total internal volume of pipework was estimated to be 1.095e-6 m³ based on the bore of the Swagelock pipes. The total volume of the gas vessel is 2.543e-3 m³. This was obtained from density calculations after filling it with water and weighing it.

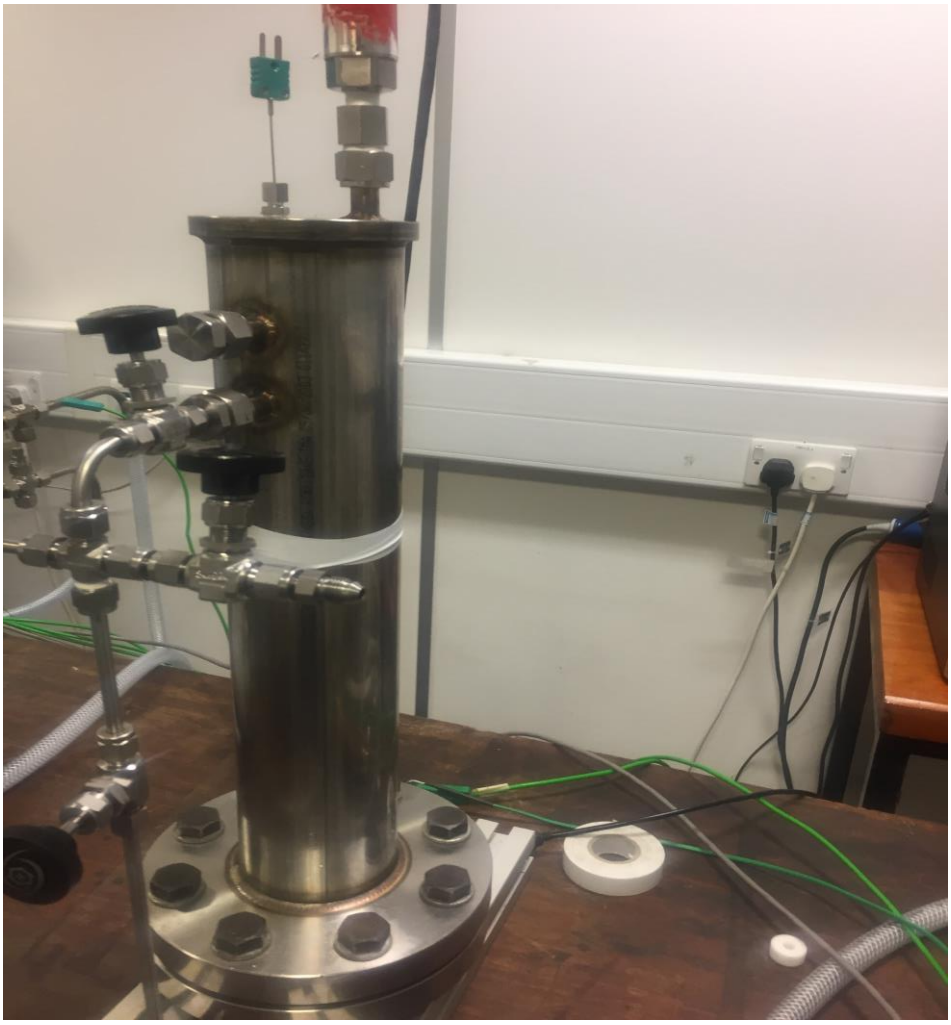

Figure 4-6: Ammonia gas vessel and pipework

The whole gas system was tested for leaks using two processes. First by connecting the system to a source of compressed air at 7 bar and using soap lather to test the potential leak sources. Second, by charging/filling the system with compressed air and observing the pressure reading from the system over a period of time for any change. As a last measure, the charged system may be dipped into a pool of water, any leaks would lead to the formation of bubbles.

4.2.2 Temperature Control

4.2.2.1 Water Heat Exchanger Loop

Two thermal circulating baths (Huber Unichiller OLE 012w and Huber Ministat 240 (datasheets provided in Appendix 3 and Appendix 4)) were used to provide the temperature jump required in the test cell. The thermal baths have the capacity to maintain the heat transfer fluid that goes through the test cell at a desired temperature.

Two heat transfer fluids (distilled water and Silicone oil) were used to supply the test cell depending on required temperatures. The heat transfer fluid was conveyed to the test cell by a network of copper tubes and PVC hoses as seen in Figure 4-7 for lower temperature experiments. For high temperature salts tests, the PVC hoses and copper tubes were replaced with Swagelok tubes as shown in Figure 4-8.

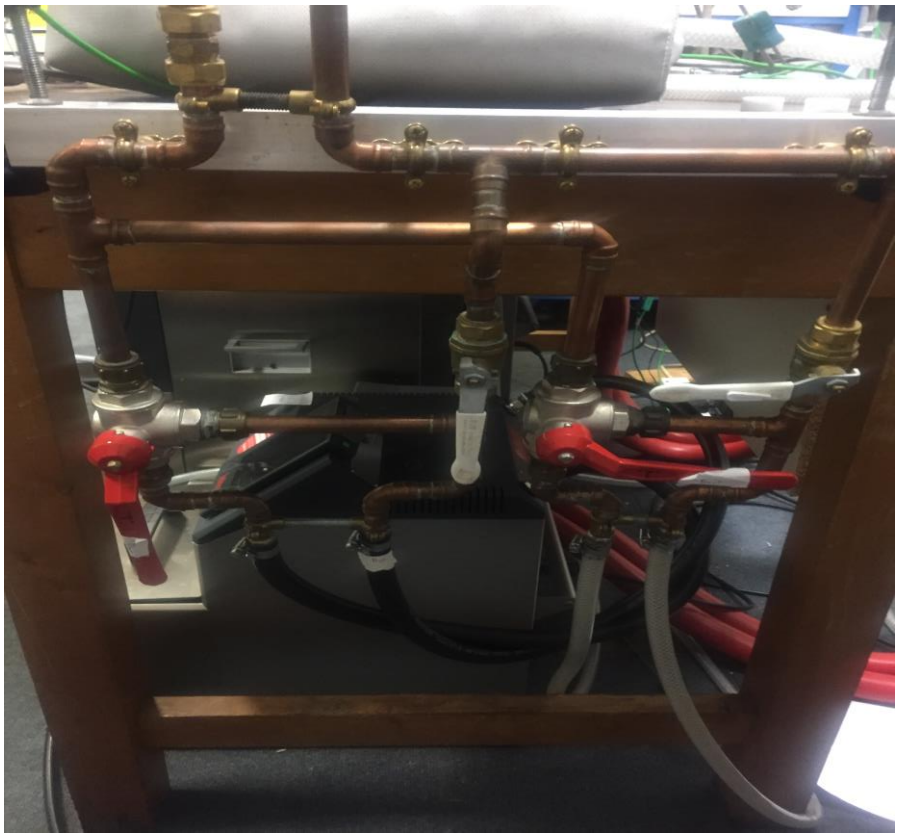

Figure 4-7: Copper tubes and PVC hoses

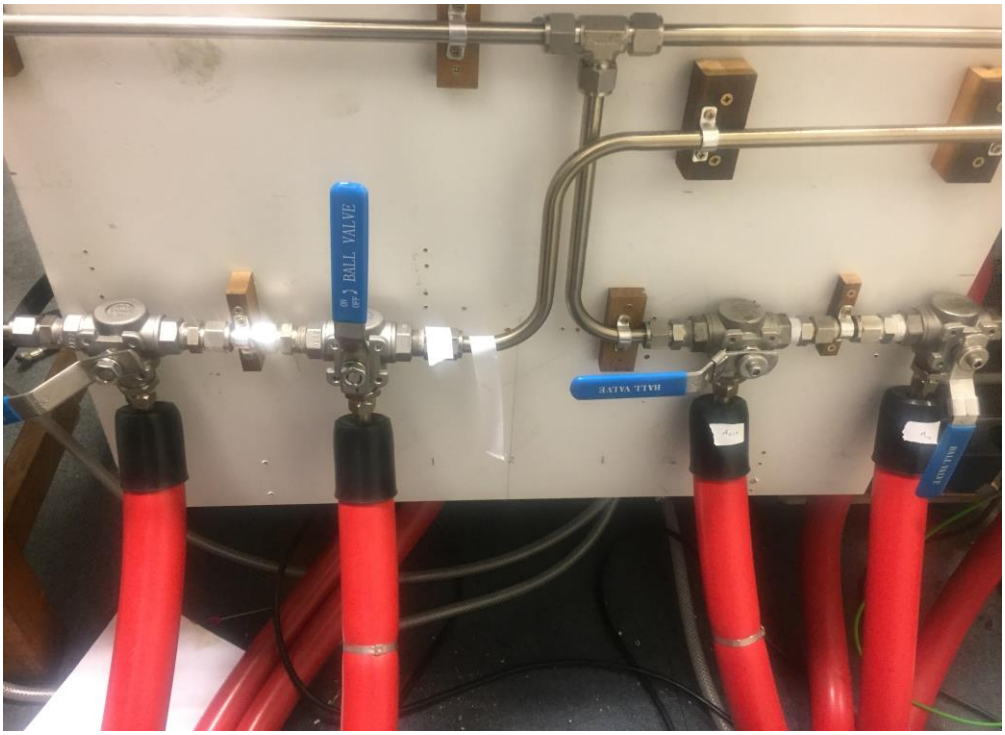

Figure 4-8: Swagelok tubes

The heat was transmitted to the sample through a heat exchanger in form of eleven holes which are drilled underneath the test cell. The holes form part of the heat exchange circuit, the heat transfer fluid is conveyed to the test cell through one end of the test cell and out the other end back to the circulating baths. A view of the heat exchanger holes is shown in Figure 4-9. Each of the channels is 7mm in diameter and 120mm long. The diameter and length of the holes were carefully chosen based on the flow rates of the circulating baths so that an adequate heat transfer fluid flow rate was obtained.

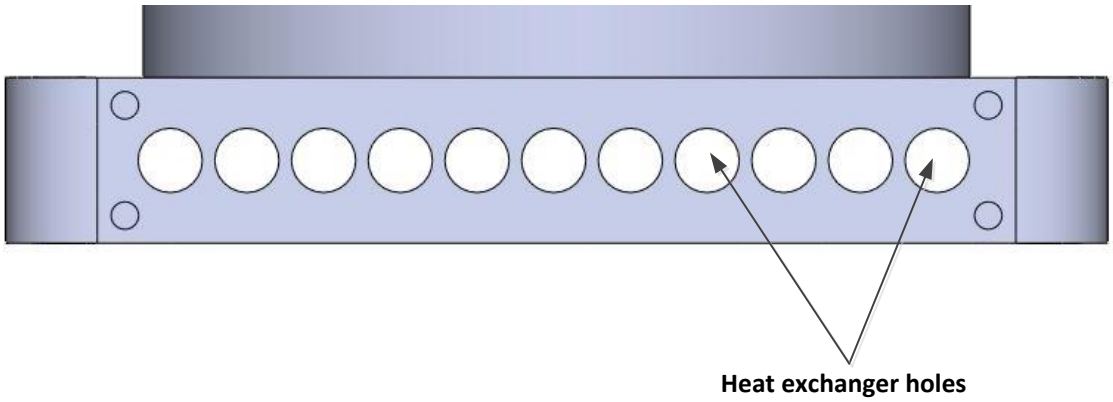

Figure 4-9: View of test cell showing the heat exchanger holes drilled beneath

The inner base of the test cell would be inaccessible for temperature measurements during experiments. Therefore, the transient heat transfer from the heat transfer fluid to the testcell base must be modelled in order provide a necessary boundary condition in the subsequent modelling of heat transfer through the sample. Essentially, the transient change in temperature of the test cell inner base with the heat transfer fluid is studied by considering heat transfer fluid flow through one of the 11 channels passing through the test cell as shown in Figure 4-10.

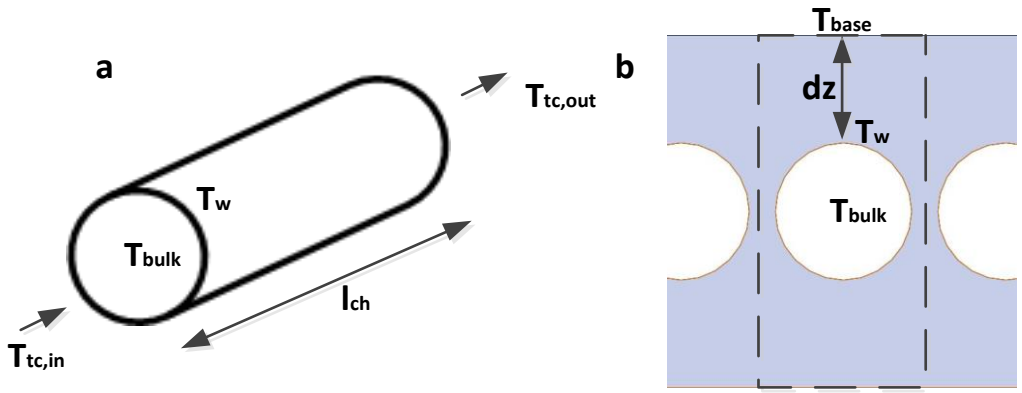

Figure 4-10: Flow through one of the channels. a) Longitudinal view of one channel b) Cross-sectional view of one channel in test cell base

It is important to ascertain what type of flow is present in order to select an appropriate analysis approach. This is done by obtaining the Reynolds number based on the volumetric flow rate of the thermal bath used. Reynolds number is given by Equation (4.7).

$$\mathrm{Re} = \frac{\dot{\psi} D_{tube}}{v_{htf} A_{tube}} \tag{4.7}$$

The volumetric flow rate ($\dot{\psi}$) of the flow in one channel is obtained by carrying out a mass conservation between the thermal baths and the 11 channels involved. Based on preliminary Reynold's number calculations, the flow is always turbulent for both heat transfer fluids (water and Silicone oil) used. Therefore, the following technique is used as described by Holman in [8].

$$\dot{Q} = \dot{m} C_p (T_{tc,out} - T_{tc,in}) = h_{htf} (\pi d_{ch} l_{ch})(T_w - T_{bulk}) \tag{4.8}$$

h_{htf} , the heat transfer coefficient of the heat transfer fluid can be found from the relevant heat transfer correlation shown below in Equation (4.9). T_{bulk} is an average value of the $T_{tc,out}$ and $T_{tc,in}$.

$$Nu = 0.023 \mathrm{Re}_d^{0.8} \mathrm{Pr}^{no} = \frac{h_{htf} l_{ch}}{k_{htf}} \tag{4.9}$$

$$\mathrm{Pr} = \frac{C_{phtf} \mu_{htf}}{k_{htf}} \tag{4.10}$$

In Equation(4.9), no is 0.4 for heating and 0.3 for cooling. Using the temperature of the tube wall, T_w , the temperature of the base of the test cell can be obtained. The mode of heat transfer between the tube wall and the internal base of the test cell is considered to be purely conduction. The effect of the curved nature of the T_w profile was accounted for by considering the shape factor of a cylinder in a square. The shape factor for such configuration is given by Equation (4.11) and the temperature of the base of the test cell can be obtained through Equation (4.12). Figure 4-11 shows a plot of modelled temperature based on the two different heat transfer fluids used against measured test cell base temperature. The difference between the measured and modelled test cell base temperature for the two heat transfer fluids was not significant and their profiles closely match. This means that the test cell base temperature can be modelled accurately despite being physically difficult to assess during actual large temperature jump experiments.

$$Sa = \frac{2\pi l_{ch}}{\ln\left(0.54 \delta_z / r_{ch}\right)} \tag{4.11}$$

$$\dot{Q} = -k_{aluminium} Sa (T_{base} - T_w) \tag{4.12}$$

Sa represents the shape factor of the channel within an assumed rectangular block, It has a value of 0.74m in this case. l_{ch} is the length of one channel, δ_z is the distance between the perpendicular distance between the topmost part of the channel and the test cell base. r_{ch} is the radius of a channel while $k_{aluminium}$ and T_w are thermal conductivity of the block and the temperature of the channel wall respectively. This approach is based on the following assumptions.

- The temperature of the base of the test cell, T_{base} is uniform across the entire test cell.

- There is no heat loss to the test cell walls.
- The shape of the sample has no influence on temperature profile.

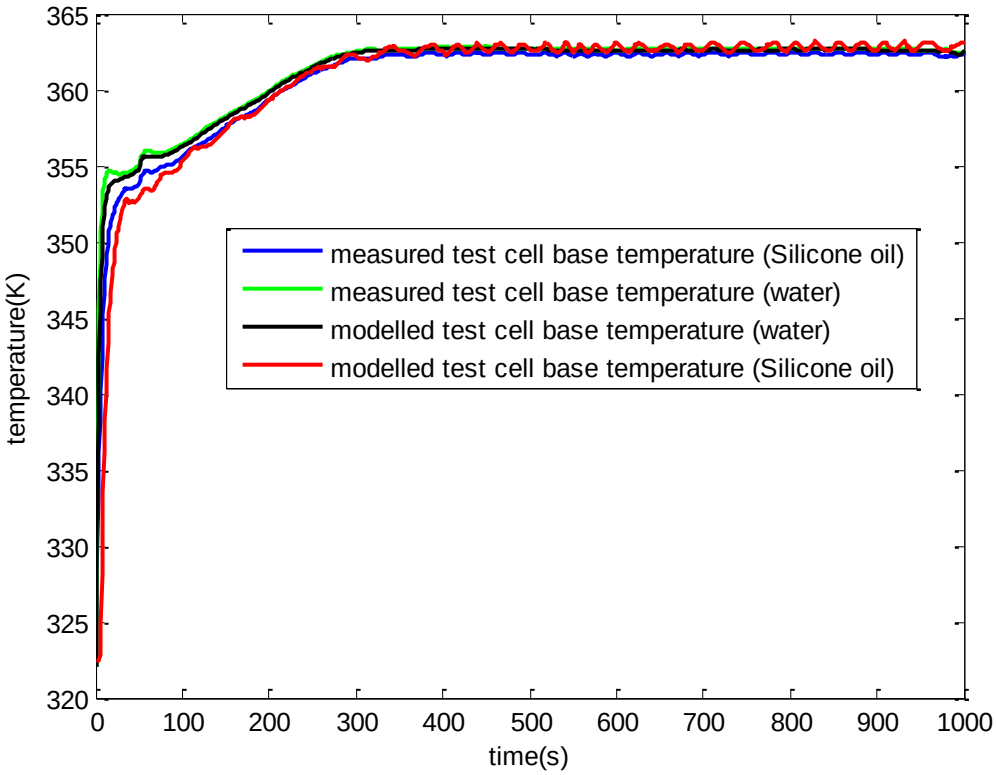

Figure 4-11: Plot of measured test cell base temperature against modelled test cell base temperature for water and silicon oil

4.2.2.2 Controlled Isothermal Container

The components that make up the gas network reside in a temperature controlled environment as fluctuations in ambient temperature could affect gas pressure measurements. To this end, two polystyrene insulation boxes were constructed. The bigger box shown in Figure 4-3 is used to control the temperature around the gas vessel so that the gas vessel temperature is protected from any external influences during experiments. Desired ambient temperatures in this bigger insulation box were attained by the use of a fan-coil system (also shown in Figure 4-3) which is supplied with heat transfer fluid (water) by a Julabo HE 4 (data sheet in Appendix 5) thermal circulating bath.

The second insulation box covers the test cell and helps to separate the test cell from the rest of the bigger box during temperature jumps so that heat from the test cell is

kept local and not dissipated to the gas vessel adversely affecting pressure measurements. This smaller box is shown in Figure 4-12.

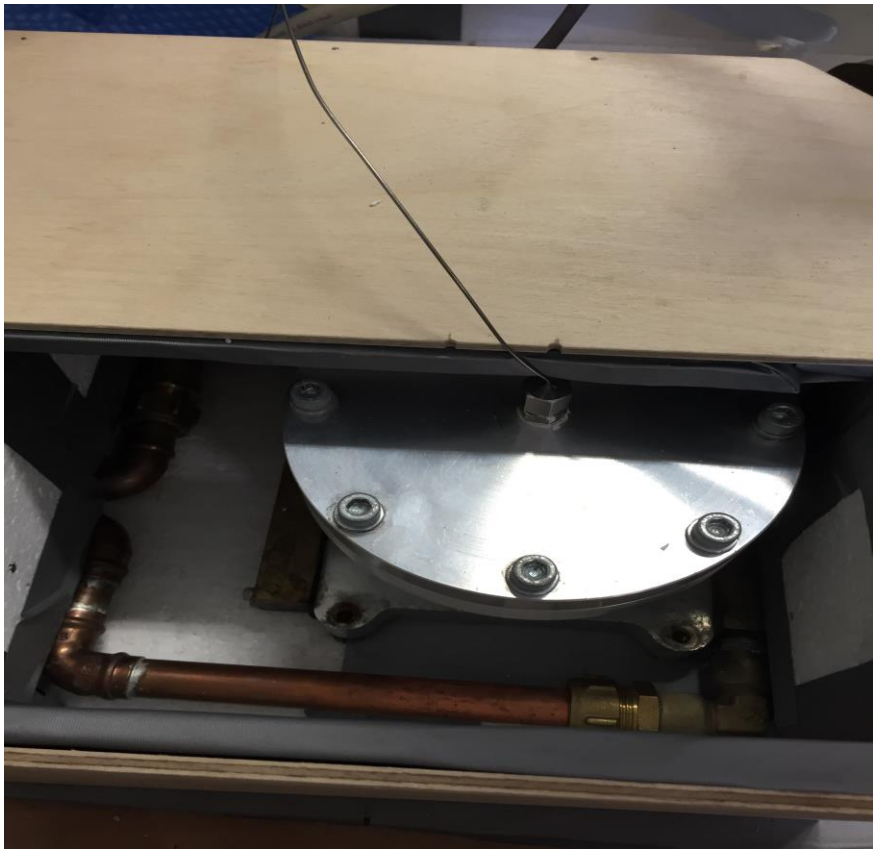

Figure 4-12: Test cell in smaller insulation box

4.2.3 Instrumentation and Control

4.2.3.1 Temperature

4.2.3.1.1 Thermocouples

Temperature measurements were taken at five points in the rig. These five points are shown in Figure 4-2 as T1, T2, T3, T4 and T5. The thermocouples used were 1mm Type K stainless steel sheathed thermocouples from TC Direct Limited. The uncertainty in their measurements was determined by bonding three thermocouples of the same specification up with a platinum resistance thermometer (PRT) and dipping them in thermal circulating baths at varying temperatures (4°C -70°C). Table 4-2 shows the results from the readings from all the thermocouples during this process. The maximum deviation (1.2°C) of the thermocouple readings compared to readings from the platinum resistance thermometer was taken as their uncertainty.

Table 4-2: Readings from the determination of uncertainty of thermocouples

PRT reading (°C)	4.70	9.75	14.85	19.90	24.93	30.04	35.00	40.00	44.96	49.99	55.00	59.87	64.99	69.90
Themocouple 1 Reading (°C)	5.73	10.53	15.42	20.24	25.13	30.11	34.88	39.74	44.63	49.54	54.31	59.32	64.20	69.05
Themocouple 2 Reading (°C)	5.90	10.70	15.65	20.52	25.36	30.31	35.15	39.74	44.87	49.73	54.66	59.55	64.45	69.38
Themocouple 3 Reading (°C)	5.80	10.60	15.40	20.32	25.20	30.09	34.86	39.82	44.65	49.50	54.40	59.24	64.21	69.06
Maximum Deviation (°C)	1.20	0.95	0.80	0.62	0.43	0.27	0.15	0.26	0.33	0.26	0.69	0.63	0.79	0.85

4.2.3.1.2 Thermal Circulating Baths

Three thermal circulating baths (Huber Ministat 240cc, Huber Unichiller OLE 012w, Julabo HE-4) feature in the large temperature jump rig and they supply heating or cooling to the test cell and the controlled isothermal container. The data sheets for the circulating baths are in Appendix 3, Appendix 4 and Appendix 5.

4.2.3.2 Pressure

The gas vessel was fitted with a gas pressure transducer (P1 in Figure 4-2) to monitor pressure change in the pressurised ammonia circuit. The pressure transducer used was a Danfoss pressure transmitter of type AKS32 (full data sheet in Appendix 6). Some of the specifications of the pressure transducer are given in Table 4-3 below.

Table 4-3: Technical details of pressure transducer

Parameter	Value
Manufacturer	Danfoss
Model	AK 32 060G2080
Pressure Range	0-40 bar
Accuracy	±0.32 %
Output Signal	0-10V

The transducer was connected to a 15V power source supplied by University of Warwick School of Engineering Electronics Store. Even though the pressure transducer was calibrated from the manufacturer and an accuracy of ±0.32% is given in the data sheet, a dead weight tester was used to ensure accuracy of the pressure measurements. Dead weight testers (shown in Figure 4-13) use known weights to apply pressure to a fluid for checking the accuracy of the readings from the pressure transducer. This level of certainty is needed as the validity of the large temperature jump method depends largely on measurements of pressure change.

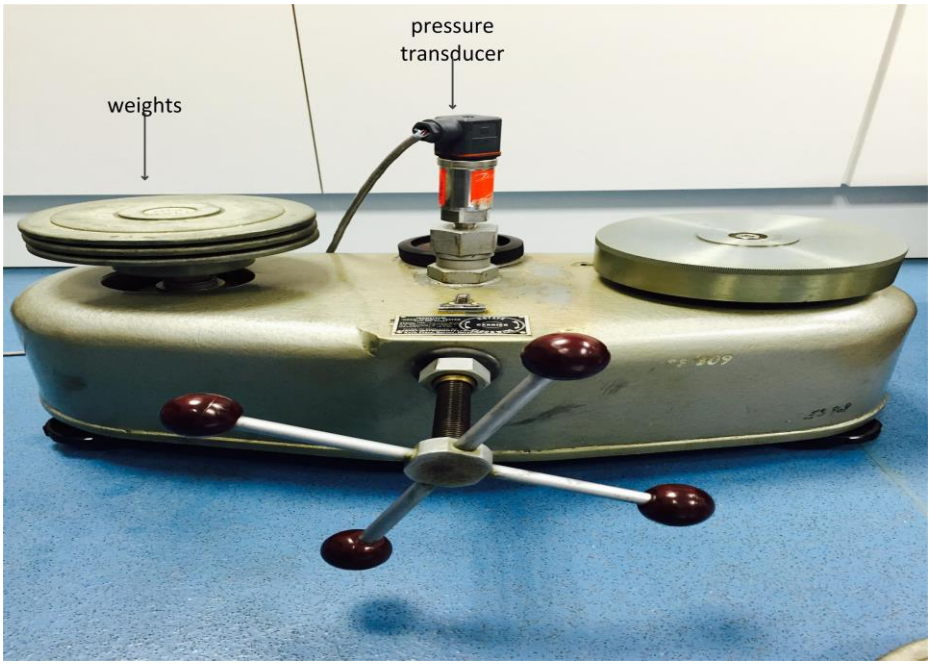

Figure 4-13: Checking the accuracy of the pressure transducer against a dead weight tester

In essence, the dead weight tester is a primary standard because it uses a known quantity, which is the weight of the masses to define the pressure of its fluid. The dead weight tester experiment showed that pressure transducer was reasonably accurate with a maximum deviation of 0.009 bar over the desired pressure range. Table 4-4 shows the deviation over all the pressure tested.

Table 4-4: Readings from pressure transducer and dead weight tester

Dead weight pressure (bar)	0.999	2.499	3.999	5.499	6.999	8.498	9.998	11.498
Pressure transducer (bar)	0.998	2.490	3.996	5.499	7.000	8.495	9.992	11.498
Deviation (bar)	0.001	0.009	0.003	0.000	0.001	0.003	0.006	0.000

4.2.3.3 Data Acquisition

All the measurement data (signals) from the pressure transducer and thermocouples were logged through an Omega OMB-DAQ-2408-2AO 8-Channel temperature/voltage input USB data acquisition system. This analogue to digital converter has a 24 bit resolution.

4.3 Experimental Procedure

4.3.1 Characterisation of Activated Carbon

Activated Carbon is a good adsorbent because of its highly porous surface. They are typically used for water treatment, industrial purification and protection against toxic gases. There are various types of activated carbon on sale commercially, the choice for this project was granular activated 208C carbon with a mesh (grain) size of 12 by 30 supplied by Chemviron Carbon. Usually, adsorption heat pumps are designed using off-the-shelf adsorbents. However, Tamainot-Telto [9] recently proposed a detailed methodology for obtaining optimum specifications of adsorbents for heat pump and refrigeration applications. These specifications may serve as a means of customising adsorbents in the future.

A Rubotherm magnetic suspension balance was used to characterise the porosity of the specific activated carbon sample used, and the following was obtained for the plot of concentration (χ) vs T/T_{sat}.

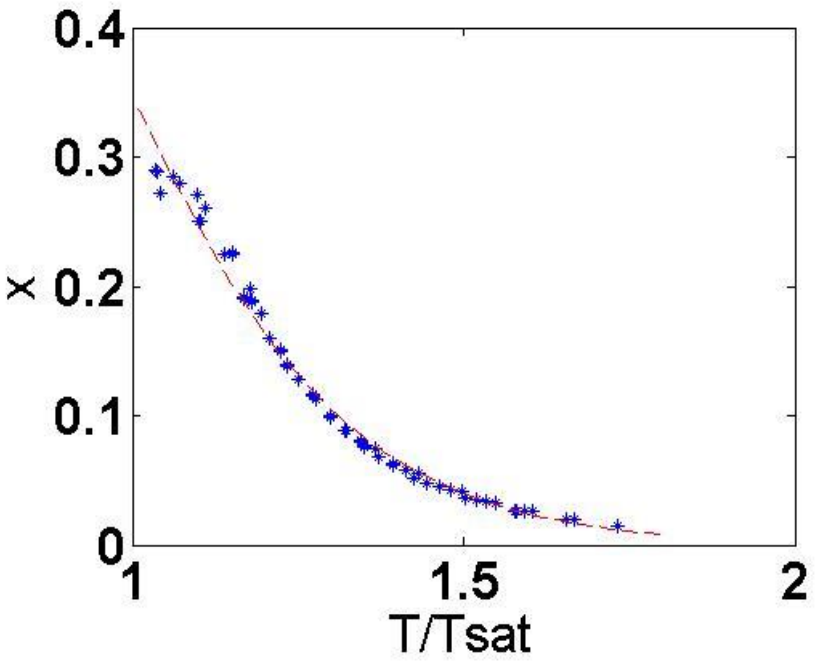

Figure 4-14: Plot of concentration (x) vs T/Tsat for the adsorbent used

As seen in Figure 4-14 above, the data has a poorer fit towards the left hand side of the graph. This is due to the presence of capillary condensation as the sample approaches saturation [10]. Capillary condensation is a phenomenon in which the

pores of the sample are filled with condensed gas since condensation occurs below the saturation vapour pressure due to the pressure exerted by the meniscus between the liquid-vapour interfaces. Therefore, it is important to operate within the area of good curve fit with regards to the large temperature jump experiments. The values of the Dubinin Astakhov equation constants ($x_{\max}$, K and n) obtained from the characterisation were 0.3431, 4.4854 and 1.17 respectively. These constants were applied in the modified Dubinin Astakhov equation (Equation(4.13)) to obtain the adsorbate concentration in the adsorbent.

$$x = x_{\max} \exp(-K(\frac{T}{T_{sat}} - 1)^{\varsigma}) \tag{4.13}$$

This form of the Dubinin Astakhov equation is obtained from the original form by making a direct comparison between the adsorbed phase and a saturated liquid at the same temperature [11].

4.3.2 Large Temperature Jump Testing

The layout of the apparatus is shown in Figure 4-2. First, the adsorbent is placed in an oven for 24 hours at 150◦C to remove all the moisture content of the adsorbent that may interfere with its adsorptive properties. Once the adsorbent is dried, it is quickly moved into the test cell. Once within the test cell, a vacuum pump is connected at V3 to evacuate the system for 5 hours. After this, V3 is shut and the system is filled with ammonia through V2. When pressurizing the large temperature jump system, it is important to add the correct mass of refrigerant (in this case ammonia) to stay within the reliable working range of the Dubinin Astakhov relation.

Once the sample adsorbent is in place and the system is filled with ammonia, water is run from thermal bath 1 at 40◦C through the heat exchanger circuit to the test cell containing the adsorbent material (active carbon) for 5 hours in order to reach equilibrium. This is achieved by setting three-way valve, V4 such that water flow is directed towards the test cell and opening valve V6 to allow for a circulation of the water.

Simultaneously, thermal bath 2 powers a short circuit through three-way valve V5 in order to prepare water needed for the temperature jump to 70◦C without interfering with the equilibrium in the pressurised ammonia system. Subsequently, valves V4 and

V6 are closed and V5 is directed towards the test cell. This process facilitates the temperature jump by switching the heat transfer fluid (water) supply from one bath to the other.

There was no assessment of possible pressure differences between the two vessel. The temperature (T3) of the water was taken at 1 second intervals using a type K thermocouple. The same is done with the ammonia gas at T1 and T2 while a Danfoss AKS32 pressure transmitter was used to measure the pressure change in the system at P1. All of the data is logged by an Omega OMB-DAQ-2408-2AO 8-Channel temperature/voltage input USB data acquisition system throughout the duration of the experiments. The entire duration of each experiment was 3000 seconds which was adequate to reach sorption equilibrium. However, the analysis of the experimental data focused on the first 500s of the experiment as this timescale is representative of the cycle duration in a real AHP. Table 4-6 gives further the details on these experimental results and results of analysis. A sample pressure plot result for the large temperature jump test is shown in Figure 4-15.

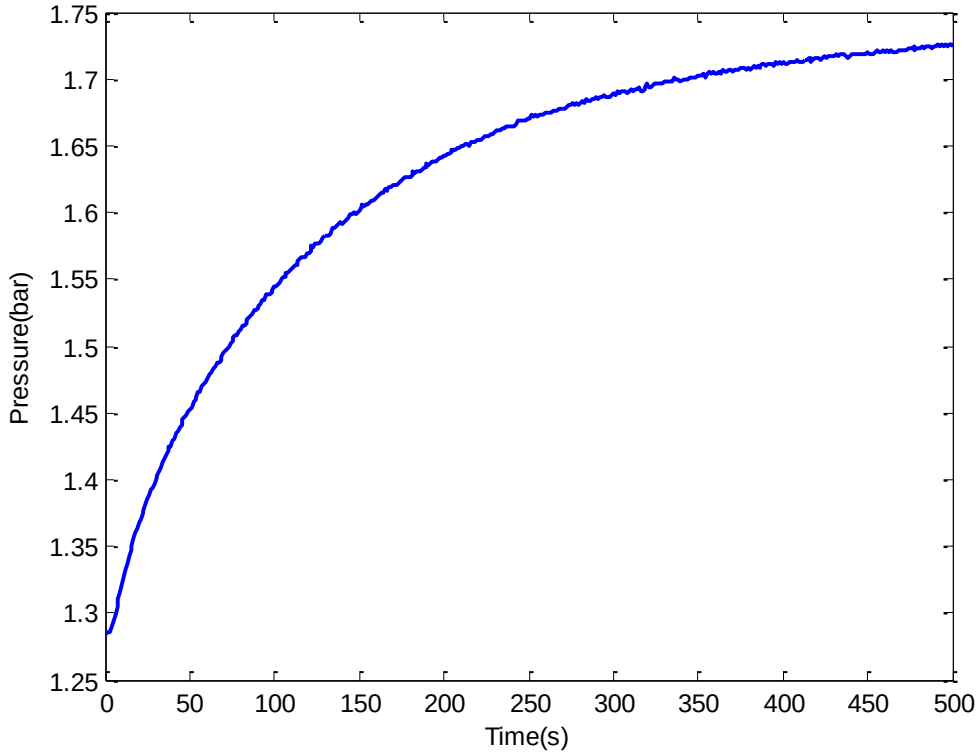

Figure 4-15: Sample result for a large temperature jump test

4.3.3 Variable Density Testing

The adsorbent was compressed in order to investigate the effect of varying packing densities on the heat transfer properties. The compression was achieved with a compression testing machine as shown in Figure 4-16. The 650 $kg.m^{-3}$ test which required a compressive force of 19.3 kN was done in a displacement control mode of 1mm/min while the 705$kg.m^{-3}$ test was done on load control mode at 40$kN.min^{-1}$ with a load of 330 kN. The other densities were obtained by merely pouring the sample loosely into the test cell. The four combinations of bed thickness and density tested are shown in Table 4-6.

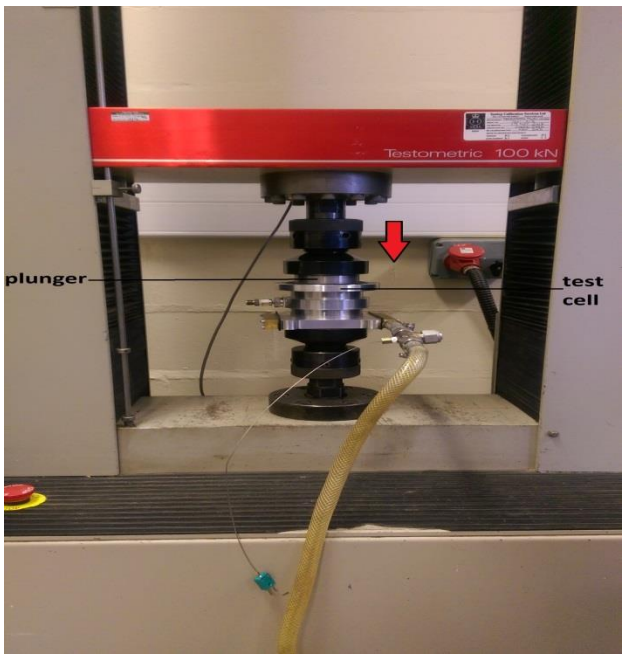

Figure 4-16: Adsorbent being compressed

4.4 Analysis

4.4.1 Standard Extraction of Heat Transfer Parameters from Large Temperature Jump Data

The linear driving force (LDF) model has been used extensively to describe large temperature jump data. The original linear driving force model is described by Glueckauf in [12] for the description of adsorption in chromatographic columns. Glueckauf found that the simple form of the linear driving force sufficiently described the studied process. In essence, it is a generally acceptable form of analysis of large temperature jump data because it is simple and it is based on the repeated averaging

of the base kinetic characteristics [13]. This simple linear driving force model is the basis for the analysis in [4, 14-17]. It is shown below.

$$\frac{dx}{dt} = \vartheta(x_{eq} - x_i) \tag{4.14}$$

Aristov et al [14] describes ϑ as a rate constant which does not change during the process of a temperature jump. This rate constant can be evaluated as $\vartheta = 1/\tau$ and τ is the characteristic time of the experiment. The driving force is the difference between the equilibrium concentration (x_{eq}) of refrigerant and the concentration (x_i) at the current time. From Equation (4.14) above, the following Equation (4.15) can be derived.

$$\frac{x_i - x_0}{x_{eq} - x_0} = (1 - \exp(t/\tau)) \tag{4.15}$$

The left hand side of the expression is the normalised, dimensionless uptake of refrigerant. According to Aristov et al in [14], this makes it more convenient to compare results for adsorption and desorption. Veselovskaya et al in [15] obtained an overall heat transfer coefficient (shown in Equation (4.16)) parameter making use of the aforementioned characteristic time (τ).

$$\alpha_{standard} = \frac{m_a((c_{p,a} + xc_{p,a})dT - Hdx)}{A \times DTD_{\max} \times \tau} \tag{4.16}$$

The equation above obtains an overall heat transfer parameter, $\alpha_{standard}$ which is a combination of the heat transfer coefficient (h) and the thermal conductivity (k) of the adsorbent. The time constant (τ) is obtained by fitting the normalised uptake measured data to the exponential expression in Equation (4.15). A sample fit for Run 1 of this work is shown below in Figure 4-17.

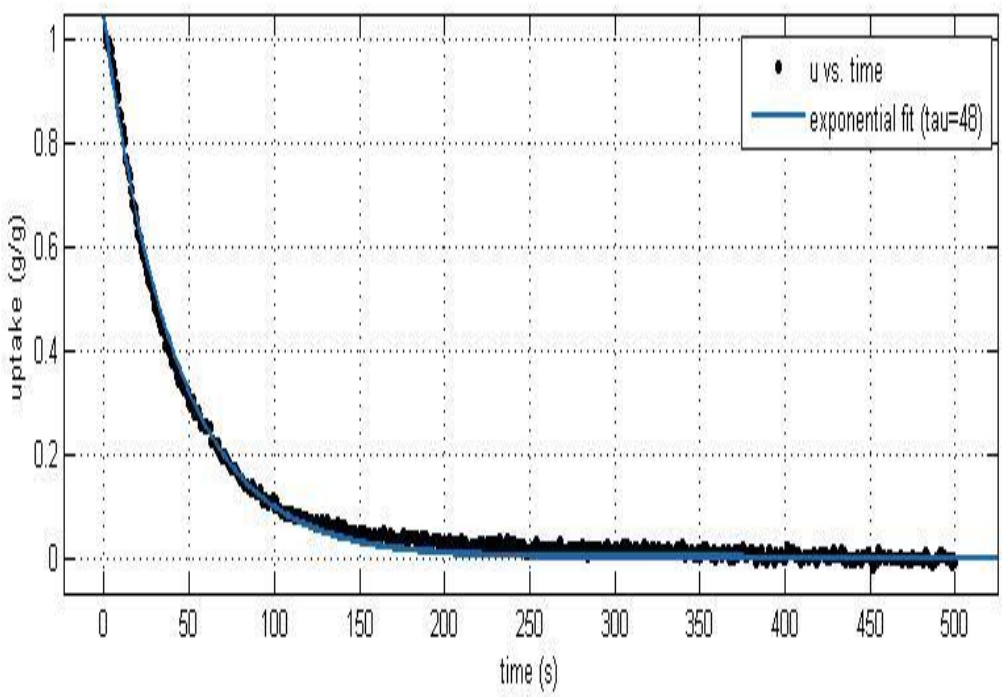

Figure 4-17: Modelling of Run 1 LTJ data using method in [14-16]

4.4.2 Separation of Heat Transfer Parameters in Large Temperature Jump Data

The technique used in this work to analyse large temperature jump data separates the k and h terms, treating them as distinct properties. It involves explicit discretisation of the adsorbent as shown in Figure 4-18. The model is run using a range of k and h values, then the combination that results in the least root mean square error (RMSE) between the experimental pressure and simulated pressure is selected as best fit.

The adsorbent bed is divided into discrete domains (Figure 4-18) and an inbuilt Matlab function, "fzero" is used to find the increase in saturation temperature (T_{sat}) value that satisfies the condition that the total mass of ammonia in the system is constant upon every time index of the experiment. The total mass of gas in the system can be expressed as shown in Equation (4.17).

$$m_{NH_3(sys)} = m_{NH_3(tc,pw\&bv)} + m_{NH_3(ads)} \tag{4.17}$$

The analysis for a time i is done using temperature and pressure conditions from the previous time step i-1. The mass of gas in the test cell, pipework and buffer volume ($m_{NH_3(tc,pw\&bv)}$) is determined through the ideal gas equation as seen in Equation (4.18). The adsorbed mass of gas ($m_{NH_3(ads)}$) is determined from the concentration (X) obtained with Equation (4.19)) and the mass of adsorbent.

$$m_{NH_3(tc,pw\&bv)i} = \frac{P_{i\text{-}1}V_{tc}}{R_{NH_3}T_{tc}} + \frac{P_{i\text{-}1}(V_{bv}+V_{pw})}{R_{NH_3}T_{bv}} \tag{4.18}$$

$$x = \frac{m_{NH_3(ads)}}{m_a} \tag{4.19}$$

The temperature profile in the bed is determined by carrying out a thermal energy balance of the discretised bed shown in Figure 4-18.

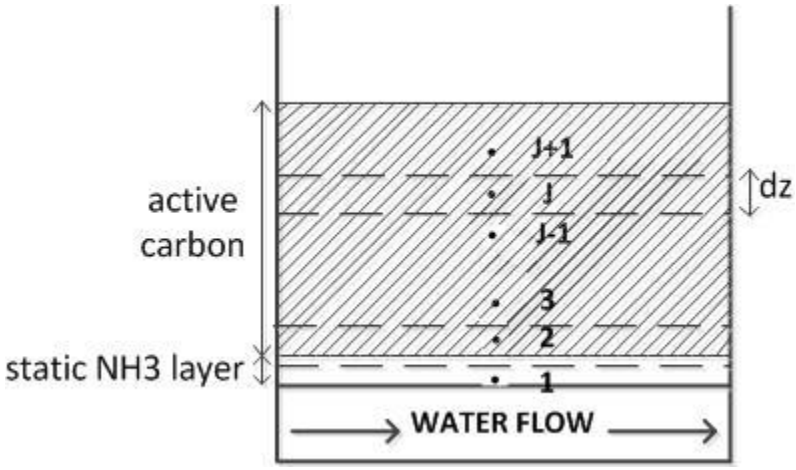

Figure 4-18: Domain discretisation of adsorbent sample

Heat transfer through the sample is considered to be one-dimensional. In light of this assumption, the samples were made with a low height to diameter ratio (0.1 at most) so as to minimise the effects of radial heat transfer. There is a node (1) on the base the test cell and each of the domains has a node at its centre. The temperature at node 1 is determined by the analysis of the heat transfer fluid temperature which was described in Sub-section 4.2.2.1. On any of the nodes after the first node in the carbon bed, the energy balance is generally as in Figure 4-19:

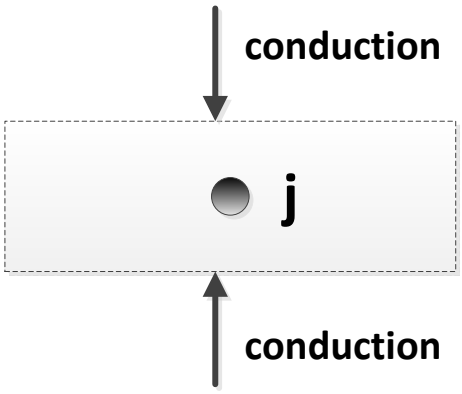

Figure 4-19: Energy balance on a discrete volume

The position of a node in the entire sample is represented by j while the time step of the simulation is represented by i. The temperature profile of each layer of the adsorbent bed is determined by accounting for the change in heat content of the adsorbent per unit mass of adsorbent. This is typically a combination of the sensible heat and heat of desorption (H), which is obtained as in Equation (4.20) [11].

$$kA\left(\frac{T_{i-1}^{j-1} - T_{i-1}^{j}}{dz}\right) + kA\left(\frac{T_{i-1}^{j+1} - T_{i-1}^{j}}{dz}\right) - \frac{Hdx}{dt} = m_a c_{p,a} \frac{T_i^j - T_{i-1}^j}{dt} \qquad (4.20)$$

The specific heat capacity ($c_{p,a}$) of the adsorbent bed without the adsorbed gas is determined from Equation (4.21). The expression was obtained by means of a differential scanning calorimeter in [18] for the same adsorbent used in this work. The heat of sorption, H can be obtained using Equation (4.22).

$$c_{p,a} = 175 + 2.245T_i \qquad (4.21)$$

$$H_i^j = R_{NH_3} E \qquad (4.22)$$

The heat transfer resistance between the first node (test cell inner base) and the second node (first adsorbent node) is made up of adsorbent material and an assumed static ammonia layer that allows us to account for the contact resistance (h). The thermal energy balance on the second node is given by Equation (4.23) below.

$$\left(h + \frac{k}{0.5dz}\right) A\left(T_{i-1}^1 - T_{i-1}^2\right) + kA\left(\frac{T_{i-1}^3 - T_{i-1}^2}{dz}\right) - Hdx = c_{p,a} \frac{T_i^2 - T_{i-1}^2}{dt} \qquad (4.23)$$

During the simulation, for every new time step, only one value of the change in T_{sat} (as found by 'fzero') obeys the constant mass condition in the system. It is with this value that the corresponding simulated pressure is obtained, P_i is given by Equation (4.24).

$$P_i = \exp(Ca - \frac{E}{T_{sat}}) \tag{4.24}$$

Ca and E are constants derived for ammonia from [19] and are 11.515 and 2823.4 respectively. dx, the change in concentration of adsorbate in the adsorbent is a variable that is dependent on the temperature of the adsorbent and the system pressure and this is taken into account in the model. x is thus partially differentiated with respect to T_{sat} (representative of pressure) and T (temperature of adsorbent). The differentials are shown in Equation (4.25) and Equation (4.26).

$$\frac{\partial x}{\partial T} = -\frac{xK\varsigma}{T_{sat}}\left(\frac{T}{T_{sat}} - 1\right)^{\varsigma - 1} \tag{4.25}$$

$$\frac{\partial x}{\partial T_{sat}} = \frac{xK\varsigma T}{\left(T_{sat}\right)^2}\left(\frac{T}{T_{sat}} - 1\right)^{\varsigma - 1} \tag{4.26}$$

The best fit to the experimental data was determined by using root mean square error (shown in Equation (4.27)); the modelled pressure curve which produced the minimum root mean square error when compared to the measured pressure curve was selected as the best fit.

$$RMSE = \sum \sqrt{\frac{(P - P_e)^2}{\text{total no. of points}}} \tag{4.27}$$

4.4.3 Measurement Accuracy

As stated earlier, the pressure transmitter was calibrated using a dead weight tester and had a maximum deviation of ±0.054 bar. The thermocouples were bound together and calibrated in a thermal circulating bath with an accurate Platinum resistance thermometer, giving a maximum deviation of ±0.5°C over the range of interest. The maximum deviations for the thermocouples and pressure transmitter were taken as

their uncertainties. The scale used in measuring the mass of adsorbent had an uncertainty of ±0.01g. These uncertainties were used to obtain the overall uncertainty in the calculated values (Table 4-5). For example, the uncertainty in the calculated value of the thermal conductivity (k) was determined by Equation (4.28).

$$\varphi_k = k\sqrt{\left(\frac{\varphi_A}{A}\right)^2+\left(\frac{\varphi_T}{T}\right)^2+\left(\frac{\varphi_H}{H}\right)^2+\left(\frac{\varphi_{dz}}{dz}\right)^2+\left(\frac{\varphi_{dx}}{dx}\right)^2+\left(\frac{\varphi_{c_p}}{c_p}\right)^2} \quad (4.28)$$

The uncertainties for the different parameters obtained in this chapter are given in Table 4-5. The diameter of the samples was 70mm. The diameters for the different samples are given in Table 4-6.

Table 4-5: Uncertainties in measurement

Parameter	Uncertainty (φ)
A	±0.00008m²
H	±3%
c_p	±1.7%
x	±3.2%
T_{sat}	±1.4%
k	±4.1%
h	±20.7%

4.5 Results of Active Carbon Tests

Figure 4-20 presents the experimental result of Run 1 (see Table 4-6) with simulation results using different combinations of h and K values. As stated earlier, h here accounts for convection only.

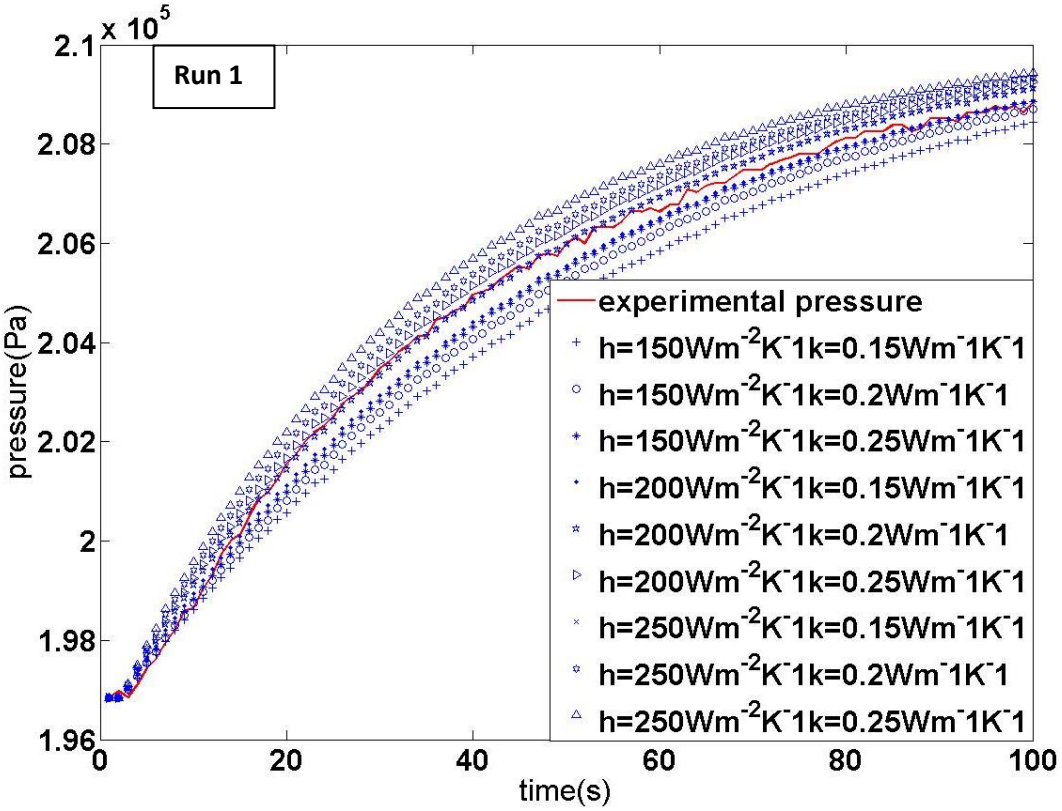

Figure 4-20: Matching modelled pressure with experimental pressure example (Run 1). The first 100 seconds of the plot is shown so as to allow for clarity between the models and the experiment curves. Total modelling/test (Table 4-6) time is 500s.

Table 4-6: Experimental details and results

Run	Thickness, t (mm)	Density, ρ (kg/m³)	Mass of Sample, (kg) m_{ads}	Thermal conductivity, k ($Wm^{-1}K^{-1}$)	Heat transfer coefficient, h ($Wm^{-2}K^{-1}$)	Root Mean Square Error , RMSE(bar)	Equivalent ammonia thickness, δ (m)
1	1.5	530	0.004	0.2	200	0.002	0.0002
2	8.5	560	0.024	0.2	250	0.0063	0.00016
3	5.2	650	0.017	0.35	450	0.0101	0.000088
4	4.8	705	0.017	0.4	400	0.0087	0.0001

To provide a useful physical analogy for the heat transfer coefficients obtained, they were translated into an equivalent thickness of ammonia gas between the metal plate and the activated carbon grains. This is done by simple heat transfer calculations (as shown in (4.29) and taking the conductivity of the layer of ammonia to be 0.04 W/mK

[19]. The thicknesses obtained are reasonable and are given in the last column of Table 4-6.

$$\delta = \frac{k_{NH_3}}{h} \tag{4.29}$$

The derivation of these thermo-physical properties plays a major role in modelling the performance of a carbon-ammonia adsorption system since the dynamics of carbon-ammonia adsorption are governed mainly by heat transfer. The mass transfer resistance is very small with ammonia and is considered negligible as explained earlier.

One of the advantages of the method proposed in this work is its suitability for thicker layers (up to about 8mm) of adsorbent. However, there is a range of thicknesses within which the apparatus can be used with confidence. As explained earlier, the sample height to diameter ratio was kept low to avoid edge effects and heat transfer from the walls. Thus the thickest sample used was 8.5mm (Run 2) and this translates to a height to diameter ratio of 0.1. This is reasonable since a real adsorption heat pump would typically have around or less than 5mm of adsorbent from centre to fin in its generator [20].

Figure 4-20 shows example matching of model to experimental measurements for the first run, Run 1. Here, the best estimate is $k=0.2 Wm^{-1}K^{-1}$ and $h=200 Wm^{-2}K^{-1}$ for the first 60 seconds. Considering the proximity of some of the model curves, it is difficult to separate k and h precisely. The thermal conductivity values obtained are in the same order as obtained in previous literature [21, 22].

There is a general trend of both k and h increasing with increasing density. Slightly anomalous behaviour was observed with the contact heat transfer coefficient for runs 3 & 4 as it decreased with an increase in density. It was assumed that this behaviour came about due to the limitations in extracting separate k and h values from the experimental data. These limitations may be attributed to experimental errors in the measurement of pressure and temperature.

A combined heat transfer parameter was also calculated to help compare with the overall heat transfer parameter obtained in [15]. For the approach detailed in this work,

this is represented by a combination of the heat transfer coefficient (h) and the thermal conductivity (k) as in Equation (4.30).

$$\alpha_{alternative} = \frac{hk}{k + 0.5hz} \tag{4.30}$$

The combined heat transfer, $\alpha_{alternative}$ for Run 1 was 114 W/m²K based on Equation (4.30). while $\alpha_{standard}$ was 73 W/m²K using Equation (4.16). The dominance of the heat transfer coefficient or the thermal conductivity can be shown to depend of the thickness of the bed. The sensitivity (S) is expressed in the equations below.

$$S_k = \frac{k}{\alpha_{alternative}} . \frac{\partial \alpha_{alternative}}{\partial k} = \frac{z\alpha_{alternative}}{2k} \tag{4.31}$$

$$S_h = \frac{h}{\alpha_{alternative}} . \frac{\partial \alpha_{alternative}}{\partial h} = \frac{\alpha_{alternative}}{h} \tag{4.32}$$

Table 4-7: Sensitivity of k and h with adsorbent thickness at k=0.2W/mK and h=200W/m²K

Bed Thickness (mm)	$\alpha_{alternative}$ **(W/m²K)**	S_k	S_h
1.5	114	0.43	0.57
3	80	0.6	0.4
5	57	0.71	0.29
8	40	0.8	0.2

This simple analysis quantifies the straightforward argument that k dominates for thicker beds (from about 3mm) and h is dominant for thinner beds with thicknesses (equal to or below 1.5mm).

4.6 Summary

The details of the design and fabrication of the large temperature jump rig were presented. In order to validate the rig, experiments were conducted on a well known adsorbent- activated carbon. The results obtained were meaningful and it shows that two properties (k and h) with physical meaning can be extracted from large temperature jump data. This provides an opportunity to relate the performance to real thermo-physical properties rather than empirically derived constants as in [15]. Also,

the effect of a change in bulk packing density on these thermo-physical properties was investigated, an increase of k and h with density was observed and quantified.

4.7 References

1. *Volumetric — Gravimetric Measurements*, in *Gas Adsorption Equilibria*. 2005, Springer US. p. 181-234.
2. van Bokhoven, J.J.G.M., *Refinement Of A Calorimetric Method Of Measuring Heats Of Adsorption And A Comparison With An Alternative Method.* Thermochimica Acta, 1985. **86**: p. 257-271.
3. Demir, H., M. Mobedi, and S. Ülkü, *A Review On Adsorption Heat Pump: Problems And Solutions.* Renewable and Sustainable Energy Reviews, 2008. **12**(9): p. 2381-2403.
4. Aristov, Y.I., *Adsorption Dynamics in Adsorptive Heat Transformers: Review of New Trends.* Heat Transfer Engineering, 2013. **35**(11-12): p. 1014-1027.
5. Bird, R.B., W.E. Stewart, and E.N. Lightfoot, *Transport Phenomena*. 2007: Wiley.
6. Tamainot-Telto, Z. and R.E. Critoph, *Thermophysical Properties Of Monolithic Carbon.* International Journal of Heat and Mass Transfer, 2000. **43**(11): p. 2053-2058.
7. Budynas, R.G., J.K. Nisbett, and J.E. Shigley, *Shigley's Mechanical Engineering Design*. 2008, Singapore; London: McGraw-Hill.
8. Holman, J.P., *Heat Transfer*. 2010: McGraw Hill Higher Education.
9. Tamainot-Telto, Z., *Towards Optimum Specifications of Adsorbents for Heat Pump and Refrigeration Applications*, in *Heat Powered Cycles*. 2016: Nottingham.
10. Bansal, R., C. and M. Goyal, *Activated Carbon Adsorption*, in *Activated Carbon Adsorption*. 2005, CRC Press.
11. Critoph, R.E.C., *Chapter 10 - Adsorption Refrigerators and Heat Pumps*, in *Carbon Materials for Advanced Technologies*, T.D. Burchell, Editor. 1999, Elsevier Science Ltd: Oxford. p. 303-340.
12. Glueckauf, E., *Theory Of Chromatography. Part 10.-Formulae For Diffusion Into Spheres And Their Application To Chromatography.* Transactions of the Faraday Society, 1955. **51**(0): p. 1540-1551.

13. Sircar, S. and J.R. Hufton, *Why Does the Linear Driving Force Model for Adsorption Kinetics Work?* Adsorption, 2000. **6**(2): p. 137-147.
14. Aristov, Y.I., et al., *A New Methodology Of Studying The Dynamics Of Water Sorption/Desorption Under Real Operating Conditions Of Adsorption Heat Pumps: Experiment.* International Journal of Heat and Mass Transfer, 2008. **51**(19–20): p. 4966-4972.
15. Veselovskaya, J.V. and M.M. Tokarev, *Novel Ammonia Sorbents "Porous Matrix Modified By Active Salt" For Adsorptive Heat Transformation: 4. Dynamics Of Quasi-Isobaric Ammonia Sorption And Desorption On Bacl2/Vermiculite.* Applied Thermal Engineering, 2011. **31**(4): p. 566-572.
16. Aristov, Y.I., *Optimal Adsorbent For Adsorptive Heat Transformers: Dynamic Considerations.* International Journal of Refrigeration, 2009. **32**(4): p. 675-686.
17. Aristov, Y.I., *Experimental And Numerical Study Of Adsorptive Chiller Dynamics: Loose Grains Configuration.* Applied Thermal Engineering, 2013. **61**(2): p. 841-847.
18. Turner, L.H., *Improvement Of Activated Charcoal-Ammonia Adsorption Heat Pumping/Refrigeration Cycles : Investigation Of Porosity And Heat/Mass Transfer Chacteristics*, in *School of Engineering*. 1992, University of Warwick.
19. *Thermodynamic and Physical Properties of Ammonia R717*. 1981, Paris: International Institute of Refrigeration.
20. Tamainot-Telto, Z., S.J. Metcalf, and R.E. Critoph, *Novel Compact Sorption Generators For Car Air Conditioning.* International Journal of Refrigeration, 2009. **32**(4): p. 727-733.
21. Rivero-Pacho, A.M., *Thermodynamic And Heat Transfer Analysis Of A Carbon – Ammonia Adsorption Heat Pump*, in *Engineering*. 2014, University of Warwick.
22. Aghbalou, F., et al., *Heat And Mass Transfer During Adsorption Of Ammonia In A Cylindrical Adsorbent Bed: Thermal Performance Study Of A Combined Parabolic Solar Collector, Water Heat Pipe And Adsorber Generator Assembly.* Applied Thermal Engineering, 2004. **24**(17–18): p. 2537-2555.

Chapter 5 : Testing and Dynamic Analysis of $BaCl_2/CaCl_2/MgCl_2$-NH_3 Reactions Using the Large Temperature Jump

5.1 Introduction

The previous chapter focuses on large temperature jump experiments using a physical adsorbent (Activated Carbon). The inherent issue with physical adsorbents is the limitation with regards to the amount of refrigerant they can hold or release per kilogram. The best performing physical adsorbent may take up or release refrigerant up to 20% of its mass per cycle [1]. Chemical salts have shown potential to hold more refrigerant per kilogram, and as such allow for improved specific heating power and COP. Calcium Chloride ($CaCl_2$) is a good example with an adsorption ability of up to 1.05 kg of Ammonia (NH_3) per kg of $CaCl_2$[2].

This chapter focuses on the experimental study and analysis of the reactions between three metal chlorides and NH_3. The experiments were conducted on the Large Temperature Jump set-up described in Chapter 4 over a number of relevant reactions between $BaCl_2$, $CaCl_2$, $MgCl_2$, and NH_3. These Chlorides were chosen because the range of their reacting temperatures is compatible with thermochemical heat pump applications. $BaCl_2$ is considered a low temperature salt, $CaCl_2$ a middle temperature salt while $MgCl_2$ is a high temperature salt. Subsection 5.2 of this Chapter presents further details about the mechanism of the reactions between these Metal Chlorides and NH_3.

The salts have an inherent problem of swelling and agglomeration. One of the methods used to prevent this is the impregnation of the salts into host matrices that allow them swelling space. Vermiculite is one of the matrices which have been used in the literature[3]. However, vermiculite by its very nature has a low thermal conductivity (0.3-0.5$Wm^{-1}K^{-1}$) which is detrimental to heat transfer within the sample. Expanded graphite has proved to be a better matrix in terms of thermal conductivity (1-5 $Wm^{-1}K^{-1}$). Its use as a salt matrix was pioneered by Coste et al [4] where it was used with varying proportions of salt to determine the sorption performance of different salts matrices.

The heat produced by the reactions between these salts and NH_3 is only useful if harvested at high power levels and at temperatures suitable for heat pump application. If the heat is to be harvested at high power levels, then the salts will usually be partially converted so that there is no tailing off at the end of the reaction. It is therefore necessary to study the rate of the reaction in order to precisely understand the length of time needed to reach certain conversion levels. This is information that is vital in the design of thermochemical heat pumps.

The rates of the reactions for the different salts were investigated by obtaining a kinetic parameter from a model, which couples the kinetics and heat transfer of the reacting sample. Usually, the rate of reaction should depend on a combination of heat transfer, mass transfer and reaction kinetics. In this work, it was assumed that mass transfer resistance was negligible due to high ammonia pressures and the porous nature of the samples that were used. Calculations on the validity of this assumption are shown later on in this chapter.

Further, in this chapter, each of the salts was modelled separately as an ideal single effect heat pump with a reactor-condenser-evaporator set-up in order to determine the performance implications of different levels of reaction advancement based on obtained kinetic parameters. The specific condensing powers (SConP) during the decomposition phase for each of the salts individually were determined at typical condensation temperatures with the aim of identifying the reaction time that produced the highest condensation power per kilogram of salt used. In addition, the coefficient of performance (COP) for a range of conversion levels was determined to ascertain the sensitivity of performance to different levels of reaction completion. Figure 5-1 shows the general operating mode of a single effect thermochemical heat pump under thermodynamic equilibrium conditions in a Clausius-Clapeyron diagram.

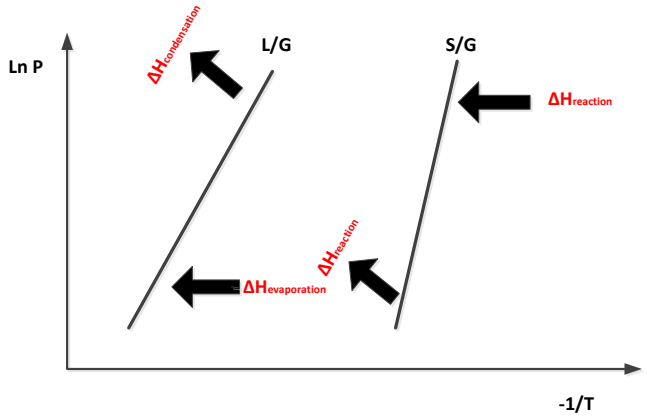

Figure 5-1: Operating mode of a single effect chemical heat pump shown on a Clausius Clapeyron diagram. L/G is the liquid-gas saturation line while S/G is the solid-gas equilibrium line

5.2 Mechanism of the Reactions

Unlike physical adsorption which has been explored previously in Chapter 4, each of the reactions explored in this chapter is defined by one equilibrium condition and the maximum amount of refrigerant reacted cannot be higher than the stoichiometric value given by the relevant equation of reaction. The general form of the equations of reaction is shown below in Equation (5.1).

$$Salt + nGas \rightleftharpoons Salt.n.(Gas) + nHeat\,of\,reaction \tag{5.1}$$

Therefore, at a given sample temperature, synthesis can only occur if the system pressure surpasses the equilibrium pressure and decomposition can only occur if the system pressure goes below the equilibrium pressure. Essentially, the reactions are based on a monovariant equilibrium. The equilibrium of chloride-NH_3 reactions obey the Clausius-Clapeyron equation as shown in Equation (5.2).

$$\ln(P_{eq}) = -\frac{\Delta H}{RT} + \frac{\Delta S}{R} \tag{5.2}$$

P_{eq} is in Pa while T is in Kelvin. The subsections (5.2.1, 5.2.2 and 5.2.3) below describe in more detail the relevant reactions between the different metal chlorides ($BaCl_2$, $CaCl_2$ and $MgCl_2$) of interest and NH_3.

5.2.1 $BaCl_2$ - NH_3

The reaction between pure Barium Chloride ($BaCl_2$) and NH_3 has been studied and

reported in the literature by Deunas et al [5]. Unlike many other salt-NH_3 reactions, the reaction between $BaCl_2$ and NH_3 is quite simple, one mole of $BaCl_2$ reacts with eight moles of NH_3 in a single stage reaction as shown in Equation (5.3).

$$R1:\ BaCl_2 + 8NH_3 \rightleftharpoons BaCl_2.8NH_3 \qquad (5.3)$$

The equilibrium conditions for the $BaCl_2$-NH_3 reaction were determined in-house on a vermiculite-$BaCl_2$ composite using a Rubotherm ISOSORP2000 magnetic suspension balance. Magnetic suspension balances allow the changes in weight that act on samples under controlled environments (pressure and temperature) to be measured accurately. The combination of temperature and pressure points where the reaction occurred were used to obtain the equilibrium line. The ΔH and ΔS values obtained in house for the decomposition and synthesis between $BaCl_2$ and NH_3 are shown in Table 5-1. Table 5-1 also shows the equilibrium values obtained in literature (Deunas et al, [5]).

Table 5-1: Comparison of equilibrium values obtained in-house and those obtained in literature [5]

	ΔH ($Jmol^{-1}$) (In-House)	ΔH ($Jmol^{-1}$) ([5])	ΔS ($Jmol^{-1}K^{-1}$)(In-House)	ΔS ($Jmol^{-1}K^{-1}$) ([5])
Synthesis	41055	41711	241.19	243.6
Decomposition	42493	41711	244.93	243.6

A comparison between equilibrium values obtained by Deunas et al[5] using Differential Scanning Calorimetry (DSC) and those obtained in-house from the Rubotherm results is shown in Figure 5-2 below. Even though the two sets of results are generally comparable, the values given in Deunas et al[5] represent a single transition line for both decomposition and synthesis. This is different for the in-house results as the decomposition synthesis occur at different points, meaning that there is an area of pseudo equilibrium between the two reactions where the reaction rate is zero.

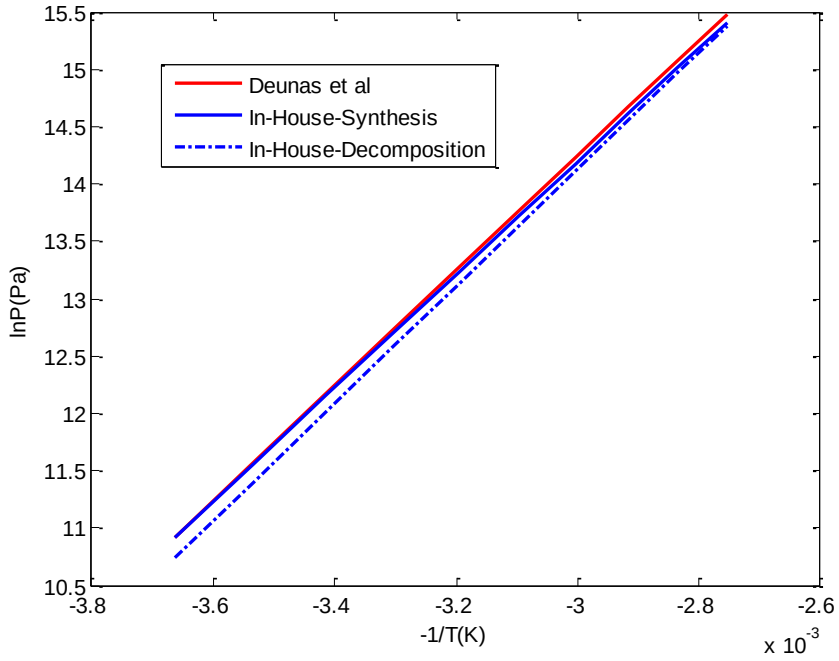

Figure 5-2: Comparison between in-house (Rubotherm) obtained equilibrium lines and line obtained in Deunas et al [5] for the $BaCl_2$-NH_3 reactions

5.2.2 $CaCl_2$ - NH_3

Calcium Chloride ($CaCl_2$) is generally considered a middle temperature salt and there are two reactions between $CaCl_2$ and NH_3 that could be relevant to a CHP, the two reactions are shown below in Equations (5.4) and (5.5). This dual nature of the reaction between Calcium Chloride and Ammonia has been debated. Some researchers have observed the two stages of the reaction while others have not. The two reactions were observed during the experiments carried out for this work.

$$R1: CaCl_2.8NH_3 \rightleftharpoons CaCl_2.4NH_3 + 4NH_3 \quad (5.4)$$

$$R2: CaCl_2.4NH_3 \rightleftharpoons CaCl_2.2NH_3 + 2NH_3 \quad (5.5)$$

The equilibrium values for the $CaCl_2$ - NH_3 reactions which were obtained from Oliveira et al [6], and are shown in Table 5-2. Also, the value obtained from in-house tests on the Rubotherm ISOSORP2000 magnetic suspension balance are shown in Table 5-2.

Table 5-2: Equilibrium values for $CaCl_2$-NH_3 reaction from Oliveira et al[6]

	ΔH ($Jmol^{-1}$) (In-House)	ΔH ($Jmol^{-1}$) ([6])	ΔS ($Jmol^{-1}K^{-1}$)(In-House)	ΔS ($Jmol^{-1}K^{-1}$) ([6])
R1	45644	41413	245.01	230.3
R2	51422	42286	259.39	229.92

The plot shown in Figure 5-3 below compares the equilibria obtained in literature (Oliveira et al[6]) with those obtained in-house for the two $CaCl_2$ - NH_3 reactions. It can be observed in both cases that the equilibria of the first (R1) and second (R2) reactions are close to each other. The implication of this is the very limited temperature and pressure (about Δ7°C at 6bar) window between the two reactions when it comes to the design of large temperature jump experiments or ultimately a heat pump.

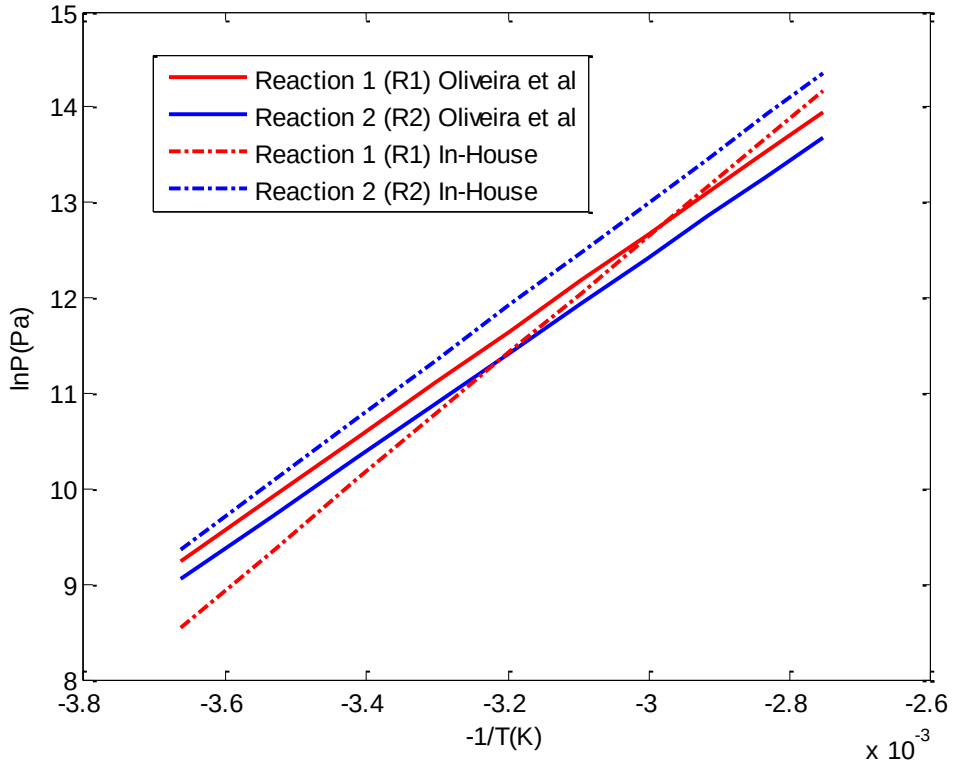

Figure 5-3: Comparison between in-house (Rubotherm) obtained equilibrium lines and line obtained in Oliveira et al[6] for the $CaCl_2$-NH_3 reactions

5.2.3 $MgCl_2$ - NH_3

Magnesium Chloride ($MgCl_2$) is a high temperature salt for CHP applications. The reaction between $MgCl_2$ and NH_3 has been found to occur in stages in some literature[7]. Many of these studies are ambiguous. However, they are all consistent about the existence of a hexa-ammonia complex and a di-ammonia complex.

Therefore, this work focused on the direct reaction between 4 moles of NH_3 and the complex $MgCl_2.2NH_3$ as shown in Equation(5.6).

$$R1: MgCl_2.6NH_3 \rightleftharpoons MgCl_2.2NH_3 + 4NH_3 \quad (5.6)$$

The equilibrium conditions for the reaction above were investigated by Bevers et al[8] and the results of the investigation in form of ΔH and ΔS values for decomposition and synthesis are given in Table 5-3. Table 5-3 also provides values for ΔH and ΔS obtained in house using the Rubotherm ISOSORP2000 magnetic suspension balance.

Table 5-3: Equilibrium values for $MgCl_2$-NH_3 reaction from Bevers et al [3]

	ΔH ($Jmol^{-1}$) (In-House)	ΔH ($Jmol^{-1}$) ([3])	ΔS ($Jmol^{-1}K^{-1}$)(In-House)	ΔS ($Jmol^{-1}K^{-1}$) ([3])
Synthesis	47805	46677	118.81	118.53
Decomposition	61324	60456	147.82	145.06

The equilibrium values obtained in Bevers et al[8] were used as a guide to conduct in-house tests on a $MgCl_2$ sample using the Rubotherm ISOSORP2000 magnetic suspension balance. The Clausius Clapeyron diagram for the reactions as observed by both in house tests and in literature (Bevers et al[8]) are shown in Figure 5-4.

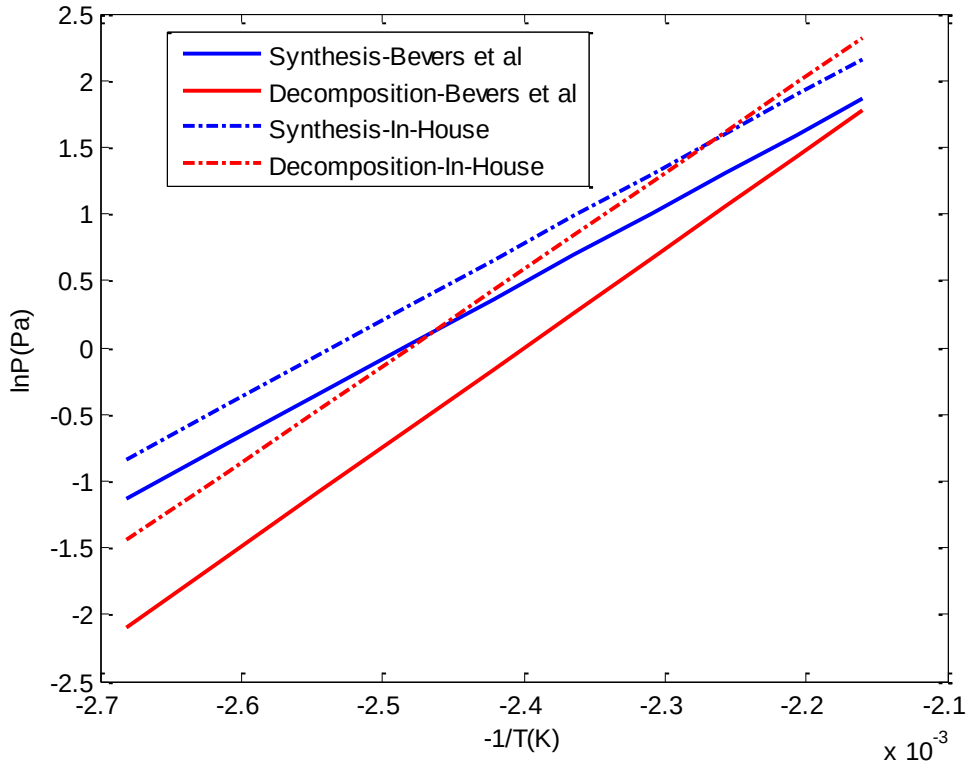

Figure 5-4: Equilibrium lines for the $MgCl_2$-NH_3 reaction according to Bevers et al[8]

5.3 Preparation of the Test Samples for Large Temperature Jump Experiments

Test samples were made of each of the aforementioned salts used in this work. The $BaCl_2$ samples were prepared using vermiculite as host matrix while the $CaCl_2$ and $MgCl_2$ samples were prepared using Expanded Graphite (ENG) as host matrix. One sample of $BaCl_2$ -Vermiculite, two samples of $CaCl_2$-ENG and one sample of $MgCl_2$-ENG were prepared. The vermiculite that was used was horticultural grade vermiculite obtained from Wilko Retail Store while the expanded graphite matrix was sourced from Mersen UK Portsdale Limited. The vermiculite and expanded graphite matrices are inert materials and therefore should not show any reactivity with NH_3. In-house large temperature jump tests show that they absorbed less than 3% of NH_3 when exposed to a temperature jump from 10 to 90°C at 5bar. Table 5-4, Table 5-5 and Table 5-6 below provide information regarding the samples' dimensions and composition.

Table 5-4: Details of $BaCl_2$-Vermiculite sample

	Mass of Vermiculite (g)	Mass of $BaCl_2$ (g)
Sample 1	1.623	1.328

Table 5-5: Details of $CaCl_2$-ENG samples

	Thickness (mm)	Diameter (mm)	Mass of ENG (g)	Mass of $CaCl_2$ (g)	Density (kgm^{-3})
Sample 1	4.00	50	1.026	0.774	205
Sample 2	7.30	50	1.026	1.264	205

Table 5-6: Details of $MgCl_2$-ENG sample

	Thickness(mm)	Diameter (mm)	Mass of ENG (g)	Mass of $MgCl_2$ (g)	Density (kgm^{-3})
Sample 1	4.00	50	0.775	0.585	173.25

As shown in Table 5-4, Table 5-5 and Table 5-6 above, the composition by mass of the salt for the $BaCl_2$ sample was 45% while that of the $CaCl_2$ and $MgCl_2$ samples was 43% with densities of 205 kgm^{-3} and 173.25 kgm^{-3} respectively. There was no specific reason behind choice of these density values. It could be useful to try a range of densities in the future, to investigate the effects of the density of the sample on the dynamics of the reaction. The density of the $BaCl_2$ sample could not be ascertained accurately due to the loose and varying nature of a naturally occurring vermiculite matrix.

5.3.1 Preparation of $BaCl_2$-Vermiculite Sample

The $BaCl_2$-Vermiculite composite was prepared in the same fashion as in Veselovskaya et al [3]. This was essentially through wet impregnation of vermiculite with Barium Chloride. To prepare the sample, first the beaker in which the sample was to be put was weighed on a scale and its mass was recorded.

Once the empty beaker was weighed, the right amount of anhydrous Barium Chloride crystals supplied by Fisher Scientific was added to the beaker. This step is important and inaccuracies here could have implications down the line during analysis of experimental data. For example, for 45% wt. of $BaCl_2$ in a 5g sample, exactly 2.25g of $BaCl_2$ crystals should be added. After, the above step was performed, a solution was made in the beaker. Water was added to make a 22% solution. So for 2.25g of $BaCl_2$, 7.97g of water was required. The water was added by means of a pipette for accuracy.

After adding the water, the solution was stirred slowly using a magnetic stirrer to ensure that all the crystals of barium chloride were dissolved and a clear solution was obtained. The required mass of vermiculite was measured in a separate beaker, poured into the aqueous Barium Chloride solution and weighed on a scale. This weigh was important so as to know how much water was expelled during drying later. The vermiculite was dried prior to this stage at 200◦C for 5 hours in an oven to ensure that it contained no moisture. Thereafter, the containing beaker was covered with a watch glass and placed in the oven at 250◦C. The mass of the beaker was checked at one hour intervals until there was no more moisture loss. It is assumed that the loss of Barium Chloride through the process of producing the sample is negligible.

5.3.2 Preparation of $CaCl_2$/$MgCl_2$-ENG Samples

The procedure used for preparing the $CaCl_2$-ENG and $MgCl_2$-ENG samples was the same. The $CaCl_2$ and $MgCl_2$ samples were prepared by impregnating pure fused granular salts ($CaCl_2$ and $MgCl_2$) supplied by Fisher Scientific UK in expanded graphite (ENG). First, the expanded graphite was weighed based on the desired salt concentration (43% for both) and density (205 kgm^{-3} for the $CaCl_2$ sample and 173.25 kgm^{-3} for the $MgCl_2$ sample) of the sample. The masses of the expanded graphite and pure salt used were 17.96g and 13.54g respectively in both cases. This was calculated based on the initial graphite to salt mass ratio at the start of the sample production.

22% solutions of the salts were prepared using distilled water as solvent for $CaCl_2$ and Ethanol as solvent for $MgCl_2$. Water was not used as a solvent for $MgCl_2$ because of the potential of an irreversible formation of Hydrochloric Acid (HCl) in the resulting solution. The temperatures of the solutions were then raised to just below boiling point (depending on the strength of the solution) to increase solubility. The heating was done using an IKA RCT Basic hot plate magnetic stirrer so that the solution was being stirred during the heating as shown in Figure 5-5.

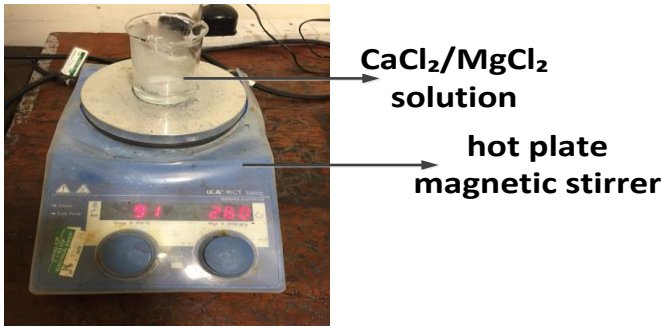

Figure 5-5: $CaCl_2/MgCl_2$ solution being heated and stirred

The weighed expanded graphite for each sample was placed in the oven for 30 minutes so that it was at the same temperature as the salt solutions before they were mixed by hand. Afterwards, the thick mixtures were poured into a pre-fabricated mould and compressed into the desired density. The resulting rectangular block measuring 40mm x60mm x 64mm was cut into a cylindrical shape (diameter-50mm, height-40mm) as shown in Figure 5-6. The direction of the cut was perpendicular to the direction of compression. This is done because the conductivity of the composite is expected to be lower in the direction of compression. It will be useful to investigate the density distribution through the composite in the future. The volume ratio of the rectangular block to the cylinder was 1.95. This implies that almost half of the material is lost during the cylinder cutting.

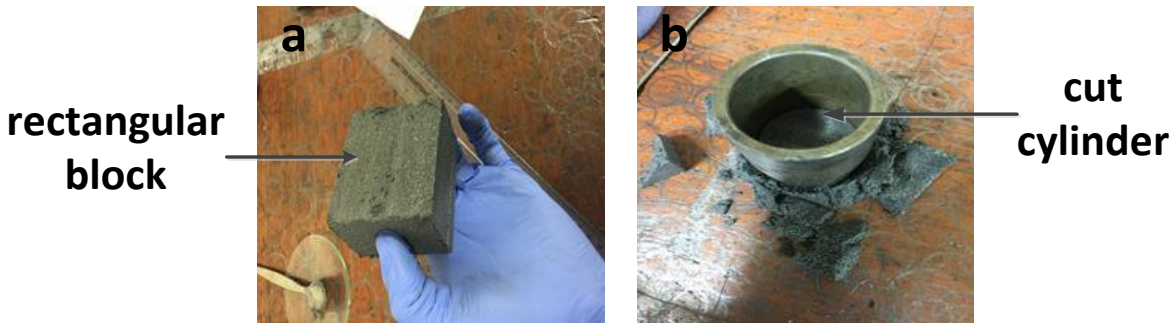

Figure 5-6: a) Compressed rectangular block b) Rectangular block being cut into cylinder

Thereafter, the cylinders were cut into discs of the required thicknesses using a mechanical saw. The discs were dried in an oven. The temperature of the drying was increased in stages, first to 80◦C for 4 hours and then to 250◦C for 20 hours. The $MgCl_2$ sample was dried in the presence of an inert gas, Argon to prevent any reaction

between $MgCl_2$ and moisture from air to permanently form Hydrogen Chloride (HCl). In future sample preparations, more attention should be paid to the accuracy of the salt concentration. Using the current method, salt losses to the walls of the mould and the mixer beaker could throw the concentration of the salt in the composite off. A possible rectification could be weighing the sample at every stage to observe and record any changes in mass.

5.4 Experimental Procedure

The experimental procedure involved in this Chapter comprises of the large temperature jump experiments, used to determine the reaction kinetics of the samples' reaction with NH_3 and the Anter thermal conductivity experiments which were used to determine the thermal conductivity of the samples. Subsections 5.4.1 and 5.4.2 describe the two procedures.

5.4.1 Large Temperature Jump Experiments

These experiments were performed using the large temperature jump method, a volumetric method that allows samples to be put through real heat pump operating conditions: the synthesis and decomposition stages of a sorption cycle. It entails the initiation of the synthesis/decomposition reactions using temperature jumps under quasi-isobaric conditions.

The LTJ method has been used in the literature [9, 10] for the same purpose and comprehensive details of its design and fabrication were given in the previous chapter (Chapter 4). The absence of a condenser or evaporator in the experimental set-up to impose constant pressure conditions in the reactor means that the experiments must be planned such that the resultant pressure change is kept to a barest minimum, consistent with accurate measurement.

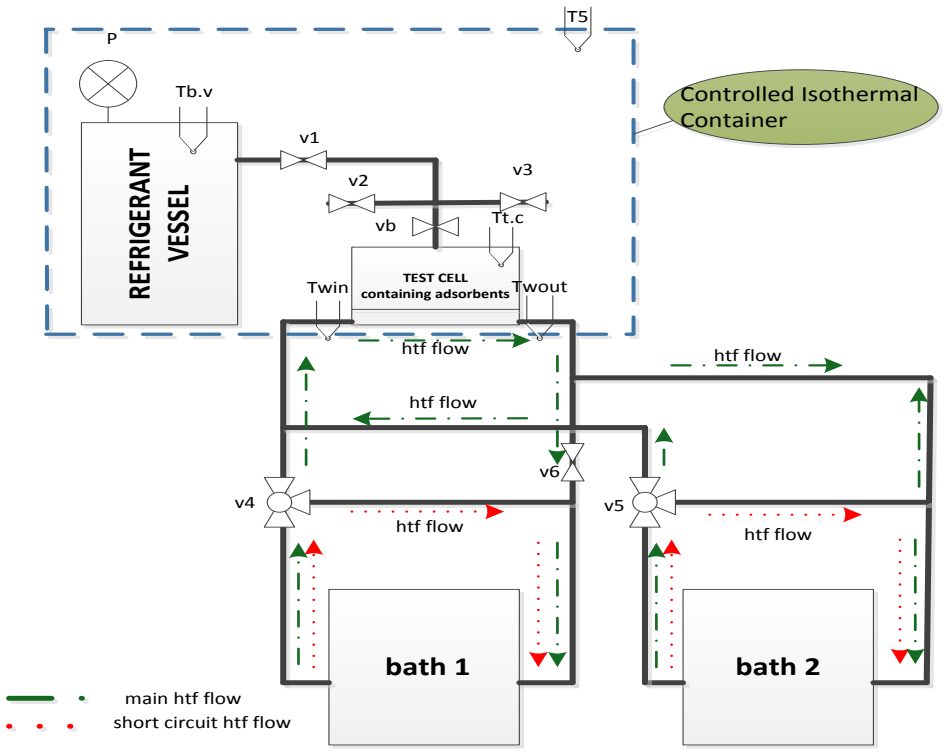

Figure 5-7: Schematic of large temperature jump set-up

The experimental procedure for this work began with evacuation of gas from the system (refrigerant vessel pipework and test cell as shown in Figure 5-7) for 1 hour through valve, v3. Then valve vb was shut so that the test cell is isolated from the rest of the system. The sample was put into the test cell straight from the oven while Silicone oil at 120◦C from thermal bath 2 was run through the heat exchanger circuit to prevent any absorption of moisture into the sample.

Once, the sample was inserted, valve vb was reopened so that the system could be evacuated again for 1 hour. After evacuation, valve vb was shut again to isolate the test cell while the rest of the system was charged with NH_3 to a predetermined level through valve v2. This predetermined level must account for possible pressure drop at a later stage due to the test cell volume and ammonia-salt synthesis. The temperature of the isothermal controller was set (to 50◦C in this case) such that any condensation of NH_3 was avoided and the entire system was allowed to settle for another hour. During this hour, Silicone oil from bath 1 was run through the heat exchanger circuit at the intended initial lower temperature of the experiment to be performed. When the system settled, valve vb was opened so that NH_3 flowed into the test cell. At this point, synthesis began to occur and the system was allowed to settle again. The amount of

NH_3 reacted was determined through the difference in total NH_3 available after this point as shown in Equation (5.7) using the steady state pressure readings from the pressure transducer before (P_b) and after (P_a) opening valve vb for the last time.

$$m_{gas(reacted)} = \frac{m_{NH_3}}{R}\left(\left(\frac{P_b\left(V_{b.v}+V_{p.w}\right)}{T_{b.v}}\right)-\left(\left(\frac{P_a\left(V_{b.v}+V_{p.w}\right)}{T_{b.v}}\right)+\left(\frac{P_a V_{tc}}{T_{t.c}}\right)\right)\right) \quad (5.7)$$

Once the system was settled, the desired sample temperature was imposed on the sample using bath 2. The temperature (T3) of the water was taken at 1 second intervals using a type K thermocouple supplied by TC Direct. The same was done with the NH_3 gas at $T_{b.v}$ and $T_{t.c}$ while a Danfoss AKS32 pressure transmitter was used to measure the pressure change in the system at P. All of the data was logged by an Omega DAQ-2408 data acquisition system throughout the duration of the experiments. The duration of the experiments varied based on the amount of time that was needed to reach sorption equilibrium.

5.4.1.1 Accuracy of Measurements

The pressure transmitter was calibrated using a dead weight tester and had a maximum deviation of ±0.054 bar. The thermocouples were bound together and calibrated in a thermal circulating bath with an accurate Platinum resistance thermometer, giving a maximum deviation of ±0.5°C over the range of interest. The maximum deviations for the thermocouples and pressure transmitter were taken as their uncertainties. The scale used for mass measurements during the preparation of the samples had an uncertainty of ±0.01g. The extent of the accuracy of the salt/graphite concentrations was not measured.

5.4.2 Anter Thermal Conductivity Tests

The thermal conductivities of the samples were measured separately on a guarded heat flow Anter Quickline-10 machine in order to limit the number of unknowns when obtaining the kinetic parameter (A) and the reaction order (yo) further down in the analysis of the large temperature jump test data. The Anter tests for thermal parameters were conducted on an unreacted sample and as such did not consider any changes in thermal conductivity due to the reactions.

The Anter machine operates based on the ASTM E1530 guarded hot plate method[11]. The test samples were constrained (as shown in Figure 5-8) using two smooth metal surfaces under a reproducible compressive force. The two smooth metal surfaces were maintained at different temperatures. The thermal resistance to heat transfer through the sample was measured using the axial steady state temperature gradient established in the stack. This method has its best accuracy when the test sample thickness is below 40mm. Therefore, the samples used in this work were kept below this thickness.

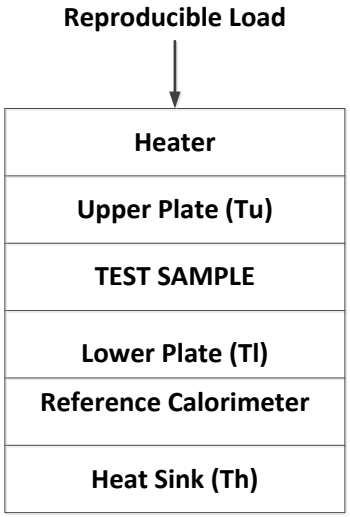

Figure 5-8: Schematic of sample in Anter Quickline 10 machine

At equilibrium, the total thermal resistance (W_{total}) between the upper plate and the lower plate is a summation of the thermal resistance of the test sample (W_{sample}) and the interface resistance (W_{int}) between the sample and the surface plates. An expression of the total thermal resistance using the Fourier heat flow equation shown in Equation (5.8)

$$\frac{T_u - T_l}{Q} = W_{sample} + W_{\text{int}} \tag{5.8}$$

W_{sample} , the thermal resistance of the sample is given by Equation (5.9)

$$W_{sample} = \frac{\delta_{sample}}{k_{sample}} \tag{5.9}$$

The heat flux (Equation (5.10)) across the sample is determined by measuring the temperature difference across the reference calorimeter which is embedded within a heat flux transducer.

$$Q = h_{r.c}(T_l - T_h) \tag{5.10}$$

Equation (5.11) below can then be obtained for the sample thermal resistance W_{sample} by combining Equations (5.8) and (5.10)

$$W_{sample} = F\left[\frac{T_u - T_l}{T_l - T_h}\right] - W_{\text{int}} \tag{5.11}$$

F, a proportionality constant is the inverse of $h_{r.c}$, the heat transfer coefficient of the reference calorimeter in the heat flux transducer. Considering the linear relationship between the temperature difference ratio $\frac{T_u - T_l}{T_l - T_h}$ and W_{sample}, then F and W_{int} can be determined by measuring the $\frac{T_u - T_l}{T_l - T_h}$ and W_{sample} for several samples of known resistances. The slope and y-intersect of the graph of $\frac{T_u - T_l}{T_l - T_h}$ against W_{sample} for the several samples are F and W_{int}. In this work two sets of materials were used for calibration depending on the salt sample to be tested. For the Barium Chloride-Vermiculite samples, Polyether ether ketone (PEEK) disks of different thicknesses were used for calibration. Table 5-7 and Figure 5-9 show details of the calibration samples and the resulting plot of $\frac{T_u - T_l}{T_l - T_h}$ against W_{sample} respectively.

Table 5-7: Calibration materials details for $BaCl_2$-Vermiculite samples

Material	Thickness (mm)	Thermal Conductivity ($Wm^{-1}K^{-1}$)
PEEK	2.5	0.29
PEEK	5.0	0.29
PEEK	10.0	0.29
PEEK	20.0	0.29
PEEK	30.0	0.29

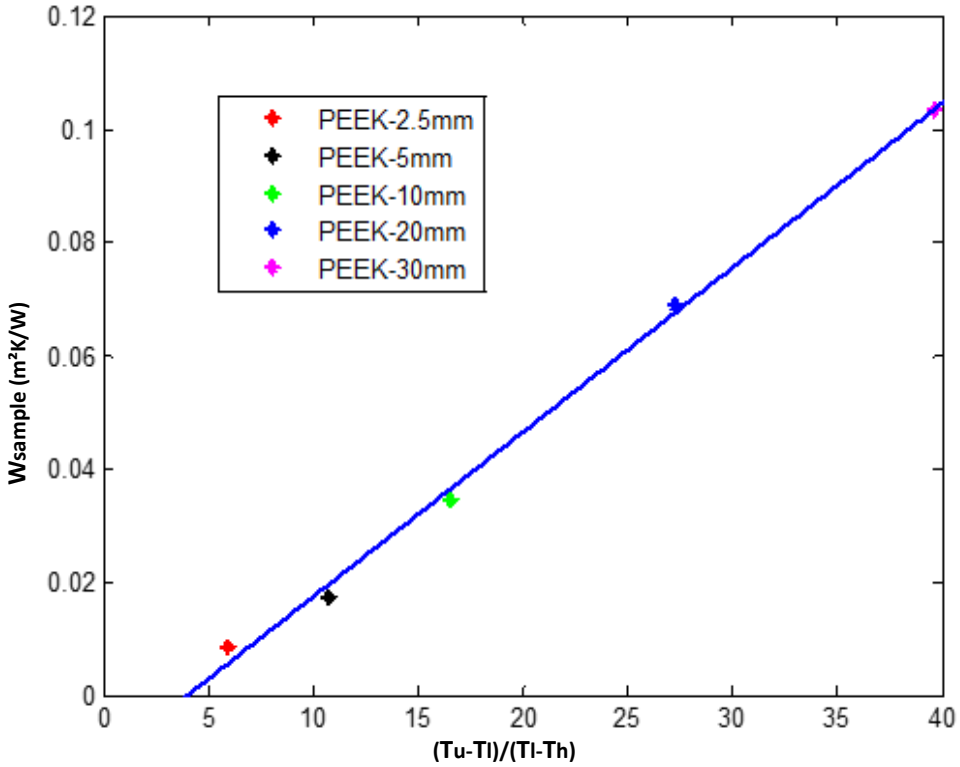

Figure 5-9: Plot of calibration line for $BaCl_2$-Vermiculite samples

Because expanded graphite (ENG) has a much higher thermal conductivity range, Vespel and Steel were used to calibrate the Anter Quickline 10 machine for the $CaCl_2$ and $MgCl_2$ samples. Table 5-8 and Figure 5-10 show details of the calibration samples and the resulting plot of $\frac{T_u - T_l}{T_l - T_h}$ against W_{sample} respectively.

Table 5-8: Calibration materials details for $CaCl_2$ and $MgCl_2$-ENG samples

Material	Thickness(mm)	Thermal Conductivity ($Wm^{-1}K^{-1}$)
Vespel	6.4	0.32
Stainless Steel	12.7	14.65

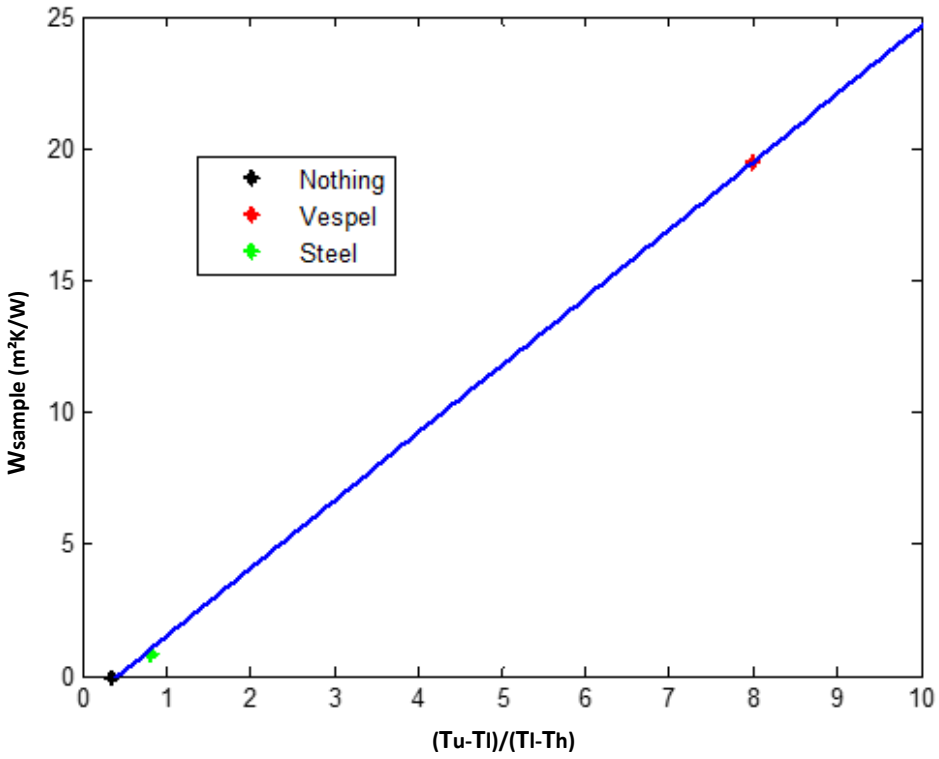

Figure 5-10: Plot of calibration line for $CaCl_2$ and $MgCl_2$-ENG samples

5.4.2.1 $BaCl_2$-Vermiculite Samples Thermal Conductivity Testing

Due to the grainy nature of the vermiculite-$BaCl_2$ samples, they were measured on the Anter Quickline 10 machine in a square cross-section sample holder (shown in Figure 5-11) which held them in loose form. The sample holder is made up of two Aluminium square blocks, which measure 50.8 mm x 50.8 mm x 10 mm and 4 low conductivity polymer plates. It is important to note that the PEEK calibration performed earlier was not done with these Aluminium sample holder. Polymer plates of varying sizes were made so that the thickness (3mm, 7mm and 11mm) of the test sample could be varied. By removing the fourth plate, there was access to fill up the sample holder with the sample. Afterwards, the last wall was screwed on and the sample holder was inserted between the upper and lower plates of the Anter Quickline 10 machine.

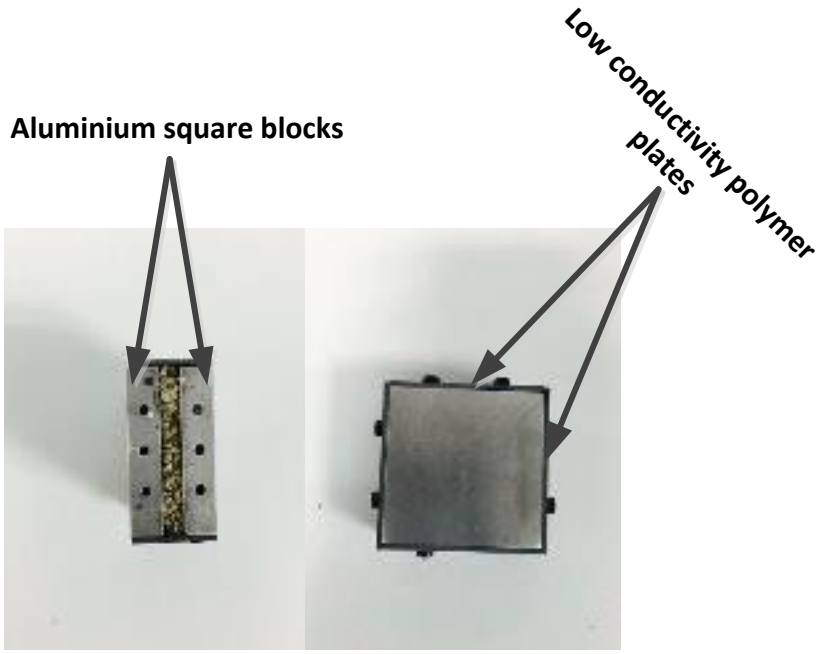

Figure 5-11: Sample holder for $BaCl_2$-Vermiculite sample

The Aluminium walls were made of Aluminium 6082-T6 and have a thermal conductivity of 180$Wm^{-1}K^{-1}$ which is three orders of magnitude higher than the average thermal conductivity of the $BaCl_2$-Vermiculite samples. This ensured that the Aluminium did not become a significant thermal barrier to the sample.

5.4.2.2 $CaCl_2$/$MgCl_2$-ENG Samples Thermal Conductivity Testing

The $CaCl_2$ and $MgCl_2$ samples were compacted and mechanically stable and did not require the sample holders used for the $BaCl_2$-Vermiculite samples. However, they were sealed in polythene to prevent any chemical damage to the upper and lower plates of the Anter Quickline 10 machine. These polythene bags were used during the calibration also. To avoid contact resistance between the base of the samples and the plates of the Anter Quickline 10 machine, a high conductivity grease SG500(6023) from ACC Silicones Ltd with a thermal conductivity of 0.77 $Wm^{-1}K^{-1}$ was applied to the top and bottom of the sample holders and polythene bags before the experiment.

5.4.2.3 Accuracy of Measurement

Thermal conductivity measurements on the Anter Quickline-10 have an estimated accuracy between ±3% to ±8% depending on the thermal resistance of the sample being measured. The level of accuracy increases when the ratio $W_{int}:W_{sample}$ is small.

5.5 Model of the Reaction Process

Three factors are responsible in the reaction mechanism of the reactions relevant to this work. They are mass transfer resistance, heat transfer resistance and reaction kinetics. The mass transfer resistance was assumed negligible due to the porous nature of the materials and the high pressure systems in use, making it possible for pressure to be uniform across the layers of the material.

The model utilised in this work is a global model, i.e it only attempts to replicate a physical effect of the reaction rather than provide a detailed description of the reaction at pellet-level[13, 14]. The model used coupled thermal and kinetic phenomena in two differential equations.

1. A thermal energy balance that accounts for conductive heat transfer within the sample and for the heat source/sink due to reaction heat.
2. A kinetic law representing the progression of the reaction with thermodynamic conditions[15].

The model is based on the following assumptions:

- Heat transfer through the sample is one dimensional.
- Pressure is uniform throughout the sample (as shown above).
- Variations in the thermal conductivity with the reaction progression is not taken into account.

The thermal part of the model follows the general form of the partial differential equation for the one-dimensional heat equation as given in Equation (5.12) below.

$$a\frac{\partial^2 T}{\partial z^2} = b\frac{\partial T}{\partial t} \tag{5.12}$$

If $b=0$ and $a \neq 0$, then this indicates that the problem being modelled is not time dependent and essentially steady state. This type of problem is called elliptic. If $b \neq 0$ and $a \neq 0$, then the problem is time dependent or transient, this type of problem is called parabolic. The heat transfer problem considered here is time dependent (transient) and as such is modelled with a simple parabolic one-dimensional heat equation with the addition of a term to represent the enthalpy change due to the reaction which may be akin to a heat generation or heat sink term depending on the

type (decomposition or synthesis) of reaction taking place. It is represented in Equation (5.13) for decomposition and Equation (5.14) for synthesis.

$$mC_p \frac{\partial T}{\partial t} = k \frac{\partial^2 T}{\partial z^2} - N_{NH_3} \Delta H \frac{\partial X}{\partial t} \tag{5.13}$$

$$mC_p \frac{\partial T}{\partial t} = k \frac{\partial^2 T}{\partial z^2} + N_{NH_3} \Delta H \frac{\partial X}{\partial t} \tag{5.14}$$

The enthalpy change term (far right of Equation(5.13)) factors in the rate of change of advancement ($\frac{\partial X}{\partial t}$) of the reactants to products in the fixed finite volume and the total number of reacted moles (N_{NH_3}) of Ammonia in the entire reaction. The advancement (X) is a normalised measure of the reacted/unreacted NH_3 quantity and therefore goes from a minimum of 0 to a maximum of 1 when each reaction is treated separately. The physical definition of the advancement is given by Equation (5.15) for decomposition and Equation (5.16) for synthesis.

$$X_{des} = 1 - \frac{m_{NH_3 i}}{m_{NH_3 initial}} \tag{5.15}$$

$$X_{syn} = \frac{m_{NH_3 i}}{m_{NH_3 final}} \tag{5.16}$$

m_{NH_3} is the mass of reacted NH_3 for synthesis or unreacted NH_3 for decomposition. The rate of change of advancement term makes up the second part of the model. Basically, it is a kinetic law representing the progression of the reaction with thermodynamic conditions[15]. It is represented in Equation (5.17) for the case of synthesis. In the case of decomposition, the kinetic law is given by Equation (5.18) below. The difference between the equilibrium pressure and gas pressure is reversed so that the driving pressure force stays positive.

$$\frac{\partial X_{syn}}{\partial t} = \left(1 - X_{syn}\right)^{yo} A \frac{P - P_{eq}\left(T\right)}{P} \tag{5.17}$$

$$\frac{\partial X_{des}}{\partial t} = \left(1 - X_{des}\right)^{yo} A \frac{P_{eq}\left(T\right) - P}{P} \tag{5.18}$$

According to Mazet et al[16], ' *yo* ' represents the pseudo-order of the reaction and has no physical meaning whatsoever. A is a kinetic parameter which is a direct indicator of the kinetics of the reactions. This kinetic law (Equation(5.17)) is of the basic form (Equation (5.19)) described by Lebrun and Spinner [17].

$$v = \frac{dX}{dt} = f(X)\,p(P,T) \tag{5.19}$$

The p-term represents the effects of temperature and pressure deviations from equilibrium conditions. The f-term represents the evolution of the reaction process with changes in the physical configuration of the sample.

5.6 Numerical Solution of the Model of the Reaction Process

The model was resolved by using a physical approach as proposed by Croft et al [18]. The sample was treated as a control volume discretised into layers, which each contain a node as shown in Figure 5-12. The very first node is different from the others, it does not exist within a layer of sample but on the floor of the test cell. Therefore, there is a combination of a layer of NH_3 and half of a sample layer between the first node and the second node.

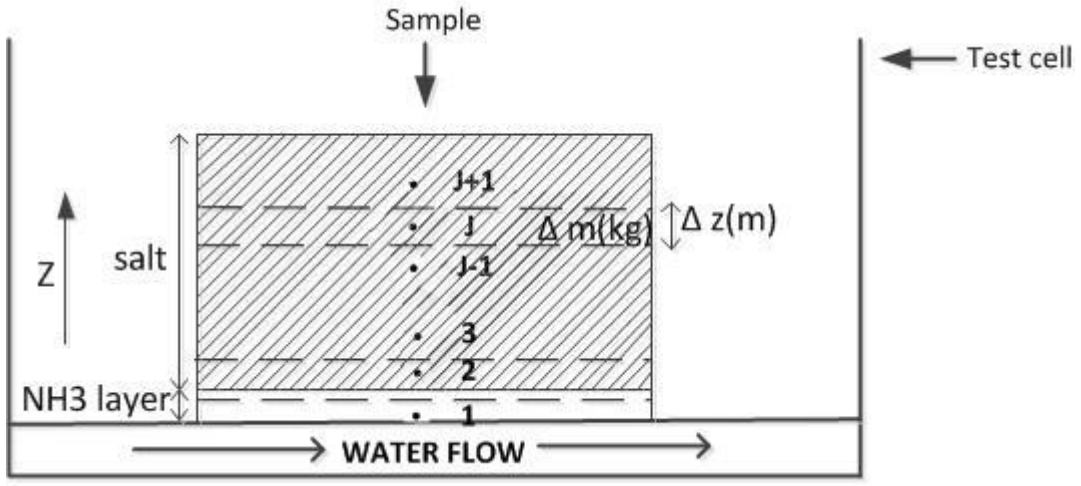

Figure 5-12: Schematic of discretised sample

The discretised forms of the thermal and kinetic equations are shown in Equations (5.20) and (5.23) for decomposition and Equations (5.21) and (5.22) for synthesis. They both obtain present conditions at a time (i) from conditions for a previous time

(i-1). The net heat conducted into a node (j) was determined by a summation of the heat gained from the preceding node (j-1) and the heat lost to the succeeding node ($j+1$).

$$\Delta m C_p \left(\frac{T_i^j - T_{i-1}^j}{\Delta t} \right) = kS \left(\frac{T_{i-1}^{j-1} - T_{i-1}^j}{\Delta z} \right) + kS \left(\frac{T_{i-1}^{j+1} - T_{i-1}^j}{\Delta z} \right) - N_{NH_3} \Delta H \frac{\Delta X_i^j}{\Delta t} \quad (5.20)$$

$$\Delta m C_p \left(\frac{T_i^j - T_{i-1}^j}{\Delta t} \right) = kS \left(\frac{T_{i-1}^{j-1} - T_{i-1}^j}{\Delta z} \right) + kS \left(\frac{T_{i-1}^{j+1} - T_{i-1}^j}{\Delta z} \right) + N_{NH_3} \Delta H \frac{\Delta X_i^j}{\Delta t} \quad (5.21)$$

$$\frac{\Delta X_i^j}{\Delta t} = \left(1 - X_{i-1}^j\right)^y A \frac{P_{i-1} - P_{eqi}^j}{P_{i-1}} \quad (5.22)$$

$$\frac{\Delta X_i^j}{\Delta t} = \left(1 - X_{i-1}^j\right)^y A \frac{P_{eqi}^j - P_{i-1}}{P_{i-1}} \quad (5.23)$$

The advancement (X_i^j) in each layer was determined simply as shown in Equation (5.24) adding the obtained change in advancement.

$$X_i^j = X_{i-1}^j + \Delta X_i^j \quad (5.24)$$

When two reactions occur simultaneously as can happen in the case of $CaCl_2$, the advancement of the second reaction can be obtained in a similar way as in the first reaction and denoted by Y instead of X. The mass of NH_3 available for the advancement of the second reaction at a time i is given by Equation(5.25).

$$m_{NH_3Y,i}^j = m_{NH_3Y,i-1}^j - N_{NH_3Y} N_{salt} M_{NH_3} \Delta Y_i^j + N_{NH_3X} N_{salt} M_{NH_3} \Delta X_i^j \quad (5.25)$$

N and M are the number of reacted moles and molar mass respectively. The average simulated advancement of all the layers at a given time i was taken as the modelled global advancement (shown in Equation(5.26)) for the reaction. The measured global advancement (shown in Equation(5.27)) was simply obtained from a normalisation of the measured pressure data. This normalisation doesn't take into account the temperature changes in the small volume of gas in the test cell. Accounting for these changes in temperature had no significant effect (<2% in the worst case) on the results and thus this approximation is good enough.

$$X_i^{global,sim} = \frac{\sum^j X_i^j}{n} \tag{5.26}$$

$$X_i^{global,mes} = \frac{P_{mes,i} - P_{mes,initial}}{P_{mes,final} - P_{mes,initial}} \tag{5.27}$$

The specific heat capacity (C_p) of reacted and unreacted salts was obtained from Oliveira et al [6] for Calcium Chloride and Bevers et al [8] for Magnesium Chloride. The numerical solution described above demands that initial conditions and boundary conditions be set. The boundary conditions can be of Dirichlet or Neumann type. A typical Dirichlet boundary condition would give the temperature of the boundary at every time interval while a Neumann boundary condition would state the flux going through the boundary at every time interval. The two boundaries (top and bottom) in this case are given Neumann type boundary conditions as shown in Equations (5.28) and (5.29). The top boundary is considered adiabatic while the boundary condition for the bottom boundary accounts for the heat transfer coefficient, h of the ammonia layer between the first node (surface of the test cell base) and the bottom of the sample as shown in Figure 5-12. The initial conditions are given by Equation (5.30) , essentially all the nodes are set to the temperature of the low temperature thermal bath before the jump.

$$\frac{\partial T}{\partial z}_{topboundary} = 0 \tag{5.28}$$

$$\frac{\partial T}{\partial z}_{bottomboundary} = h\left(T_i^1 - T_i^2\right) \tag{5.29}$$

$$T(t=0)_{allFDV} = T_1^j \tag{5.30}$$

For each experiment, the combination of yo and A that produces the simulated global advancement that best fits the measured global advancement was selected as optimal. The selection was done by minimising a root mean square error between the simulated and the measured global advancements as shown in Equation(5.31).

$$RMSE = \sqrt{\frac{\sum^{tp} (X_i^{global,sim} - X_i^{global,mes})^2}{\text{total no. of points}}} \quad (5.31)$$

5.7 Results

This subsection presents the results for the Anter thermal conductivity tests and those for the analysis of the large temperature jump tests results for all the four samples involved in this work.

5.7.1 Anter Thermal Conductivity Results

Table 5-9 shows the thermal conductivity values obtained from the Anter tests on all the samples.

Table 5-9: Anter thermal conductivity results

		Thermal Conductivity ($Wm^{-1}K^{-1}$)
$BaCl_2$	Sample 1	0.22
$CaCl_2$	Sample 1	4.98
$CaCl_2$	Sample 2	4.66
$MgCl_2$	Sample 1	4.12

5.7.2 Large Temperature Jump Results

The large temperature jump results for various experiments were analysed to produce a kinetic parameter *A* and pseudo-order *yo* for the reactions between Calcium Chloride and Ammonia and Magnesium Chloride and Ammonia. These kinetic parameter and pseudo-order values are given in Table 5-10. The $CaCl_2$-NH_3 account for the two samples involved (Sample 1 and Sample 2). The results of the specific experiments conducted for the different reactions are presented in Appendix 1.

Table 5-10: Average kinetic parameter (A) and pseudo-order (yo) values for the reactions between $CaCl_2$ and NH_3 and $MgCl_2$ and NH_3

		A (s^{-1})	yo
$BaCl_2$-NH_3 (R1)	a	0.07	0.72
	b	0.007	0.70
$CaCl_2$-NH_3 (R1)	a	0.037	0.72
	b	0.02	0.71
$CaCl_2$-NH_3 (R2)	a	0.0069	0.81
	b	0.0057	0.83
$MgCl_2$-NH_3 (R1)	a	0.00013	0.64
	b	0.000056	0.72

5.8 Discussion

All the experiments carried out helped to identify the best fit kinetic parameters (A) for the different relevant reactions between $BaCl_2$, $CaCl_2$, $MgCl_2$ and NH_3. All the average values obtained were checked against each experiment between 10% and 80% completion to ensure a good fit was produced. The decision to only consider between 10% and 80% of the reaction was based on a strange behaviour observed between 0% and 10% in some of the experimental results which could not be thoroughly investigated due to time limitations. Figure 5-13 shows an example using the measured pressure profile for Experiment 2a (see Appendix 1 for more details about all the experiments). This behaviour is believed to be due to the effect of contact resistance between the test cell base and the sample which caused an initial stall in the reaction progression.

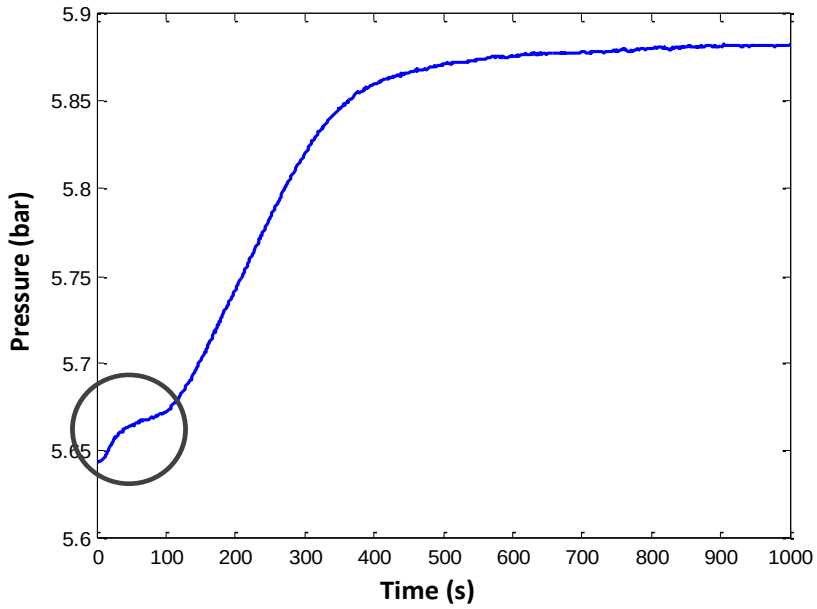

Figure 5-13: Pressure profile for Experiment 2a with 0%-10% area circled

Sections 5.8.1 discusses the results for each of the different salts considered.

5.8.1 The General Trends in the Kinetics of the Reactions

Only one pair of decomposition and synthesis experiments was conducted for the $BaCl_2$ -NH_3 experiment. This is because the $BaCl_2$ -NH_3 working pair would not be

used in subsequent heat pump design and was not considered important. The $BaCl_2$ -NH_3 working pair is a low temperature working pair and out of the temperature range which is being considered in this work. The $BaCl_2$ -NH_3 working pair would be more suitable for low temperature heat pump/chiller applications. For example, low temperature thermochemical chillers which can use waste heat from a data centre which is usually at low temperature to provide much needed cooling at the data centre.

In the single experiment pair conducted for the $BaCl_2$ -NH_3 reaction, the decomposition experiment appeared to be about five times faster than the corresponding synthesis experiments. However for the $CaCl_2$ -NH_3 reaction where more experiments were conducted, the rate of the reactions seemed to be influenced by the magnitude of the driving temperature difference involved. For instance, in Experiment 1a and 1b (see Appendix 1), there is a driving temperature difference of 4.71°C for 1a (decomposition) and 22.15°C for 1b (synthesis). Here, the synthesis reaction is three times faster than the decomposition reaction based on measured advancement. The situation is however reversed in the case of Experiment 9a and 9b where the driving temperature differences are 8.78°C and 6.91°C respectively. Here the decomposition reaction is three times faster than the synthesis reaction. A similar trend was observed for the $MgCl_2$ -NH_3 reaction. These can be observed in Figure 5-14a-d which show the measured advancement, experimental best fit and average reaction best fit for Experiments 1a, 1b, 9a and 9b. The average reaction best fit is obtained using the average of the *A* values obtained for all the experiments for a particular reaction.

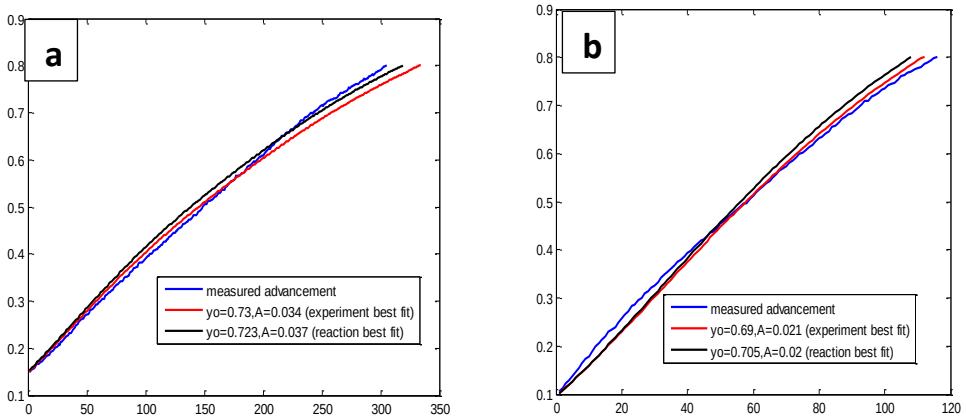

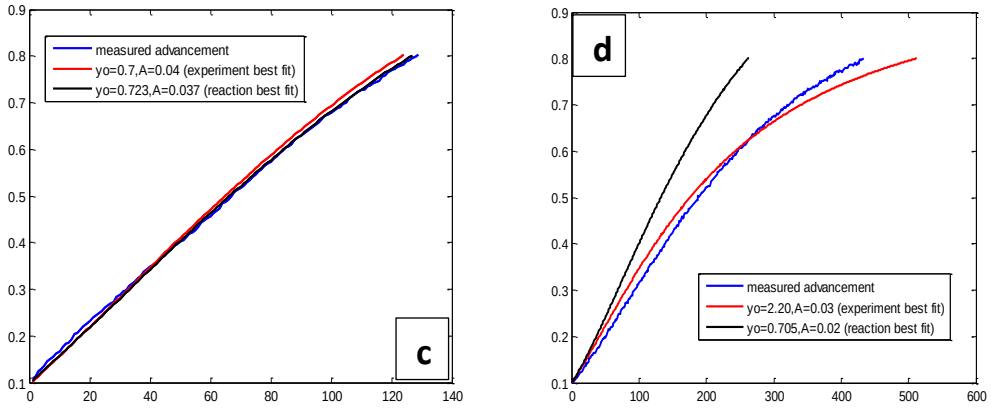

Figure 5-14: Measured advancement vs experimental best fit and average reaction best fit for Experiments 1a (in a), 1b (in b), 9a (in c) and 9b (in d)

Generally, for driving temperatures in the same range, the $MgCl_2$ -NH_3 reactions appeared to be slower than the $CaCl_2$ -NH_3 reactions. For example, Experiment 31b and 19b both have driving temperature differences of 17.36°C and 22.85°C respectively. However, the $MgCl_2$ -NH_3 (30b) takes 1006s compared to 205s for the $CaCl_2$ -NH_3 (19b) reaction to reach 80% completion from 10%. This means that when the salts are cascaded in a heat pump design in Chapter 6, the Magnesium Chloride salt would limit the system because of its slower rate compared to the Calcium Chloride reaction. Figure 5-15a-b shows the measured advancement, experimental best fit and average reaction best fit for Experiments 30b and 19b.

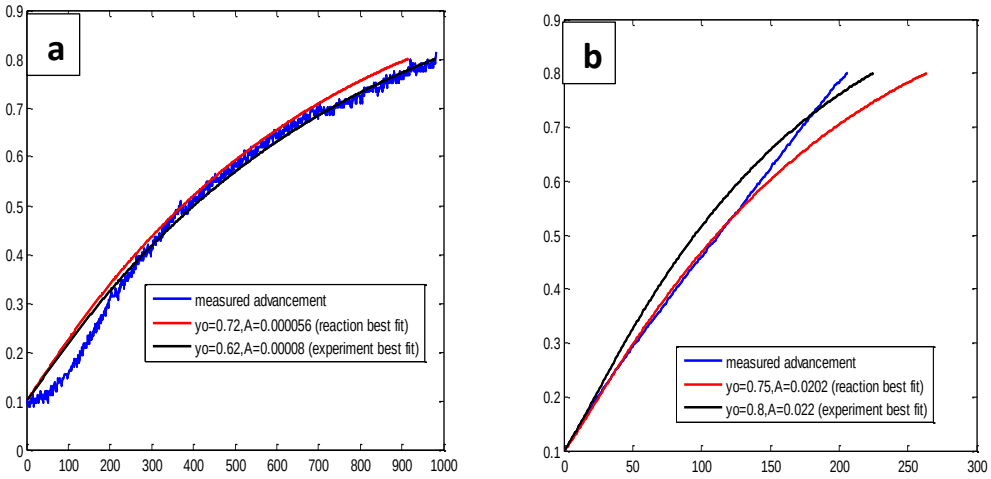

Figure 5-15: Measured advancement vs experimental best fit and average reaction best fit for Experiments 30b (in a- $MgCl_2$-NH_3), 19b (in b- $CaCl_2$-NH_3)

5.8.2 Trend of A-Values with Driving Temperature Difference

The A values seem consistent and show no prominent relationship with driving temperature difference. However, there seemed to be a major deviation in the trend of A values in certain cases. These were typically the experiments where the driving temperature difference was lowest. For instance, as shown in Figure 5-17, the values of A were about a magnitude of 10 more than the average reaction A values when driving temperature difference dropped to 5.7ºC $CaCl_2$-NH_3 (R2). The same was observed for $CaCl_2$-NH_3 (R1) as shown in Figure 5-16 These deviations have been put down to inadequate driving temperature difference and they therefore represent a limitation of the model used in this work in such situations. These low driving temperature cases were excluded when obtaining the average reaction A and y_0. In Figure 5-16 and Figure 5-17, the legend is formed by the temperature jump for the respective experiments and the experiment number in bracket.

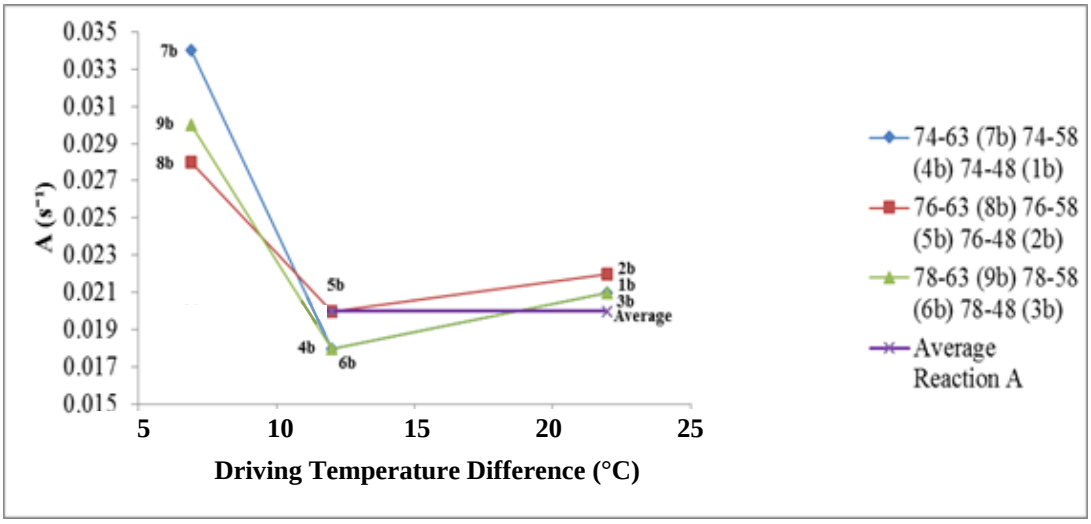

Figure 5-16: A values against driving temperature difference for $CaCl_2$-NH_3 (R1) synthesis reaction (Sample 1)

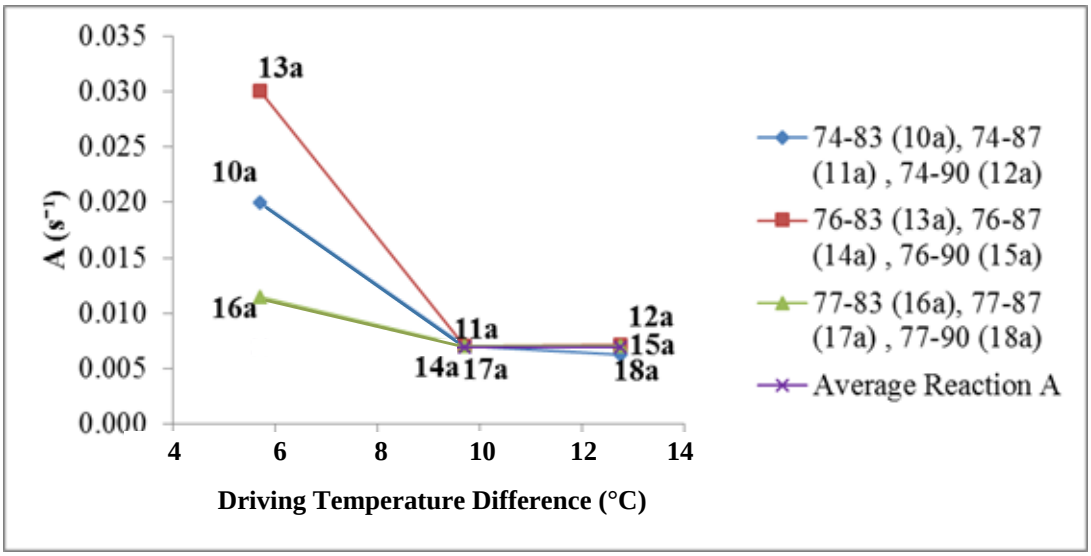

Figure 5-17: A values against driving temperature difference for $CaCl_2$-NH_3 (R2) decomposition reaction (Sample 1)

5.8.3 Advancement and Concentration in Thinner Samples vs Thicker Samples

The values of advancement for each layer of the discretised sample cannot be determined experimentally. However, the kinetic model that was utilised allowed for the determination of an advancement parameter (X) for each discrete layer which is synonymous with the completion level of the reaction in that layer. X will usually start from 0 at the beginning of the reaction and progress with a decaying exponential towards a maximum value of 1 when all of the reaction has taken place.

Figure 5-18 shows an example of the advancement profile for different layers of Sample 1 ($CaCl_2$) in Experiment 2a.

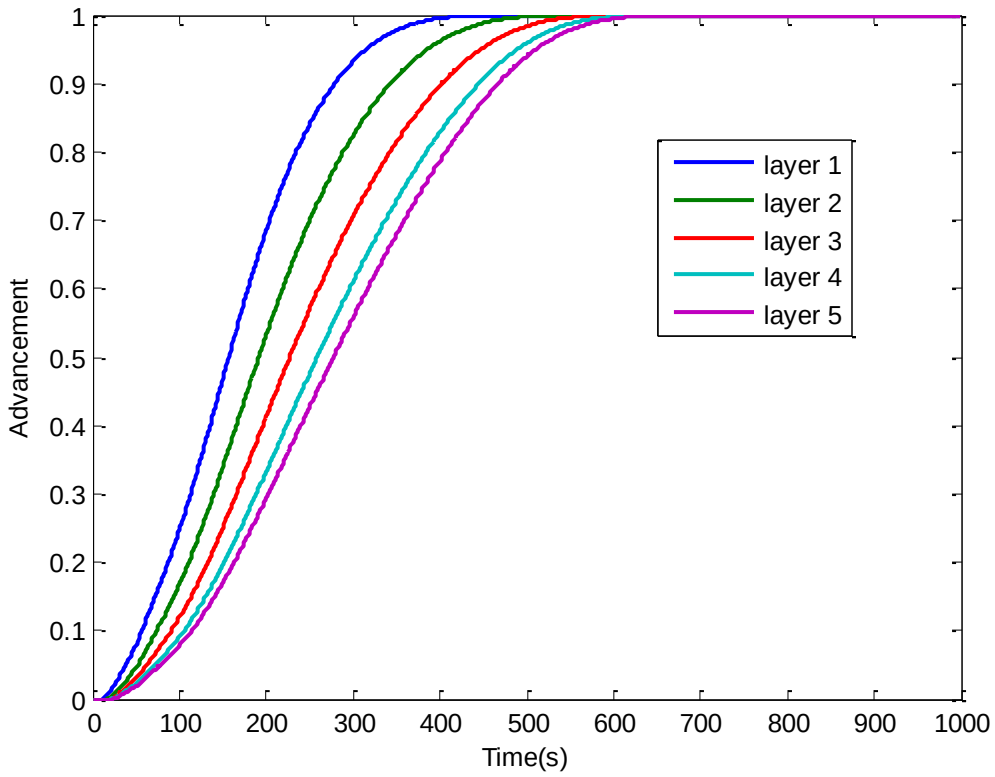

Figure 5-18: Example advancement profile for Experiment 2a

Strong advancement gradients occurred between the discrete layers in some simulations of the experimental cases. For example, these gradients were more pronounced in the thicker samples for the $CaCl_2$ sample as seen in Figure 5-19 and Figure 5-20 which show the advancement profile across the two $CaCl_2$ samples at 1s, 30s, 40s, 60s, 90s ,100s, 120s, and 150s for Experiments 2a and 20a. At the same point (150s) of similar experiments in the two samples, there was an advancement gradient of $0.02mm^{-1}$ in the thinner 4mm sample while there was a much higher advancement gradient of $0.06mm^{-1}$ in the thicker sample.

There are distinctive areas where advancement is low (i.e temperature below or close to the equilibrium value) and there are also regions where the reaction is completed early because of temperature attainments which are far above or below the equilibrium temperature depending on the type of experiment. These are typically the regions located close to the test cell base which is the source/sink of the heat. This means that the time for full transformation or a complete reaction gets higher the further away from the bottom of the sample or heat source and this highlights the influence of heat

transfer on the reaction rates. Further, the effect of the thickness of the bed can be quantified through an observation of the inert period of similar points in the thinner and thicker sample. The inert period is the time during which the point being studied does not react at all. i.e advancement is 0. This is a phenomenon that could greatly affect the overall power output of a reactor and it means there is a need for a detailed optimisation of the reaction bed thickness in the subsequent design of a thermochemical heat pump.

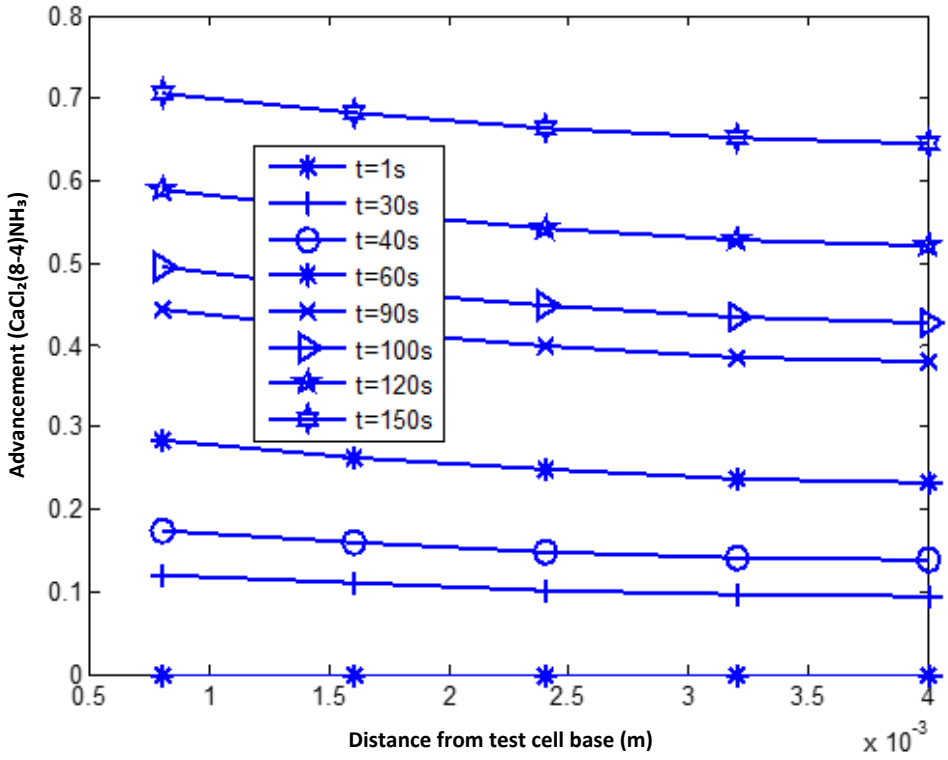

Figure 5-19: Advancement at different points in Sample 1 for Experiment 2a

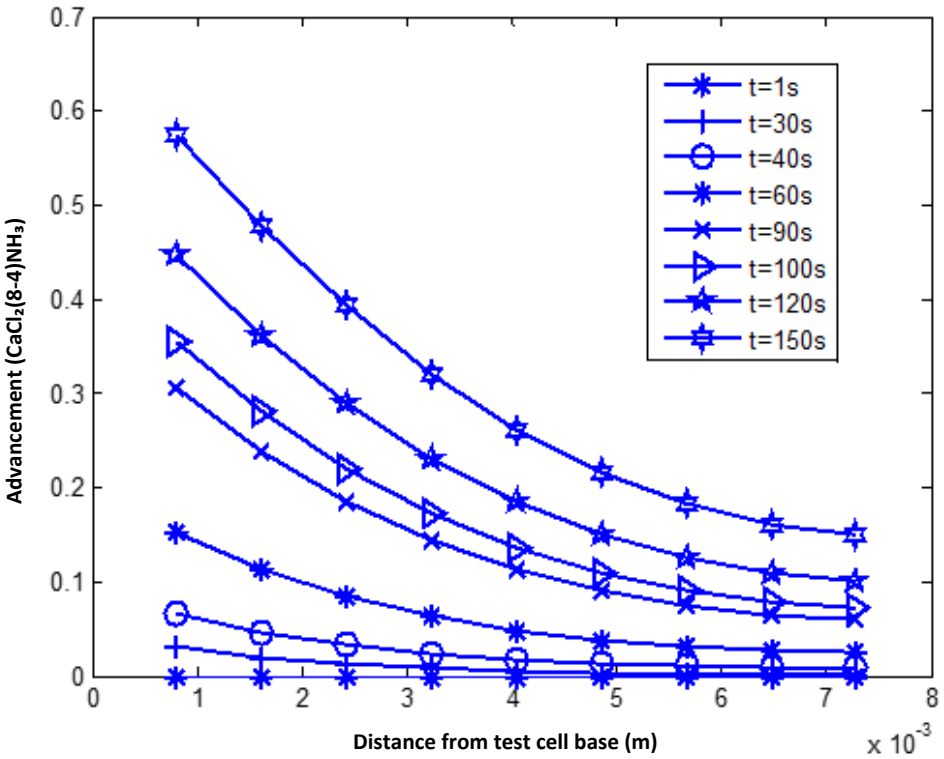

Figure 5-20: Advancement at different points in Sample 2 for Experiment 20a

5.8.4 Temperature Profile in Thinner Samples vs Thicker Samples

Generally, the temperature profiles like the advancement profiles for the thicker $CaCl_2$ sample show larger temperature differences between the layers compared to the thinner samples. This is in line with the way the modelling was done- a connection between the heat transfer and the kinetics of the reactions.

For instance, for the $CaCl_2$ samples in Experiment 2a and 20a, a stronger gradient can be observed in the thicker sample as shown in Figure 5-21 and Figure 5-22. The thicker (7.3mm) sample showed a maximum gradient of 0.36K/mm over the sample compared to only 0.17K/mm at most in the thinner (4mm) sample. Figure 5-19 and Figure 5-20 show a plot of temperature differences between the bottom and top layers of $CaCl_2$ Samples 1 and 2 during the initial 1000s of Experiments 2a and 20a. These strong variations in temperature will adversely affect the power attainable from the sample because certain portions of the sample stay at thermodynamic conditions which are lower than reaction equilibrium conditions for longer periods of time.

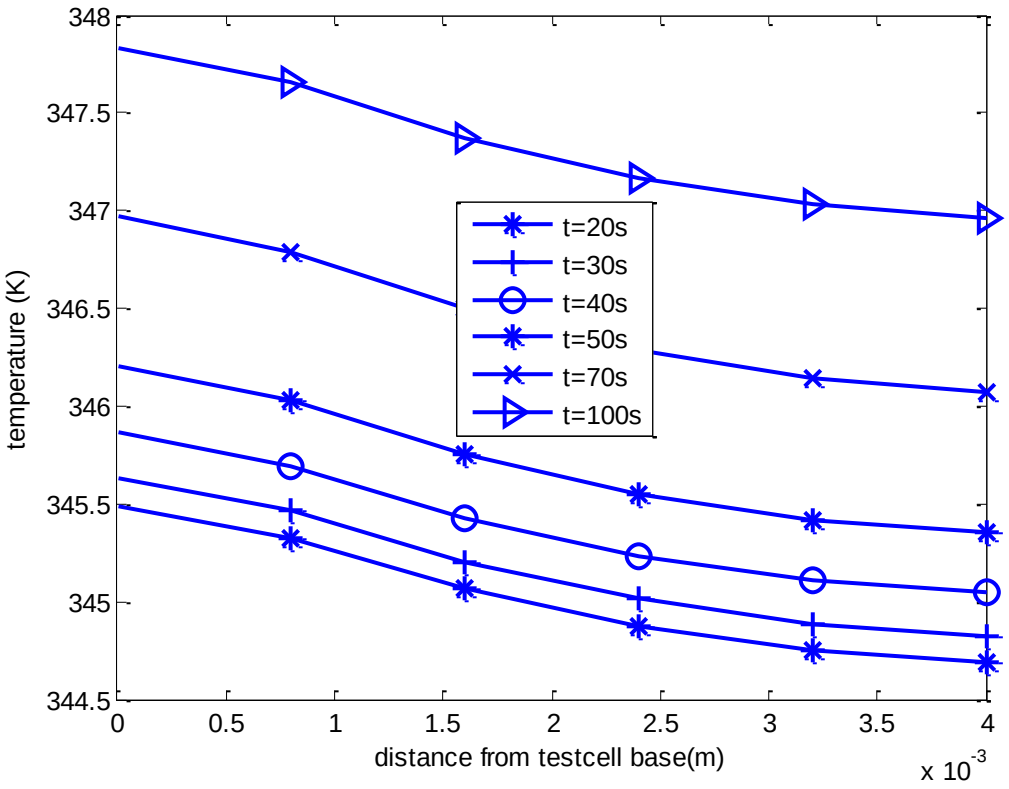

Figure 5-21: Temperature gradient for different points across Sample 1 for Experiment 2a

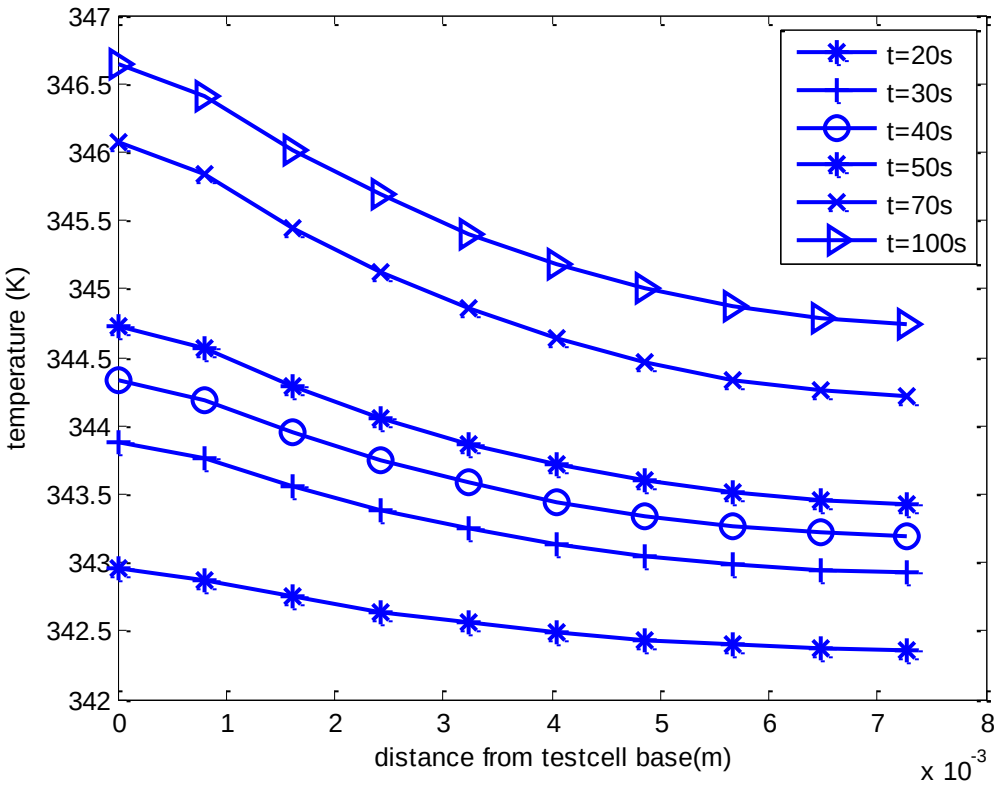

Figure 5-22: Temperature gradient for different points across Sample 2 for Experiment 20a

5.8.5 Sensitivity Study of the Specific Heat Capacity and Thermal Conductivity

The model utilised in this work has two parameters (k and C_p) which were identified outside of the model's two differential equations. Previous work in literature has identified that the sensitivity of the thermal conductivity is largely due to the physical make-up of the sample. Mazet et al[1] for example identified an increase in thermal conductivity with the proportion of binder (expanded graphite)used.

Sensitivity studying of the thermal conductivity on all the samples used in this work was carried out. In each case, the conductivity was halved and doubled and held constant for the entire reaction. Figure 5-23 and Figure 5-24 show that changes in the thermal conductivity have a huge influence on the modelled advancement profiles in the samples and consequently the advancements of reactions.

The specific heat capacity of the samples on the other hand did not seem to show much influence on the modelled pressure profiles as seen in Figure 5-25 and Figure 5-26.

However, the specific heat capacity has a small influence (not visible unless the plot is zoomed) at the beginning of the pressure profile due to the consumption of sensible heat by the reaction. Overall, it is evident that the thermal conductivity has a larger influence on the reaction rate than the heat capacity. This goes to emphasise the need for the thermal conductivity to be determined accurately and precisely when using the Anter Quickline 10 machine.

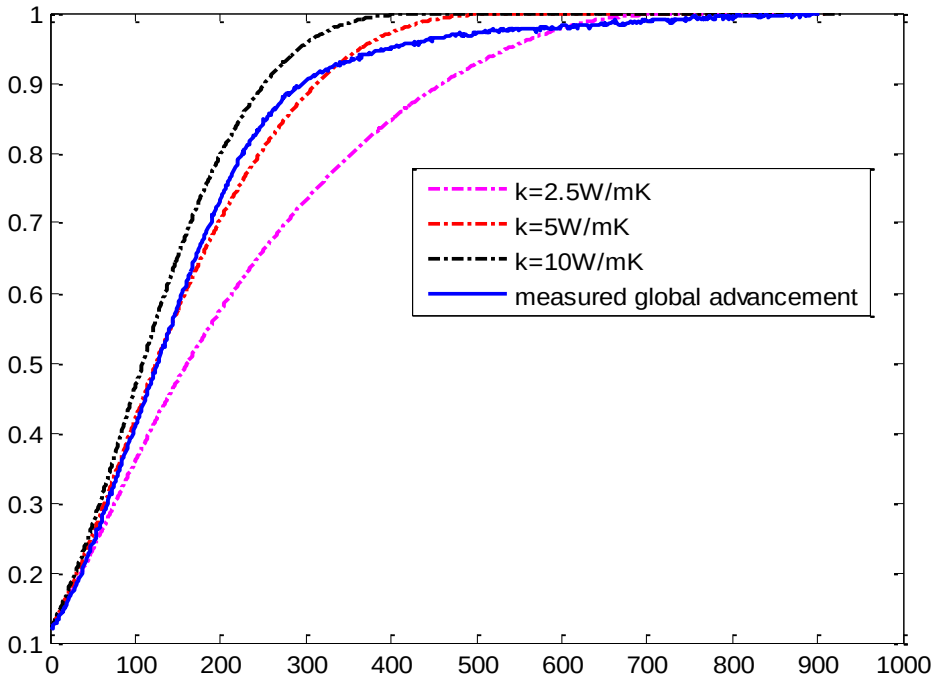

Figure 5-23: Modelled and experimental pressure profiles when thermal conductivity is varied (2.5, 5, 10$Wm^{-1}K^{-1}$) for $CaCl_2$ Sample 1 in Experiment 5a

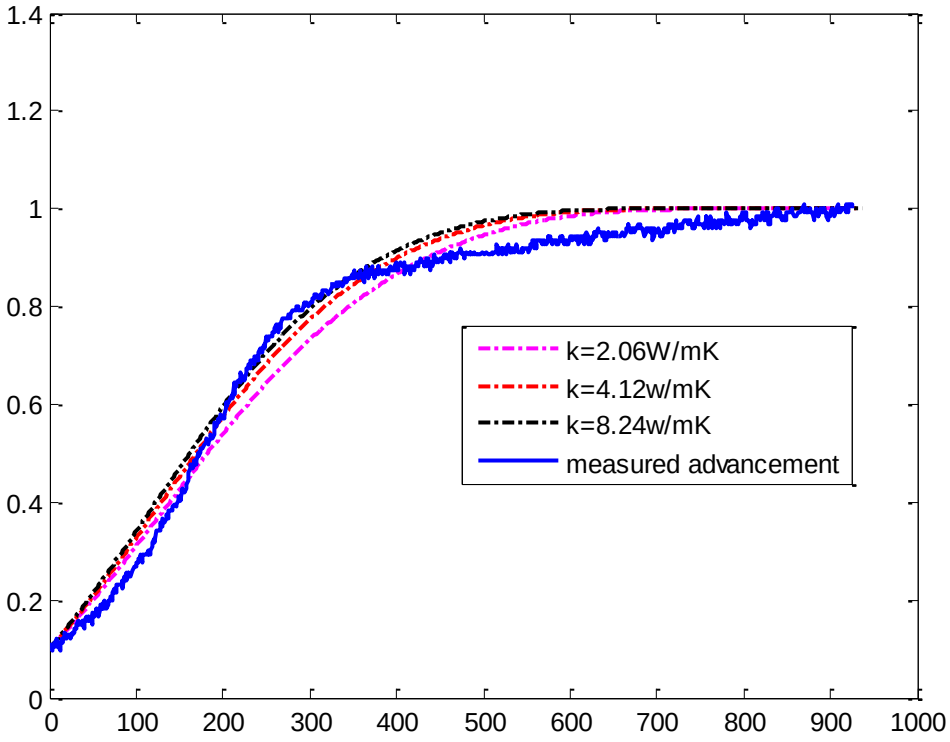

Figure 5-24: Modelled and experimental pressure profiles when thermal conductivity is varied (2.06, 4.12, 8.24$Wm^{-1}K^{-1}$) for $MgCl_2$ Sample 1 in Experiment 33a

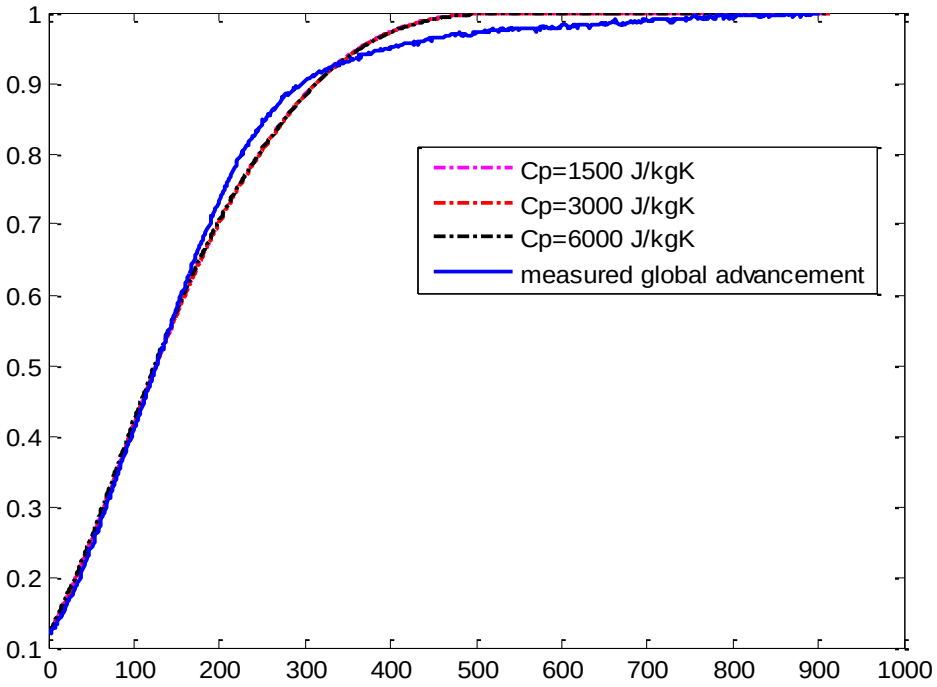

Figure 5-25: Modelled and experimental pressure profiles when specific heat capacity is varied (1000, 3000, 6000Jkg^{-1}K^{-1} for $CaCl_2$ Sample 1 in Experiment 5a

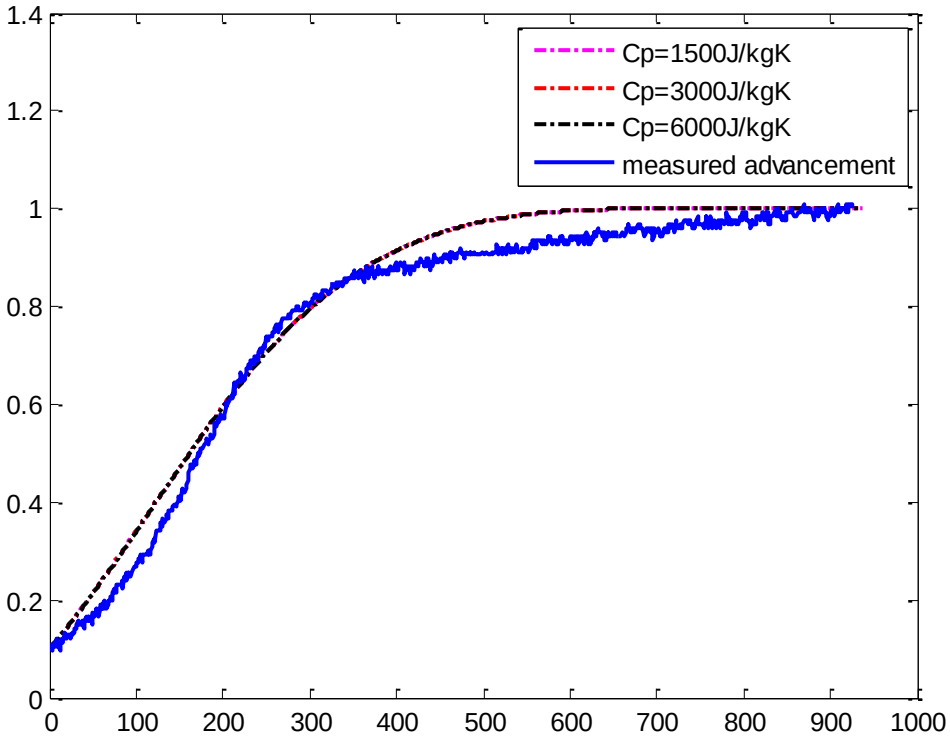

Figure 5-26: Modelled and experimental pressure profiles when specific heat capacity is varied (1000, 3000, 6000Jkg^{-1}K^{-1}) for $MgCl_2$ Sample 1 in Experiment 33a

5.9 Summary

The coupling between heat transfer and the kinetics of the reaction between certain chlorides and Ammonia was investigated using the large temperature jump rig described in the previous chapter. The model was used to derive best fit reaction rate constant (A) for all the reactions considered. The model also helped to obtain the local advancement and temperature profiles of the different layers of the samples. Sensitivity studies showed that model is sensitive to changes in thermal conductivity but not sensitive to changes in the specific heat capacity of the samples.

5.10 References

1. Zheng, W., et al., *Activated Carbon Fiber Composites For Gas Phase Ammonia Adsorption.* Microporous and Mesoporous Materials, 2016. **234**: p. 146-154.
2. Wang, L., et al., *Adsorption Performances And Refrigeration Application Of Adsorption Working Pair Of Cacl2−NH3.* Science in China Series E: Technological Sciences, 2004. **47**(2): p. 173-185.

3. Veselovskaya, J.V., M.M. Tokarev, and Y.I. Aristov, *Novel Ammonia Sorbents "Porous Matrix Modified By Active Salt" For Adsorptive Heat Transformation: 1. Barium Chloride In Various Matrices.* Applied Thermal Engineering, 2010. **30**(6–7): p. 584-589.
4. Coste, C., G. Crozat, and S. Mauran, *Gaseous-Solid Reaction*, in *Patent 4595774*, EUA, Editor. 1986.
5. Dueñas, C., et al., *Dynamic Study Of The Thermal Behaviour Of Solar Thermochemical Refrigerator: Barium Chloride-Ammonia For Ice Production.* Solar Energy Materials and Solar Cells, 2001. **70**(3): p. 401-413.
6. Oliveira, R.G. and R.Z. Wang, *A Consolidated Calcium Chloride-Expanded Graphite Compound For Use In Sorption Refrigeration Systems.* Carbon, 2007. **45**(2): p. 390-396.
7. Guangming, L., et al., *Investigation Of Thermal Decomposition Of Mgcl 2hexammoniate And Mgcl 2biglycollate Biammoniate By Dtaâ€"TG, XRD And Chemical Analysis.* Thermochimica Acta 2004. **412**(1-2): p. 149-153.
8. Bevers, E.R.T., et al., *Investigation Of Thermodynamic Properties Of Magnesium Chloride Amines By HPDSC And TG.* Journal of Thermal Analysis and Calorimetry, 2007. **90**(3): p. 923-929.
9. Jegede, O.O. and R.E. Critoph, *Extraction Of Heat Transfer Parameters In Active Carbon–Ammonia Large Temperature Jump Experiments.* Applied Thermal Engineering, 2016. **95**: p. 499-505.
10. Aristov, Y.I., et al., *A New Methodology Of Studying The Dynamics Of Water Sorption/Desorption Under Real Operating Conditions Of Adsorption Heat Pumps: Experiment.* International Journal of Heat and Mass Transfer, 2008. **51**(19–20): p. 4966-4972.
11. A.S.T.M, *Standard Test Method for Evaluating the Resistance to Thermal Transmission of Materials by the Guarded Heat Flow Meter Technique*. 2011: West Conshohocken, PA.
12. Han, J.H. and K.-H. Lee, *Gas Permeability Of Expanded Graphite–Metallic Salt Composite.* Applied Thermal Engineering, 2001. **21**(4): p. 453-463.
13. Tykodi, R.J., *Thermodynamics Of Steady States: &Ldquo;Resistance Change&Rdquo; Transitions In Steady-State Systems.* Bulletin of the Chemical Society of Japan, 1979. **52**(2): p. 564-570.

14. Goetz, V. and A. Marty, *A Model For Reversible Solid-Gas Reactions Submitted To Temperature And Pressure Constraints: Simulation Of The Rate Of Reaction In Solid-Gas Reactor Used As Chemical Heat Pump.* Chemical Engineering Science, 1992. **47**(17): p. 4445-4454.
15. Mazet, N. and M. Amouroux, *Analysis Of Heat Transfer In A Non-Isothermal Solid-Gas Reacting Medium.* Chemical Engineering Communications, 1991. **99**(1): p. 175-200.
16. Mazet, N., M. Amouroux, and B. Spinner, *Analysis And Experimental Study Of The Transformation Of A Non-Isothermal Solid/Gas Reacting Medium.* Chemical Engineering Communications, 1991. **99**(1): p. 155-174.
17. Lebrun, M. and B. Spinner, *Models Of Heat And Mass Transfers In Solid—Gas Reactors Used As Chemical Heat Pumps.* Chemical Engineering Science, 1990. **45**(7): p. 1743-1753.
18. CROFT, D.R.A. and D.G. Lilley, *Heat Transfer Calculations Using Finite Difference Equations*. 1977: Applied Science Pub.

Chapter 6 : Concept Design and Performance Analysis of a Double Effect Thermochemical Heat Pump Using the $CaCl_2$-NH_3 and the $MgCl_2$-NH_3 Pairs

6.1 Introduction

Single effect thermochemical heat pumps can attain COPs which are higher than those of physical adsorption heat pumps based on activated carbon, silica or zeolites. However, these COPs could be even higher if the sensible heat which is lost during the synthesis phase of the cycle can be reutilised within the system utilising internal heat recovery. The sensible heat from synthesis in one reactor is recovered and used to drive decomposition in another reactor.

The earliest instances of the use of the heat recovery concept were in adsorption systems were found in Douss et al[1] and Tchernev[2] in the form of regenerative cycles. At the beginning of the cycle described by Tchernev, the heat from one Zeolite bed during its adsorption stage was used to preheat the heating fluid for desorption in another Zeolite bed, thereby reducing the heat required from an external boiler and improving efficiency. A more recent example based on the activated carbon-methanol working pair was described by Wang et al [3]. Here, the regenerative cycles attained COP levels which were 20% higher than those for a basic cycle without heat recovery.

The internal heat recovery cycle which was used in this work is a cascading cycle which involves two different working pairs (Magnesium Chloride-Ammonia and Calcium Chloride-Ammonia) which have different equilibrium temperatures at a specific evaporation or condensation pressure. The heat of reaction from the synthesis of the higher temperature salt ($MgCl_2$) and the sensible heat of the higher temperature salt are transferred to the lower temperature salt ($CaCl_2$) for decomposition. There are recent instances [4-6] in the literature that document thermochemical systems which are based on this internal heat recovery principle. However, none of these systems use $MgCl_2$ and $CaCl_2$ in a heating application. Possible real world applications include at the high temperature (290°C) level of the external heat supply in this work include:

1. Producing cooling from process steam condensate in the food processing industry. Typical temperature range- 190°C-300°C.

2. Heat pumping using heat recovered from the cooling water from annealing furnaces. Typical temperature range- 150°C-450°C.
3. Producing cooling using heat recovered from drying, baking and curing ovens. Typical temperature range- 90°C-450°C.

In this work, a design and the working principle of the aforementioned cascading thermo-chemical heat pump is presented. This is followed by a presentation of the equations which are relevant to the design of the heat pump. There are a number of parameters which influence the performance of a chemical heat pump. A model was developed to investigate the effect of the parameters on the performance (COP and SHP) and to compare with single salt systems.

6.2 System Design and Working Principle

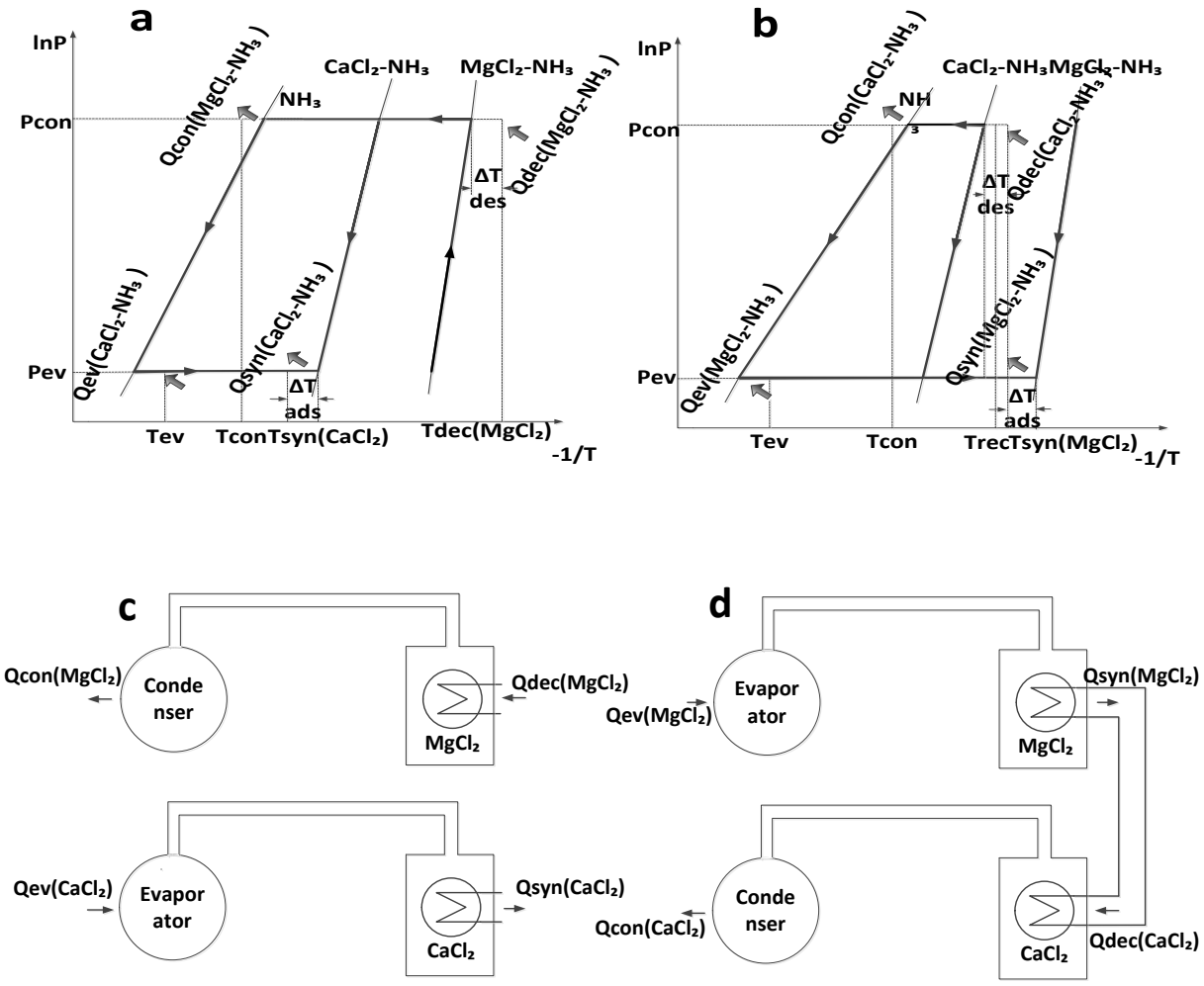

Figure 6-1: Clapeyron diagram and schematics for $MgCl_2$-NH_3 and $CaCl_2$-NH_3 cascading cycle: a,c) Phase 1-decomposition of $MgCl_2$ and synthesis of $CaCl_2$ b,d) Phase 2-decomposition of $CaCl_2$ and synthesis of $MgCl_2$ and internal heat recovery

Figure 6-1 shows the operating principle of the double effect thermo-chemical heat pump which was proposed in this work. The system comprises two salt reactors (one for the Magnesium Chloride salt and another for the Calcium Chloride salt), a condenser and an evaporator. The operation of this double effect system is in two phases. It begins with a first phase (Figure 6-1a and Figure 6-1c) where there is an application of heat through an external heat source to the Magnesium Chloride ($MgCl_2$) reactor for decomposition. This initial decomposition causes NH_3 gas to flow into the condenser and condense at T_{con} releasing a first portion of useful heat

($Q_{con(MgCl_2\text{-}NH_3)}$). At the same time, the Calcium Chloride ($CaCl_2$) reactor is being cooled and it synthesises at $T_{syn(CaCl_2)}$ with NH_3 gas which is evaporated from the evaporator at T_{ev}. This synthesis process produces second portion of useful heat ($Q_{syn(CaCl_2\text{-}NH_3)}$) at $T_{syn}(CaCl_2)$.

In the second working phase of the system (Figure 6-1b and Figure 6-1d), the $MgCl_2$ reactor undergoes synthesis at $T_{syn(MgCl_2)}$ with NH_3 gas from the evaporator producing heat ($Q_{syn(MgCl_2\text{-}NH_3)}$). This heat is transferred to the $CaCl_2$ reactor for decomposition through an internal recovery process and removing the need for an external heat source to decompose the $CaCl_2$. The decomposition in the $CaCl_2$ reactor causes refrigerant to travel into the condenser, producing a third portion of useful heat ($Q_{con(CaCl_2\text{-}NH_3)}$). In all, three streams of useful heat are obtained from the system by the application of one high temperature heat input.

6.3 The Working Pairs

The working pairs ($CaCl_2$-NH_3 and $MgCl_2$-NH_3) used in the design of a thermochemical heat pump in this chapter were studied in the previous chapter. The focus was on the kinetics of the reactions which are relevant to this work. To this end, a kinetic parameter (A) and pseudo-order (yo) were obtained for each reaction which will be used in this chapter. The A and yo values which were obtained for each of the reactions are shown in Table 6-1.

Table 6-1: A and yo values obtained for the $CaCl_2$-NH_3 and $MgCl_2$-NH_3 reactions

		A (s^{-1})	yo
$CaCl_2$-NH_3 (R1)	a	0.037	0.72
	b	0.02	0.71
$CaCl_2$-NH_3 (R2)	a	0.0069	0.81
	b	0.0057	0.83
$MgCl_2$-NH_3 (R1)	a	0.00013	0.64
	b	0.000056	0.72

The aforementioned salts were not chosen at random. Preliminary calculations showed that these salts were compatible for the internal heat recovery process which occurs in the second phase of the operation of the system.

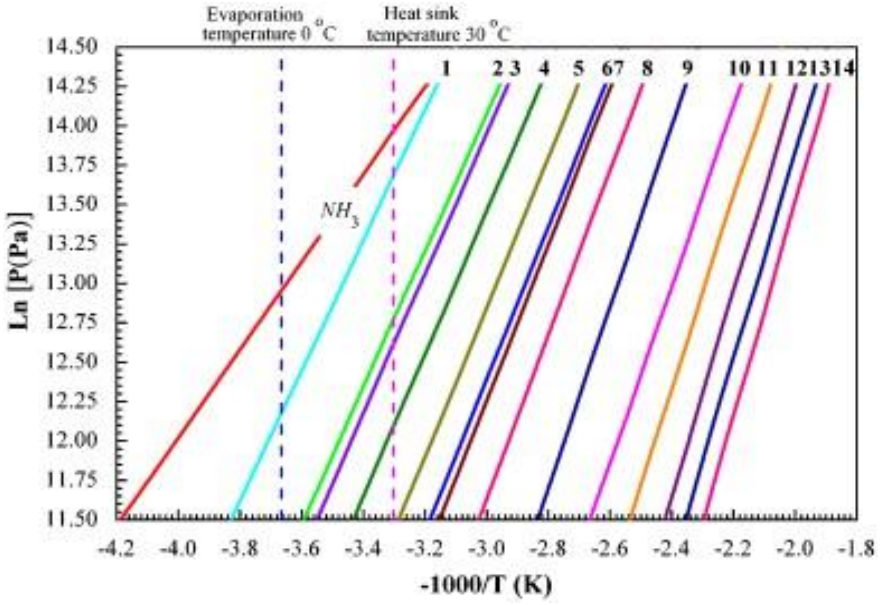

Figure 6-2: Metal chloride-Ammonia lines shown on a Clapeyron diagram[5]. 1=$PbCl_2$ (8/3.25); 2=$BaCl_2$ (8/0); 3=$LiCl_2$ (4/3); 4=$AgCl_2$ (3/1.5); 5=$CaCl_2$ (8/4); 6=$SrCl_2$ (8/1); 7=$CaCl_2$ (4/2); 8=$CdCl_2$ (6/2); 9=$ZnCl_2$ (6/2); 10=$MnCl_2$ (6/2); 11=$FeCl_2$ (6/2); 12=$CoCl_2$ (6/2); 13=$MgCl_2$ (6/2); 14=$NiCl_2$ (6/2)

Figure 6-2 shows the equilibrium lines for other common metal chloride ammonia reactions. When selecting salts from this plot for the design of a double effect thermochemical heat pump, two fundamental conditions must be satisfied. Using the system proposed in this work (Figure 6-2) as an example, they are:

1. $T_{syn(CaCl_2)}$, the lowest salt-NH_3 equilibrium in the system must be greater than T_{con} to keep the $CaCl_2$-NH_3 safe distance away from any potential of condensation of refrigerant on the wrong side of the system.
2. Internal heat recovery as described in this work is only possible when the synthesis heat of the $MgCl_2$-NH_3 reaction is greater than the decomposition heat required for the subsequent $CaCl_2$-NH_3 reaction and there is a sufficient temperature difference (ΔT_{des}) to drive the process as shown in Figure 6-1b. Therefore, $T_{syn(MgCl_2)}$ must be greater than $T_{dec(CaCl_2)}$.

6.4 Energy and Performance Equations

The summation of all the energy which goes in and out of the heat pump must be zero. It is in this light that the following equations were obtained for each of the different

components of the system. Each of the solid-gas reactor are modelled based on the method described in the previous chapter which is based on a coupling between heat transfer and reaction kinetics. The following assumptions are used.

- All of the process happens at constant volume and so no work is done
- The two reactors are identical and only differ in length, which is directly related to the mass of salt each contains
- The ammonia gas pressure throughout the reactor is uniform
- Heat transfer in the reactors is radial alone
- There are no heat losses to the environment

6.4.1 The Reactors

Assuming an initial $MgCl_2$ mass of 1kg. The amount of NH_3 which reacts with 1kg of $MgCl_2$ can be obtained using Equation (5.32)

$$m_{NH3(MgCl2)} = \frac{N m_{MgCl2} M_{NH3}}{M_{MgCl2}} \tag{5.32}$$

The maximum possible mass of $CaCl_2$ which is required is determined by the amount of heat energy produced by the synthesis stage of the $MgCl_2$-NH_3 reaction. The decomposition energy process in the two reactors can be described by Figure 6-3 and Equation (5.33) , Equation (5.34), Equation (5.35), Equation (5.36) and Equation (5.37). Here, the temperature of the loaded salt is taken from T_{syn} to T_{dec}. The total heat input here is a combination of the sensible heat ($\Delta H_{sensible}$) of the loaded salt and the heat of reaction ($\Delta H_{reaction}$).

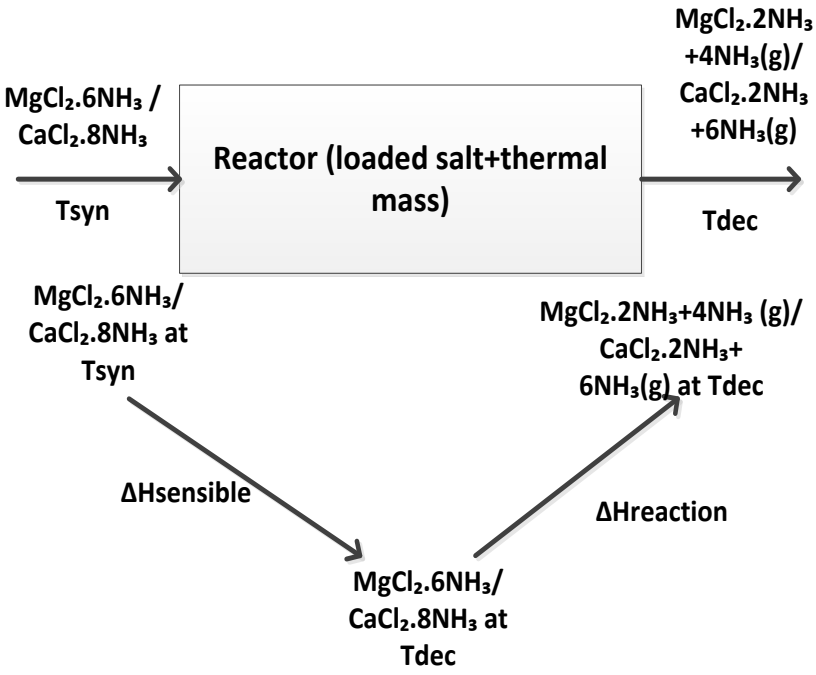

Figure 6-3: Decomposition energy flow in the $MgCl_2$ reactor

$$Q_{dec} = \Delta H_{sensible} + \Delta H_{reaction} \tag{5.33}$$

$$Q_{dec(MgCl_2)} = \int_{T_{syn(MgCl_2)}}^{T_{dec(MgCl_2)}} m_{MgCl_2+ENG+NH_3} Cp_{MgCl_2+ENG+NH_3} dT + m_{NH_3(MgCl_2)} \Delta H_{MgCl_2(6\text{-}2)NH_3}$$

(5.34)

$$Q_{dec(MgCl_2)} = m_{MgCl_2+ENG+NH_3} Cp_{MgCl_2+ENG+NH_3} \left(T_{dec(MgCl_2)} - T_{syn(MgCl_2)}\right) + m_{NH_3(MgCl_2)} \Delta H_{MgCl_2(6\text{-}2)NH_3}$$

(5.35)

$$Q_{dec(CaCl_2)} = \int_{T_{syn(CaCl_2)}}^{T_{dec(CaCl_2)}} m_{CaCl_2+ENG+NH_3} Cp_{CaCl_2+ENG+NH_3} dT + m_{NH_3(CaCl_2)} \Delta H_{CaCl_2(8\text{-}2)NH_3}$$

(5.36)

$$Q_{dec(CaCl_2)} = m_{CaCl_2+ENG+NH_3} Cp_{CaCl_2+ENG+NH_3} \left(T_{dec(CaCl_2)} - T_{syn(CaCl_2)}\right) + m_{NH_3(CaCl_2)} \Delta H_{CaCl_2(8\text{-}2)NH_3}$$

(5.37)

6.4.1.1 Heat Transfer within the Reactor

The reactor is modelled as a stainless steel tube heat transfer tube surrounded radially by salt composite. Heat is transferred to or taken from the salt composite through a constant temperature heat source contained in the heat transfer tube. The heat transfer is modelled only in one dimension in the radial direction and the temperature profile is considered constant axially. The cross-section of the reactor model is shown in Figure 6-4.

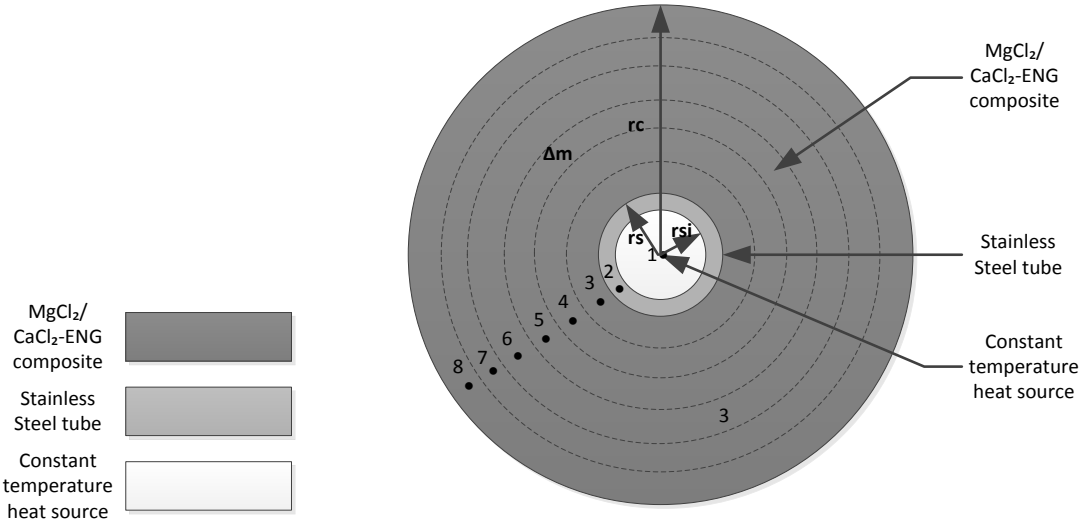

Figure 6-4: Cross-sectional view of the reactor

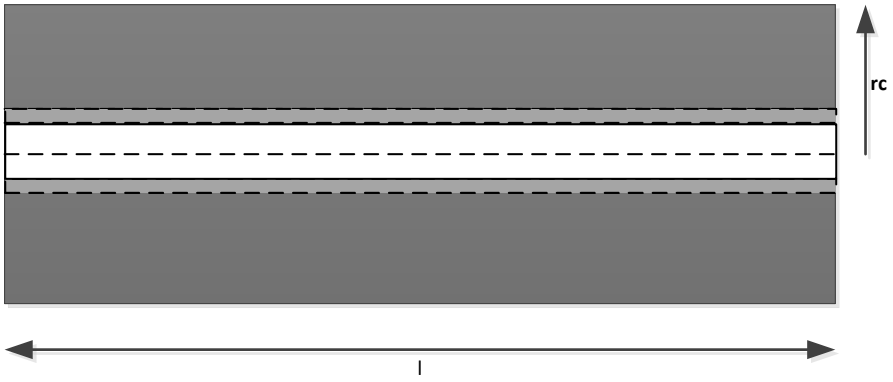

Figure 6-5: Longitudinal view of reactor

The one dimensional heat transfer model used was similar to that which was used in previous chapters. The reactor is divided into discrete finite difference volumes. Each volume contains a node. The first node (1) is the constant temperature heat source, the

second node (2) is midway into the thickness of the stainless steel tube. The rest of the nodes are spread out in the composite salt in equal distances.

The temperature of node 1 was set as a Dirichlet boundary condition. For each of the other nodes, an energy balance was conducted in terms of the rate of heat flow into it from neighbouring nodes and the heat produced and consumed as a result of the reactions between the salts and NH_3. Taking node 4 as an example, the energy balance is conducted in terms of the rate of heat flow from node 3 and node 5.

Equations (5.38), (5.39) and (5.40) give the energy balance for the second node, the middle nodes and the last node respectively for a decomposition reaction, highlighting the relevant thermal resistances in each case.

$$\Delta mC_{pi}{}^{2}\left(\frac{T_i^2 - T_{i-1}^2}{\Delta t}\right) = \left(\frac{T_i^1 - T_{i-1}^2}{1/h_{htf}S + \ln\left(rs/rsi\right)/2\pi k_{steel}l}\right) + \left(\frac{T_{i-1}^3 - T_{i-1}^2}{\ln\left(r3/r2\right)/2\pi k_{salt}l}\right)$$

(5.38)

$$\Delta mC_{pi}{}^{j}\left(\frac{T_i^j - T_{i-1}^j}{\Delta t}\right) = \left(\frac{T_{i-1}^{j-1} - T_{i-1}^j}{\ln\left(r_j/r_{j-1}\right)/2\pi k_{salt}l}\right) + \left(\frac{T_{i-1}^{j+1} - T_{i-1}^j}{\ln\left(r_{j+1}/r_j\right)/2\pi k_{salt}l}\right) - N_{NH_3}\Delta H\frac{\Delta X_i^j}{\Delta t}$$

(5.39)

$$\Delta mC_{pi}{}^{8}\left(\frac{T_i^8 - T_{i-1}^8}{\Delta t}\right) = \left(\frac{T_{i-1}^7 - T_{i-1}^8}{\ln\left(r_8/r_7\right)/2\pi k_{salt}l}\right) - N_{NH_3}\Delta H\frac{\Delta X_i^8}{\Delta t} \qquad (5.40)$$

In these case of synthesis reaction, the heat loss to incoming cold gas from the evaporator must be taken into account. Therefore, Equation (5.39) and Equation (5.40) become Equation (5.41) and Equation (5.42).

$$\Delta mC_{pi}{}^{j}\left(\frac{T_i^{j}-T_{i-1}^{j}}{\Delta t}\right)=\left(\frac{T_{i-1}^{j-1}-T_{i-1}^{j}}{\ln\left(r_j/r_{j-1}\right)/2\pi k_{salt}l}\right)+\left(\frac{T_{i-1}^{j+1}-T_{i-1}^{j}}{\ln\left(r_{j+1}/r_j\right)/2\pi k_{salt}l}\right)+N_{NH_3}\Delta H\frac{\Delta X_i^{j}}{\Delta t}-\Delta mx_i^{j}C_{p,NH_3}\left(\frac{T_{i-1}^{j}-T_{ev}}{\Delta t}\right)$$

(5.41)

$$\Delta mC_{pi}{}^{8}\left(\frac{T_i^{8}-T_{i-1}^{8}}{\Delta t}\right)=\left(\frac{T_{i-1}^{7}-T_{i-1}^{8}}{\ln\left(r_8/r_7\right)/2\pi k_{salt}l}\right)+N_{NH_3}\Delta H\frac{\Delta X_i^{8}}{\Delta t}-\Delta mx_i^{8}C_{p,NH_3}\left(\frac{T_{i-1}^{8}-T_{ev}}{\Delta t}\right)$$

(5.42)

In the equations above, the superscript (j) on the different terms represents the position of the node in the discretised space while the subscript (i) is the simulation time.

6.4.2 Condenser

The superheated gas leaving the $MgCl_2$/ $CaCl_2$ reactor condenses in the condenser and the heat released makes up the first portion of useful heat in this system in the case of the $MgCl_2$ and the third portion in the case of $CaCl_2$. These portions of heat are made up of the sensible heat and the heat of condensation of the refrigerant. Figure 6-6 shows the flow of energy through the condenser. Equation (5.43), Equation (5.44), Equation (5.45), Equation (5.46), and Equation (5.47) show the energy balance in the condenser.

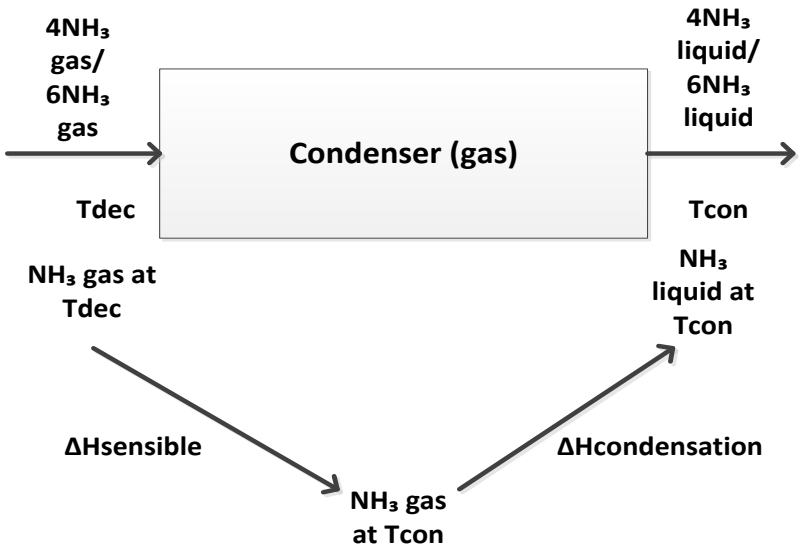

Figure 6-6: 1st condensation energy flow

$$Q_{con} = \Delta H_{sensible} + \Delta H_{condensation} \tag{5.43}$$

$$Q_{con(MgCl_2)} = \int_{T_{con}}^{T_{dec(MgCl_2)}} m_{NH_3(MgCl_2)} Cp_{NH_3(g)} dT + m_{NH_3(MgCl_2)} \Delta H_{con(MgCl_2)} \tag{5.44}$$

$$Q_{con(MgCl_2)} = m_{NH_3(MgCl_2)} \left(\Delta H_{con(MgCl_2)} + (Cp_{gNH_3} (T_{dec(MgCl_2)} - T_{con})) \right) \tag{5.45}$$

$$Q_{con(CaCl_2)} = \int_{T_{con}}^{T_{dec(CaCl_2)}} m_{NH_3(CaCl_2)} Cp_{NH_3(g)} dT + m_{NH_3(CaCl_2)} \Delta H_{con(CaCl_2)} \tag{5.46}$$

$$Q_{con(CaCl_2)} = m_{NH_3(CaCl_2)} \left(\Delta H_{con(CaCl_2)} + (Cp_{NH_3(g)} (T_{dec(CaCl_2)} - T_{con})) \right) \tag{5.47}$$

6.4.3 Evaporator

The condensed liquid NH_3 goes into the evaporator where it boils. The summation of the heat at this stage is the sensible heat and the heat of vaporisation of the refrigerant. The energy flow for the evaporation process is shown in Figure 6-7 and Equation (5.48) , Equation (5.49) and Equation (5.50) show the energy balance in evaporation.

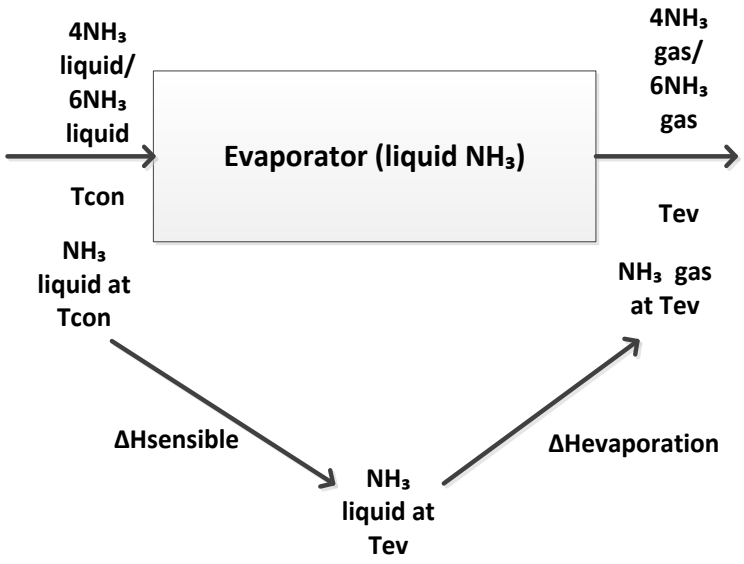

Figure 6-7: Evaporation energy flow

$$Q_{ev(MgCl_2)} = \Delta H_{sensible} + \Delta H_{evaporation} \tag{5.48}$$

$$Q_{ev(MgCl_2)} = \int_{T_{ev}}^{T_{con}} m_{NH_3(MgCl_2)} Cp_{gNH_3} dT + m_{NH_3(MgCl_2)} \Delta H_{evap(NH_3)} \tag{5.49}$$

$$Q_{ev(MgCl_2)} = m_{NH_3(MgCl_2)} \left(\Delta H_{evap(MgCl_2)} + (Cp_{gNH3}(T_{con} - T_{ev})) \right) \tag{5.50}$$

$$Q_{ev(CaCl_2)} = \int_{T_{ev}}^{T_{con}} m_{NH_3(CaCl_2)} Cp_{NH_3(g)} dT + m_{NH_3(CaCl_2)} \Delta H_{evap(NH_3)} \tag{5.51}$$

$$Q_{ev(CaCl_2)} = m_{NH_3(CaCl_2)} \left(\Delta H_{evap(CaCl_2)} + (Cp_{NH3(g)}(T_{con} - T_{ev})) \right) \tag{5.52}$$

6.4.4 Internal Heat Recovery

The internal heat recovery was idealised by assuming an overall heat transfer coefficient (UA) between the $MgCl_2$ and $CaCl_2$ reactor tubes. At every time step through the heat recovery period, the heat lost by the $MgCl_2$ reactor tube is exactly the same as the heat gained by the $CaCl_2$ reactor tube. Equation (5.53) and Equation (5.54) describe the internal heat recovery process.

$$-dQ_{MgCl_2 tube} = dQ_{CaCl_2 tube} \tag{5.53}$$

$$-m_{MgCl_2 tube} Cp_{steel} \Delta T_{MgCl_2 tube} = m_{CaCl_2 tube} Cp_{steel} \Delta T_{CaCl_2 tube} = UA\Delta T_{(MgCl_2 tube\text{-}CaCl_2 tube)} \quad (5.54)$$

6.4.5 Coefficient of Performance

6.4.5.1 Single Effect

The coefficient of performance (COP) of a single effect system using only either $MgCl_2$ or $CaCl_2$ is given by Equation (5.55) or Equation (5.56).

$$COP_{CaCl_2} = \frac{Q_{con(CaCl_2)} + Q_{syn(CaCl_2)}}{Q_{dec(CaCl_2)}} \quad (5.55)$$

$$COP_{MgCl_2} = \frac{Q_{con(MgCl_2)} + Q_{syn(MgCl_2)}}{Q_{dec(MgCl_2)}} \quad (5.56)$$

6.4.5.2 Double Effect

The coefficient of performance (COP) of a double effect system using both $MgCl_2$ and $CaCl_2$ is given by Equation (5.57).

$$COP_{CaCl_2 \& MgCl_2} = \frac{Q_{con(MgCl_2)} + Q_{con(MgCl_2)} + Q_{syn(CaCl_2)} + Q_{syn(MgCl_2)} - Q_{dec(CaCl_2)}}{Q_{dec(MgCl_2)}} \quad (5.57)$$

6.4.6 Specific Heating Power

6.4.6.1 Single Effect

The specific heating power (SHP) of a single effect system using only either $MgCl_2$ or $CaCl_2$ is given by Equation (5.58) or Equation (5.59). The SHP is measured in W/m^3 rather than W/kg. This is because it is more important to minimise the volume of the reactor rather than the mass.

$$SHP_{CaCl_2} = \frac{Q_{con(CaCl_2)} + Q_{syn(CaCl_2)}}{V_{CaCl_2}} \quad (5.58)$$

$$SHP_{MgCl_2} = \frac{Q_{con(MgCl_2)} + Q_{syn(MgCl_2)}}{V_{MgCl_2}} \quad (5.59)$$

6.4.6.2 Double Effect

The specific heating power (SHP) of a double effect system using both $MgCl_2$ and $CaCl_2$ is given by Equation (5.60).

$$SHP_{CaCl_2 \& MgCl_2} = \frac{Q_{con(CaCl_2)} + Q_{con(MgCl_2)} + Q_{syn(CaCl_2)} + Q_{syn(MgCl_2)} - Q_{dec(CaCl_2)}}{V_{CaCl_2 \& MgCl_2}} \quad (5.60)$$

6.5 Simulated System Performance Analysis

A dynamic model was developed to simulate the system with internal heat recovery between the two reactors. The kinetics and heat transfer within the individual reactions was modelled using the heat transfer-kinetics coupling which was described in Chapter 5. Mass transfer resistance was ignored because of the high pressure in the system and the porous nature of the salt-ENG composites. The parameters used in the performance analysis are shown in Table 6-2.

Table 6-2: Reactor Parameters

Parameter	$MgCl_2$	$CaCl_2$
Density (kgm^{-3})	205	205
% Mass of Salt Content	43	43
Thermal Conductivity ($Wm^{-1}K^{-1}$)	4.12	4.82
No of NH_3 moles reacted per mole of salt (mol)	4	6
Specific Heat Capacity ($Jkg^{-1}K^{-1}$)	747	657
Molar Mass ($kgmol^{-1}$)	0.11098	0.095211

The mass of the $MgCl_2$ in the $MgCl_2$ reactor was set to 1kg while the mass of the $CaCl_2$ in the $CaCl_2$ reactor was determined based on the amount of heat produced by the $MgCl_2$-NH_3 synthesis reaction in order to complete the $CaCl_2$ reaction. The system performance in this work is measured through the coefficient of performance (COP) and the specific heating power (SHP). The COP and SHP were analysed by going through a series of cases. The results of the analyses are discussed in sub-sections 6.5.1, 6.5.2, 6.5.3, 6.5.4, 6.5.5 and 6.5.6.

6.5.1 The Working Process of the Heat Pump Model (Evolution of Time, Pressure and Concentration and Clapeyron Diagram)

The evolution of the temperature, pressure and concentration of NH_3 in the two different reactors are presented in Figure 6-8, Figure 6-9 and Figure 6-10.The general baseline parameter details used to generate these profiles are shown in Table 6-3.

Table 6-3: Baseline parameters

Parameter	Value
Condenser Temperature (K)	323.15
Evaporator Temperature (K)	263.15
$CaCl_2/MgCl_2$ Mass Ratio (-)	1.79
Cycle Time (s)	2400

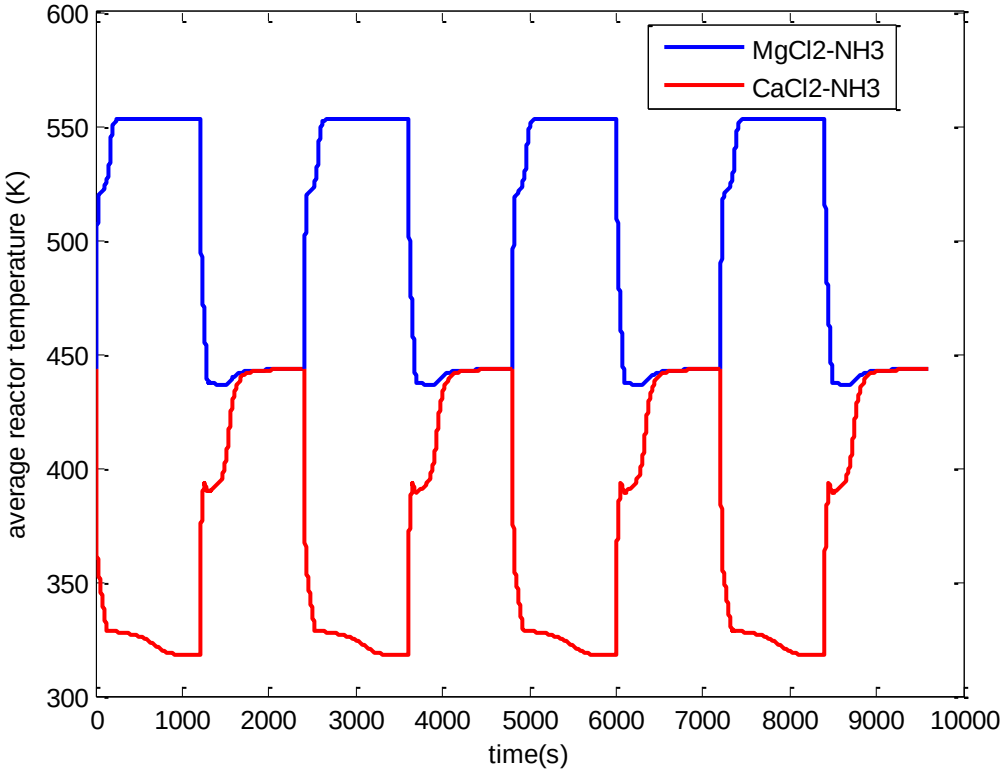

Figure 6-8: Average temperature in the reactors

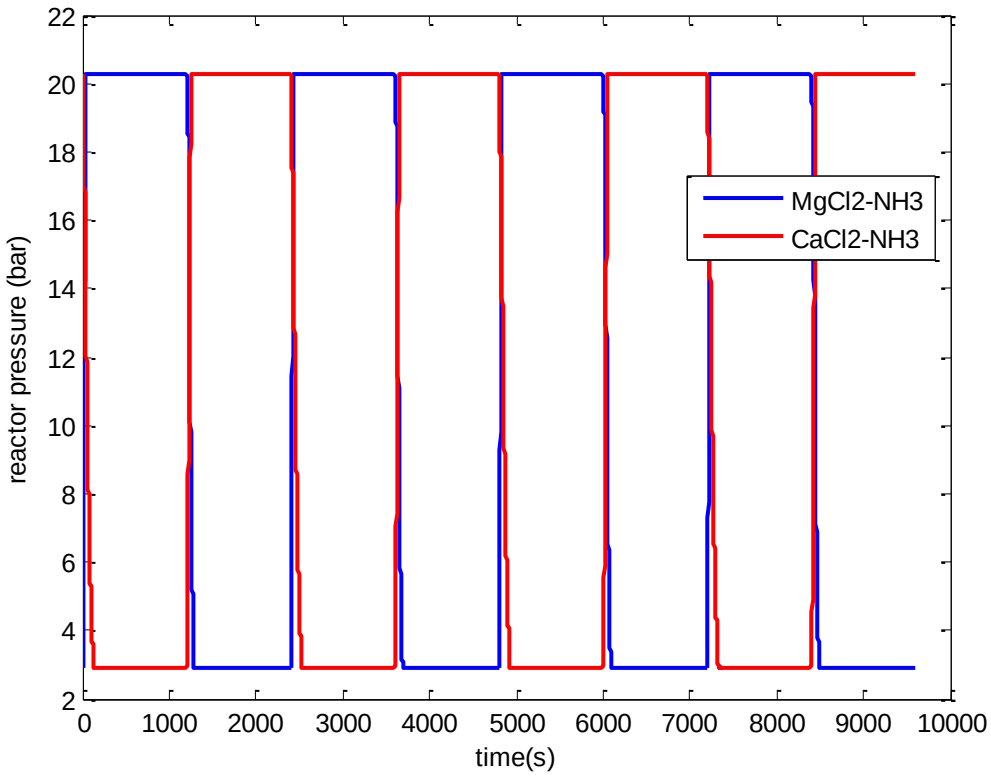

Figure 6-9: Pressure in the reactors

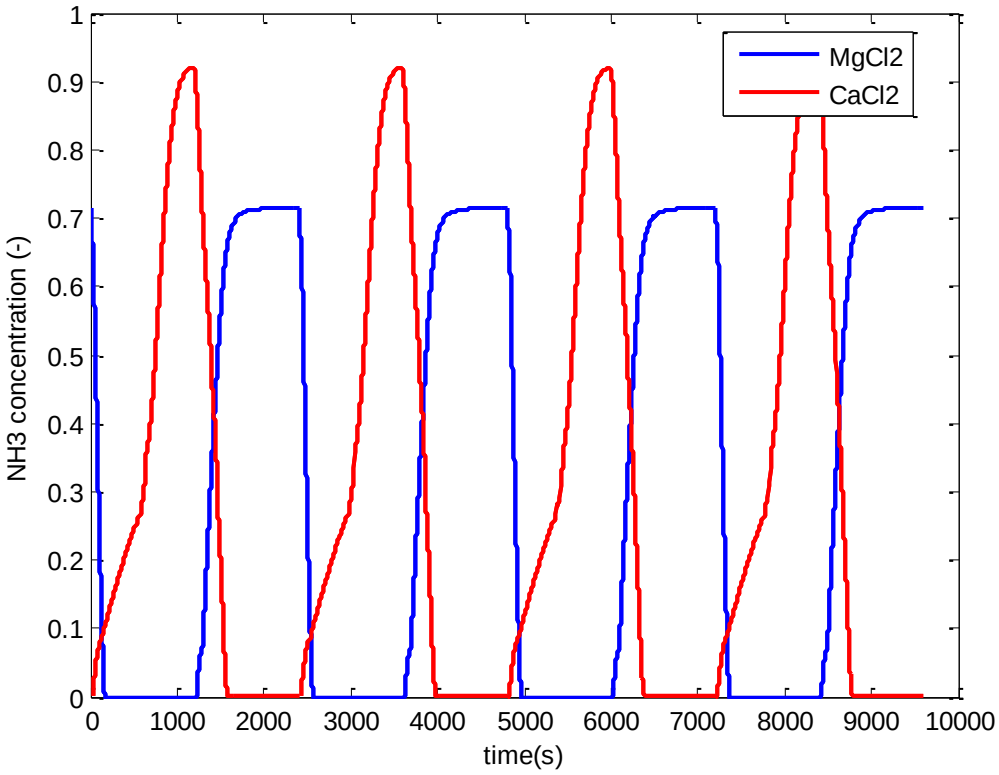

Figure 6-10: NH3 concentration in the two salts (kg of NH_3 per kg of salt)

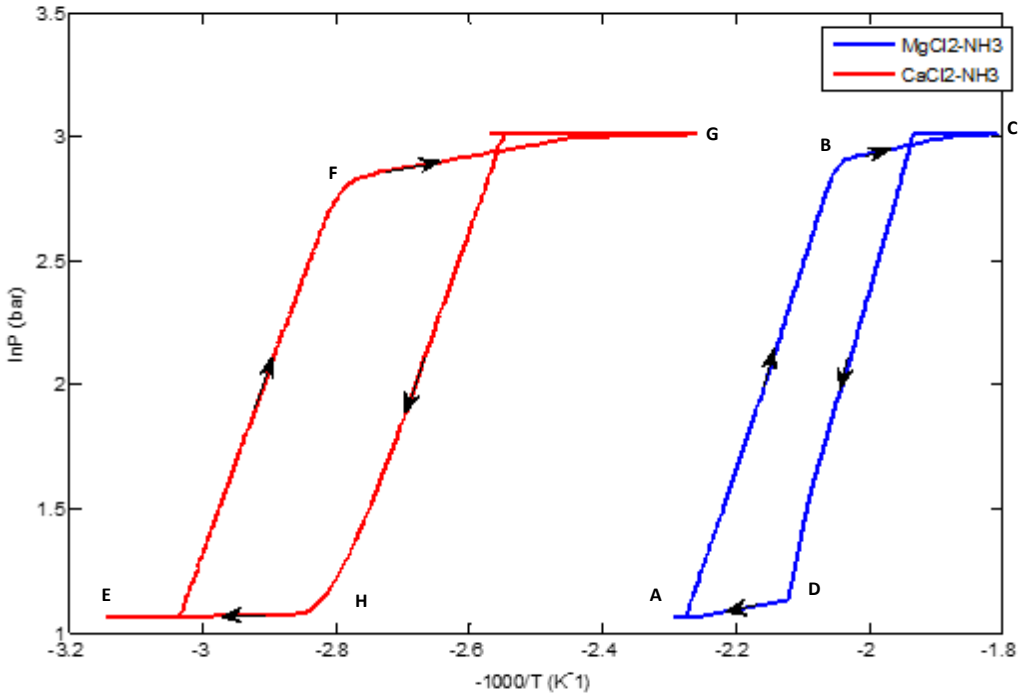

Figure 6-11: Clapeyron diagram for the two reactions

The temperature profile for four consecutive cycles is shown above in Figure 6-8. In the first phase of a cycle, the average temperature of the $MgCl_2$ reactor is raised by an external heat source to $T_{dec(MgCl_2)}=286°C$ shown by the blue line. The $CaCl_2$ on the other hand is cooled by an external cooler shown by the red line at $T_{syn(CaCl_2)}=45°C$. In phase 2, there is a heat recovery process between the $MgCl_2$ reactor and the $CaCl_2$ reactor bringing their temperatures $T_{dec(MgCl_2)}=286°C$ and $T_{syn(CaCl_2)}=45°C$ respectively to $T_{rec}=167°C$. During this phase, it is important that the $CaCl_2$ reactor is sized such that the heat from the $MgCl_2$-NH_3 synthesis process is sufficient for the $CaCl_2$-NH_3 decomposition process.

Figure 6-9 also shows the evolution of the pressure profile over time. Since the reactors are not linked, the pressures are different. In the first phase, when the $MgCl_2$ reactor is being decomposed, the pressure in the reactor increases steadily until before reaching a constant pressure of 20bar which is imposed by the condenser. At the same

time the $CaCl_2$ reactor loses pressure until it is kept constant by the evaporator at 2.9bar as shown in Figure 6-9. For the second phase, the cases are simply reversed.

The concentration of NH_3 in the salts is shown in Figure 6-10. The periods of increasing concentration correspond with periods of decreasing pressure in the reactor because synthesis reactions remove NH_3 gas from the reactor. The maximum concentration of 6 moles of NH_3 in $CaCl_2$ was 0.92 kg/kg while the maximum concentration of 4 moles of NH_3 in $MgCl_2$ was 0.71 kg/kg. The Clausius Clapeyron diagram shown in Figure 6-11 describes the cycle used in this work. Points D to A and H to E represent the synthesis phase of the two salts while points B to C and F to G represent the decomposition phase in the two reactors. The concentration of NH_3 in the salts is at its lowest at C and G for the $MgCl_2$ and the $CaCl_2$ respectively and at the highest at A and E respectively.

6.5.2 Effects of External Heat Source Temperature

The temperature of the external heating source is an important parameter in the design of thermochemical heat pumps which must be studied. Figure 6-12 shows how variations of the external heat source temperatures affect the SHP and the COP level. These results suggest that the changes in heating and cooling fluid temperature which were made had effects on both the SHP and the COP. Specifically, higher external heat source temperatures produced better SHP levels but lower COP levels. Nevertheless, there is an unusual kink in the curves at around 240°C which requires further study. This may be due to the plateauing of any improvements in reaction rates based on increase in external heat temperature, meaning that nearly the same condensation heat is obtained at the expense of more heat input.

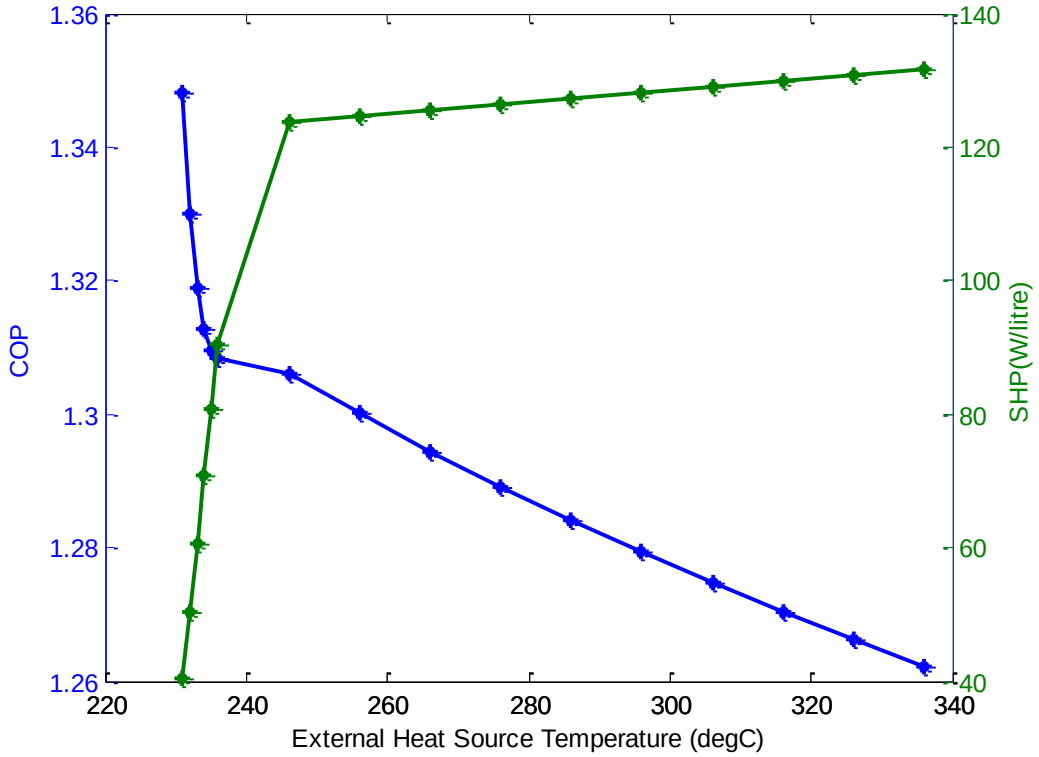

Figure 6-12: Effect of external heat source temperature

Zhang et al [7] suggests that the improvement in SHP with increasing external heat source temperature is due to a higher heat transfer rate which occurs when the heating fluid temperature is increased or the cooling fluid temperature is decreased, producing shorter cycle times. The shorter cycle times also explain why the COP decreases when the external heat source temperature is increased or the cooling temperature is decreased. Shorter cycles mean that the full extent of the different heat outputs may not be realised even as temperature of heat input increases. The rate of the improvement of the SHP drops once the external heat source temperature of 250°C is reached.

6.5.3 Effects of Condensing and Evaporating Temperature

Figure 6-13 and Figure 6-14 show the evolution of the COP and SHP with changing condensation and evaporation temperatures respectively. The figures show how the the COP of the system increases when the evaporating temperature is increased or the condensing temperature is lowered. When the evaporating temperature was increased from -10°C to 10°C, the COP of the system increased from 1.3 to 1.335. The SHP also rose from 124.8W per litre to 128.4W per litre in response to the aforementioned

increase in evaporating temperature. However, as condensation temperature was increased from 30°C to 60°C, the COP decreased from 1.39 to 1.26 while the SHP also decreased from 130W per litre to 121W per litre The effects of the condensing and evaporating temperature found in this work tally with those obtained for a single effect $CaCl_2$-NH_3 system in Wang et al[3].

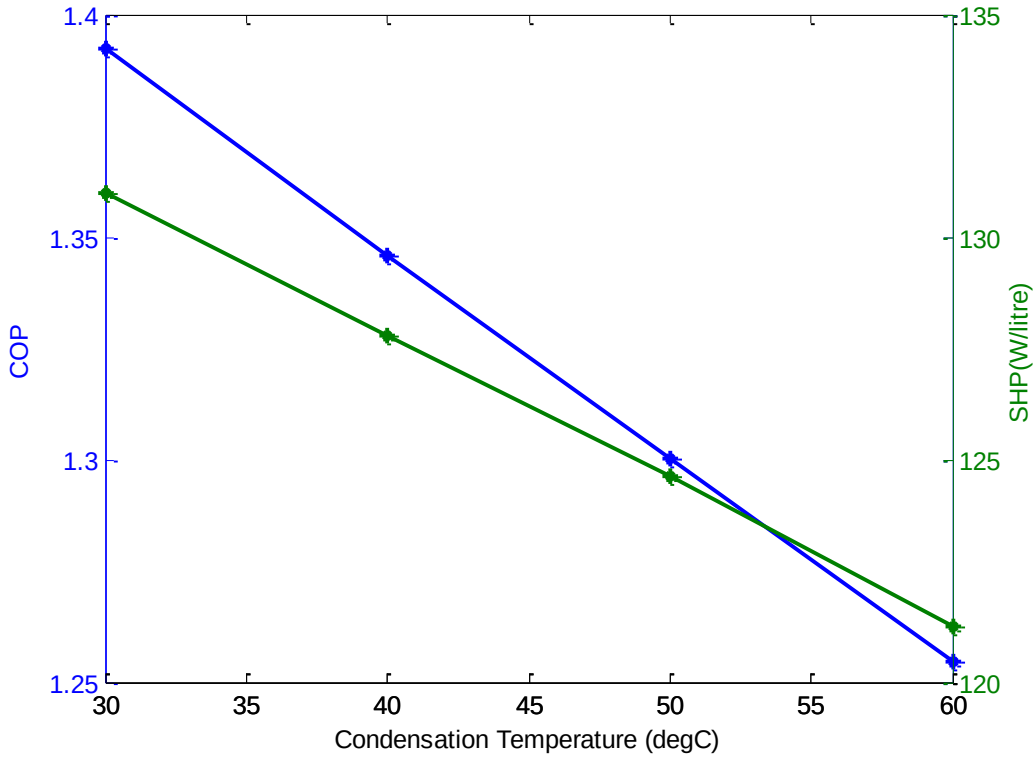

Figure 6-13: Effect of condensation temperature

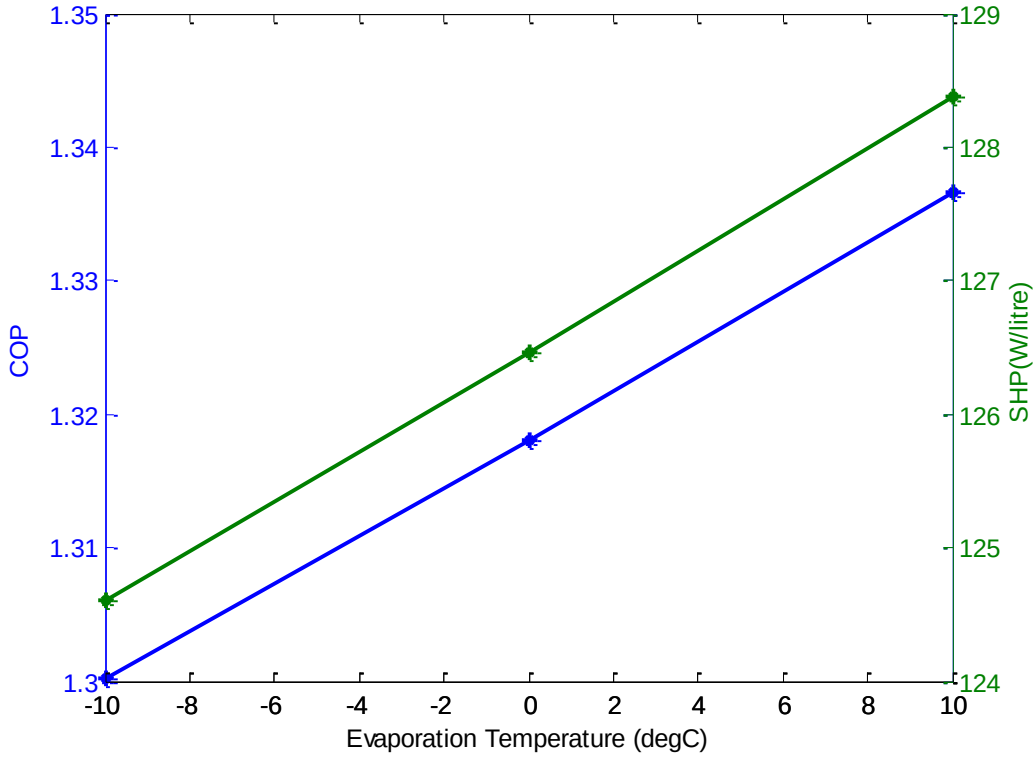

Figure 6-14: Effect of evaporation temperature

6.5.4 Effects of Cycle Time

Here, the effects of the cycle time on the performance of the system are investigated. Figure 6-15 shows the evolution of the COP and SHP over a series of cycle times between 600s and 3000s. The shortest cycle time of 600s produced a lower COP (1.2134) but a higher SHP (311.6W per litre) compared to the longest cycle time of 3000s which produced a much higher COP of 1.3059 but a lower SHP of 81.95W per litre. The longest cycle time of 3000s produced the best COP compared to the other cycle times here because the reactors get the time to reach a much higher generation temperature and also react more refrigerant yielding a higher useful heat output both in the condenser and reactors[8]. This advantage however comes with a trade-off of lower power in the system and a balance must therefore be struck.

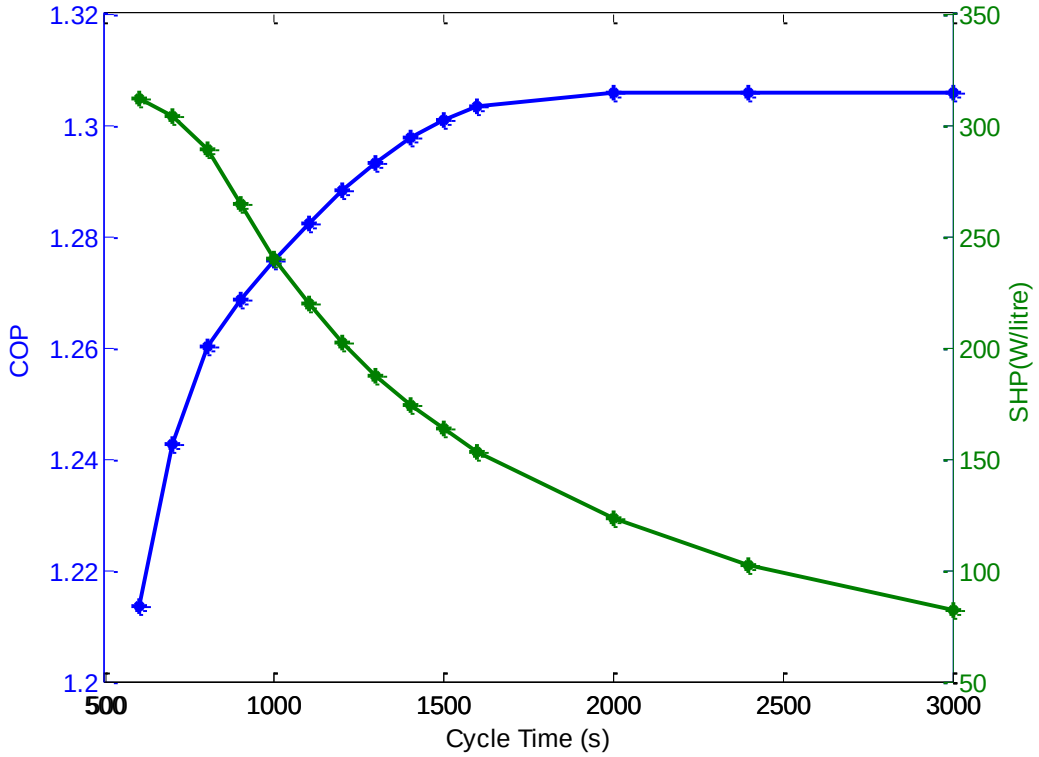

Figure 6-15: Effect of cycle time on COP and SHP

6.5.5 Effects of $MgCl_2$-$CaCl_2$ Mass Ratio

The ratio of the two salt masses in the reactors is an important consideration in the system. 12 different ratios of the $MgCl_2$-$CaCl_2$ masses were considered with the aim of determining what effect it has on the SHP and COP levels. Figure 6-16 and Figure 6-17 show the results obtained for different cycle times. The COP level reduced as the $MgCl_2$-$CaCl_2$ mass ratio increases but the SHP increases when the $MgCl_2$-$CaCl_2$ mass ratio increases. The reduction in COP is due to the reduced level of condensation heat from the $CaCl_2$ side of the system. Also, the heat of reaction from the $CaCl_2$ side of the system is reduced when the ratio is higher (i.e the mass of $CaCl_2$ is smaller). Much lower $MgCl_2$-$CaCl_2$ ratios were not considered as they would produce very low COP levels because of insufficient heat available to decompose the $CaCl_2$ reactor.

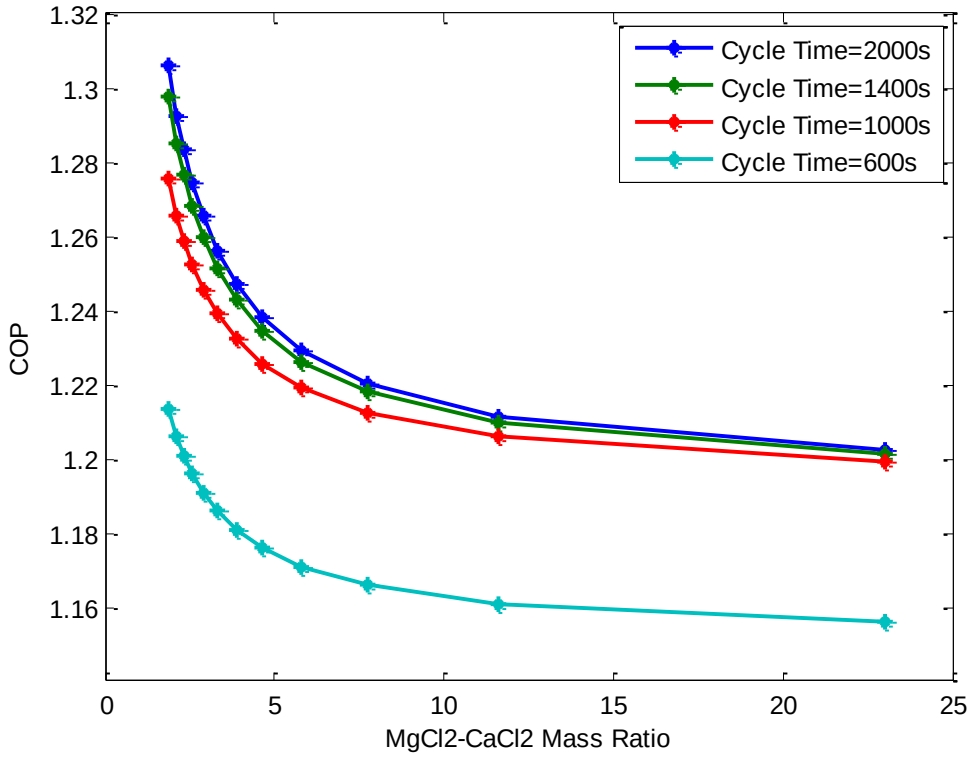

Figure 6-16: Effect of $MgCl_2$-$CaCl_2$ mass ratio on COP

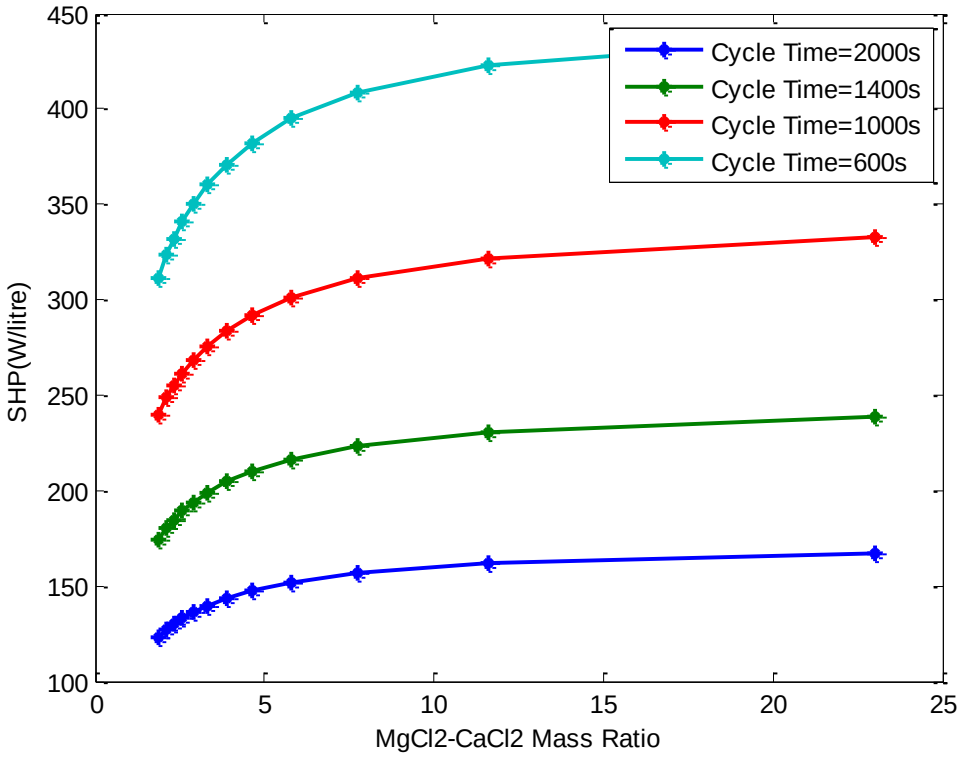

Figure 6-17: Effect of $MgCl_2$-$CaCl_2$ mass ratio on SHP

6.5.6 Single Effect Vs Double Effect

Overall, the best obtained COP values for the cases of the single salts separately showed that the $MgCl_2$ system produced a higher COP than the $CaCl_2$ system as shown in Figure 6-18. However, the double effect $MgCl_2$-$CaCl_2$ system showed an improvement in COP of 13.4% and 17.4% compared to the single $MgCl_2$ and the $CaCl_2$ systems respectively. The single effect systems were simulated using the same model used for the double effect system but with appropriate modifications. The operating conditions for which the result shown in Figure 6-18, were given in Table 6-3.

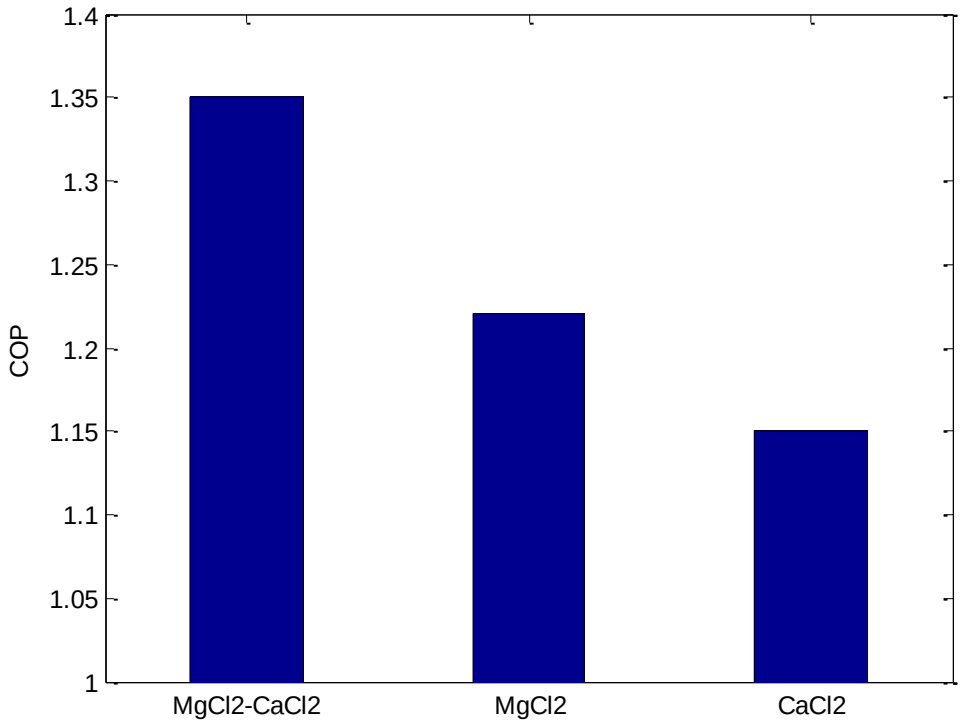

Figure 6-18: Single vs double effect

6.6 Summary

In this chapter, the concept of a double effect thermochemical heat pump was introduced based on the $MgCl_2$-NH_3 and the $CaCl_2$-NH_3 working pairs. The heat produced by the synthesis of the $MgCl_2$-NH_3 was used in the decomposition of the $CaCl_2$-NH_3 eliminating the need for an external heat source for that process. The underlying idea was to obtain improved performance levels compared to a single effect

system based on either of the two working pairs. Simulation results showed that the double effect system could produce a COP which is 13.4% and 17.4% higher compared to the $MgCl_2$-NH_3 and the $CaCl_2$-NH_3 single effect systems respectively. Furthermore, increasing the external heat source temperature increased the SHP but reduced the COP. Higher evaporation temperatures produced higher levels of both the COP and SHP as expected from thermodynamic principles. Conversely, higher condensation temperatures produced lower COP and SHP values. Increasing the cycle time also increased the COP and decreased the SHP. Lower COP and higher SHP was observed when the $MgCl_2$-$CaCl_2$ mass ratio was increased.

6.7 References

1. Douss, N., F.E. Meunier, and L.M. Sun, *Predictive Model And Experimental Results For A Two-Adsorber Solid Adsorption Heat Pump*. Industrial & Engineering Chemistry Research, 1988. **27**(2): p. 310-316.
2. Tchernev, D.I., *Regenerative Zeolite Heat Pump*, in *Studies in Surface Science and Catalysis*, P.A. Jacobs and R.A.v. Santen, Editors. 1989, Elsevier. p. 519-526.
3. Wang, R., Wang, L., Wu, J.,, *Adsorption Refrigeration Technology*. 2014, Singapore: Wiley.
4. Goetz, V., B. Spinner, and E. Lepinasse, *A Solid-Gas Thermochemical Cooling System Using Bacl2 And Nicl2*. Energy, 1997. **22**(1): p. 49-58.
5. Li, T.X., et al., *A Conceptual Design And Performance Analysis Of A Triple-Effect Solid–Gas Thermochemical Sorption Refrigeration System With Internal Heat Recovery*. Chemical Engineering Science, 2009. **64**(14): p. 3376-3384.
6. Neveu, P. and J. Castaing, *Solid-Gas Chemical Heat Pumps: Field Of Application And Performance Of The Internal Heat Of Reaction Recovery Process.* Heat Recovery Systems and CHP, 1993. **13**(3): p. 233-251.
7. Zhang, L.Z. and L. Wang, *Performance Estimation Of An Adsorption Cooling System For Automobile Waste Heat Recovery.* Applied Thermal Engineering, 1997. **17**(12): p. 1127-1139.
8. Xu, S.Z., R.Z. Wang, and L.W. Wang, *Temperature–Heat Diagram Analysis Method For Heat Recovery Physical Adsorption Refrigeration Cycle – Taking*

Multi-Stage Cycle As An Example. International Journal of Refrigeration, 2017. **74**: p. 254-268.

Chapter 7 : Conclusions and Recommendations for Further Work

7.1 Conclusions

The essence of this chapter is to make conclusions on the work that has been done in relation to the aims and objectives which were set at the beginning of the project. The aim of the project was to design in concept a double effect thermochemical heat pump based on the calcium chloride-ammonia and magnesium chloride-ammonia pair. The objectives which were set initially in order to achieve the aforementioned aim are given below.

- To study the underlying theory behind adsorption systems
- To conduct a literature review of the state of the art systems in the area of thermochemical systems.
- To study the heat transfer and kinetic behaviour of the relevant reactions- calcium chloride-ammonia and magnesium chloride-ammonia.
- To design and develop a Matlab model to simulate a representative double effect thermochemical heat pump based on the chosen reactions

All the above objectives which were initially set were met.

The work began with a detailed study of theory which is relevant to adsorption heat pumps, setting the foundation of knowledge on which the work was built upon. The topics which were covered included the adsorption equations of state, the mechanisms of both physical adsorption and chemical adsorption, a kinetic model for chemical adsorption and the thermodynamics of the adsorption cycle. This theoretical background can be found in Chapter 2.

The theory was followed by a literature review which highlighted other multiple stage systems which are available both in the market and the literature. This served two purposes. It helped to be up to date with the state of the art and also to ensure that the system being developed in this work was not a repetition of a system which has been built in the past. In addition to multiple stage system, systems based on other advanced cycles such as the thermal wave were presented in the literature review. This part of the work can be found in Chapter 3.

The heat transfer and kinetic behaviour of the relevant reactions was studied as planned. A large temperature jump rig was built to achieve this aim. Experiments on the large temperature jump rig began with a better understood adsorbent-active carbon. This way, the large temperature jump rig was validated before beginning experiments on thermochemical reactions. The thermochemical reactions experimental results were simulated with a model based on a heat transfer-kinetics coupling in order to identify a kinetic parameter (A) for the different relevant reactions. Chapter 4 and Chapter 5 detail the experiments carried out on the active carbon, magnesium chloride and calcium chloride samples.

The kinetic parameters obtained from the modelling of the large temperature jump experiments were used to dynamically model an entire double effect thermochemical heat pump. With the dynamic model, the optimum conditions of the operation of the thermochemical heat pump were obtained. This part of the work was detailed in Chapter 6.

7.1.1 Specific Contributions to Knowledge and Wider Field

The specific contributions to knowledge which are obtainable from this thesis are listed as follows.

- Method for extraction of heat transfer parameters (thermal conductivity and heat transfer coefficient) from large temperature jump data. This could help the adoption of the large temperature jump method as a more holistic technique in the design of adsorption systems and not just dynamics study only.
- Kinetic study of two reactions ($CaCl_2$-NH_3 and $MgCl_2$-NH_3) which haven't previously been studied for thermochemical heat pump application. The kinetic parameters obtained for these reactions could be useful in any field where these working pairs are used and there's a goal to understand their particular kinetic behaviour.
- Concept design and performance analysis of a thermochemical heat pump using the reactions which were studied- $CaCl_2$-NH_3 and $MgCl_2$-NH_3. Such high temperature thermochemical heat pump could be applied to produce cooling or heating in food processing or metal works industries.

7.2 Recommendation for Further Work

Further work is recommended on three levels.

- Detailed analysis of the experimental process should be carried out with the aim of identifying the cause of the sudden change in the rate of the reaction in the initial stages of some of the salt-ammonia experiments as seen in subsection 5.8 of Chapter 5.
- More experiments should be conducted over a wider temperature and pressure range for the relevant salt-ammonia reactions. This would help to further validate the kinetic parameters which have been obtained.
- Furthermore, a full representative prototype of the system may be built to further validate the simulation results which were obtained in this work.

Appendices

Appendix 1 (A1): Experimental and Analysis Results for Chapter 5 (LTJ Experiments on $CaCl_2$-NH_3 and $MgCl_2$-NH_3)

The experiments are numbered numerically in these results tables. The letters 'a' and 'b' are used to denote decomposition and synthesis respectively. After the results tables, plots of global advancement against modelled advancement (denoted by 'i') based on a number of A and yo combinations are presented between 10% and 100% reaction completion. Also, for cases where there were multiple experiments for one reaction, plots which compared the best fit yo and A were was obtained for every experiment to the average best fit yo and A obtained for each reaction between 10% and 80% reaction completion were presented and denoted by 'ii'. Beneath all the results tables, there is a smaller 2 by 2 table which shows the average best fit values of yo and A between 10% and 80% reaction completion obtained for the relevant reaction. Table Table A1:1 shows a key to the results tables headings for further understanding.

No	Numerical identification for experiment
Type	a for deconmposition and b for synthesis
T Jump (°C)	Temperature jump (initial temeprature and final temeperature for experiment)
P-Jump (bar)	Resultant pressure jump from temperature jump
Teq (°C)	Equilibrium temperature at starting pressure
t(0.1 to 0.8) model (s)	Time taken by simulation from 10% to 80% reaction completion, this is based on a predetermined reaction yo and A combination
t(0.1 to 0.8) measured (s)	Time measured during experiment from 10% to 80% reaction completion
% difference	Percentage time difference between simulated and measurred time from 10% to 80% completion
t (0 to 0.1) model (s)	Time taken by simulation from 0% to 10% reaction completion, this is based on a predetermined reaction yo and A combination
t(0 to 0.1) experiment (s)	Time measured during experiment from 0% to 10% reaction completion
yo	yo which produced lowest RMSE for the particular experiment
A (s^{-1})	A which produced lowest RMSE for the particular experiment
n (moles)	Number of Ammonia moles reacted per mole of salt
RMSE	Root mean square error
Texp (mins)	Total time of experiment

Table A1:1: Key to results tables headings

$BaCl_2$ -NH_3

					The columns below are all based on average reaction yo and A									
No	Type	T Jump (°C)	P-Jump (bar)	Teq (°C)	t(0.1 to 0.8)model (s)	t(0.1 to 0.8)measured (s)	% difference	t(0 to 0.1)model(s)	t(0 to 0.1)experiment(s)	yo	A(s^{-1})	n(moles)	RMSE	Texp(mins)
0	a	10.0-78	2.15-2.55	25.22	-	-	-	-	-	0.72	0.071	7.31	0.002	60
	b	78-10	2.55-2.16	25.02	-	-	-	-	-	0.7	0.007	7.28	0.034	90
					$BaCl_2$-NH_3 (R1) (a)	$BaCl_2$-NH_3 (R1) (b)								
					yo=0.72, A=0.07	yo=0.70, A=0.007								

Table A1:2: Results for $BaCl_2$-NH_3 (R1) reaction (Sample 1)

$CaCl_2$ -NH_3

					The columns below are all based on average reaction yo and A									
No	Type	T Jump (°C)	P-Jump (bar)	Teq (°C)	t(0.1 to 0.8)model (s)	t(0.1 to 0.8)measured (s)	% difference	t(0 to 0.1)model(s)	t(0 to 0.1)experiment(s)	yo	A(s^{-1})	n(moles)	RMSE	Texp(mins)
1	a	48-74	5.71-5.96	69.29	305	304	-0.33	122	122	0.73	0.034	3.1	0.0197	60
	b	74-48	5.96-5.72	70.15	111	115	3.48	33	21	0.69	0.021	3	0.0176	60
2	a	48-76	5.64-5.90	69	218	207	-5.31	97	118	0.72	0.039	3.23	0.0096	60
	b	76-48	5.90-5.65	69.9	122	123	0.81	40	23	0.70	0.022	2.96	0.0143	60
3	a	48-78	5.60-5.87	68.84	179	177	-1.13	68	89	0.67	0.040	2.98	0.0084	60
	b	78-48	5.89-5.64	69.86	123	120	-2.50	41	23	0.71	0.021	2.85	0.021	60
4	a	58-74	5.68-5.88	69.16	221	216	-2.31	58	67	0.70	0.040	2.72	0.0088	60
	b	74-58	5.88-5.67	69.97	207	208	0.48	66	32	0.70	0.018	2.99	0.0147	60
5	a	58-76	5.66-5.89	69.07	173	174	0.57	36	56	0.81	0.042	2.94	0.0155	60
	b	76-58	5.89-5.66	70.01	229	240	4.58	75	41	0.75	0.020	2.82	0.0159	60
6	a	58-78	5.67-5.89	69.14	154	141	-9.22	30	38	0.71	0.028	2.63	0.0072	60
	b	78-58	5.89-5.67	70.01	234	228	-2.63	88	47	0.68	0.018	2.97	0.0161	60
7	a	63-74	5.60-5.82	68.85	190	195	2.56	37	47	0.72	0.039	2.59	0.0069	60
	b	74-63	5.82-5.63	69.73	304	425	28.47	111	62	2.20	0.034	2.31	0.0338	90
8	a	63-76	5.69-5.90	69.22	158	152	-3.95	32	40	0.60	0.040	2.83	0.0079	60
	b	76-63	5.90-5.69	70.06	296	442	33.03	124	504	2.20	0.028	2.26	0.0394	90
9	a	63-78	5.69-5.90	69.22	123	128	3.91	23	33	0.70	0.040	2.72	0.009	60
	b	78-63	5.90-5.69	69.91	297	432	31.25	134	76	2.20	0.030	2.68	0.0354	90

$CaCl_2$-NH_3 (R1) (a)	$CaCl_2$-NH_3 (R1) (b)
yo=0.723, A=0.037	yo=0.705, A=0.02

Table A1:3: Results for $CaCl_2$-NH_3 (R1) reaction (Sample 1)

					The columns below are all based on average reaction yo and A										
No	Type	T Jump (°C)	P-Jump (bar)	Teq (°C)	t(0.1 to 0.8)model (s)	t(0.1 to 0.8)measured (s)	% difference	t(0 to 0.1)model(s)	t(0 to 0.1)experiment(s)	yo	A(s^{-1})	n(moles)	RMSE	Texp(mins)
10	a	74-83	5.84-5.94	77.46	1052	283	-271.73	110	38	1.6	0.02	1.31	0.032	90
	b	83-74	5.95-5.85	80.72	236	229	-3.06	85	94	0.76	0.0049	1.36	0.007	60
11	a	74-87	5.78-5.92	77.24	386	366	-5.46	63	100	0.81	0.007	1.46	0.002	60
	b	87-74	5.92-5.79	80.72	268	261	-2.68	148	80	0.87	0.0064	1.49	0.001	60
12	a	74-90	5.79-5.91	77.26	134	139	3.60	26	38	0.83	0.0063	1.58	0.0068	60
	b	90-74	5.92-5.79	80.73	300	293	-2.39	182	78	0.86	0.0059	1.69	0.001	60
13	a	76-83	5.83-5.92	77.34	825	130	-534.62	119	26	1.6	0.03	1.4	0.069	90
	b	83-76	5.9-5.81	80.66	815	749	-8.81	226	140	0.76	0.0059	1.2	0.0169	90
14	a	76-87	5.81-5.92	77.33	128	125	-2.40	26	42	0.86	0.007	1.6	0.01	60
	b	87-76	5.93-5.82	80.76	869	847	-2.60	272	140	0.8	0.005	1.39	0.031	90
15	a	76-90	5.81-5.94	77.36	88	87	-1.15	19	30	0.77	0.0072	1.45	0.021	60
	b	90-76	5.94-5.83	80.68	1404	1052	-33.46	365	104	0.7	0.04	1.38	0.1	90
16	a	77-83	5.77-5.89	77.18	330	110	-200.00	21	34	0.7	0.0115	1.38	0.066	90
17	a	77-87	5.81-5.91	77.34	117	128	8.59	24	36	0.79	0.0071	1.3	0.0185	60
18	a	77-90	5.79-5.86	77.23	95	99	4.04	18	30	0.8	0.007	1.48	0.019	60
					$CaCl_2$-NH_3 (R2) (a)	$CaCl_2$-NH_3 (R2) (b)								
					yo=0.81, A=0.0069	yo=0.83, A=0.0057								

Table A1:4: Results for $CaCl_2$-NH_3 (R2) reaction (Sample 1)

					The columns below are all based on average reaction yo and A									
No	Type	T Jump (℃)	P-Jump (bar)	Teq (°C)	t(0.1 to 0.8)model (s)	t(0.1 to 0.8)measured (s)	% difference	t(0 to 0.1)model(s)	t(0 to 0.1)experiment(s)	yo	A(s^{-1})	n(moles)	RMSE	Texp(mins)
19	a	48-74	5.76-6.12	69.36	894	789	-13.31	192	171	0.71	0.039	3.69	0.010	90
	b	74-48	6.14-5.79	70.85	224	205	-9.27	44	43	0.80	0.022	3.67	0.005	60
20	a	48-76	5.67-6.03	68.97	453	414	-9.42	143	147	0.83	0.035	3.68	0.019	60
	b	76-48	6.04-5.68	70.46	229	206	-11.17	45	44	0.73	0.022	3.75	0.016	60
21	a	48-78	5.61-5.97	68.69	367	365	-0.55	101	142	0.74	0.031	3.90	0.011	60
	b	78-48	6.00-5.68	70.48	428	397	-7.81	67	74	0.80	0.016	3.90	0.020	60
22	a	58-74	5.66-5.99	68.93	408	413	1.21	89	120	0.73	0.029	3.48	0.011	60
	b	74-58	5.99-5.67	70.45	367	360	-1.94	64	63	0.71	0.022	3.62	0.011	60
23	a	58-76	5.66-5.99	68.95	309	317	2.52	78	119	0.73	0.032	3.75	0.015	60
	b	76-58	6.00-5.67	70.46	362	369	1.90	64	63	0.70	0.019	3.59	0.012	60
24	a	58-78	5.66-6.00	68.94	235	235	0.00	53	81	0.79	0.038	3.75	0.023	60
					$CaCl_2$-NH_3 (R1) (a)	$CaCl_2$-NH_3 (R1) (b)								
					yo=0.76, A=0.034	yo=0.75, A=0.0202								

Table A1:5: Results for $CaCl_2$-NH_3 (R1) reaction (Sample 2)

					The columns below are all based on average reaction yo and A									
No	Type	T Jump (°C)	P-Jump (bar)	Teq (°C)	t(0.1 to 0.9)model (s)	t(0.1 to 0.9)measured (s)	% difference	t(0 to 0.1)model(s)	t(0 to 0.1)experiment(s)	yo	$A(s^{-1})$	n(moles)	RMSE	Texp(mins)
25	a	76-87	5.77-5.92	77.19	-	-	-	-	-	0.8	0.008	1.57	0.02	60
	b	87-76	5.92-5.77	78.12	-	-	-	-	-	0.78	0.007	1.55	0.034	90
					$CaCl_2$-NH_3 (R2) (a)	$CaCl_2$-NH_3 (R2) (b)								
					yo=0.8, A=0.008	yo=0.78, A=0.007								

Table A1:6: Results for $CaCl_2$-NH_3 (R2) reaction (Sample 2)

					The columns below are all based on average reaction yo and A									
No	Type	T Jump (°C)	P-Jump (bar)	Teq (°C)	t(0.1 to 0.9)model (s)	t(0.1 to 0.9)measured (s)	% difference	t(0 to 0.1)model(s)	t(0 to 0.1)experiment(s)	yo	$A(s^{-1})$	n(moles)	RMSE	Texp(mins)
26	a	48-58	2.81-3.12	53.41	-	-	-	-	-	0.71	0.016	3.52	0.0074	60
	b	58-48	3.12-2.83	55.66	-	-	-	-	-	0.83	0.0053	2.92	0.009	60
27	a	48-74	2.89-3.37	53.96	-	-	-	-	-	0.89	0.023	3.74	0.0176	60
	b	74-48	3.38-2.98	57.43	-	-	-	-	-	0.77	0.0061	3.85	0.0367	60
					$CaCl_2$-NH_3 (R1) (a)	$CaCl_2$-NH_3 (R1) (b)								
					yo=0.8, A=0.0195	yo=0.8, A=0.0057								

Table A1:7: Results for $CaCl_2$-NH_3 (R1) reaction (Sample 2)

$MgCl_2$ -NH_3

					The columns below are all based on average reaction yo and A									
No	Type	T Jump (°C)	P-Jump (bar)	Teq (°C)	t(0.1 to 0.8)model (s)	t(0.1 to 0.8)measured (s)	% difference	t(0 to 0.1)model(s)	t(0 to 0.1)experiment(s)	yo	A(s^{-1})	n(moles)	RMSE	Texp(mins)
28	a	110-166	1.73-1.92	156.36	1523	1480	-2.91	256	141	0.61	0.00010	3.28	0.013	120
	b	166-110	1.92-1.72	137.10	660	735	10.20	72	157	0.69	0.00009	3.20	0.025	90
29	a	110-176	1.74-1.90	156.77	608	619	1.78	146	117	0.78	0.00010	3.60	0.030	90
	b	176-110	1.91-1.73	137.45	1085	1287	15.70	120	70	0.78	0.00006	3.62	0.023	120
30	a	110-186	1.70-1.88	157.03	516	612	15.69	89	62	0.6	0.00020	2.91	0.026	90
	b	186-110	1.89-1.74	137.35	982	1006	2.39	92	72	0.62	0.00007	3.43	0.030	120
31	a	120-166	1.73-1.92	156.95	800	790	-1.27	175	118	0.6	0.00010	3.26	0.014	120
	b	166-120	1.92-1.75	137.36	914	982	6.92	99	153	0.62	0.00008	3.35	0.021	120
32	a	120-176	1.70-1.91	157.08	531	507	-4.73	113	89	0.61	0.00030	3.06	0.032	90
	b	176-120	1.91-1.73	137.20	1243	1222	-1.72	132	133	0.77	0.00005	2.97	0.010	120
33	a	120-186	1.72-1.93	157.16	383	449	14.70	65	83	0.7	0.00010	2.95	0.030	90
	b	186-120	1.91-1.74	137.53	1524	1474	-3.39	174	79	0.8	0.00006	3.41	0.040	120
34	a	130-166	1.71-1.88	156.08	1477	1412	-4.60	200	98	0.61	0.00008	3.62	0.026	120
	b	166-130	1.89-1.72	138.30	1104	1038	-6.36	212	306	0.8	0.00004	3.78	0.026	120
35	a	130-176	1.72-1.87	156.47	648	714	9.24	111	207	0.69	0.00010	2.76	0.030	90
	b	176-130	1..88-1.73	137.22	1175	1027	-14.41	234	278	0.68	0.00004	2.93	0.021	120
36	a	130-186	1.73-1.92	156.86	347	328	-5.79	55	103	0.66	0.00010	3.71	0.021	90
	b	186-130	1.92-1.73	137.57	1198	1130	-6.02	278	284	0.72	0.00002	3.62	0.038	120
					$CaCl_2$-NH_3 (R1) (a)	$CaCl_2$-NH_3 (R1) (b)								
					yo=0.64, A=0.00013	yo=0.72, A=0.000056								

Table A1:8: Results for $MgCl_2$-NH_3 (R1) reaction (Sample 1)

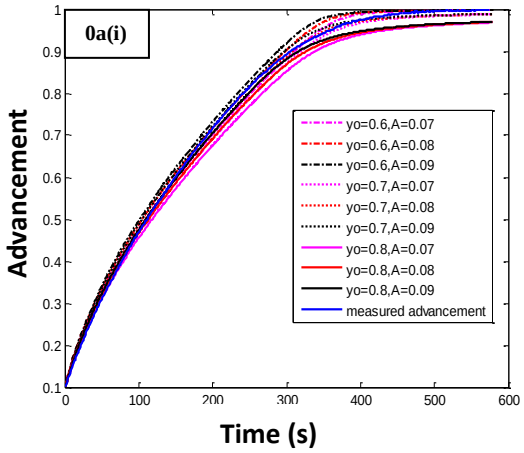
0a(i)
Advancement
Time (s)
yo=0.6,A=0.07
yo=0.6,A=0.08
yo=0.6,A=0.09
yo=0.7,A=0.07
yo=0.7,A=0.08
yo=0.7,A=0.09
yo=0.8,A=0.07
yo=0.8,A=0.08
yo=0.8,A=0.09
measured advancement

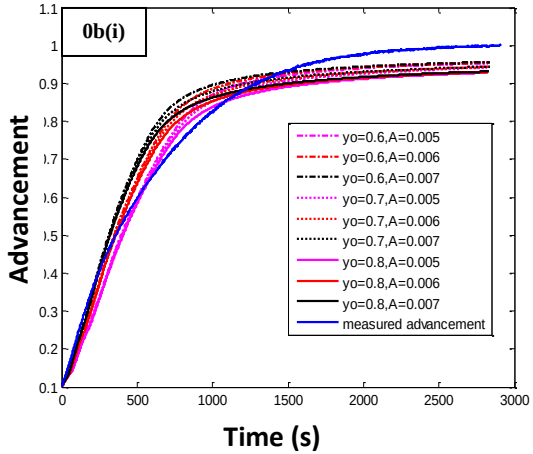
0b(i)
Advancement
Time (s)
yo=0.6,A=0.005
yo=0.6,A=0.006
yo=0.6,A=0.007
yo=0.7,A=0.005
yo=0.7,A=0.006
yo=0.7,A=0.007
yo=0.8,A=0.005
yo=0.8,A=0.006
yo=0.8,A=0.007
measured advancement

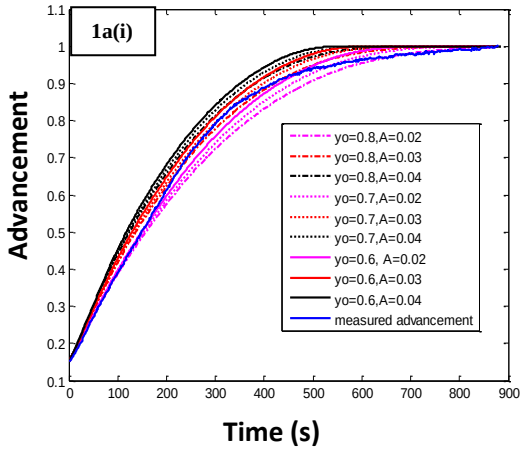
1a(i)
Advancement
Time (s)
yo=0.8,A=0.02
yo=0.8,A=0.03
yo=0.8,A=0.04
yo=0.7,A=0.02
yo=0.7,A=0.03
yo=0.7,A=0.04
yo=0.6, A=0.02
yo=0.6,A=0.03
yo=0.6,A=0.04
measured advancement

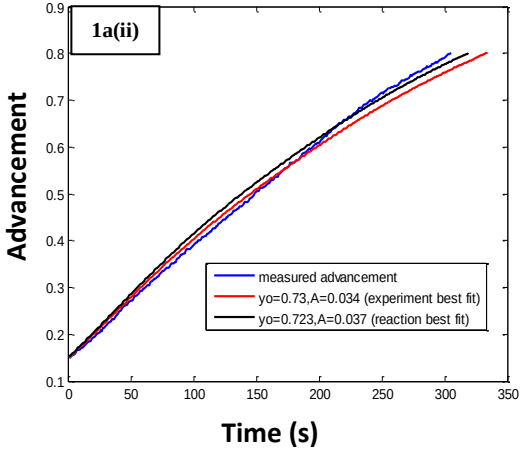
1a(ii)
Advancement
Time (s)
measured advancement
yo=0.73,A=0.034 (experiment best fit)
yo=0.723,A=0.037 (reaction best fit)

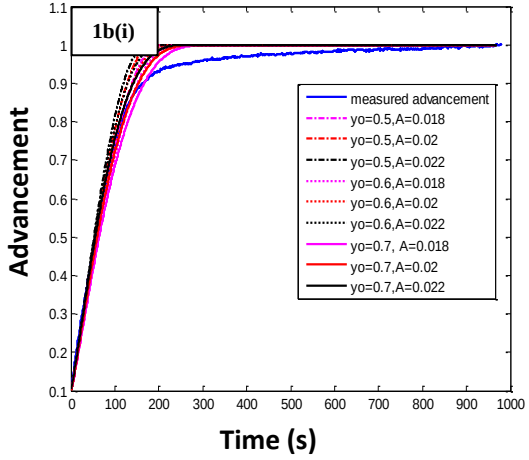
1b(i)
Advancement
Time (s)
measured advancement
yo=0.5,A=0.018
yo=0.5,A=0.02
yo=0.5,A=0.022
yo=0.6,A=0.018
yo=0.6,A=0.02
yo=0.6,A=0.022
yo=0.7, A=0.018
yo=0.7,A=0.02
yo=0.7,A=0.022

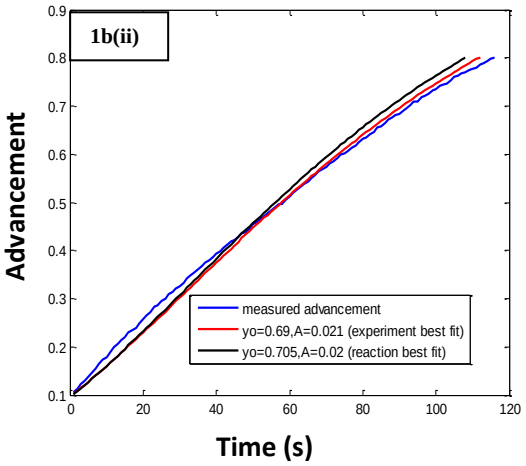
1b(ii)
Advancement
Time (s)
measured advancement
yo=0.69,A=0.021 (experiment best fit)
yo=0.705,A=0.02 (reaction best fit)

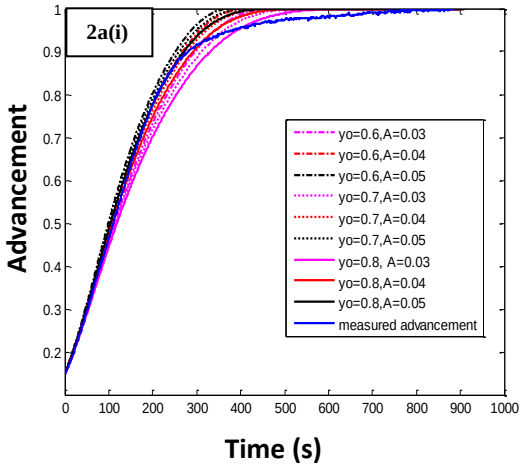
2a(i)
Advancement
Time (s)
yo=0.6,A=0.03
yo=0.6,A=0.04
yo=0.6,A=0.05
yo=0.7,A=0.03
yo=0.7,A=0.04
yo=0.7,A=0.05
yo=0.8, A=0.03
yo=0.8,A=0.04
yo=0.8,A=0.05
measured advancement

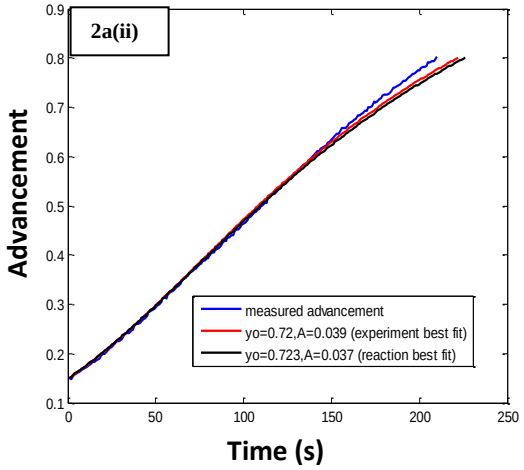
2a(ii)
Advancement
Time (s)
measured advancement
yo=0.72,A=0.039 (experiment best fit)
yo=0.723,A=0.037 (reaction best fit)

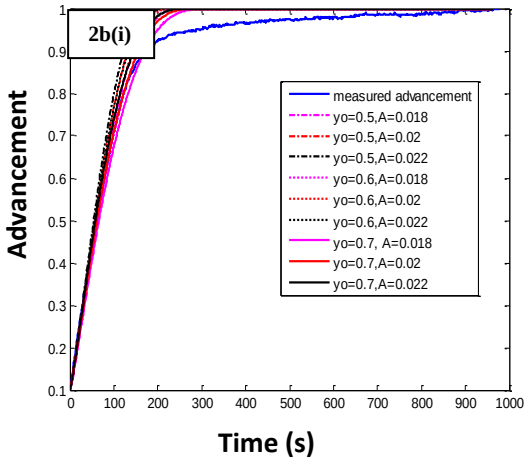
2b(i)
Advancement
Time (s)
measured advancement
yo=0.5,A=0.018
yo=0.5,A=0.02
yo=0.5,A=0.022
yo=0.6,A=0.018
yo=0.6,A=0.02
yo=0.6,A=0.022
yo=0.7, A=0.018
yo=0.7,A=0.02
yo=0.7,A=0.022

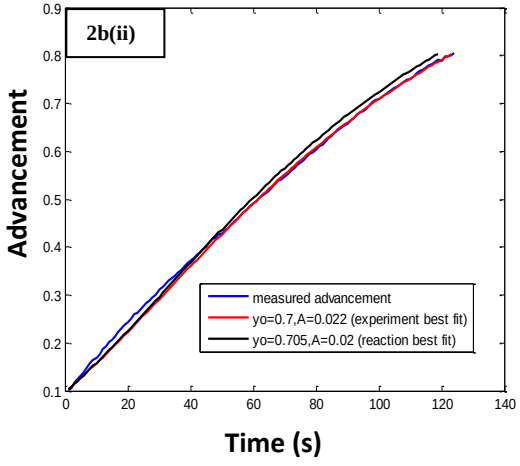
2b(ii)
Advancement
Time (s)
measured advancement
yo=0.7,A=0.022 (experiment best fit)
yo=0.705,A=0.02 (reaction best fit)

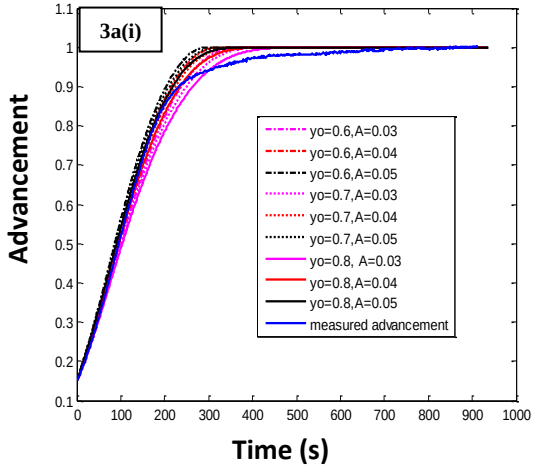
3a(i)
Advancement
Time (s)
yo=0.6,A=0.03
yo=0.6,A=0.04
yo=0.6,A=0.05
yo=0.7,A=0.03
yo=0.7,A=0.04
yo=0.7,A=0.05
yo=0.8, A=0.03
yo=0.8,A=0.04
yo=0.8,A=0.05
measured advancement

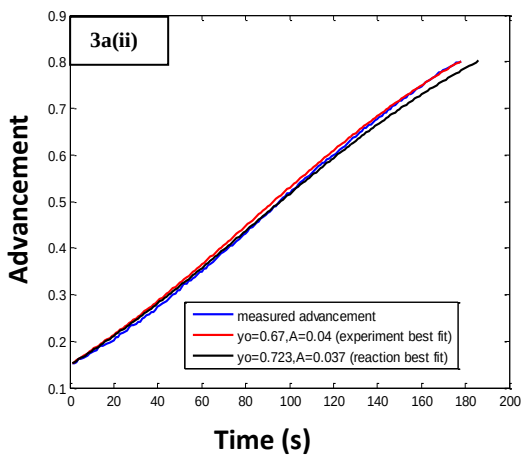
3a(ii)
Advancement
Time (s)
measured advancement
yo=0.67,A=0.04 (experiment best fit)
yo=0.723,A=0.037 (reaction best fit)

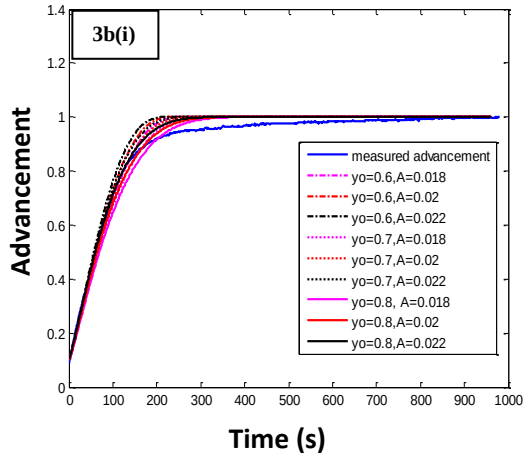
3b(i)
Advancement
Time (s)
measured advancement
yo=0.6,A=0.018
yo=0.6,A=0.02
yo=0.6,A=0.022
yo=0.7,A=0.018
yo=0.7,A=0.02
yo=0.7,A=0.022
yo=0.8, A=0.018
yo=0.8,A=0.02
yo=0.8,A=0.022

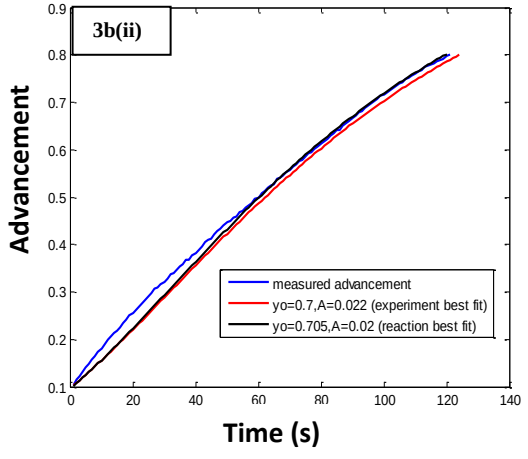
3b(ii)
Advancement
Time (s)
measured advancement
yo=0.7,A=0.022 (experiment best fit)
yo=0.705,A=0.02 (reaction best fit)

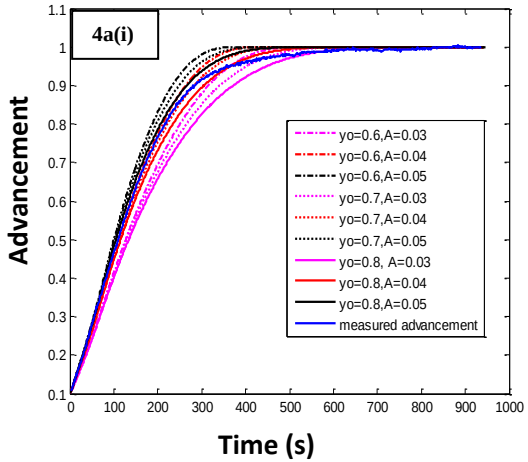
4a(i)
Advancement
Time (s)
yo=0.6,A=0.03
yo=0.6,A=0.04
yo=0.6,A=0.05
yo=0.7,A=0.03
yo=0.7,A=0.04
yo=0.7,A=0.05
yo=0.8, A=0.03
yo=0.8,A=0.04
yo=0.8,A=0.05
measured advancement

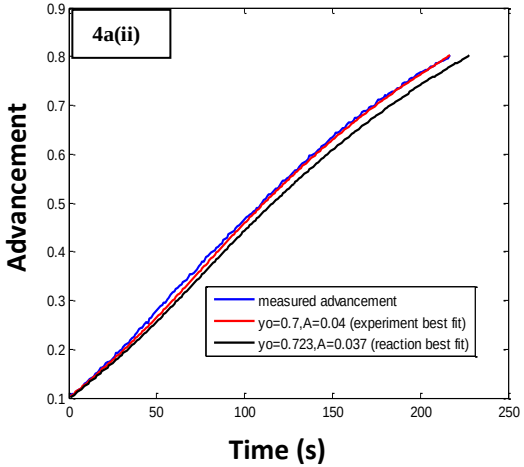
4a(ii)
Advancement
Time (s)
measured advancement
yo=0.7,A=0.04 (experiment best fit)
yo=0.723,A=0.037 (reaction best fit)

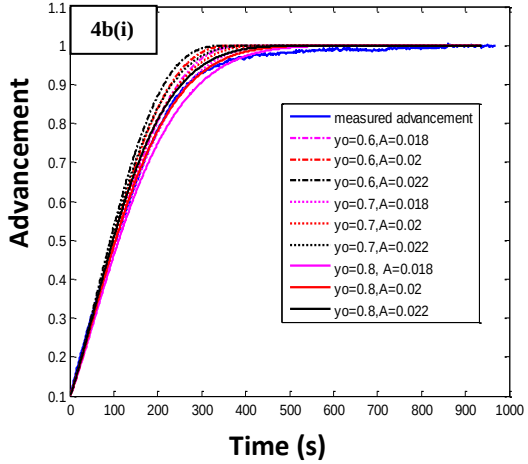
4b(i)
Advancement
Time (s)
measured advancement
yo=0.6,A=0.018
yo=0.6,A=0.02
yo=0.6,A=0.022
yo=0.7,A=0.018
yo=0.7,A=0.02
yo=0.7,A=0.022
yo=0.8, A=0.018
yo=0.8,A=0.02
yo=0.8,A=0.022

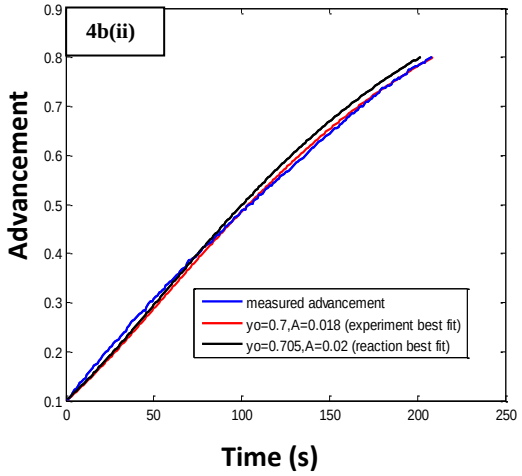
4b(ii)
Advancement
Time (s)
measured advancement
yo=0.7,A=0.018 (experiment best fit)
yo=0.705,A=0.02 (reaction best fit)

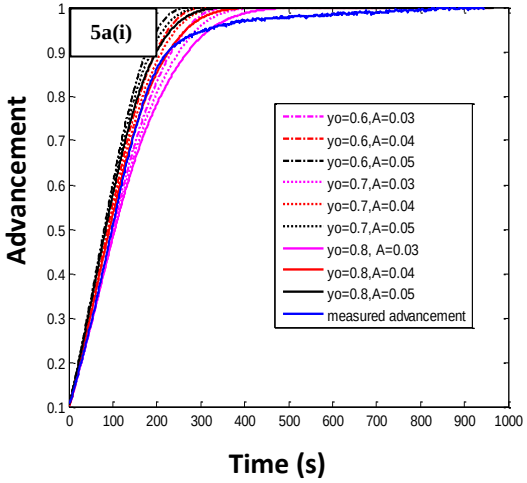
5a(i)
Advancement
Time (s)
yo=0.6,A=0.03
yo=0.6,A=0.04
yo=0.6,A=0.05
yo=0.7,A=0.03
yo=0.7,A=0.04
yo=0.7,A=0.05
yo=0.8, A=0.03
yo=0.8,A=0.04
yo=0.8,A=0.05
measured advancement

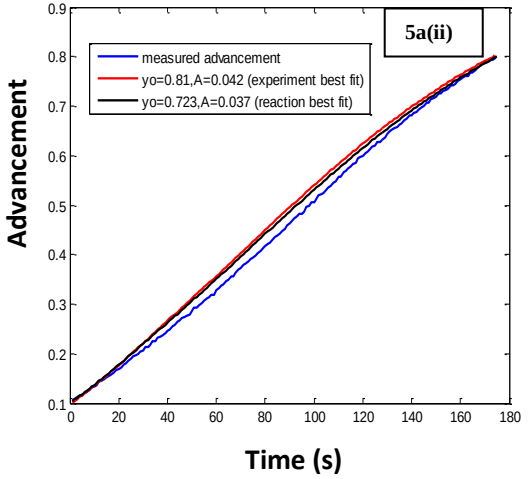
5a(ii)
Advancement
Time (s)
measured advancement
yo=0.81,A=0.042 (experiment best fit)
yo=0.723,A=0.037 (reaction best fit)

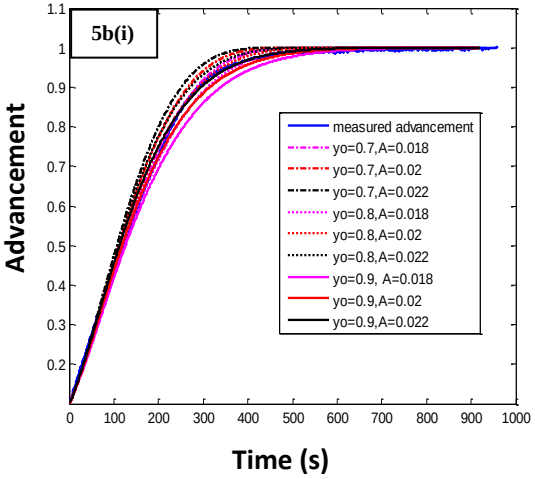
5b(i)
Advancement
Time (s)
measured advancement
yo=0.7,A=0.018
yo=0.7,A=0.02
yo=0.7,A=0.022
yo=0.8,A=0.018
yo=0.8,A=0.02
yo=0.8,A=0.022
yo=0.9, A=0.018
yo=0.9,A=0.02
yo=0.9,A=0.022

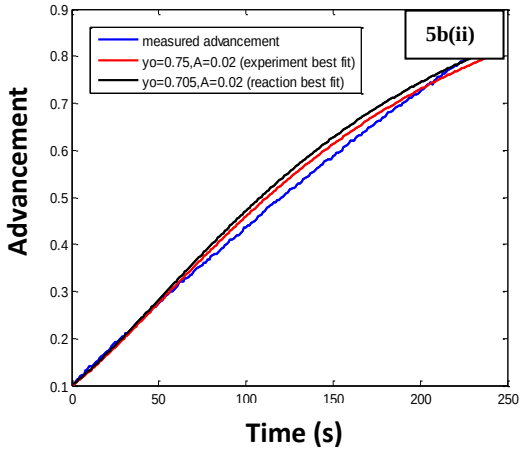
5b(ii)
Advancement
Time (s)
measured advancement
yo=0.75,A=0.02 (experiment best fit)
yo=0.705,A=0.02 (reaction best fit)

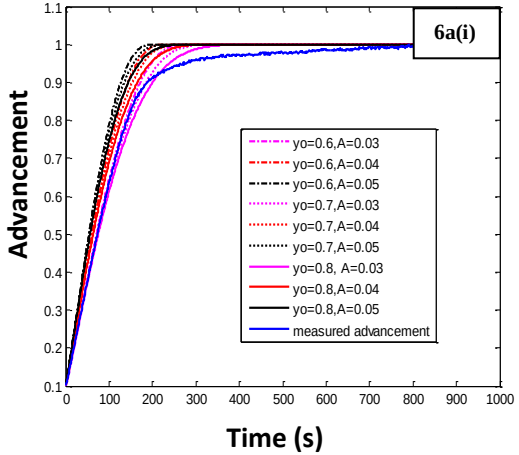
6a(i)
Advancement
Time (s)
yo=0.6,A=0.03
yo=0.6,A=0.04
yo=0.6,A=0.05
yo=0.7,A=0.03
yo=0.7,A=0.04
yo=0.7,A=0.05
yo=0.8, A=0.03
yo=0.8,A=0.04
yo=0.8,A=0.05
measured advancement

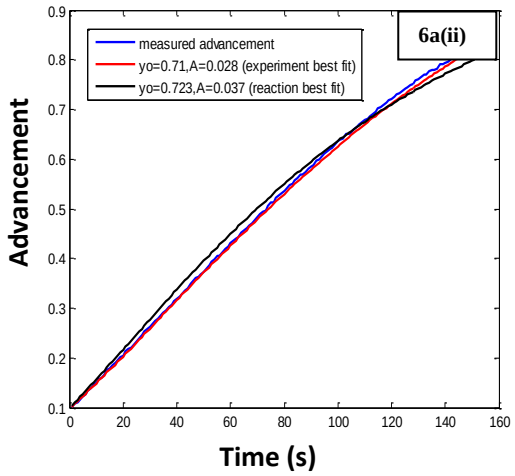
6a(ii)
measured advancement
yo=0.71,A=0.028 (experiment best fit)
yo=0.723,A=0.037 (reaction best fit)
Advancement
Time (s)

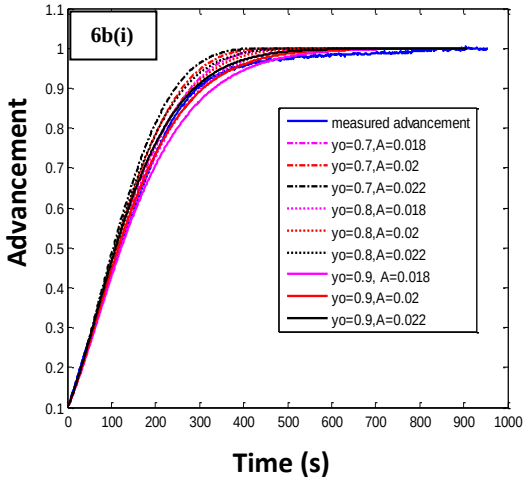
6b(i)
measured advancement
yo=0.7,A=0.018
yo=0.7,A=0.02
yo=0.7,A=0.022
yo=0.8,A=0.018
yo=0.8,A=0.02
yo=0.8,A=0.022
yo=0.9, A=0.018
yo=0.9,A=0.02
yo=0.9,A=0.022
Advancement
Time (s)

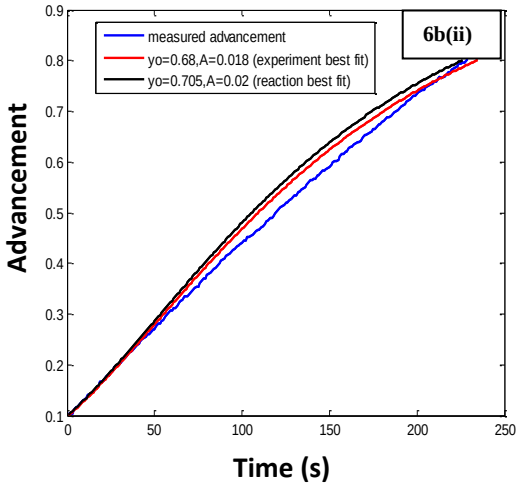
6b(ii)
measured advancement
yo=0.68,A=0.018 (experiment best fit)
yo=0.705,A=0.02 (reaction best fit)
Advancement
Time (s)

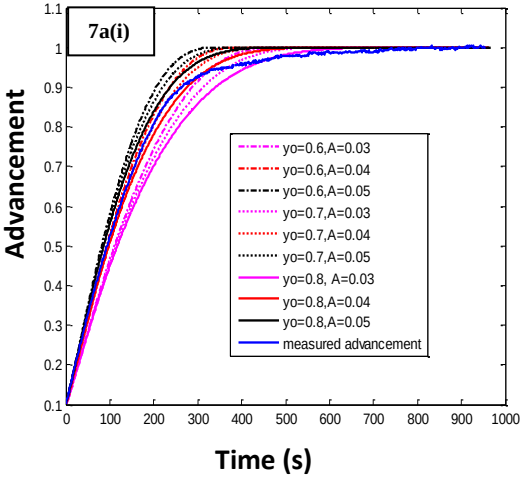
7a(i)
yo=0.6,A=0.03
yo=0.6,A=0.04
yo=0.6,A=0.05
yo=0.7,A=0.03
yo=0.7,A=0.04
yo=0.7,A=0.05
yo=0.8, A=0.03
yo=0.8,A=0.04
yo=0.8,A=0.05
measured advancement
Advancement
Time (s)

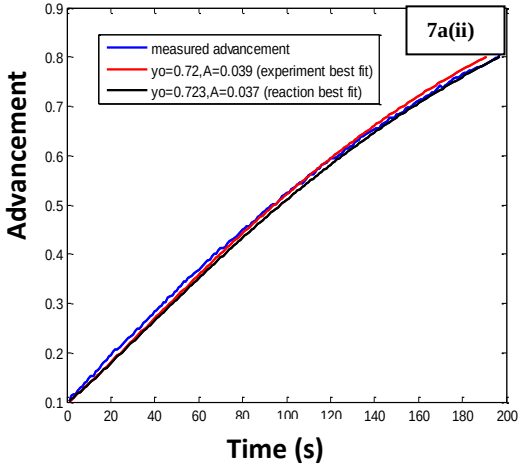
7a(ii)
measured advancement
yo=0.72,A=0.039 (experiment best fit)
yo=0.723,A=0.037 (reaction best fit)
Advancement
Time (s)

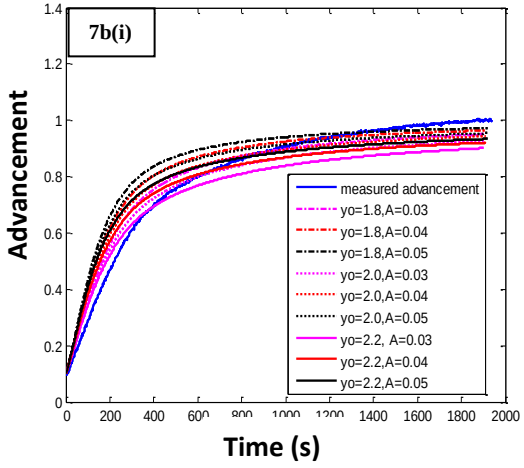
7b(i)
measured advancement
yo=1.8,A=0.03
yo=1.8,A=0.04
yo=1.8,A=0.05
yo=2.0,A=0.03
yo=2.0,A=0.04
yo=2.0,A=0.05
yo=2.2, A=0.03
yo=2.2,A=0.04
yo=2.2,A=0.05
Advancement
Time (s)

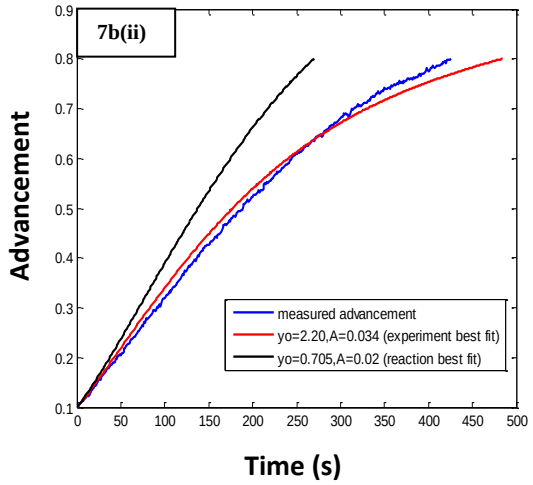
7b(ii)
Advancement
Time (s)
measured advancement
yo=2.20,A=0.034 (experiment best fit)
yo=0.705,A=0.02 (reaction best fit)

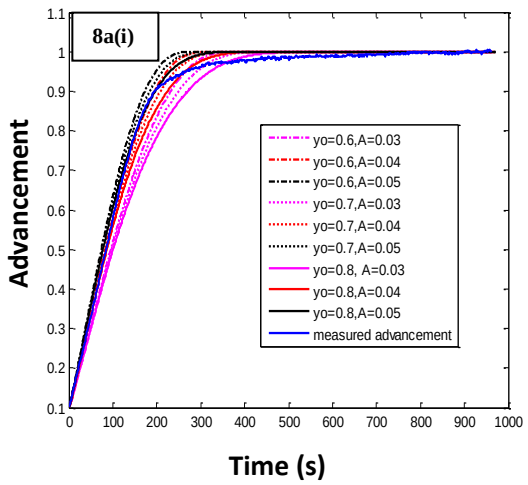
8a(i)
Advancement
Time (s)
yo=0.6,A=0.03
yo=0.6,A=0.04
yo=0.6,A=0.05
yo=0.7,A=0.03
yo=0.7,A=0.04
yo=0.7,A=0.05
yo=0.8, A=0.03
yo=0.8,A=0.04
yo=0.8,A=0.05
measured advancement

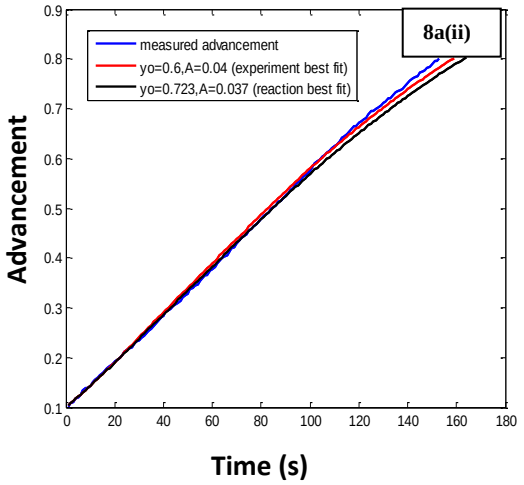
8a(ii)
Advancement
Time (s)
measured advancement
yo=0.6,A=0.04 (experiment best fit)
yo=0.723,A=0.037 (reaction best fit)

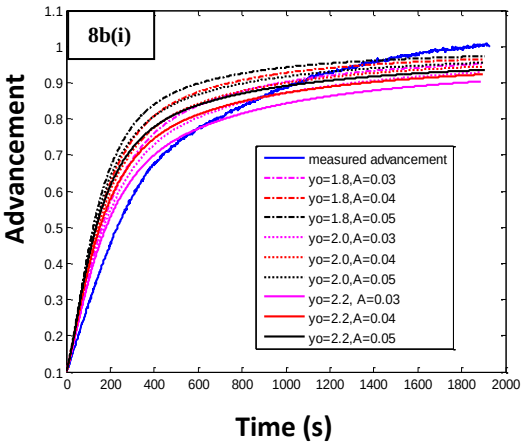
8b(i)
Advancement
Time (s)
measured advancement
yo=1.8,A=0.03
yo=1.8,A=0.04
yo=1.8,A=0.05
yo=2.0,A=0.03
yo=2.0,A=0.04
yo=2.0,A=0.05
yo=2.2, A=0.03
yo=2.2,A=0.04
yo=2.2,A=0.05

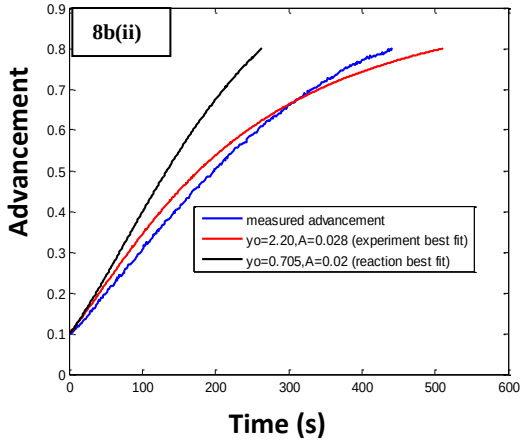
8b(ii)
Advancement
Time (s)
measured advancement
yo=2.20,A=0.028 (experiment best fit)
yo=0.705,A=0.02 (reaction best fit)

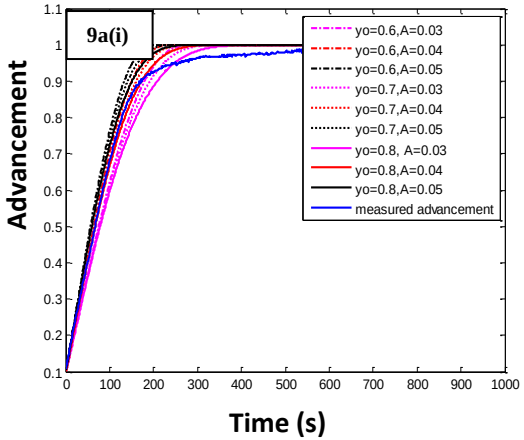
9a(i)
Advancement
Time (s)
yo=0.6,A=0.03
yo=0.6,A=0.04
yo=0.6,A=0.05
yo=0.7,A=0.03
yo=0.7,A=0.04
yo=0.7,A=0.05
yo=0.8, A=0.03
yo=0.8,A=0.04
yo=0.8,A=0.05
measured advancement

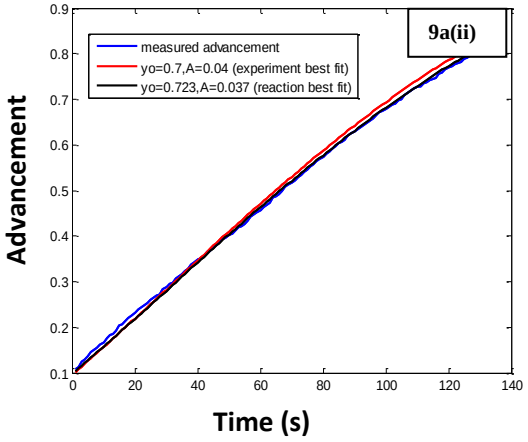
9a(ii)
measured advancement
yo=0.7,A=0.04 (experiment best fit)
yo=0.723,A=0.037 (reaction best fit)
Advancement
Time (s)

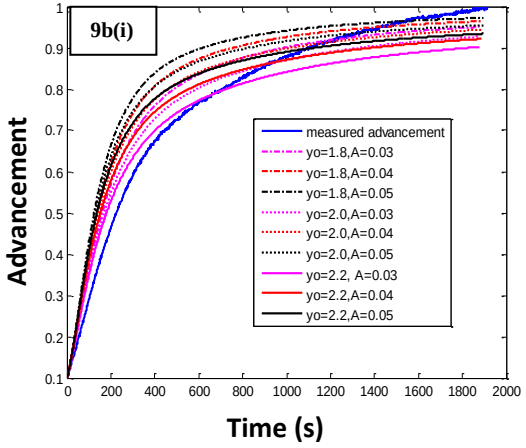
9b(i)
measured advancement
yo=1.8,A=0.03
yo=1.8,A=0.04
yo=1.8,A=0.05
yo=2.0,A=0.03
yo=2.0,A=0.04
yo=2.0,A=0.05
yo=2.2, A=0.03
yo=2.2,A=0.04
yo=2.2,A=0.05
Advancement
Time (s)

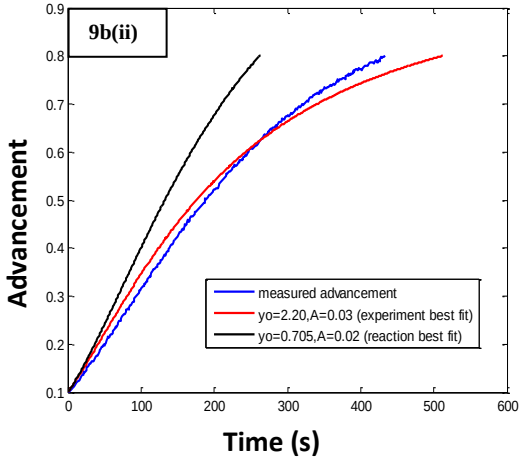
9b(ii)
measured advancement
yo=2.20,A=0.03 (experiment best fit)
yo=0.705,A=0.02 (reaction best fit)
Advancement
Time (s)

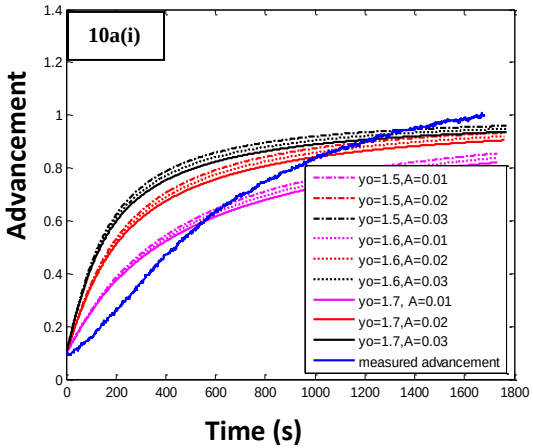
10a(i)
yo=1.5,A=0.01
yo=1.5,A=0.02
yo=1.5,A=0.03
yo=1.6,A=0.01
yo=1.6,A=0.02
yo=1.6,A=0.03
yo=1.7, A=0.01
yo=1.7,A=0.02
yo=1.7,A=0.03
measured advancement
Advancement
Time (s)

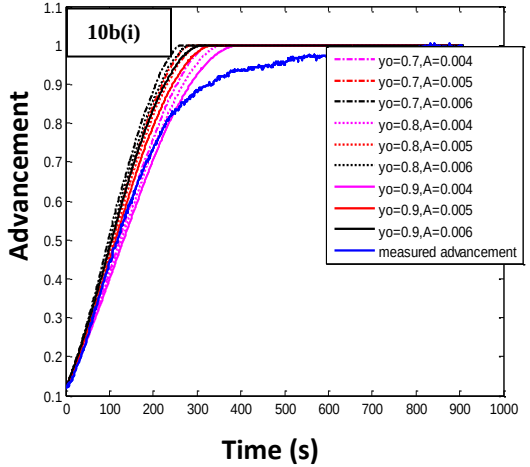
10b(i)
yo=0.7,A=0.004
yo=0.7,A=0.005
yo=0.7,A=0.006
yo=0.8,A=0.004
yo=0.8,A=0.005
yo=0.8,A=0.006
yo=0.9,A=0.004
yo=0.9,A=0.005
yo=0.9,A=0.006
measured advancement
Advancement
Time (s)

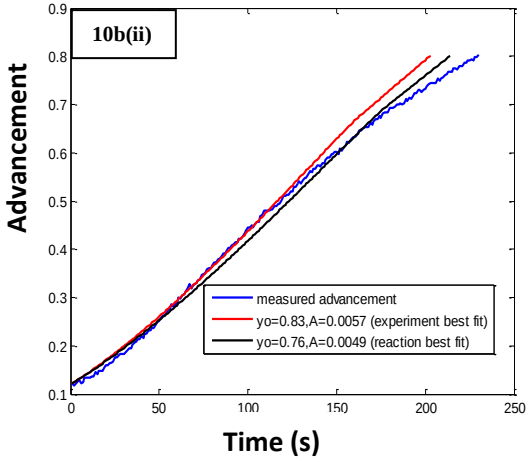
10b(ii)
measured advancement
yo=0.83,A=0.0057 (experiment best fit)
yo=0.76,A=0.0049 (reaction best fit)
Advancement
Time (s)

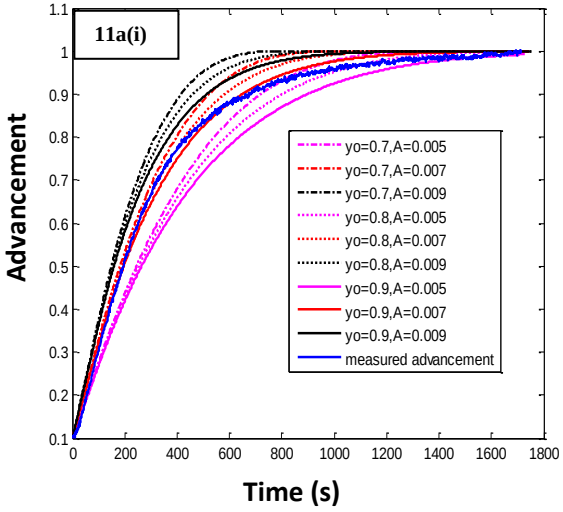
11a(i)
Advancement
Time (s)
yo=0.7,A=0.005
yo=0.7,A=0.007
yo=0.7,A=0.009
yo=0.8,A=0.005
yo=0.8,A=0.007
yo=0.8,A=0.009
yo=0.9,A=0.005
yo=0.9,A=0.007
yo=0.9,A=0.009
measured advancement

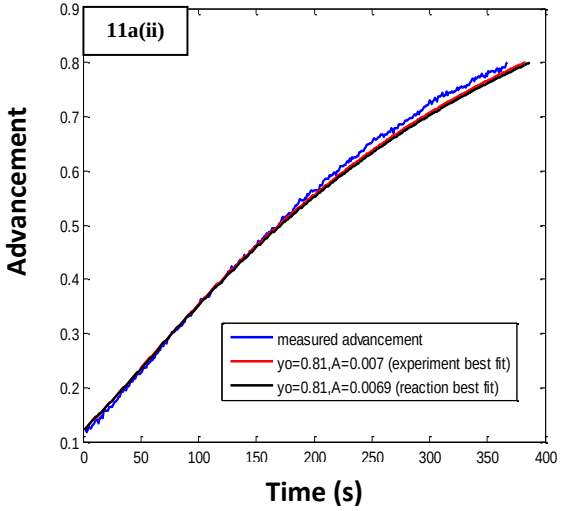
11a(ii)
Advancement
Time (s)
measured advancement
yo=0.81,A=0.007 (experiment best fit)
yo=0.81,A=0.0069 (reaction best fit)

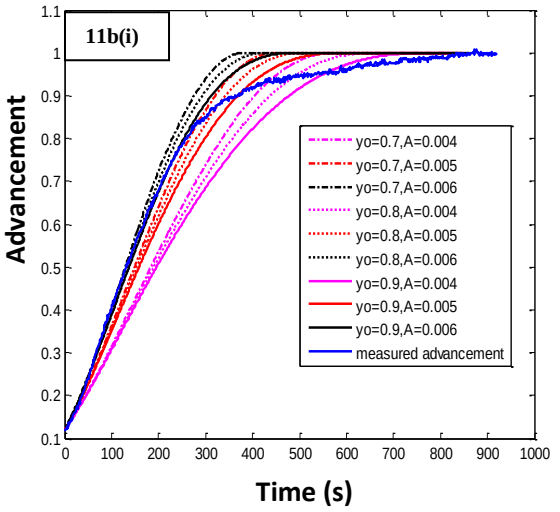
11b(i)
Advancement
Time (s)
yo=0.7,A=0.004
yo=0.7,A=0.005
yo=0.7,A=0.006
yo=0.8,A=0.004
yo=0.8,A=0.005
yo=0.8,A=0.006
yo=0.9,A=0.004
yo=0.9,A=0.005
yo=0.9,A=0.006
measured advancement

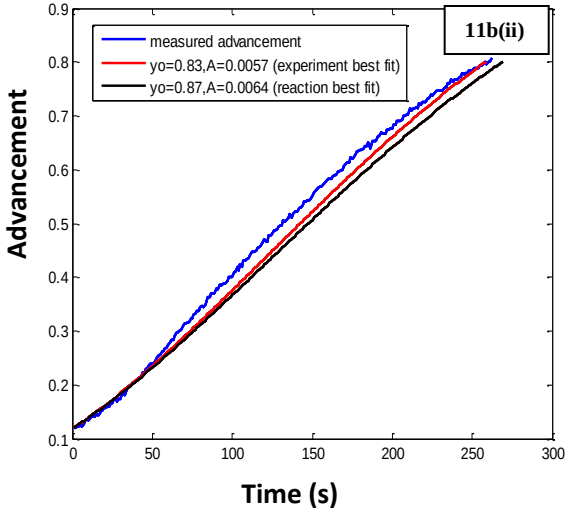
11b(ii)
Advancement
Time (s)
measured advancement
yo=0.83,A=0.0057 (experiment best fit)
yo=0.87,A=0.0064 (reaction best fit)

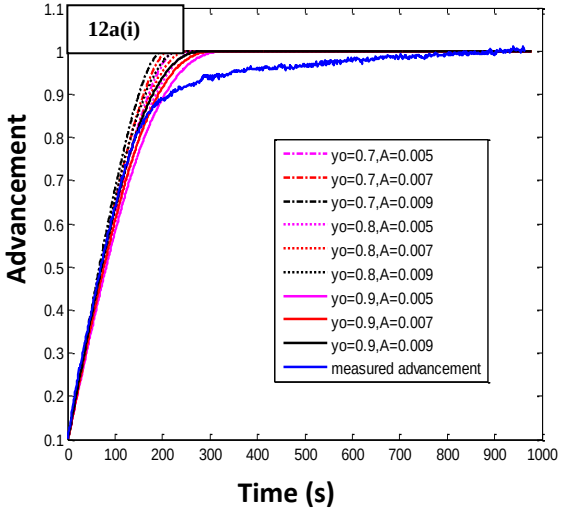
12a(i)
Advancement
Time (s)
yo=0.7,A=0.005
yo=0.7,A=0.007
yo=0.7,A=0.009
yo=0.8,A=0.005
yo=0.8,A=0.007
yo=0.8,A=0.009
yo=0.9,A=0.005
yo=0.9,A=0.007
yo=0.9,A=0.009
measured advancement

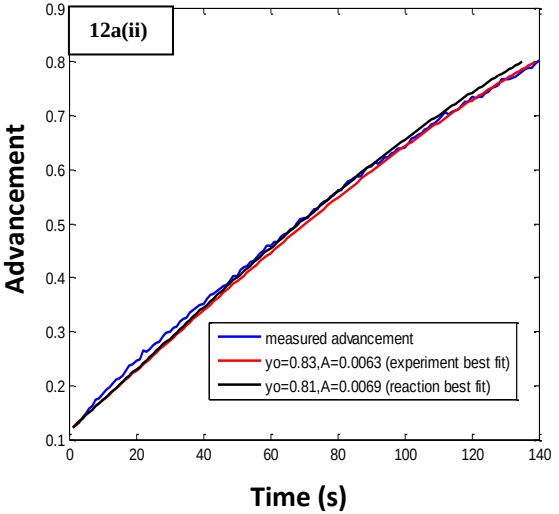
12a(ii)
Advancement
Time (s)
measured advancement
yo=0.83,A=0.0063 (experiment best fit)
yo=0.81,A=0.0069 (reaction best fit)

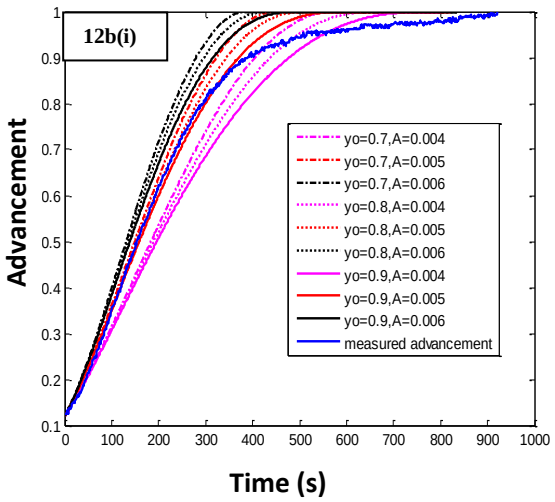
12b(i)
Advancement
Time (s)
yo=0.7,A=0.004
yo=0.7,A=0.005
yo=0.7,A=0.006
yo=0.8,A=0.004
yo=0.8,A=0.005
yo=0.8,A=0.006
yo=0.9,A=0.004
yo=0.9,A=0.005
yo=0.9,A=0.006
measured advancement

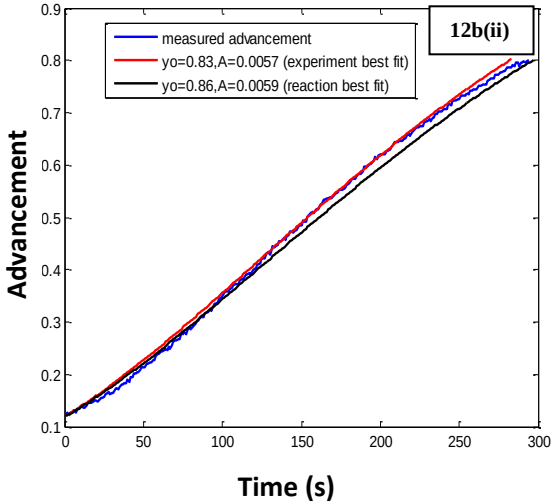
12b(ii)
Advancement
Time (s)
measured advancement
yo=0.83,A=0.0057 (experiment best fit)
yo=0.86,A=0.0059 (reaction best fit)

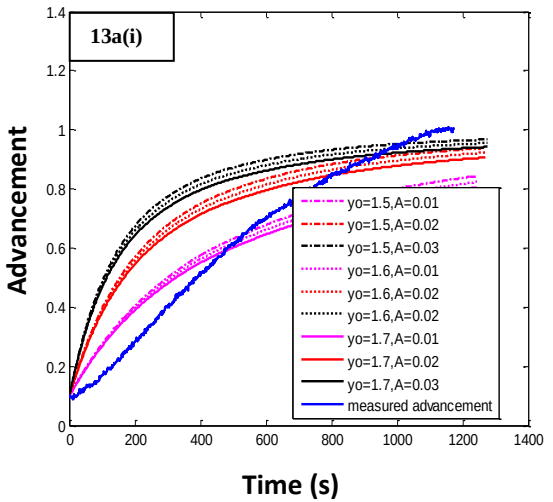
13a(i)
Advancement
Time (s)
yo=1.5,A=0.01
yo=1.5,A=0.02
yo=1.5,A=0.03
yo=1.6,A=0.01
yo=1.6,A=0.02
yo=1.6,A=0.02
yo=1.7,A=0.01
yo=1.7,A=0.02
yo=1.7,A=0.03
measured advancement

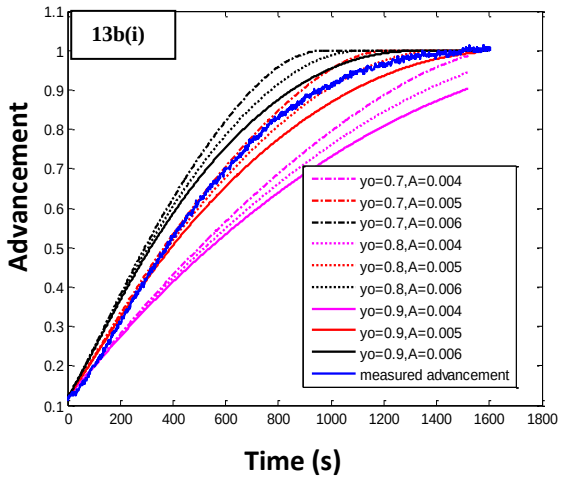
13b(i)
Advancement
Time (s)
yo=0.7,A=0.004
yo=0.7,A=0.005
yo=0.7,A=0.006
yo=0.8,A=0.004
yo=0.8,A=0.005
yo=0.8,A=0.006
yo=0.9,A=0.004
yo=0.9,A=0.005
yo=0.9,A=0.006
measured advancement

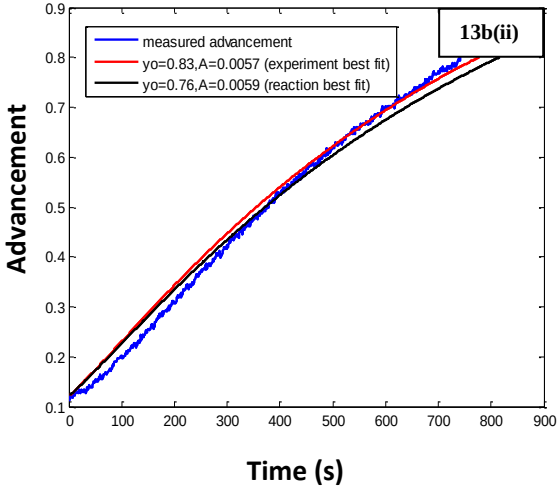
13b(ii)
Advancement
Time (s)
measured advancement
yo=0.83,A=0.0057 (experiment best fit)
yo=0.76,A=0.0059 (reaction best fit)

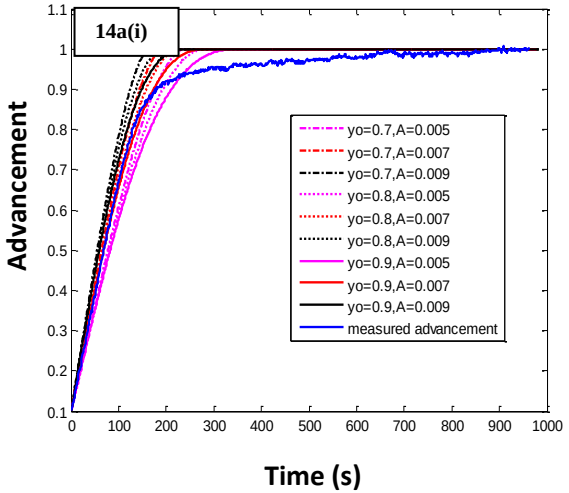
14a(i)
Advancement
Time (s)
yo=0.7,A=0.005
yo=0.7,A=0.007
yo=0.7,A=0.009
yo=0.8,A=0.005
yo=0.8,A=0.007
yo=0.8,A=0.009
yo=0.9,A=0.005
yo=0.9,A=0.007
yo=0.9,A=0.009
measured advancement

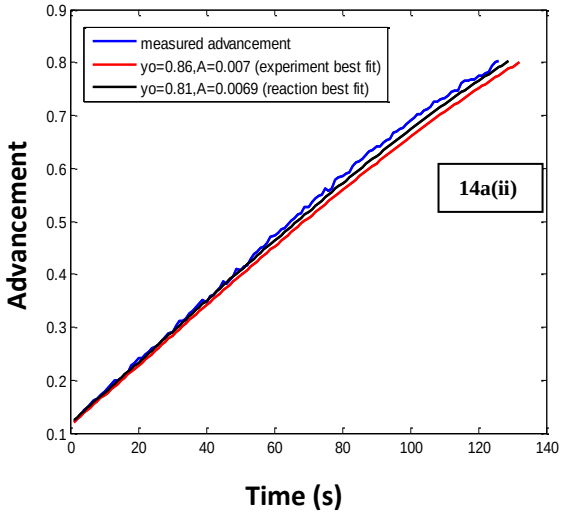
measured advancement
yo=0.86,A=0.007 (experiment best fit)
yo=0.81,A=0.0069 (reaction best fit)
14a(ii)
Advancement
Time (s)

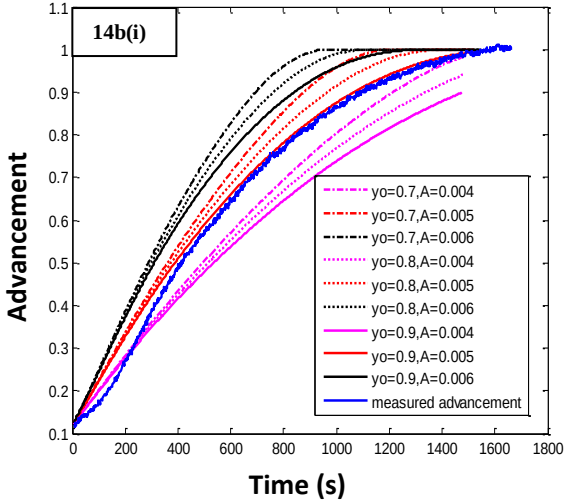
14b(i)
yo=0.7,A=0.004
yo=0.7,A=0.005
yo=0.7,A=0.006
yo=0.8,A=0.004
yo=0.8,A=0.005
yo=0.8,A=0.006
yo=0.9,A=0.004
yo=0.9,A=0.005
yo=0.9,A=0.006
measured advancement
Advancement
Time (s)

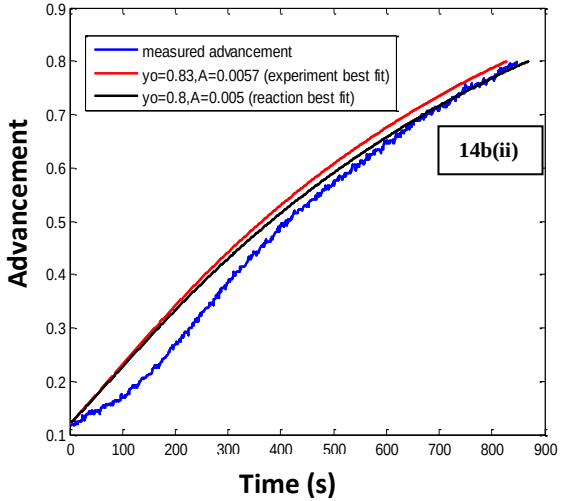
measured advancement
yo=0.83,A=0.0057 (experiment best fit)
yo=0.8,A=0.005 (reaction best fit)
14b(ii)
Advancement
Time (s)

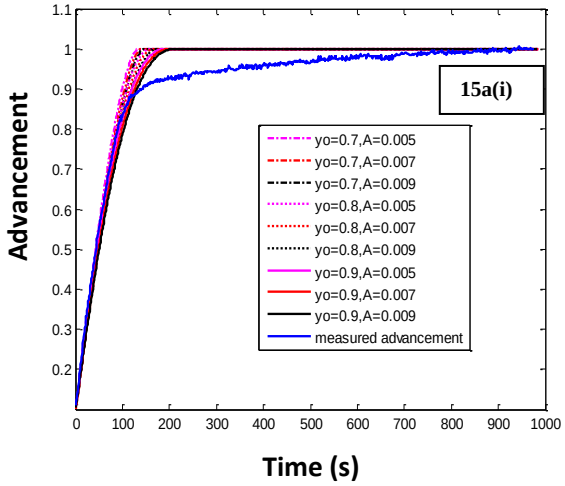
15a(i)
yo=0.7,A=0.005
yo=0.7,A=0.007
yo=0.7,A=0.009
yo=0.8,A=0.005
yo=0.8,A=0.007
yo=0.8,A=0.009
yo=0.9,A=0.005
yo=0.9,A=0.007
yo=0.9,A=0.009
measured advancement
Advancement
Time (s)

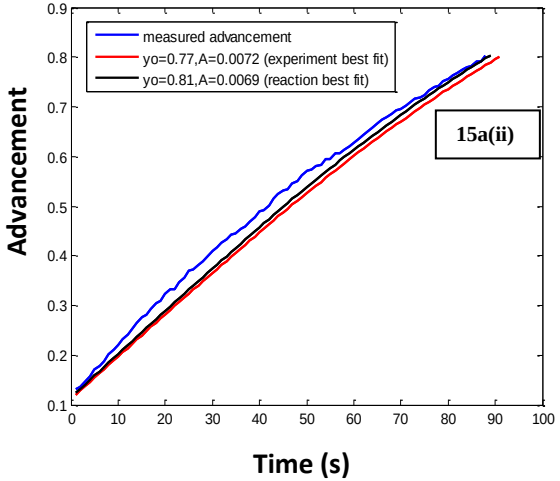
measured advancement
yo=0.77,A=0.0072 (experiment best fit)
yo=0.81,A=0.0069 (reaction best fit)
15a(ii)
Advancement
Time (s)

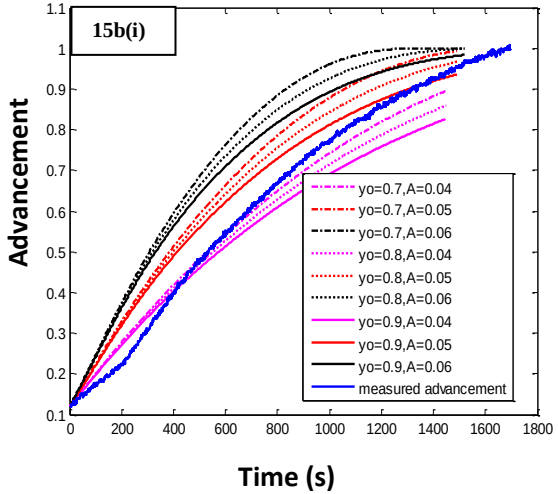
15b(i)
yo=0.7,A=0.04
yo=0.7,A=0.05
yo=0.7,A=0.06
yo=0.8,A=0.04
yo=0.8,A=0.05
yo=0.8,A=0.06
yo=0.9,A=0.04
yo=0.9,A=0.05
yo=0.9,A=0.06
measured advancement
Advancement
Time (s)

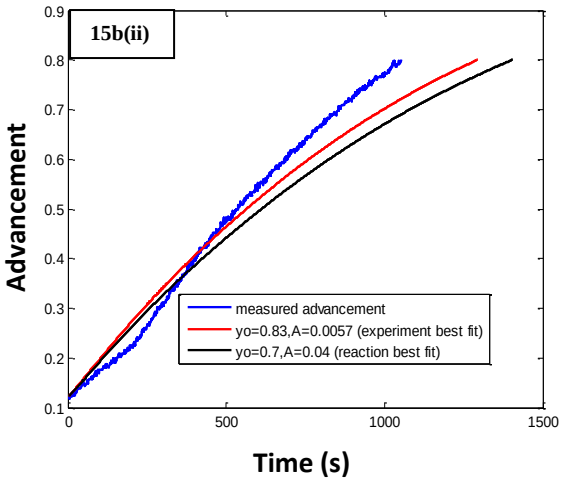
15b(ii)
Advancement
Time (s)
measured advancement
yo=0.83,A=0.0057 (experiment best fit)
yo=0.7,A=0.04 (reaction best fit)

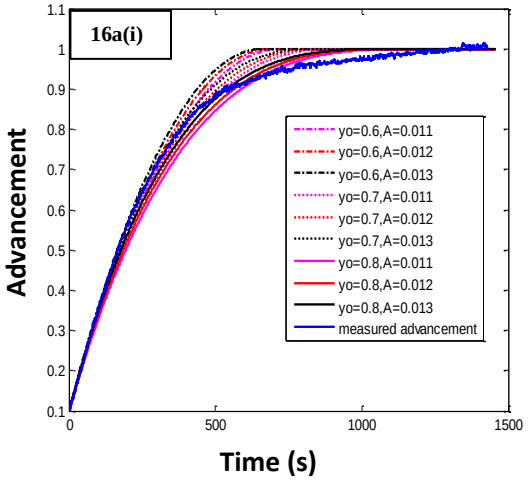
16a(i)
Advancement
Time (s)
yo=0.6,A=0.011
yo=0.6,A=0.012
yo=0.6,A=0.013
yo=0.7,A=0.011
yo=0.7,A=0.012
yo=0.7,A=0.013
yo=0.8,A=0.011
yo=0.8,A=0.012
yo=0.8,A=0.013
measured advancement

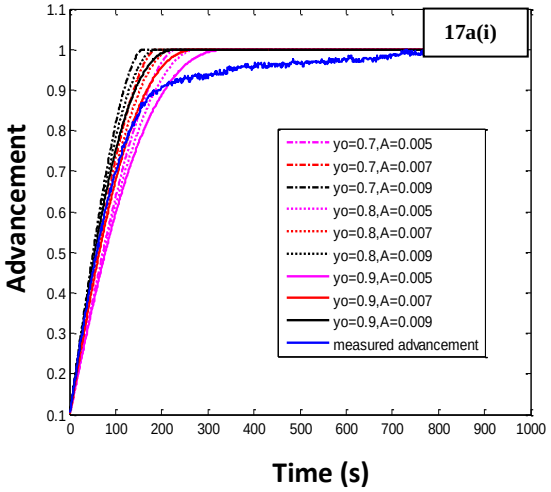
17a(i)
Advancement
Time (s)
yo=0.7,A=0.005
yo=0.7,A=0.007
yo=0.7,A=0.009
yo=0.8,A=0.005
yo=0.8,A=0.007
yo=0.8,A=0.009
yo=0.9,A=0.005
yo=0.9,A=0.007
yo=0.9,A=0.009
measured advancement

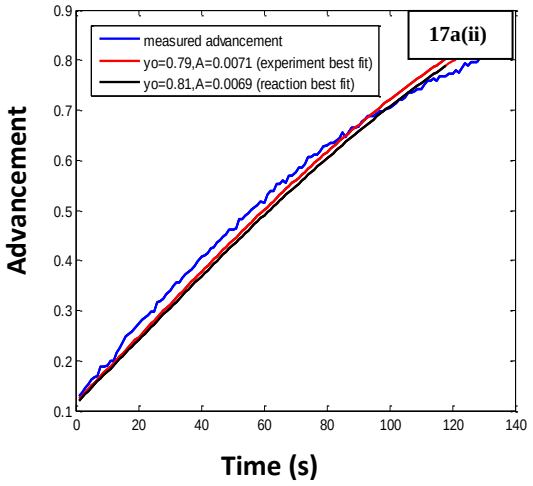
17a(ii)
Advancement
Time (s)
measured advancement
yo=0.79,A=0.0071 (experiment best fit)
yo=0.81,A=0.0069 (reaction best fit)

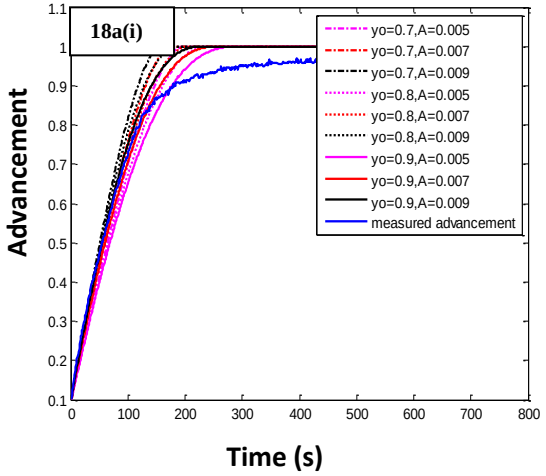
18a(i)
Advancement
Time (s)
yo=0.7,A=0.005
yo=0.7,A=0.007
yo=0.7,A=0.009
yo=0.8,A=0.005
yo=0.8,A=0.007
yo=0.8,A=0.009
yo=0.9,A=0.005
yo=0.9,A=0.007
yo=0.9,A=0.009
measured advancement

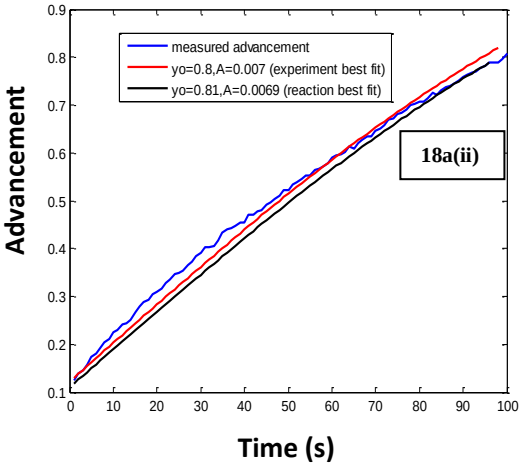
18a(ii)
Advancement
Time (s)
measured advancement
yo=0.8,A=0.007 (experiment best fit)
yo=0.81,A=0.0069 (reaction best fit)

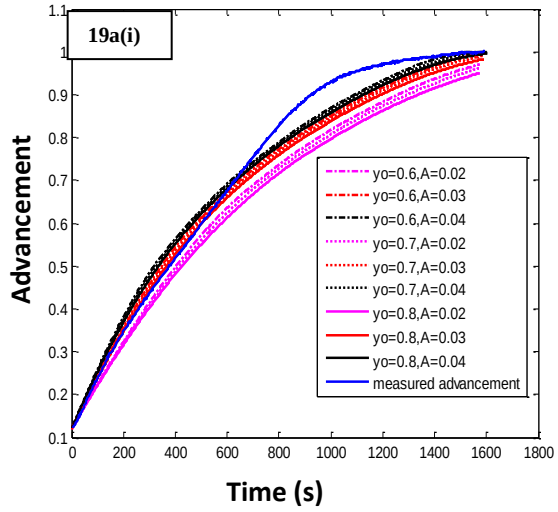
19a(i)
Advancement
Time (s)
yo=0.6,A=0.02
yo=0.6,A=0.03
yo=0.6,A=0.04
yo=0.7,A=0.02
yo=0.7,A=0.03
yo=0.7,A=0.04
yo=0.8,A=0.02
yo=0.8,A=0.03
yo=0.8,A=0.04
measured advancement

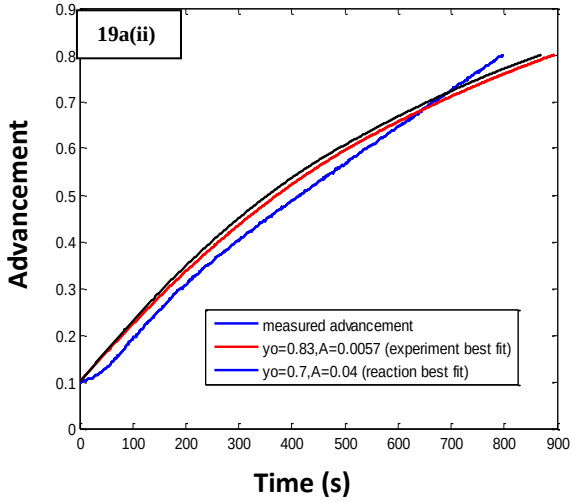
19a(ii)
Advancement
Time (s)
measured advancement
yo=0.83,A=0.0057 (experiment best fit)
yo=0.7,A=0.04 (reaction best fit)

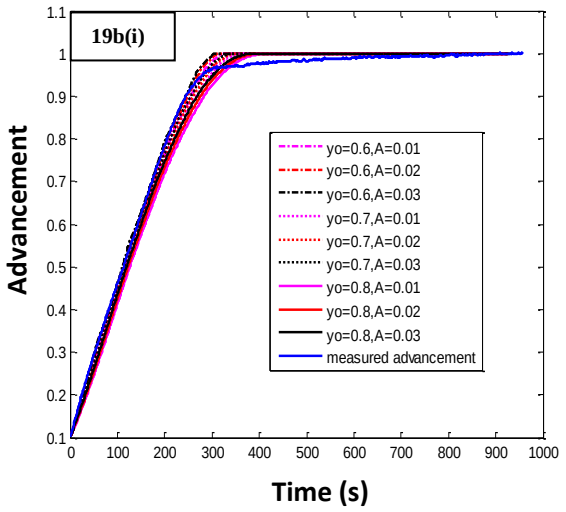
19b(i)
Advancement
Time (s)
yo=0.6,A=0.01
yo=0.6,A=0.02
yo=0.6,A=0.03
yo=0.7,A=0.01
yo=0.7,A=0.02
yo=0.7,A=0.03
yo=0.8,A=0.01
yo=0.8,A=0.02
yo=0.8,A=0.03
measured advancement

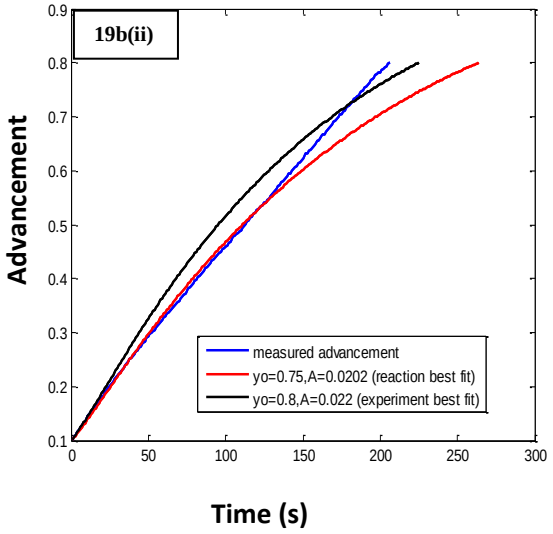
19b(ii)
Advancement
Time (s)
measured advancement
yo=0.75,A=0.0202 (reaction best fit)
yo=0.8,A=0.022 (experiment best fit)

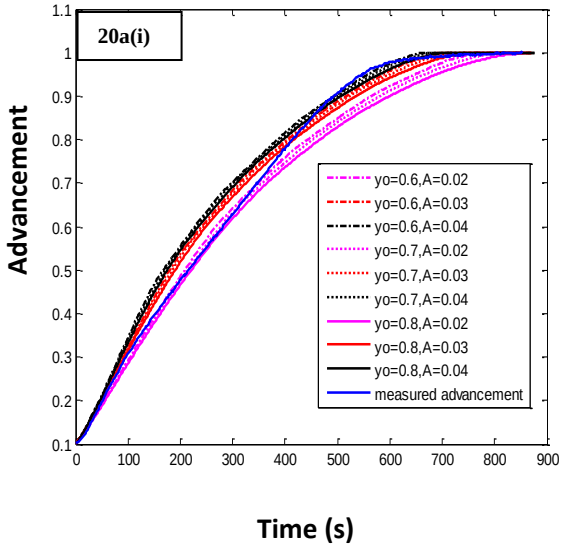
20a(i)
Advancement
Time (s)
yo=0.6,A=0.02
yo=0.6,A=0.03
yo=0.6,A=0.04
yo=0.7,A=0.02
yo=0.7,A=0.03
yo=0.7,A=0.04
yo=0.8,A=0.02
yo=0.8,A=0.03
yo=0.8,A=0.04
measured advancement

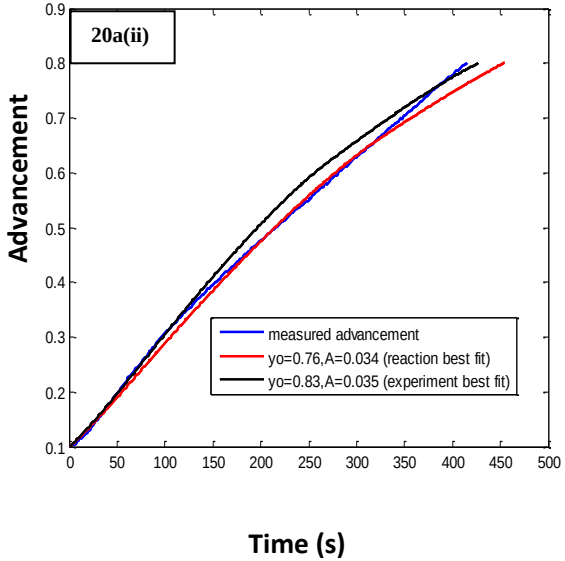
20a(ii)
Advancement
Time (s)
measured advancement
yo=0.76,A=0.034 (reaction best fit)
yo=0.83,A=0.035 (experiment best fit)

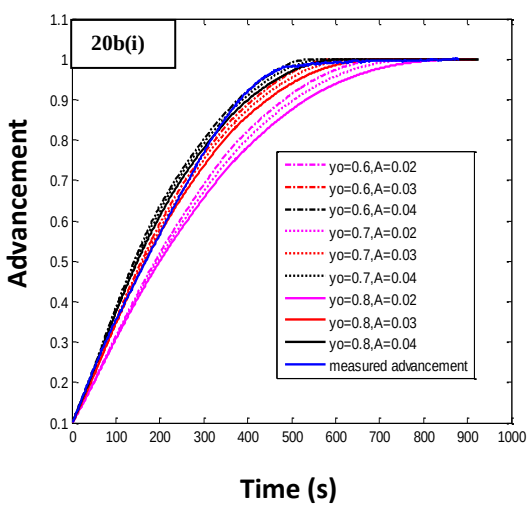
20b(i)
Advancement
Time (s)
yo=0.6,A=0.02
yo=0.6,A=0.03
yo=0.6,A=0.04
yo=0.7,A=0.02
yo=0.7,A=0.03
yo=0.7,A=0.04
yo=0.8,A=0.02
yo=0.8,A=0.03
yo=0.8,A=0.04
measured advancement

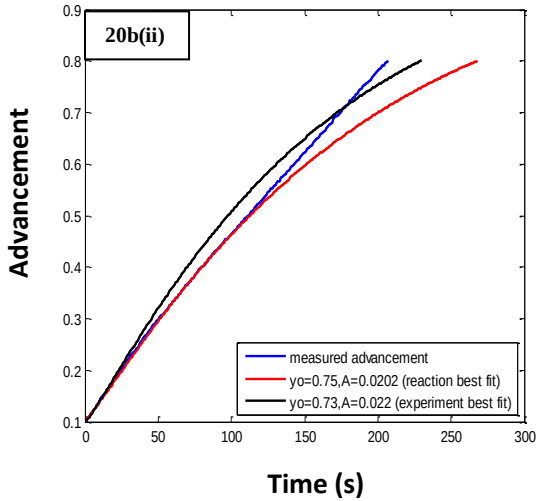
20b(ii)
Advancement
Time (s)
measured advancement
yo=0.75,A=0.0202 (reaction best fit)
yo=0.73,A=0.022 (experiment best fit)

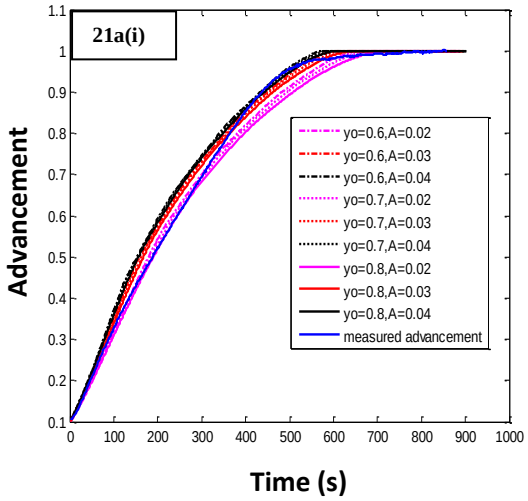
21a(i)
Advancement
Time (s)
yo=0.6,A=0.02
yo=0.6,A=0.03
yo=0.6,A=0.04
yo=0.7,A=0.02
yo=0.7,A=0.03
yo=0.7,A=0.04
yo=0.8,A=0.02
yo=0.8,A=0.03
yo=0.8,A=0.04
measured advancement

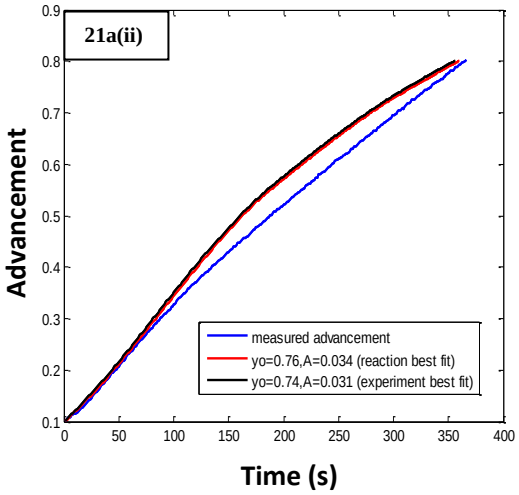
21a(ii)
Advancement
Time (s)
measured advancement
yo=0.76,A=0.034 (reaction best fit)
yo=0.74,A=0.031 (experiment best fit)

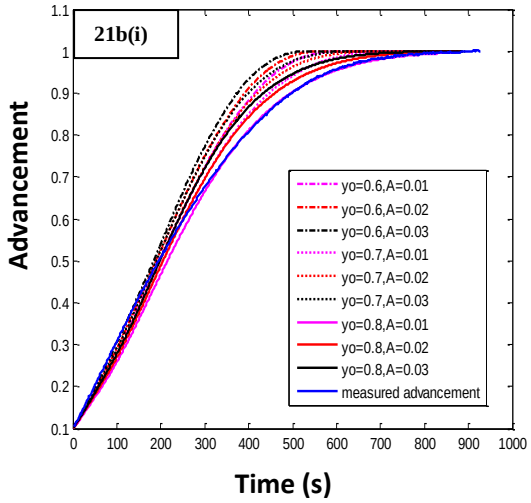
21b(i)
Advancement
Time (s)
yo=0.6,A=0.01
yo=0.6,A=0.02
yo=0.6,A=0.03
yo=0.7,A=0.01
yo=0.7,A=0.02
yo=0.7,A=0.03
yo=0.8,A=0.01
yo=0.8,A=0.02
yo=0.8,A=0.03
measured advancement

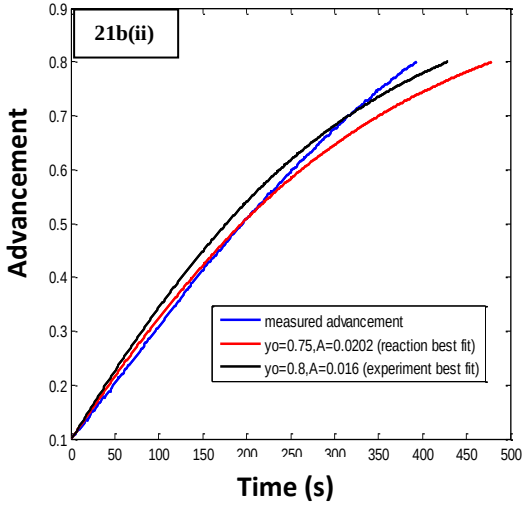
21b(ii)
Advancement
Time (s)
measured advancement
yo=0.75,A=0.0202 (reaction best fit)
yo=0.8,A=0.016 (experiment best fit)

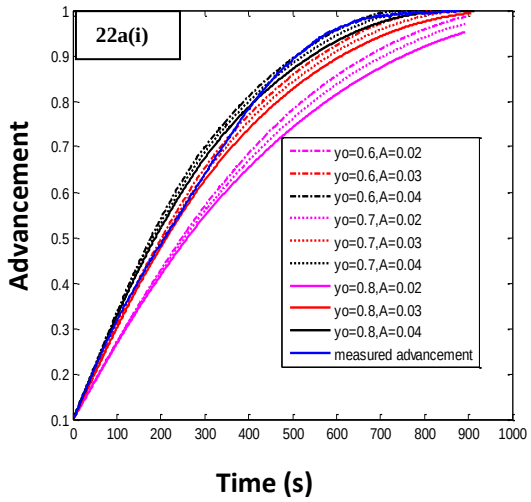
22a(i)
Advancement
Time (s)
yo=0.6,A=0.02
yo=0.6,A=0.03
yo=0.6,A=0.04
yo=0.7,A=0.02
yo=0.7,A=0.03
yo=0.7,A=0.04
yo=0.8,A=0.02
yo=0.8,A=0.03
yo=0.8,A=0.04
measured advancement

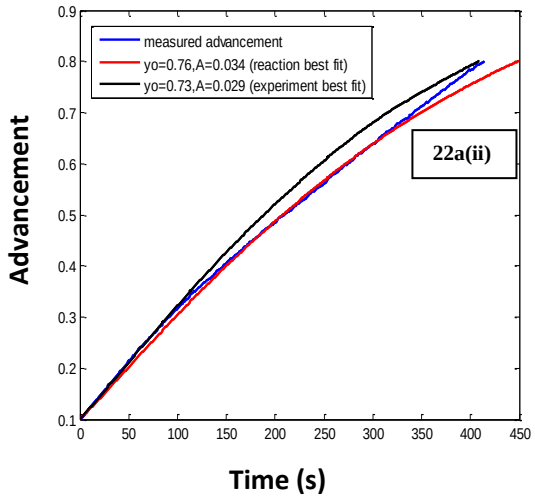
22a(ii)
Advancement
Time (s)
measured advancement
yo=0.76,A=0.034 (reaction best fit)
yo=0.73,A=0.029 (experiment best fit)

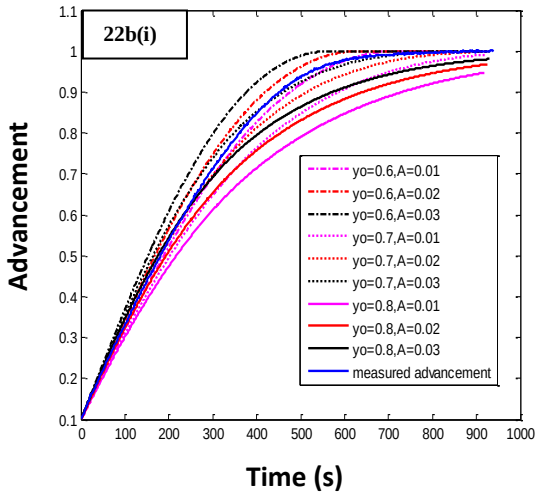
22b(i)
Advancement
Time (s)
yo=0.6,A=0.01
yo=0.6,A=0.02
yo=0.6,A=0.03
yo=0.7,A=0.01
yo=0.7,A=0.02
yo=0.7,A=0.03
yo=0.8,A=0.01
yo=0.8,A=0.02
yo=0.8,A=0.03
measured advancement

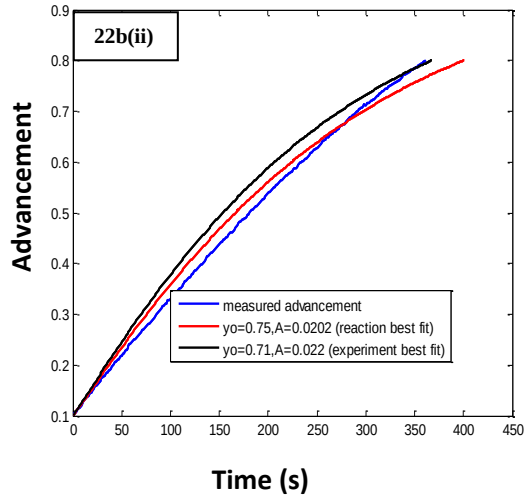
22b(ii)
Advancement
Time (s)
measured advancement
yo=0.75,A=0.0202 (reaction best fit)
yo=0.71,A=0.022 (experiment best fit)

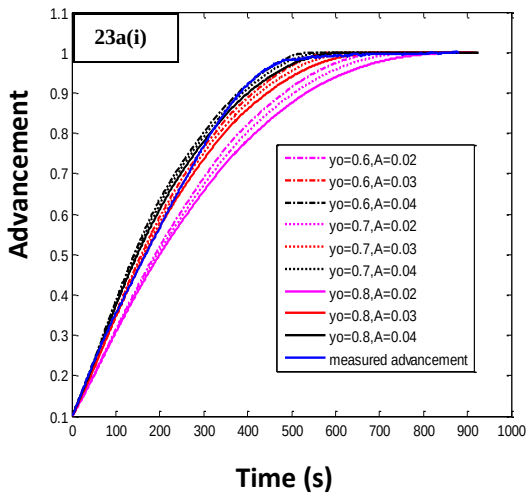
23a(i)
Advancement
Time (s)
yo=0.6,A=0.02
yo=0.6,A=0.03
yo=0.6,A=0.04
yo=0.7,A=0.02
yo=0.7,A=0.03
yo=0.7,A=0.04
yo=0.8,A=0.02
yo=0.8,A=0.03
yo=0.8,A=0.04
measured advancement

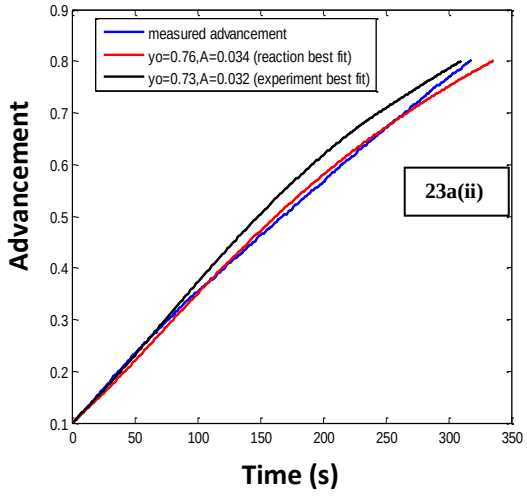
23a(ii)
Advancement
Time (s)
measured advancement
yo=0.76,A=0.034 (reaction best fit)
yo=0.73,A=0.032 (experiment best fit)

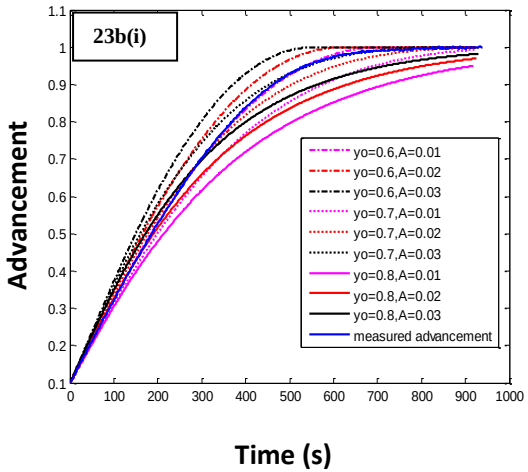
23b(i)
Advancement
Time (s)
yo=0.6,A=0.01
yo=0.6,A=0.02
yo=0.6,A=0.03
yo=0.7,A=0.01
yo=0.7,A=0.02
yo=0.7,A=0.03
yo=0.8,A=0.01
yo=0.8,A=0.02
yo=0.8,A=0.03
measured advancement

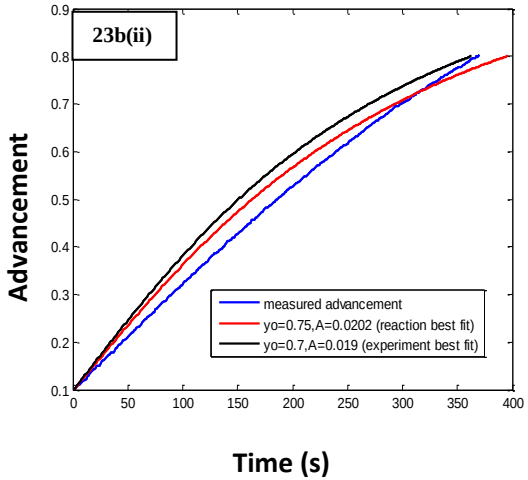
23b(ii)
Advancement
Time (s)
measured advancement
yo=0.75,A=0.0202 (reaction best fit)
yo=0.7,A=0.019 (experiment best fit)

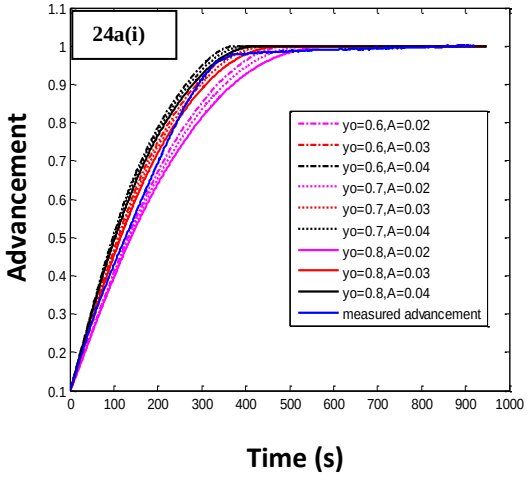
24a(i)
Advancement
Time (s)
yo=0.6,A=0.02
yo=0.6,A=0.03
yo=0.6,A=0.04
yo=0.7,A=0.02
yo=0.7,A=0.03
yo=0.7,A=0.04
yo=0.8,A=0.02
yo=0.8,A=0.03
yo=0.8,A=0.04
measured advancement

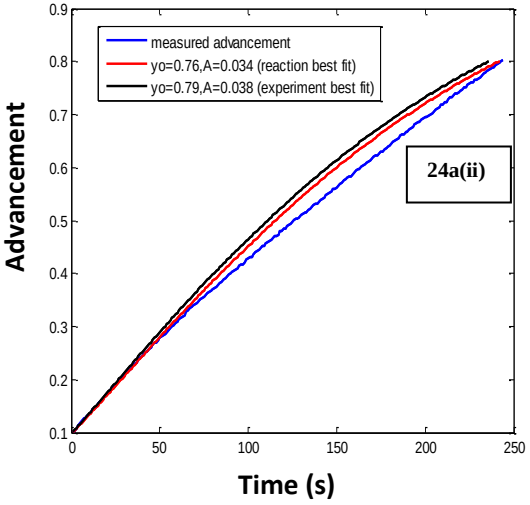
24a(ii)
Advancement
Time (s)
measured advancement
yo=0.76,A=0.034 (reaction best fit)
yo=0.79,A=0.038 (experiment best fit)

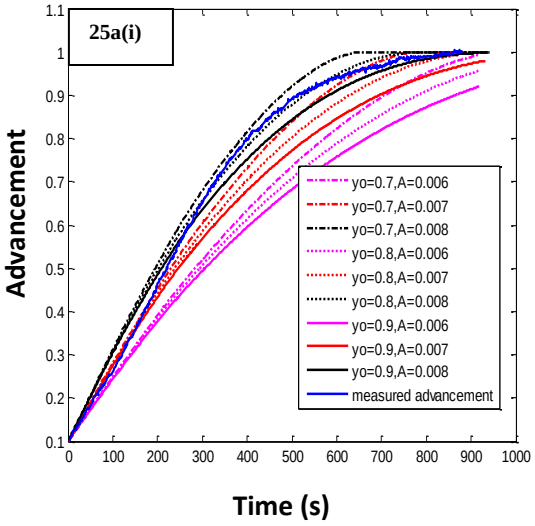
25a(i)
Advancement
Time (s)
yo=0.7,A=0.006
yo=0.7,A=0.007
yo=0.7,A=0.008
yo=0.8,A=0.006
yo=0.8,A=0.007
yo=0.8,A=0.008
yo=0.9,A=0.006
yo=0.9,A=0.007
yo=0.9,A=0.008
measured advancement

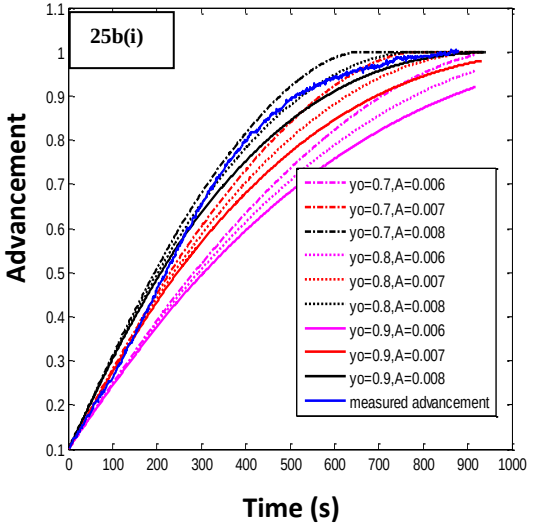
25b(i)
Advancement
Time (s)
yo=0.7,A=0.006
yo=0.7,A=0.007
yo=0.7,A=0.008
yo=0.8,A=0.006
yo=0.8,A=0.007
yo=0.8,A=0.008
yo=0.9,A=0.006
yo=0.9,A=0.007
yo=0.9,A=0.008
measured advancement

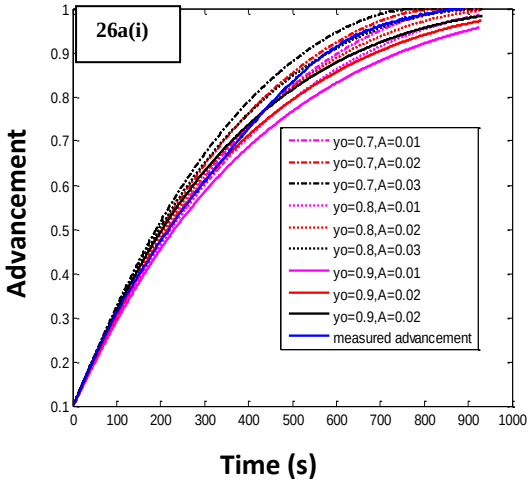
26a(i)
Advancement
Time (s)
yo=0.7,A=0.01
yo=0.7,A=0.02
yo=0.7,A=0.03
yo=0.8,A=0.01
yo=0.8,A=0.02
yo=0.8,A=0.03
yo=0.9,A=0.01
yo=0.9,A=0.02
yo=0.9,A=0.02
measured advancement

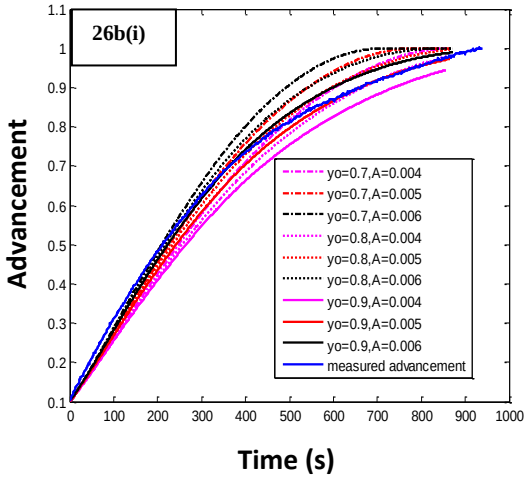
26b(i)
Advancement
Time (s)
yo=0.7,A=0.004
yo=0.7,A=0.005
yo=0.7,A=0.006
yo=0.8,A=0.004
yo=0.8,A=0.005
yo=0.8,A=0.006
yo=0.9,A=0.004
yo=0.9,A=0.005
yo=0.9,A=0.006
measured advancement

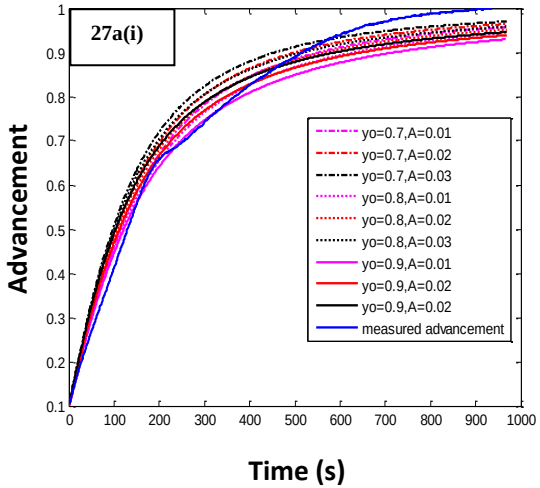
27a(i)
Advancement
Time (s)
yo=0.7,A=0.01
yo=0.7,A=0.02
yo=0.7,A=0.03
yo=0.8,A=0.01
yo=0.8,A=0.02
yo=0.8,A=0.03
yo=0.9,A=0.01
yo=0.9,A=0.02
yo=0.9,A=0.02
measured advancement

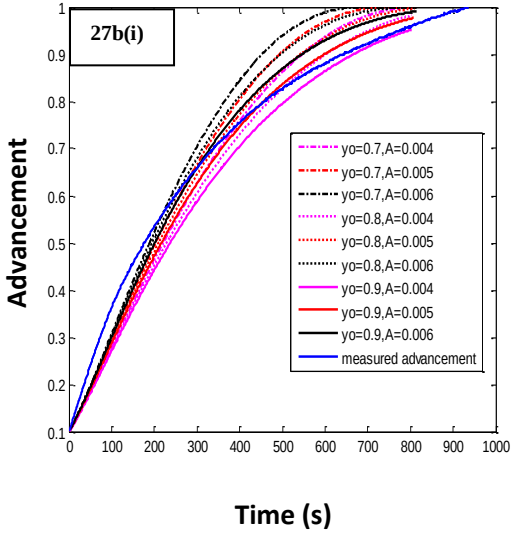
27b(i)
Advancement
Time (s)
yo=0.7,A=0.004
yo=0.7,A=0.005
yo=0.7,A=0.006
yo=0.8,A=0.004
yo=0.8,A=0.005
yo=0.8,A=0.006
yo=0.9,A=0.004
yo=0.9,A=0.005
yo=0.9,A=0.006
measured advancement

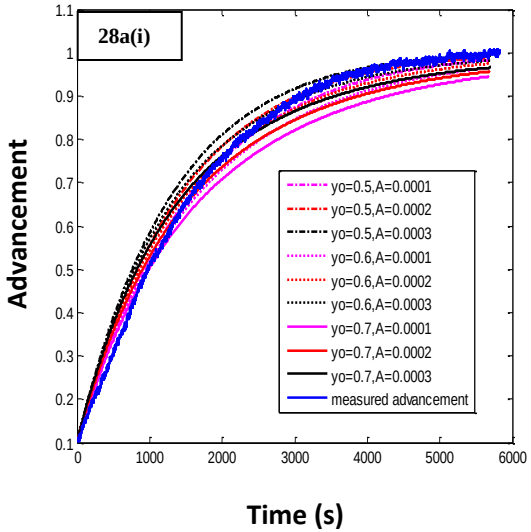
28a(i)
Advancement
Time (s)
yo=0.5,A=0.0001
yo=0.5,A=0.0002
yo=0.5,A=0.0003
yo=0.6,A=0.0001
yo=0.6,A=0.0002
yo=0.6,A=0.0003
yo=0.7,A=0.0001
yo=0.7,A=0.0002
yo=0.7,A=0.0003
measured advancement

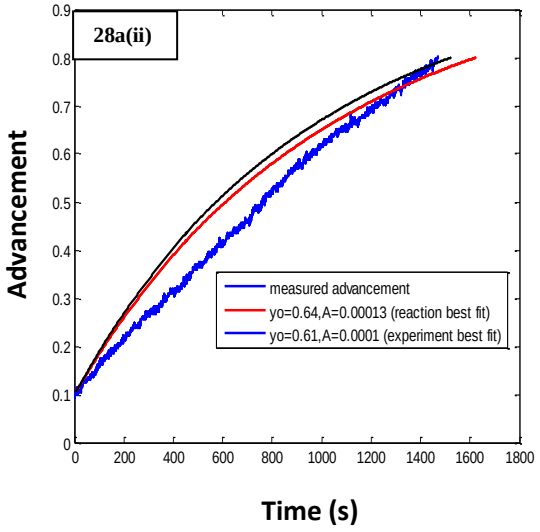
28a(ii)
Advancement
Time (s)
measured advancement
yo=0.64,A=0.00013 (reaction best fit)
yo=0.61,A=0.0001 (experiment best fit)

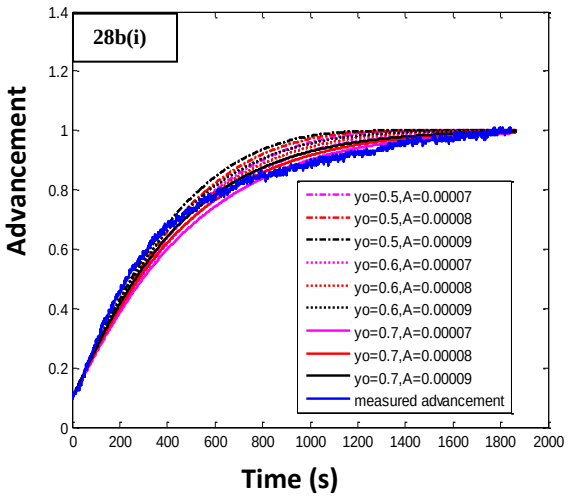
28b(i)
Advancement
Time (s)
yo=0.5,A=0.00007
yo=0.5,A=0.00008
yo=0.5,A=0.00009
yo=0.6,A=0.00007
yo=0.6,A=0.00008
yo=0.6,A=0.00009
yo=0.7,A=0.00007
yo=0.7,A=0.00008
yo=0.7,A=0.00009
measured advancement

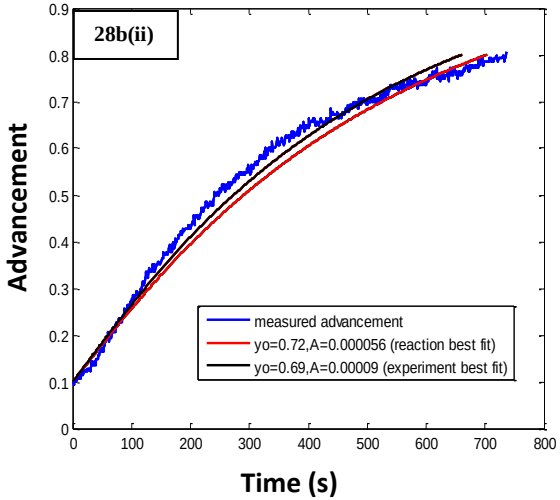
28b(ii)
Advancement
Time (s)
measured advancement
yo=0.72,A=0.000056 (reaction best fit)
yo=0.69,A=0.00009 (experiment best fit)

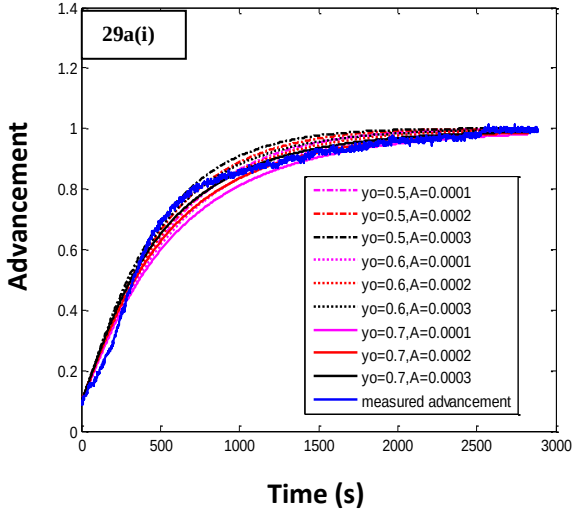
29a(i)
Advancement
Time (s)
yo=0.5,A=0.0001
yo=0.5,A=0.0002
yo=0.5,A=0.0003
yo=0.6,A=0.0001
yo=0.6,A=0.0002
yo=0.6,A=0.0003
yo=0.7,A=0.0001
yo=0.7,A=0.0002
yo=0.7,A=0.0003
measured advancement

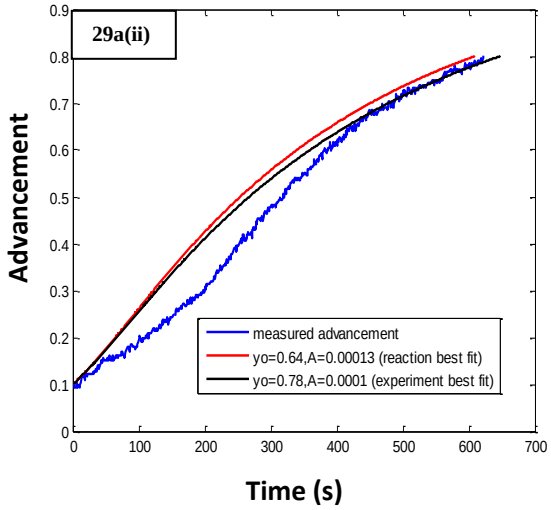
29a(ii)
Advancement
Time (s)
measured advancement
yo=0.64,A=0.00013 (reaction best fit)
yo=0.78,A=0.0001 (experiment best fit)

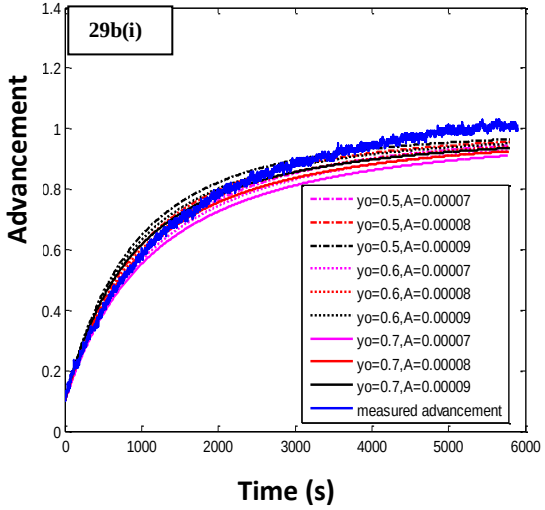
29b(i)
Advancement
Time (s)
yo=0.5,A=0.00007
yo=0.5,A=0.00008
yo=0.5,A=0.00009
yo=0.6,A=0.00007
yo=0.6,A=0.00008
yo=0.6,A=0.00009
yo=0.7,A=0.00007
yo=0.7,A=0.00008
yo=0.7,A=0.00009
measured advancement

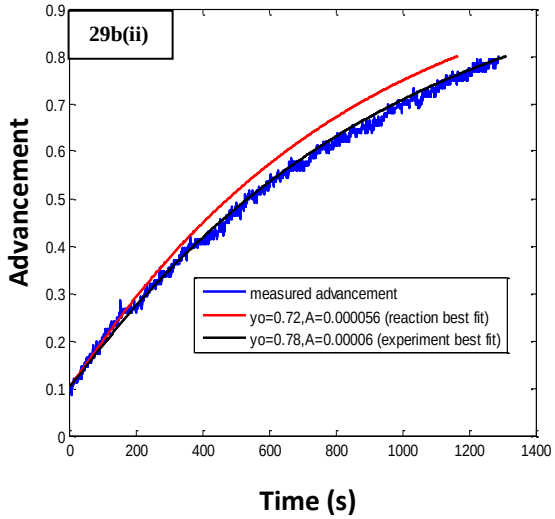
29b(ii)
Advancement
Time (s)
measured advancement
yo=0.72,A=0.000056 (reaction best fit)
yo=0.78,A=0.00006 (experiment best fit)

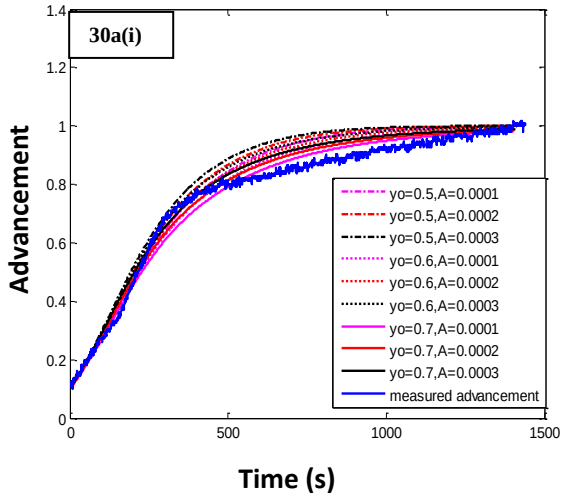
30a(i)
Advancement
Time (s)
yo=0.5,A=0.0001
yo=0.5,A=0.0002
yo=0.5,A=0.0003
yo=0.6,A=0.0001
yo=0.6,A=0.0002
yo=0.6,A=0.0003
yo=0.7,A=0.0001
yo=0.7,A=0.0002
yo=0.7,A=0.0003
measured advancement

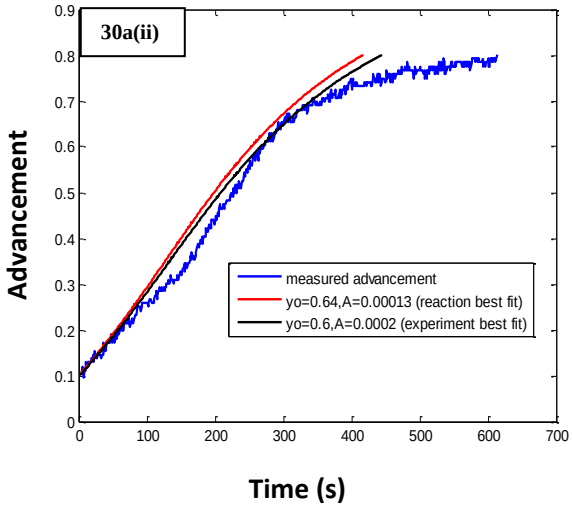
30a(ii)
Advancement
Time (s)
measured advancement
yo=0.64,A=0.00013 (reaction best fit)
yo=0.6,A=0.0002 (experiment best fit)

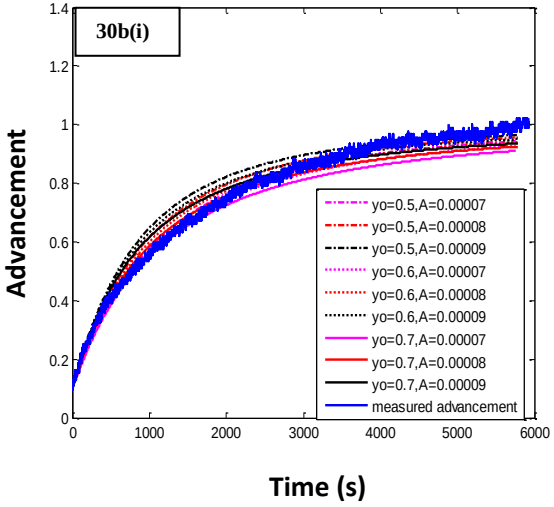
30b(i)
Advancement
Time (s)
yo=0.5,A=0.00007
yo=0.5,A=0.00008
yo=0.5,A=0.00009
yo=0.6,A=0.00007
yo=0.6,A=0.00008
yo=0.6,A=0.00009
yo=0.7,A=0.00007
yo=0.7,A=0.00008
yo=0.7,A=0.00009
measured advancement

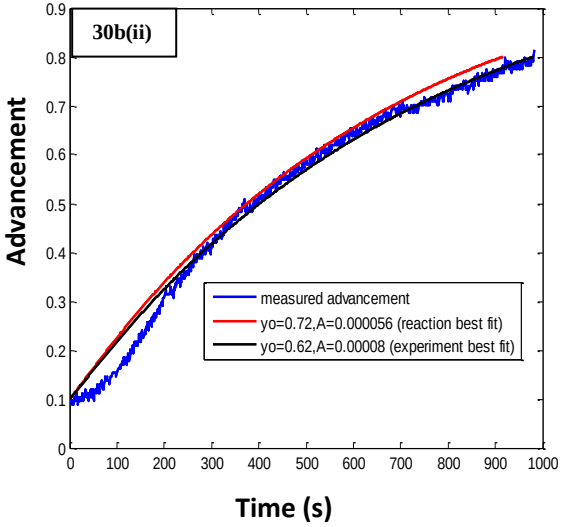
30b(ii)
Advancement
Time (s)
measured advancement
yo=0.72,A=0.000056 (reaction best fit)
yo=0.62,A=0.00008 (experiment best fit)

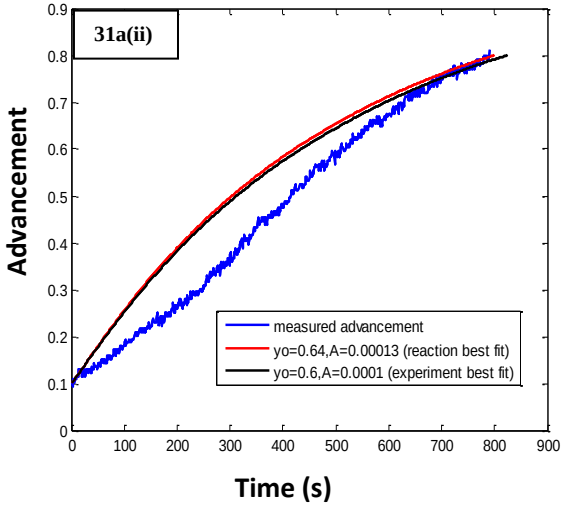
31a(ii)
Advancement
Time (s)
measured advancement
yo=0.64,A=0.00013 (reaction best fit)
yo=0.6,A=0.0001 (experiment best fit)

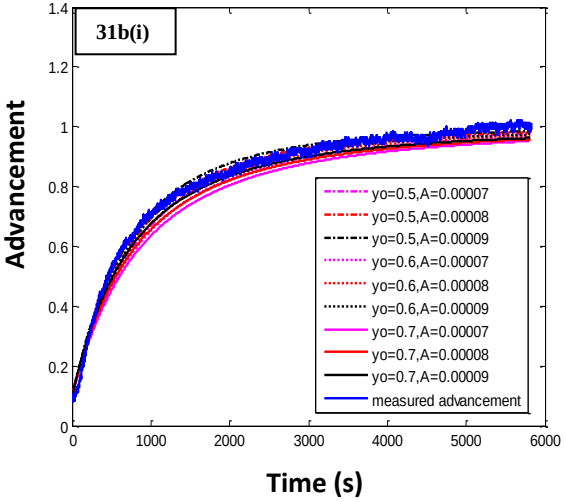
31b(i)
Advancement
Time (s)
yo=0.5,A=0.00007
yo=0.5,A=0.00008
yo=0.5,A=0.00009
yo=0.6,A=0.00007
yo=0.6,A=0.00008
yo=0.6,A=0.00009
yo=0.7,A=0.00007
yo=0.7,A=0.00008
yo=0.7,A=0.00009
measured advancement

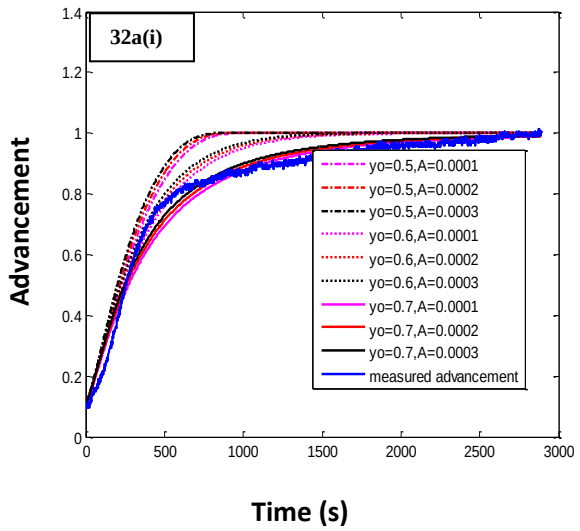
32a(i)
Advancement
Time (s)
yo=0.5,A=0.0001
yo=0.5,A=0.0002
yo=0.5,A=0.0003
yo=0.6,A=0.0001
yo=0.6,A=0.0002
yo=0.6,A=0.0003
yo=0.7,A=0.0001
yo=0.7,A=0.0002
yo=0.7,A=0.0003
measured advancement

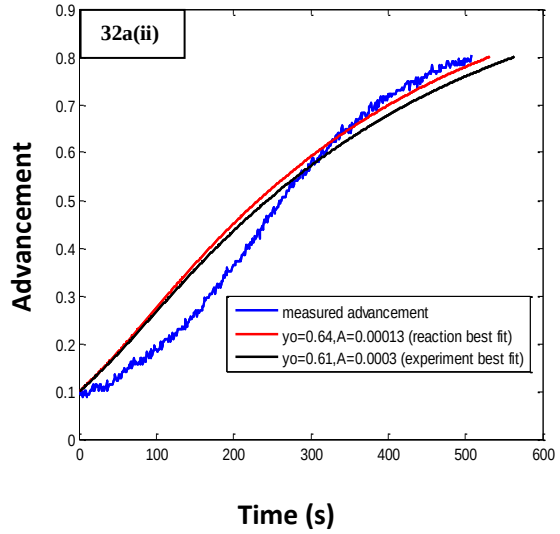
32a(ii)
Advancement
Time (s)
measured advancement
yo=0.64,A=0.00013 (reaction best fit)
yo=0.61,A=0.0003 (experiment best fit)

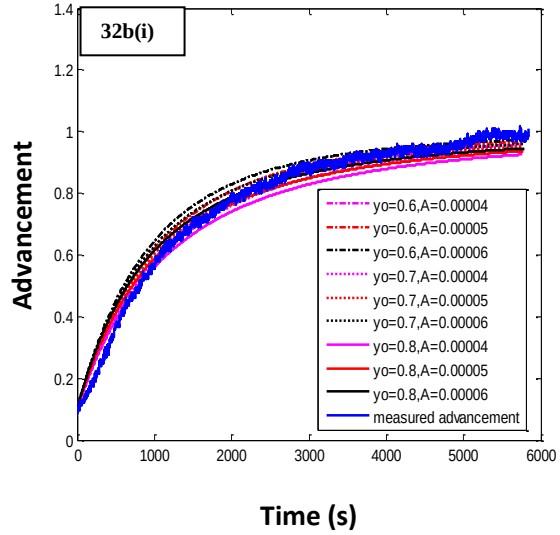
32b(i)
Advancement
Time (s)
yo=0.6,A=0.00004
yo=0.6,A=0.00005
yo=0.6,A=0.00006
yo=0.7,A=0.00004
yo=0.7,A=0.00005
yo=0.7,A=0.00006
yo=0.8,A=0.00004
yo=0.8,A=0.00005
yo=0.8,A=0.00006
measured advancement

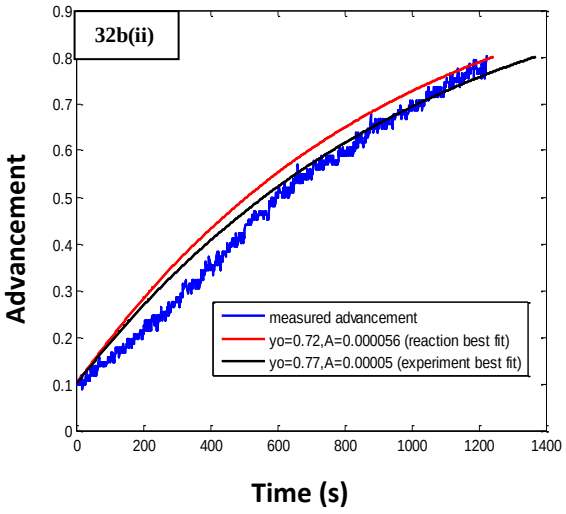
32b(ii)
Advancement
Time (s)
measured advancement
yo=0.72,A=0.000056 (reaction best fit)
yo=0.77,A=0.00005 (experiment best fit)

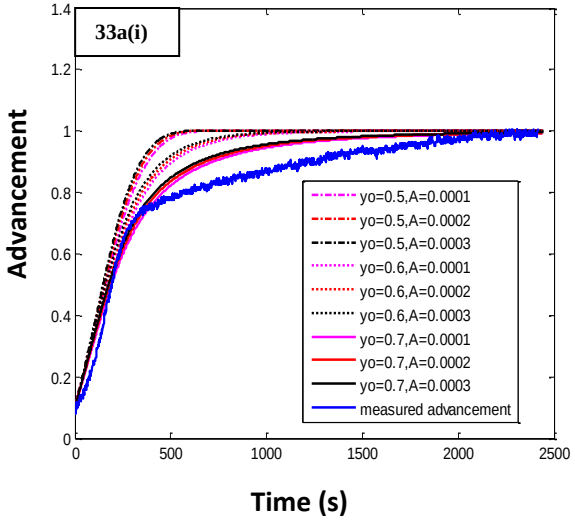
33a(i)
Advancement
Time (s)
yo=0.5,A=0.0001
yo=0.5,A=0.0002
yo=0.5,A=0.0003
yo=0.6,A=0.0001
yo=0.6,A=0.0002
yo=0.6,A=0.0003
yo=0.7,A=0.0001
yo=0.7,A=0.0002
yo=0.7,A=0.0003
measured advancement

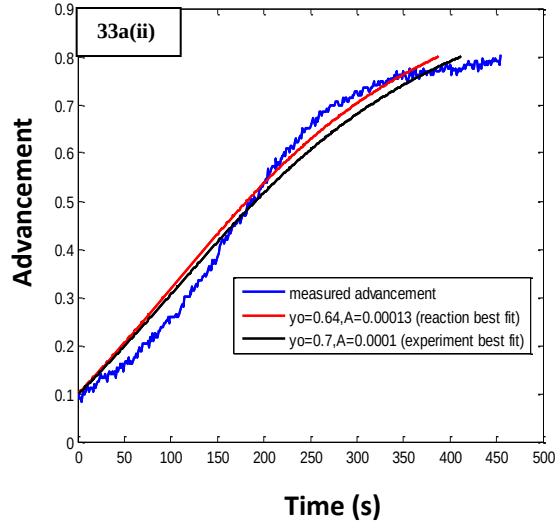
33a(ii)
Advancement
Time (s)
measured advancement
yo=0.64,A=0.00013 (reaction best fit)
yo=0.7,A=0.0001 (experiment best fit)

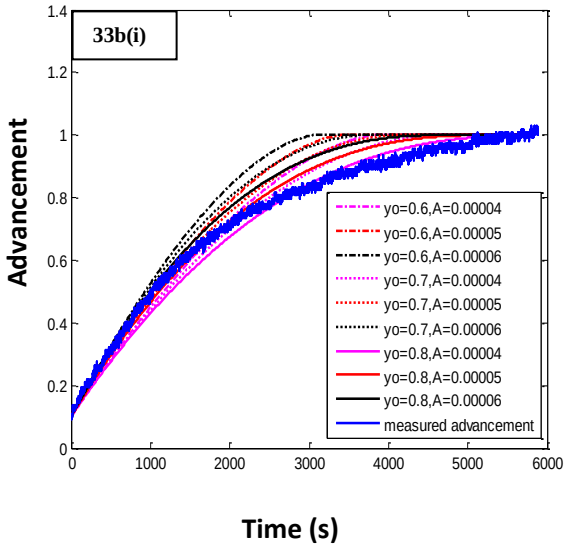
33b(i)
Advancement
Time (s)
yo=0.6,A=0.00004
yo=0.6,A=0.00005
yo=0.6,A=0.00006
yo=0.7,A=0.00004
yo=0.7,A=0.00005
yo=0.7,A=0.00006
yo=0.8,A=0.00004
yo=0.8,A=0.00005
yo=0.8,A=0.00006
measured advancement

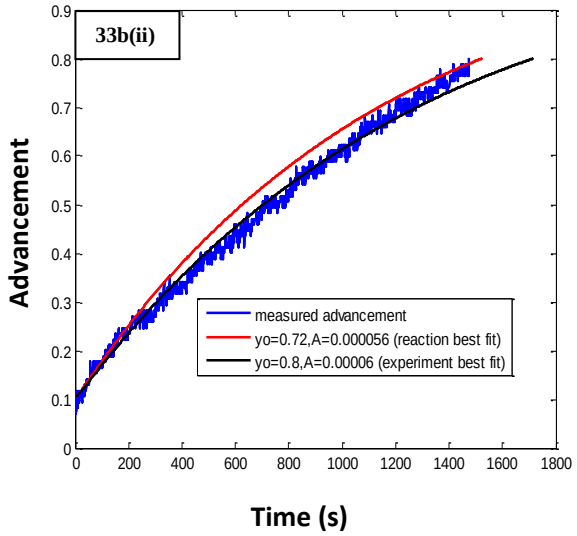
33b(ii)
Advancement
Time (s)
measured advancement
yo=0.72,A=0.000056 (reaction best fit)
yo=0.8,A=0.00006 (experiment best fit)

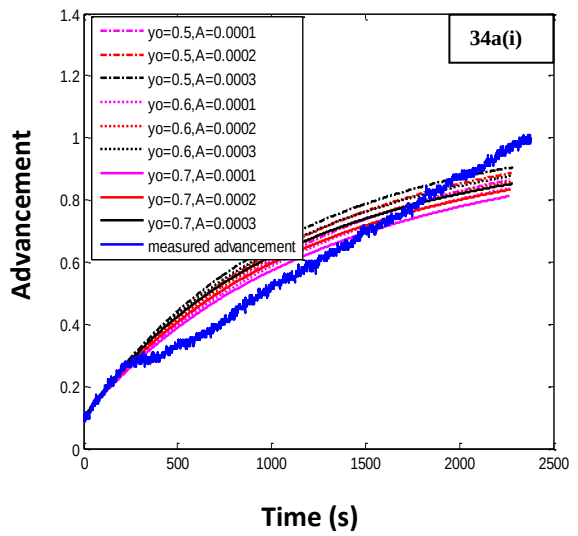
34a(i)
Advancement
Time (s)
yo=0.5,A=0.0001
yo=0.5,A=0.0002
yo=0.5,A=0.0003
yo=0.6,A=0.0001
yo=0.6,A=0.0002
yo=0.6,A=0.0003
yo=0.7,A=0.0001
yo=0.7,A=0.0002
yo=0.7,A=0.0003
measured advancement

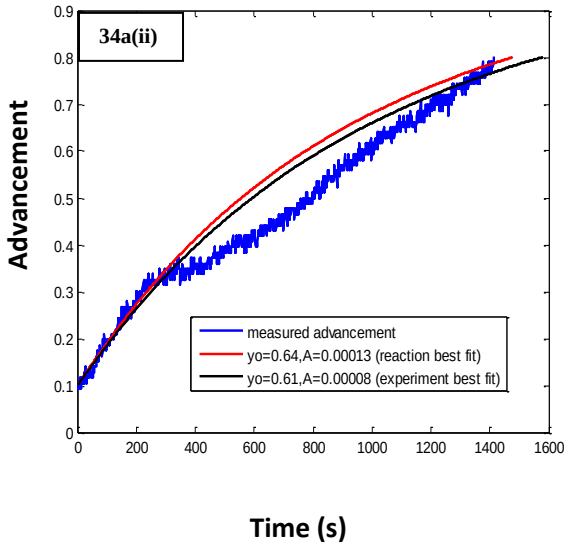
34a(ii)
Advancement
Time (s)
measured advancement
yo=0.64,A=0.00013 (reaction best fit)
yo=0.61,A=0.00008 (experiment best fit)

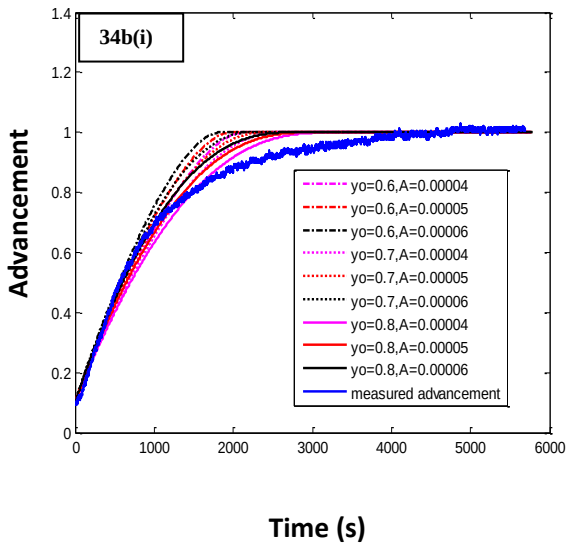
34b(i)
Advancement
Time (s)
yo=0.6,A=0.00004
yo=0.6,A=0.00005
yo=0.6,A=0.00006
yo=0.7,A=0.00004
yo=0.7,A=0.00005
yo=0.7,A=0.00006
yo=0.8,A=0.00004
yo=0.8,A=0.00005
yo=0.8,A=0.00006
measured advancement

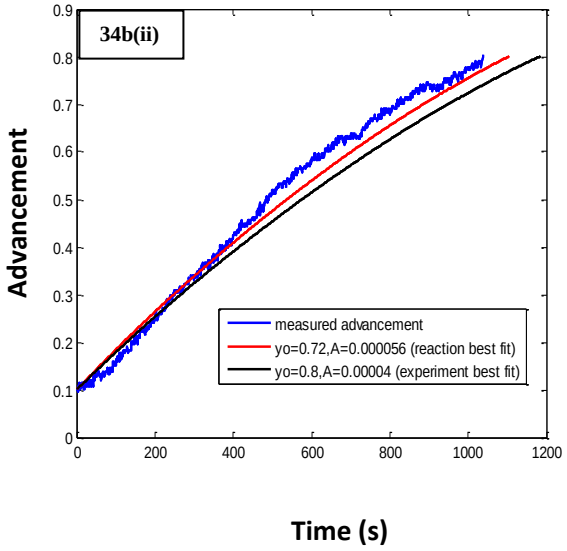
34b(ii)
Advancement
Time (s)
measured advancement
yo=0.72,A=0.000056 (reaction best fit)
yo=0.8,A=0.00004 (experiment best fit)

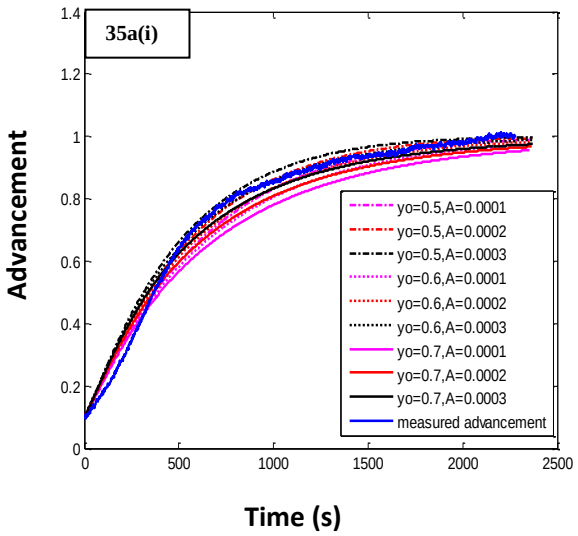
35a(i)
Advancement
Time (s)
yo=0.5,A=0.0001
yo=0.5,A=0.0002
yo=0.5,A=0.0003
yo=0.6,A=0.0001
yo=0.6,A=0.0002
yo=0.6,A=0.0003
yo=0.7,A=0.0001
yo=0.7,A=0.0002
yo=0.7,A=0.0003
measured advancement

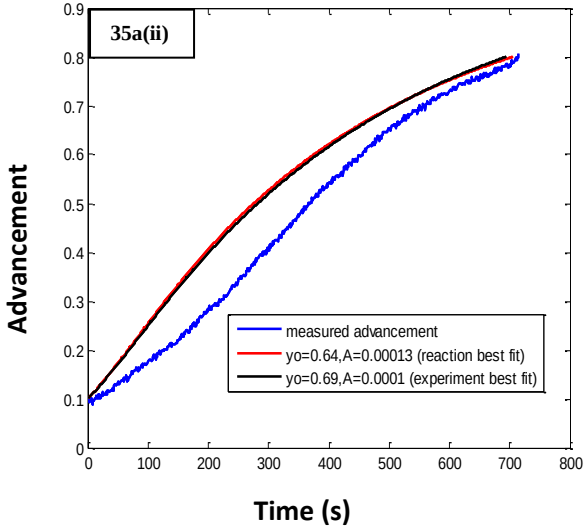
35a(ii)
Advancement
Time (s)
measured advancement
yo=0.64,A=0.00013 (reaction best fit)
yo=0.69,A=0.0001 (experiment best fit)

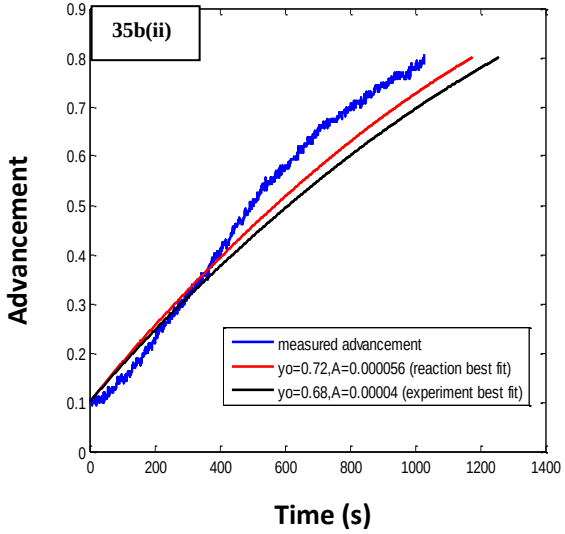
35b(ii)
Advancement
Time (s)
measured advancement
yo=0.72,A=0.000056 (reaction best fit)
yo=0.68,A=0.00004 (experiment best fit)

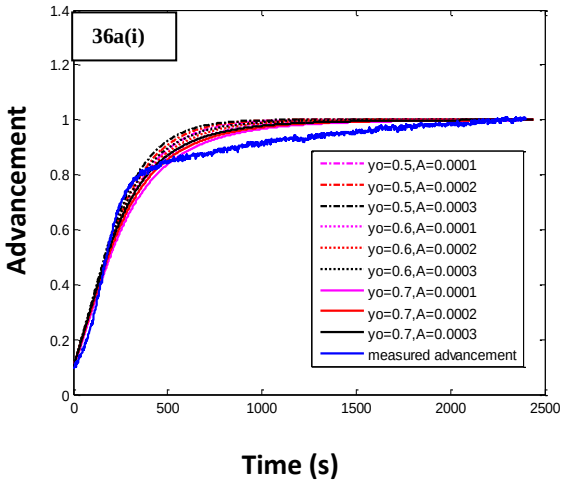
36a(i)
Advancement
Time (s)
yo=0.5,A=0.0001
yo=0.5,A=0.0002
yo=0.5,A=0.0003
yo=0.6,A=0.0001
yo=0.6,A=0.0002
yo=0.6,A=0.0003
yo=0.7,A=0.0001
yo=0.7,A=0.0002
yo=0.7,A=0.0003
measured advancement

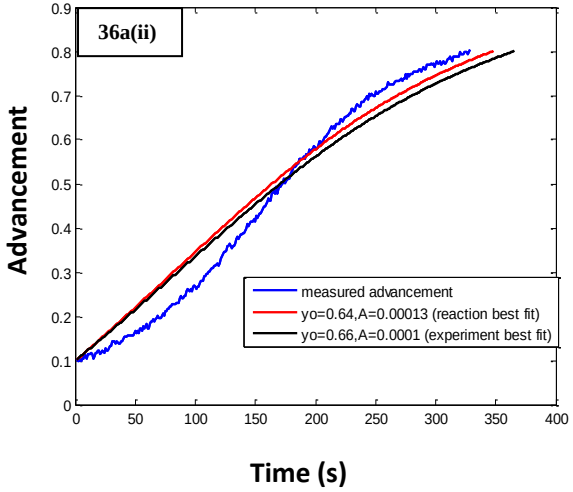
36a(ii)
Advancement
Time (s)
measured advancement
yo=0.64,A=0.00013 (reaction best fit)
yo=0.66,A=0.0001 (experiment best fit)

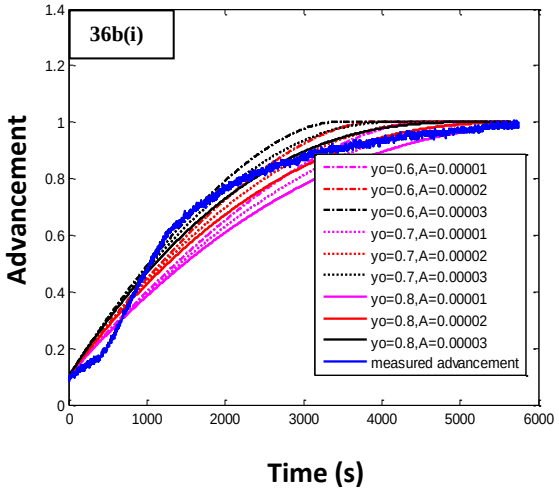
36b(i)
Advancement
Time (s)
yo=0.6,A=0.00001
yo=0.6,A=0.00002
yo=0.6,A=0.00003
yo=0.7,A=0.00001
yo=0.7,A=0.00002
yo=0.7,A=0.00003
yo=0.8,A=0.00001
yo=0.8,A=0.00002
yo=0.8,A=0.00003
measured advancement

Appendix 2: Solid Works Drawings of the Test Cell

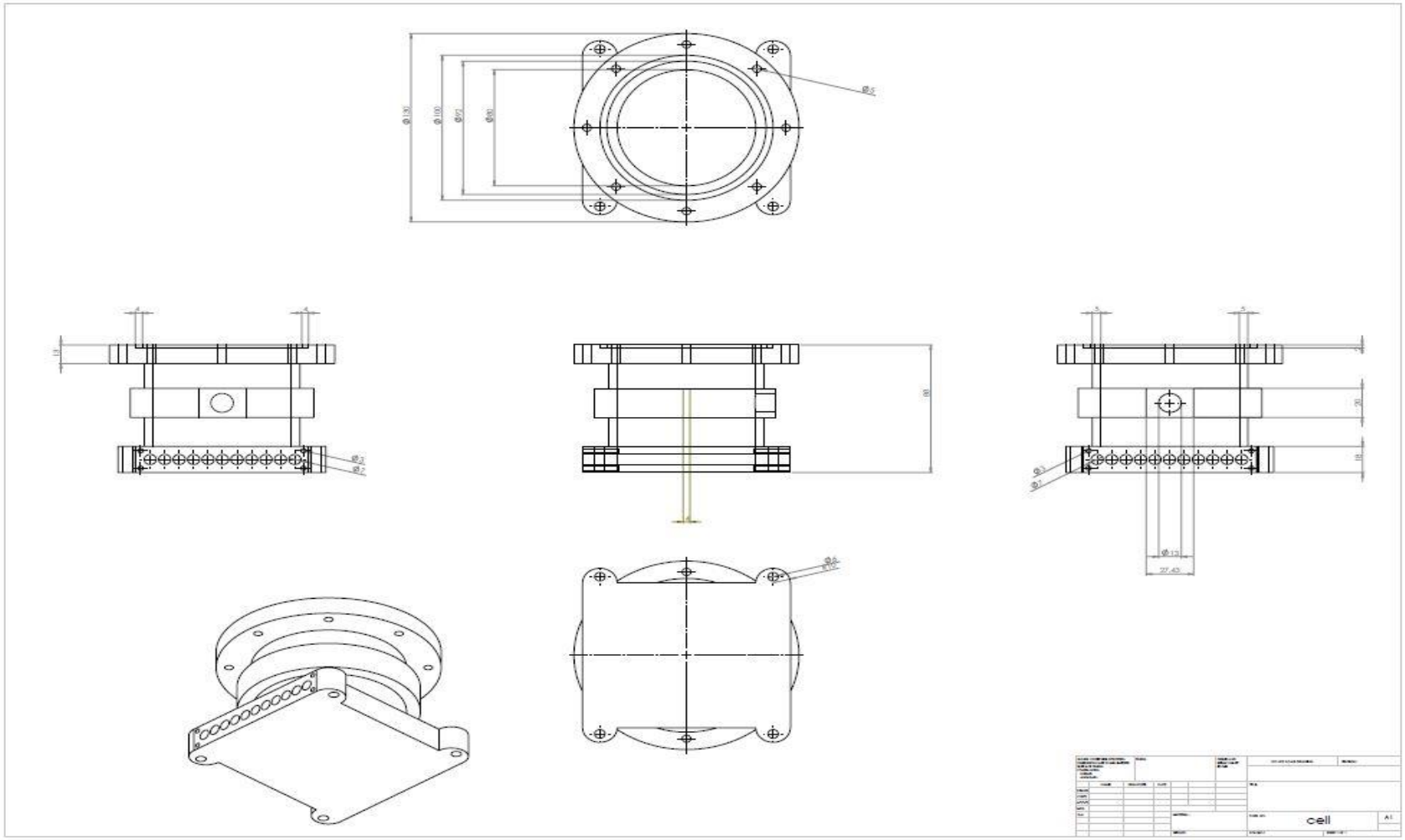

Appendix 3: Solid Works Drawings of the Test Cell Cover

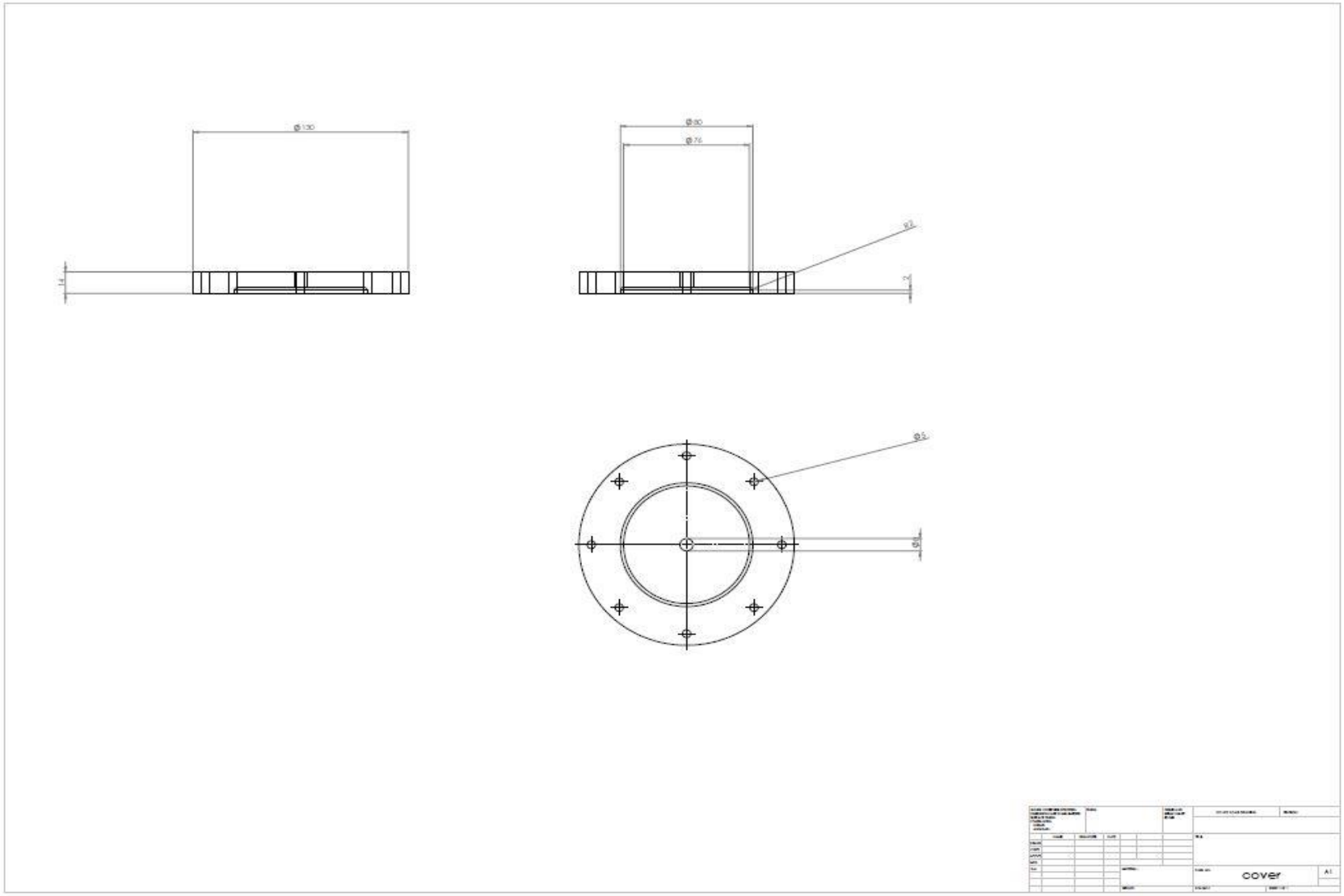

Appendix 4: Data sheet for Huber Unichiller OLE 012w

Model	Unichiller 012w OLÉ
General information & temperature controller	
Temperature range	-20...40 °C
Temperature stability	±0.5 °C
Temperature display	OLED Display
Display resolution	0.1 °C
Alarm message	optic, acoustic
Controller	OLÉ
Safety class	I / NFL
Protection class	IP20
Dimensions (W x D x H)	350 x 430 x 622 mm
Weight	52 kg
Heating / cooling capacity	
Heating capacity	Not available
Cooling capacity	15 0 -10 -20 °C 1.2 1 0.7 0.25 kW
Cooling machine	water-cooled

Refrigerant	R507 (0.34 kg)
Circulation pump	
Pressure pump max.	29 l/min ; 1.0 bar
Pump connection	G3/4 AG male
Connections	
Digital interface	USB, RS232
Operating data	
Permissible ambient temp.	5..40 °C
Filling volume min.	3.8 Litres
Volume of expansion	1.7 Litres
Cooling water connection	G1/2 AG
Cooling water differential pressure min.	3 bar
Cooling water pressure max.	6 bar
Power supply	230V 1~ 50Hz
Current max.	4.5 A

Appendix 5: Data sheet for Huber Ministat 240

Ministat 240

Refrigerated Heating Circulator Bath with air-cooled cooling machine. Powerful, variable speed, pressure and suction pump, evaporator (cooler) and housing of stainless steel, CFC and H-CFC free. With adjustable overtemperature protection according to DIN 12876.

Pilot ONE:
The new Pilot ONE controller with pioneering technology and advanced control functions brings numerous advantages to routine work. The extensive features list includes a brilliant 5,7" TFT touchscreen display, USB and network connections, an integrated technical glossary and language support in 13 languages (EN, DE, FR, IT, ES, RU, CN, PT, JP, CZ, PL, KO, TR). The Pilot ONE has a convenient navigation system with easily remembered icons and menu categories which are colour sorted to make routine work simpler. Thanks to a favourites menu and One-Click operator guidance all important information is always just a few keystrokes away. Software wizards also help you to set up, ensuring correct settings. The USB port allows connection of the system to a PC or notebook. Together with the Spy software, requirements such as remote control or data transmission are easily achieved in a cost-effective manner. Network integration is easy with the internet port.

The range of functions can be expanded very easily via E-grade at any time by entering a unit specific upgrade code:

E-grade "Exclusive": TAC (True Adaptive Control) - self optimising internal and cascade control, selectable temperature control mode (Internal/Process), programmer with 3 programs (max. 15 steps), ramp function (linear), 5 point calibration, scalable graphic display, favourites menu, display resolution 0,01 K.

E-grade "Professional": Programmer with 10 programs (max. 100 steps), ramp function for temperature gradients (linear and non-linear), 2nd set point, user menus (Administrator level), calendar start.

3-2-2 warranty - registration required.

Technical data according to DIN 12876

Operating temperature range	-45...200 °C
Temperature stability at -10°C	0,02 K
temperature set point / display	5,7" colour Touchscreen
Internal temperature sensor	Pt100
Sensor external connection	Pt100
Interface digital	Ethernet, USB (Host u. Device), RS232
Safety classification	Class III / FL
Heating power	2 kW
Cooling power	
at 100°C	0,6 kW
at 20°C	0,6 kW
at 0°C	0,55 kW
at -10°C	0,42 kW
at -20°C	0,35 kW
at -30°C	0,125 kW
at -40°C	0,05 kW
Refrigeration machine	air-cooled, natural refrigerant
Refrigerant	R290
Refrigerant quantity	0,099 kg

Gas warning sensor	without	**Order-No.: 2016.0005.01**
Pressure pump		
max. delivery	22 l/min	
max. delivery pressure	0,7 bar	
Suction pump	yes	
max. delivery (suction)	16 l/min	
max. delivery pressure (suction)	0,4 bar	
Pump connection	M16x1 male	
max. permissible kin. viscosity	50 mm²/s	
Bath volume	4,9 l	
min. filling capacity	4,5 l	
Bath capacity with displacement rack	2,8 l	
Width bath opening WxD / bath depth	205 x 85 / 157 mm	
Overall dimensions WxDxH **	300x465x516 mm	
Net weight	41 kg	

Peter Huber Kältemaschinenbau AG Werner-von-Siemens-Str. 1 D-77656 Offenburg Tel 0781/9603-0 Fax 0781/57211 www.huber-online.com

Technical data according to DIN 12876

Power supply requirement	230V 1~ 50/60Hz
max. current	12 A
Fuse (1 phase)	16 A
Degree of Protection	IP20
max. ambient temperature	40 °C
min. ambient temperature	5 °C

from Serial-No.: 160745 1.2/17

Technical details and dimensions are subject to change. No liability is accepted for errors or omissions. Illustrations can deviate from the original.

Accessories and periphery: mini-USB cable #54949*, Adapter nom. dia. 12 mm*, dummy plugs*, sleeve nuts thread M16x1*, connection tubes, drain valve, displacement insert to reduce bath volume, calibration insert * standard equipment

Output data valid for: Room temperature 20°C
in accordance with EN60034-1 the following voltage and frequency tolerances are valid:
Voltage + / - 5% with a simultaneous frequency tolerance of + / - 2%
Example -5% voltage and + 2% frequency -> not allowed!
-5% voltage and - 2% frequency -> allowed

Information to Electromagnetic compatibility:
Classification (disturbance) to EN55011: Class A, Group 1

** Please respect space requirements. See operating conditions at www.huber-online.com

Appendix 6: Data sheet for Julabo HE-4

Order No.	9212504
Model series	HighTech
Category	Heating Circulators
Working temperature range (°C)	+20 ... +250
Temperature stability (°C)	±0.01
Setting / display resolution	0.01 °C
Integrated programmer	1x10 steps
Temperature Display	VFD
Heating capacity (kW)	2
Pump capacity flow rate (l/min)	22-26
Pump capacity flow pressure (bar)	0.4-0.7
Pump capacity flow suction (bar)	0.2-0.4
Bath opening / bath depth (W x L / D cm)	13 x 15 / 15
Pump connections	M16x1
Barbed fittings diameter (inner dia. / mm)	8 / 12
Filling volume (liters)	4.5

External Pt100 sensor connection	integrated
Digital interfaces	RS232 Optional Profibus
Ambient temperature	5...40 °C
Dimensions W x L x H (cm)	21 x 42 x 40
Weight (kg)	11
Classification according to DIN12876-1	Classification III (FL)
Description	Built-in cooling coil for tap water connection for temperature applications below or near ambient temperatures are integrated.
Included with each unit	2 each barbed fittings for tubing 8 and 12 mm inner dia. (pump connections M16x1 female).
Cooling coil	integrated
Bath tank	Stainless steel

Appendix 7: Data sheet for Danfoss AKS32

Technical leaflet — **Pressure transmitters, type AKS 32 and AKS 33**

Technical data *(continued)*

Approvals

UL recognized for sale in the USA and Canada	File no. E310 24
CE marked according to the EMC directive	89/ 336/ EC

Mechanical characteristics

Housing material and material in contact with medium	DIN 17440-1.4404 (AISI 316L)
Weight	0.3 kg

Ordering

AKS 32, version 1 → 5 V

Operating range bar		Max. working pressure PB bar	Compensated temperature range °C	Code no.					
				DIN 43650 plug			Cable		
				¼ NPT [1]	G ⅜ A [2]	¼ flare [3]	¼ NPT [1]	¼ flare [3]	
LP	−1 → 6	33	−30 → +40	060G2000	060G2004	060G2068			
	−1 → 12	33	−30 → +40	060G2001	060G2005	060G2069	060G2017	060G2073	
HP	−1 → 20	40	0 → +80	060G2002	060G2006	060G2070			
	−1 → 34	55	0 → +80	060G2003	060G2007	060G2071			

AKS 32, version 0 → 10 V

Operating range bar		Max. working pressure PB bar	Compensated temperature range °C	Code no.		
				DIN 43650 plug		Cable
				¼ NPT [1]	G ⅜ A [2]	¼ flare [3]
LP	−1 → 5	33	−30 → +40		060G2038	
	−1 → 9	33	−30 → +40	060G2013	060G2036	060G2082
HP	−1 → 24	40	0 → +80	060G2014	060G2037	060G2083
	−1 → 39	60	0 → +80	060G2080	060G2079	060G2084

AKS 33, version 4 → 20 mA

Operating range bar		Max. working pressure PB bar	Compensated temperature range °C	Code no.					
				DIN 43650 plug			Cable		
				¼ NPT [1]	G ⅜ A [2]	¼ flare [3]	¼ NPT [1]	G ⅜ A [2]	¼ flare [3]
LP	−1 → 5	33	−30 → +40	060G2112	060G2108	060G2047			
	−1 → 6	33	−30 → +40	060G2100	060G2104	060G2048	060G2116	060G2120	
	−1 → 9	33	−30 → +40	060G2113	060G2111	060G2044			060G2062
	−1 → 12	33	−30 → +40	060G2101	060G2105	060G2049	060G2117		
	−1 → 20	40	0 → +80	060G2102	060G2106	060G2050	060G2118		
HP	−1 → 34	55	0 → +80	060G2103	060G2107	060G2051	060G2119		060G2065
	0 → 16	40	0 → +80	060G2114	060G2109				
	0 → 25	40	0 → +80	060G2115	060G2110			060G2127	060G2067

[1] ¼-18 NPT
[2] Thread ISO 228/1 - G ⅜ A (BSP)
[3] 7/16-20 UNF

Is also available in US-version (1 → 6 V) and with ⅛-27 NPT connection. Please contact Danfoss

Appendix 8: Matlab Model for Determining k and h in Activated Carbon Large Temperature Jump Experiments

Main Script

```
%code for conduction between layers of carbon
%determine the temperature evolution of different layers of adsorbent
clear all;%clear workspace and global values
clc;
global x k N x0 C Tsat Cpl Pd Aamm h tlad Kad n mlad Mamm i Tgtc Tgbv Vbv
Vpw Vtc dt T
% global variables used in function masserror
t=1;        % experimental time step
n=2;        % no of layers
no=n+1;     % no of nodes
tad=0.005;  % thickness of carbon bed
tlad=tad/n; % thickness of single carbon layer
Aamm=0.0050265% contact area of adsorbent
m=0.0168     % mass of adsorbent
mlad=m/n;   % mass of one layer of adsorbent
x0=0.3431   % x0 for adsorbent - Roger's data
k=4.4854    % k for adsorbent
N=1.17      % n for adsorbent1
C=2823.4;   % Slope of sat. line for NH3
Cpl=4734;   % Cp liquid ammonia
Vbv=0.00254346542;      % volume of the pressure vessel m^3
Vtc=0.000351865         % volume of test cell m^3
Vpw=0.0000010956304;  % volume of pipework m^3
Tv=Vbv+Vtc+Vpw;         % total volume of system m^3
load 'pressure.m';
Pe=pressure(1:500);           % Gauge pressure, bar, 1 column
Pe=Pe+1;              % Convert to absolute pressure
load 'gastemperature.m';% Gas temp in vessel, deg C
Tgbv=gastemperature(1:500); % Gas temp in vessel, deg C
Tgbv=Tgbv+273.15;       % convert to K
load 'gastemperaturetestcell.m'; % Gas temp in cell, deg C
Tgtc=gastemperaturetestcell(1:500);% Gas temp in cell, deg C
Tgtc=Tgtc+273.15;           % convert to K
load 'watertemperature.m';  % Water temp in cell, deg C
Tw=watertemperature(1:500); % Water temp in cell, deg C
Tw=Tw+273.15;               %convert to K
ott=0:t:(length(Pe)-1);     %old test times with first element of time zero
% interval = t sec
dt=1;                   %new test time step
ntt=0:dt:ott(end);          %new test times
tend=ntt(end);              %Final simulated time
Pe=interp1(ott,Pe,ntt);     %new pressure array
Tgbv=interp1(ott,Tgbv,ntt); %new gas temperature array
Tgtc=interp1(ott,Tgtc,ntt); %new cell temperature array
Tw=interp1(ott,Tw,ntt);     %new water temperature array
T=zeros(no,length(Tw));     %an initial matrix of zeros for all nodes and all times
```

```
x=zeros(n,length(Tw));      %an initial matrix of zeros for all nodes and all times
Twall=Tw;                   %temperature at wall
T(1:no,1)=Tw(1);            %initial temperature for all the nodes
T(1,:)=Tw;              % All first nodes set to measured water temperature
Pd(1)=Pe(1)             % Initial pressure = experimental initial pressure
Tsat(1)=2748.3/(11.515-log(Pd(1))); % Initial Tsat
x(:,1)=ones(n,1)*dub2(Tsat(1),T(1,1),x0,k,N); %Initial concentrations

%*************************************************************************
*******
% calculate total mass of gas in the system initially
%*************************************************************************
*******
Mamm=x(1,1)*m+(Pd(1)*1e5)*...
   ((Vbv+Vpw)/ramms(Pd(1),Tgbv(1)-273)/Tgbv(1) +...
   Vtc/ramms(Pd(1),Tgtc(1)-273)/Tgtc(1));
Madsinitial=x(1,1)*m
Mgasinitial=(Pe(1)*1e5)*...
   ((Vbv+Vpw)/ramms(Pe(1),Tgbv(1)-273)/Tgbv(1) +...
   Vtc/ramms(Pe(1),Tgtc(1)-273)/Tgtc(1))

%*************************************************************************
*******
% request user input for h and k
%*************************************************************************
*******
hl=input('please enter a lower boundary for h, the heat transfer coefficient')
hh=input('please enter an upper boundary for h, the heat transfer coefficient')
kl=input('please enter a lower boundary for k, the thermal conductivity')
kh=input('please enter an upper boundary for k, the thermal conductivity')
%*************************************************************************
*******
%*************************************************************************
*******
hi=[hl ((hh-hl)/2)+hl hh] %develop a 1 by 3 matrix with the lower and upper h
values given
Kadi=[kl ((kh-kl)/2)+kl kh] %develop a 1 by 3 matrix with the lower and upper k
values given
Pdkh=zeros((length(hi)*length(Kadi)),length(Tw))%creates an array of zeros for the
results (different k and h combinations)
mse=zeros((length(hi)*length(Kadi)),1)
%*************************************************************************
*******
% Begin simulation from first step after zero
%*************************************************************************
*******
for w=1:1:length(hi)%indices of heat trasnfer coefficients specified above
   h=hi(w)

   for z=1:1:length(Kadi)%indices of conductivities specified above
```

```
        Kad=Kadi(z)%combined heat conductivity of adsorbent and refrigerant
        dTsat=0; % First guess at Tsat (and hence pressure) rise in first time step
        % In later times the first guess is the previous value found

        for i=2:length(ntt) % indices of times from first step after zero to end
            dTsat;
            i;
            dTsat=fzero(@masserror,dTsat) ;% Finds dTsat so that the function
masserror is 0
        end
%**************************************************************************
*******
        % calaculate total mass of gas in the system finally

%**************************************************************************
*******
        Madsfinalsim=mean(x(:,end))*m
        Tsate=2748.3/(11.515-log(Pe(end)))
        xfinalex=dub2(Tsate,Tw(end),x0,k,N)
        Madsfinalex=xfinalex*m
        Mgasfinal=(Pe(end)*1e5)*...
            ((Vbv+Vpw)/ramms(Pe(end),Tgbv(end)-273)/Tgbv(end) +...
            Vtc/ramms(Pe(end),T(1,end)-273)/T(1,end))
        Mtotalfinalex = Mgasfinal+Madsfinalex
        Mtotalinitialex=Mgasinitial+Madsinitial

        Pdk(z,:)=Pd; %stores results for each 'Kad' in Pdk
    end
    Pdkh(((length(hi)*w)-(length(hi)-1)):(length(hi)*w),(1:length(Tw)))=Pdk%fills in
the results in the above created array for each 'h' value)
    Pee=[Pe' Pe' Pe']
    mse(((length(hi)*w)-(length(hi)-1)):(length(hi)*w),1)=sqrt((sum((Pdk'-
Pee).^2)./length(Pe))) %find root mean square error between model and
experimental
end
%**************************************************************************
*******
%         Find model with best fit
%**************************************************************************
*******
%**************************************************************************
*******
%         Final result
%**************************************************************************
*******
Tempdist=T(1:1:no,1:1:length(Tw));
figure(1)
plot(Tempdist(no,:),'g')
hold on
plot(Tgtc,'b')
```

```
plot(Tw,'r')
legend('Top of carbon','Cell temp.','Water temp.')
figure(2)
k1=num2str(Kadi(1))
k2=num2str(Kadi(2))
k3=num2str(Kadi(3))
h1=num2str(hi(1))
h2=num2str(hi(2))
h3=num2str(hi(3))
u=length(hi)*length(Kadi)
plot(Pe,'color','r')
hold on
plot(Pdkh(8,:),'color','k')
hold on
legend(['experimental pressure'],['h=',...
   h3 'k=',k2])
xlabel('time(s)','fontsize', 24);ylabel('pressure(bar)','fontsize',24)
set(gca,'fontsize',24,'fontweight','bold')
```

Other Functions

Masserror

```
function [ y ] = masserror(dTsat)
%masseror calculated change in total system mass of ammonia for assumed
%change in Tsat (dTsat). This is used by fzero to find actual dTast and dp
global x k N x0 C Tsat Cpl Pd  Aamm h tlad Kad n mlad Mamm i Tgtc Tgbv Vbv
Vpw Vtc dt T
Tsat(i)=Tsat(i-1)+dTsat; % Assumed new Tsat in K
Pd(i)=psatamm(Tsat(i));  % Assumed new pressure in bar
for j=2:n+1;
   CpC=175+(2.245*T(j,i-1));% Calculate   specific heat of node j carbon
   H=ramms(Pd(i-1),T(j,i-1)-273)*C*T(j,i-1)/Tsat(i-1);
   % Heat of adsorption in J/kg
   dxbydT=-x(j-1,i-1)*k*N/Tsat(i-1)*((T(j,i-1)/Tsat(i-1)-1)^(N-1));
   % Partial differential of x with T
   dxbydTsat=x(j-1,i-1)*k*N*((T(j,i-1)/Tsat(i-1)-1)^(N-1))*...
      T(j,i-1)/Tsat(i-1)/Tsat(i-1); %Partial differential of x with Tsat
   % Now calculate dQdot from conduction in Watts
%**********************************************************************
*******%
   if(j==2); % First carbon node
      dQdot=Aamm*((T(1,i-1)-T(2,i-1))/(1/h+tlad/2/Kad)+...
         Kad/tlad*(T(3,i-1)-T(2,i-1)));
   end
%**********************************************************************
*******
   if(j>2 && j<(n+1)) ; % middle nodes
      dQdot=Aamm*Kad/tlad*(T(j+1,i-1)-2*T(j,i-1)+T(j-1,i-1));
```

```
   end
%*************************************************************************
*******
   if(j==n+1); % end node
      dQdot=Aamm*Kad/tlad*(-T(j,i-1)+T(j-1,i-1));
   end
%*************************************************************************
*******
   dT=(dQdot*dt/mlad+dTsat*H*dxbydTsat)/(CpC+x(j-1,i-1)*Cpl -H*dxbydT);
   %Temp rise
   T(j,i)=T(j,i-1)+dT;
   % Calculate new concentration based on new pressure, new temperature
   x(j-1,i)=dub2(Tsat(i),T(j,i),x0,k,N);
end % of stepping through nodes to get new temperatures, concentrations.
%*************************************************************************
*******
%   calculate total mass of ammonia in system for assumed rise in Tsat
%*************************************************************************
*******
Madsorbed=mlad*sum(x(:,i)); % kg adsorbed ammonia in all carbon
Tcell=Tgtc(i); % Assume gas in cell at same temperature as top layer(K)
Tvessel=Tgbv(i); % Use measured value of vessel temperature (K)
Mgas=(Pd(i)*1e5)*...
   ((Vbv+Vpw)/ramms(Pd(i),Tvessel-273)/Tvessel(end) +...
   Vtc/ramms(Pd(i),Tcell-273)/Tcell);
Mamm;
Massgain=Madsorbed + Mgas - Mamm;
y = (Madsorbed + Mgas - Mamm)/Mamm;
% Returns change in total ammonia mass within system, which should be zero
end
```

Dub2

```
function x= dub2(tsat,t,x0,k,n)
% x is conc, tsat is t saturated, t is temp deg K
if tsat>=t
x=x0;
mess='saturation'
x=x0
else
x=x0*exp(-k*(((t/tsat)-1)^n));
end
```

Appendix 8: Matlab Model for Determining Kinetic Parameter in Large Temperature Jump Experiments on Salts

Main Script

```
%this routine models LTJ test on salt-NH3 reactions
clear all; %clear workspace and global values and plots
clc;
close all;  % close all previous plots

%**************************INPUT**********************************
*********
%*****************************************************************
********
mx=0.7;
Axd=[0.5,1,2];                % kinetic parameter for making storing matrices later.
same as below
for u=1:length(mx)
   mxi=mx(u);

   %********** input from user
(structure)************************************
   s.rt = 1;                        % MgCl2(8to2NH3)->1, MgCl2(2to8NH3)->3
   s.M=0.095211;                        % molar mass of salt (kg/mol)
   %*** vary anyone the following********%
   s.n=5;                          % no of discrete layers
   s.tad=0.004;                      % thickness of entire sample(m)
   s.dt=0.01;                       % time step (s)
   s.li=1000;                       % length of analysis in seconds
   s.Pc=43;                         % percentage of sample that is salt (%)
   s.mc=0.0016;                       % mass of entire sample (kg)
   s.Ax=0.003                       % kinetic parameter
   s.k=1                           % thermal conductivity of sample (W/m.K)
   s.h=8840000;                         % heat transfer coefficient (W/m^2.K)
   s.dia=5e-2;                      % contact s.diameter of sample (m)
   s.Cpg=[1000,2190,4400];

%*****************************************************************
********


%************************data**************************************
*******
   load 'pressure.m';                     % load pressure data
   Pe=pressure(1:s.li);                     % make pressure array according to input 'li'
   load 'testcell.m';                    % load test cell temperature data
   testcell=smooth(testcell(1:s.li)+273.15,100);   % make test cell temperature array
according to input 'li', convert to kelvin and smooth
   load 'water.m';                     % load water temperature data
```

```
   water=smooth(water(1:s.li)+273.15,100);        % make water temperature array
according to input 'li', convert to kelvin and smooth
   load 'vessel.m';                          % load vessel temperature data
   vessel=smooth(vessel(1:s.li)+273.15,100);      % make vessel temperature array
according to input 'li', convert to kelvin and smooth

%*************************************************************************
********

   %***************************the test rig
**********************************
   Vbv=0.00254346542;         % volume of the pressure vessel (m^3)
   Vpw=6.16e-6;              % volume of pipework (my side) (m^3)
   Vtc=(pi*((40e-3)^2)*70e-3)-(pi*((25e-3)^2)*50e-3);   % volume of test cell (m^3)

%*************************************************************************
********


%*************************************************************************
********
   s.Ps = Pe(1);               % Starting pressure (bar)
   s.tt = length(Pe)-1;          % total experimental time (s)
   s.R= 8.3145;                % gas constant (J/mol.K)
   s.dte=1;                   % experimental time step (s)
   xamax=1;                    % maximum reaction advancement

%*************************************************************************
********

   %***********************the refrigerant and
ENG*****************************
   Mg=0.017;             % molar mass of refrigerant (kg/mol)
   %Cpg=2190;             % specific heat of ammonia gas (J/kgK)
   Cpeng=890;           % Cp of expanded natural graphite (J/kgK)

%*************************************************************************
********

   %*******************calculated
properties***********************************
   [ no,tlad,ms,mlad,N0,As ]= samplechar(s.n,s.dia,s.tad,s.mc,s.M,s.Pc);  %returns
calaculated physical xteristics of the sample

%*************************************************************************
********

   %************number of reacted NH3 moles per mole of
salt******************
```

```
   n1=(Pe(1)*1e5*(Vtc+Vpw))/(s.R*testcell(1))+(Pe(1)*1e5*(Vbv))/(s.R*vessel(1));
% no of initial gas moles

n2=(Pe(end)*1e5*(Vtc+Vpw))/(s.R*testcell(end))+(Pe(end)*1e5*(Vbv))/(s.R*vessel
(end));      % no of final gas moles
   mnh31=n1*Mg;                                                    % mass of
ammonia gas in system (g)
   mnh32=n2*Mg;                                                    % mass of
ammonia gas in system (g)
   dnh3=mnh32-mnh31;                                                % mass of
ammonia lost to adsorption (g)
   s.Namm=abs((dnh3/Mg)/(ms/s.M));                                          % total
no of moles reacted NH3 per mole of salt

%*********************************************************************
********

   %******* thermodynamic properties for the chosen
reaction******************
   switch s.rt
      case(1)
         [dH, dS, CpC]= thermoprop(s.rt);            % returns equilibrium properties
for MgCl2(8-4)NH3 reaction
         Teqs= Tequilibrium(s.Ps,dH,dS,s.R);         % returns equilibrium
temperature at initial pressure (s.Ps) (K)
      case(3)
         [dH, dS, CpC]= thermoprop(s.rt);            % returns equilibrium properties
for MgCl2(2-4)NH3 reaction
         Teqs= Tequilibrium(s.Ps,dH,dS,s.R);         % returns equilibrium
temperature at initial pressure (s.Ps) (K)
   end

%*********************************************************************
*****
   %********************END OF
INPUT*****************************************

   ttotal = round(s.tt/s.dt); %calculate number of required timestes.Ps
   t=s.dt:ttotal;                          % dummy data of modeling time (s)

%*********************************************************************
******
   %*****************figure out if and which parameter has been varied *******
   N= structfun(@numel,s);         % number of element each user input parameter
has
   if (nnz(N>1)==1);              % if one of the parameters has elements greater than
one or has been varied
      C=fieldnames(s);           % declares the names of all the user input parameters
      F=C{N>1};                  % declares the name of the parameter with more than
one element
```

```
    V=s.(F);                % stores the value of the parameter above as variable V
    Pda=zeros(length(V),ttotal); % initial matrix of zeros for pressures for each
value of the varied parameter
    xd=zeros(length(V),ttotal);     % initial matrix of zeros for xd
    yd=zeros(length(V),ttotal);     % initial matrix of zeros for yd

%*****************************************************************************
********

    %***obtain modeled pressure for different values of the varied parameter***

%*****************************************************************************
********

    for l=1:length(V),          % loop through varied parameter
        s.(F)=V(l);             % declare the values for varied parameter in each loop
        [ no,tlad,ms,mlad,N0,As ]= samplechar(s.n,s.dia,s.tad,s.mc,s.M,s.Pc);
%returns calaculated physical xteristics of the sample. This line is repeated to cater
fopr the scenario of varying the s.tad, s.Pc or s.dia

        %******************make initial
matrices**************************
        ott=0:s.dte:s.tt;           % experimental time array
        ntt=0:s.dt:ott(end);        % modelling time array
        Tc=interp1(ott,water,ntt);      % interpolated matrix for water temperature
based on modelling time s.dt
        Tgbv=interp1(ott,vessel,ntt);   % interpolated matrix for vessel
temperature based on modelling time s.dt
        Tcell=interp1(ott,testcell,ntt);  % interpolated matrix for water temperature
based on modelling time s.dt
        T=zeros(no+1,ttotal);       % an initial matrix of zeros for temperature of
all nodes
        x=zeros(no,ttotal);         % an initial matrix of zeros for refigerant
concentration in each layer
        xa=zeros(no,ttotal);        % an initial matrix of zeros for local
advancement in each lay
        Peq=zeros(no,ttotal);       % an initial row vector of zeros for
equilibrium pressure of equal layer
        Peqy=zeros(no,ttotal);      % an initial row vector of zeros for
equilibrium pressure of equal layer
        Teq=zeros(1,s.li);          % an initial row vector of zeros for equilibrium
temperature
        Teqy=zeros(1,s.li);         % an initial row vector of zeros for equilibrium
temperature
        Pd=zeros(1,ttotal);         % an initial row vector of zeros for modelled
pressure
        Cp=zeros(no,ttotal);        % an initial matrix of zeros for specific heat of
each layer
        rmse=zeros(2,(length(V)*length(mx)));       % an initial matrix of zeros
for root mean square error
```

```
%**************************end*************************************

        %**********************initial
conditions***************************
        T(:,1)= Tc(1);                          % initial temperature for all the nodes
set to temeparture of water (K)
        xa(:,1)=0;                          % advancement of all nodes at time index 1
        Peq(:,1)= Pequilibrium(dH,dS,s.R,T(1,1));          % returns initial
equilibrium pressure for first MgCl2 reaction  for all nodes (bar)
        switch s.rt
           case (1)                                    % MgCl2(8-2)NH3 reaction
              x(1:no,1)=conc(s.Namm,Mg,s.M );                % initial concetration
of (8-4) in all nodes at time index 1 (kg/kg)
              msys
=((s.Ps*1e5/s.R)*(((Vbv)/Tgbv(1))+((Vpw+Vtc)/testcell(1)))*Mg)+(x(1,1)*ms); %
mass of NH3 initially in system
              Pd(1)=s.Ps;                           % initial pressure
           case(3)                                   % MgCl2(2-8)NH3 reaction
              x(1:no,end)=conc(s.Namm,Mg,s.M );              % final concetration
of (4-8) in all nodes at time index end (kg/kg)
              x(1:no,1)=0; %conc(s.Namm,Mg,s.M );              % initial
concentration of (4-8) in all nodes at time index 1 (kg/kg)
              msys =((s.Ps*1e5/s.R)*((Vbv/Tgbv(1))+((Vpw+Vtc)/testcell(1))))*Mg;
% total mass of NH3 initially in system

Pd(1)=(((msys)*s.R*Tgbv(1)*testcell(1))/(Mg*((Vbv*testcell(1))+(Tgbv(1)*(Vpw+
Vtc)))))/1e5;     % initial pressure
        end

%*****************************end*********************************
        %***************************main
model*************************************
        T(1,2:ttotal)=Tc(2:ttotal);                  % declare the temperature of
the first node i.e temperature of the test cell base
        for i=2:ttotal,                          % loop through time steps
           for jj=2:no                           % loop through discrete layers
              switch s.rt
                 case(1)
                    [xa(jj,i),T(jj,i),x(jj,i),Peq(jj,i),Cp(jj,i)]=newcon(s.dt,As,s.k,T(jj-1,i-
1),T(jj,i-1)...
                       ,T(jj+1,i-1),tlad,s.h,dH,s.R,dS,Pd(i-1),xamax,xa(jj,i-
1),s.Ax,s.Namm,N0,mlad,CpC,Cpeng,s.Cpg,...
                       Tc(i),x(jj,i-
1),x(jj,1),msys,Mg,Tgbv(i),Vtc,Vpw,Vbv,no,i,jj,s.n,s.rt,x(jj,end),mxi);          %
returns new modelled advancement,tempareture,equilibrium pressure and
concentration for decomposition reaction
                 case(3)
```

```
                    [xa(jj,i),T(jj,i),x(jj,i),Peq(jj,i),Cp(jj,i)]=newconads(s.dt,As,s.k,T(jj-
1,i-1),T(jj,i-1)...
                    ,T(jj+1,i-1),tlad,s.h,dH,s.R,dS,Pd(i-1),xamax,xa(jj,i-
1),s.Ax,s.Namm,N0,mlad,CpC,Cpeng,s.Cpg,...
                    Tc(i),x(jj,i-
1),x(jj,1),msys,Mg,Tgbv(i),Vtc,Vpw,Vbv,no,i,jj,s.n,s.rt,x(jj,end),mxi);   % returns
new modelled advancement,tempareture,equilibrium pressure and concentration for
sythesis reaction
                end
                Pd(i)=
newP1(N0,Mg,s.n,xa(:,i),s.Namm,msys,s.R,Tgbv(i),Tcell(i),Vbv,Vtc,Vpw,s.rt);     %
returns new modelled pressure
            end
        end
        xd(l,:)=mean(xa(2:no,:));  % save modelled pressure for each value of the
varied parameter
    end
    if (u==1)
        xdp((1:(length(Axd)*u)),:)=xd; %store advanacements for each mx
    else;
        xdp(((length(Axd)*(u-1)+1):(length(Axd)*u)),:)=xd; %store advanacements
for each mx
    end

  else

    %*******************make initial matrices**************************
    ott=0:s.dte:s.tt;                % experimental time array
    ntt=0:s.dt:ott(end);             % modelling time array
    Tc=interp1(ott,water,ntt);         % interpolated matrix for water temperature
based on modelling time s.dt
    Tgbv=interp1(ott,vessel,ntt);       % interpolated matrix for vessel temperature
based on modelling time s.dt
    Tcell=interp1(ott,testcell,ntt);     % interpolated matrix for water temperature
based on modelling time s.dt
    T=zeros(no+1,ttotal);              % an initial matrix of zeros for temperature of
all nodes
    x=zeros(no,ttotal);               % an initial matrix of zeros for refigerant
concentration in each layer
    xa=zeros(no,ttotal);               % an initial matrix of zeros for local
advancement in each layer
    y=zeros(no,ttotal);               % an initial matrix of zeros for refigerant
concentration in each layer
    ya=zeros(no,ttotal);               % an initial matrix of zeros for local
advancement in each layer
    Peq=zeros(no,ttotal);              % an initial row vector of zeros for equilibrium
pressure of equal layer
    Peqy=zeros(no,ttotal);             % an initial row vector of zeros for equilibrium
pressure of equal layer
```

```
    Teq=zeros(1,s.li);              % an initial row vector of zeros for equilibrium
temperature
    Teqy=zeros(1,s.li);             % an initial row vector of zeros for equilibrium
temperature
    Pd=zeros(1,ttotal);             % an initial row vector of zeros for modelled
pressure
    Cp=zeros(no,ttotal);            % an initial matrix of zeros for specific heat of
each layer

%*************************end************************************
    %**********************initial conditions**************************
    T(:,1)= Tc(1);                          % initial temperature for all the nodes set
to temeparture of water (K)
    switch s.rt
      case(1)                               % if MgCl2(8-2)NH3 reaction
        if (s.Namm<4 & s.Namm>2)                    % if the MgCl2(8-4)NH3
          xa(:,1)=0;                        % advancement of all nodes at time
index 1
          ya(:,1)=xamax;                    % advancement of all nodes at time
index 1
        else                                % if the MgCl2(4->2)NH3 or MgCl2(2-
>4)NH3
          xa(:,1)=xamax;                    % advancement of all nodes at time
index 1
          ya(:,1)=0;                        % advancement of all nodes at time
index 1
        end
      case(3)                               % if MgCl2(2-8)NH3 reaction
        if (s.Namm<4 & s.Namm>2)                    % if the MgCl2(8-4)NH3
          xa(:,1)=0;                        % advancement of all nodes at time
index 1
          ya(:,1)=xamax;                    % advancement of all nodes at time
index 1
        else                                % if the MgCl2(4->2)NH3 or MgCl2(2-
>4)NH3
          xa(:,1)=xamax;                    % advancement of all nodes at time
index 1
          ya(:,1)=0;                        % advancement of all nodes at time
index 1
        end
    end
    Peq(:,1)= Pequilibrium(dH,dS,s.R,T(1,1));       % returns initial equilibrium
pressure for first MgCl2 reaction  for all nodes (bar)
    Peqy(:,1)= Pequilibrium(dHy,dSy,s.R,T(1,1));    % returns initial
equilibrium pressure for second MgCl2 reaction for all nodes (bar)
    switch s.rt
      case (1)                                  % MgCl2(8-2)NH3 reaction
        x(1:no,1)=conc(s.Namm,Mg,s.M );             % initial concetration of
(8-4) in all nodes at time index 1 (kg/kg)
```

```
            y(1:no,1)=conc(s.Nammy,Mg,s.M);                    % initial concetration
of (4-2) in all nodes at time index 1 (kg/kg)
            msys
=((s.Ps*1e5/s.R)*(((Vbv)/Tgbv(1))+((Vpw+Vtc)/testcell(1)))*Mg)+(x(1,1)*ms+y(1,
1)*ms); % mass of NH3 initially in system
            Pd(1)=s.Ps;                                        % initial pressure
          case(3)                                             % MgCl2(2-8)NH3 reaction
            x(1:no,end)=conc(s.Namm,Mg,s.M );                  % final concetration of
(4-8) in all nodes at time index end (kg/kg)
            y(1:no,end)=conc(s.Nammy,Mg,s.M);                  % final concentration
of (2-4) in all nodes at time index end (kg/kg)
            y(1:no,1)=0;                                       % initial concentration of (2-4) in
all nodes at time index 1 (kg/kg)
            x(1:no,1)=0; %conc(s.Namm,Mg,s.M );                % initial
concentration of (4-8) in all nodes at time index 1 (kg/kg)
            msys =((s.Ps*1e5/s.R)*((Vbv/Tgbv(1))+((Vpw+Vtc)/testcell(1))))*Mg;
% total mass of NH3 initially in system

Pd(1)=(((msys)*s.R*Tgbv(1)*testcell(1))/(Mg*((Vbv*testcell(1))+(Tgbv(1)*(Vpw+
Vtc)))))/1e5;      % initial pressure
        end

        T(1,2:ttotal)=Tc(2:ttotal);                            % declare the temperature of
the first node i.e temperature of the test cell base

%*****************************end*********************************

        %**************************main
model*************************************
        T(1,2:ttotal)=Tc(2:ttotal);                            % declare the temperature of
the first node i.e temperature of the test cell base
        for i=2:ttotal,                                        % loop through time steps
           for jj=2:no                                         % loop through discrete layers
              switch s.rt
                 case(1)

[xa(jj,i),ya(jj,i),T(jj,i),x(jj,i),y(jj,i),Peq(jj,i),Peqy(jj,i),Cp(jj,i)]=newcon(s.dt,As,s.k,T(
jj-1,i-1),T(jj,i-1)...
                      ,T(jj+1,i-1),tlad,s.h,dH,s.R,dS,Pd(i-1),xamax,xa(jj,i-1),ya(jj,i-
1),s.Ax,s.Ay,s.Namm,N0,mlad,CpC,Cpeng,Cpg,...
                      Tc(i),x(jj,i-
1),x(jj,1),msys,Mg,Tgbv(i),Vtc,Vpw,Vbv,no,i,jj,dHy,dSy,s.Nammy,y(jj,i-
1),y(jj,1),s.n,s.rt,x(jj,end),mxi);          % returns new modelled
advancement,tempareture,equilibrium pressure and concentration for decomposition
reaction
                 case(3)

[xa(jj,i),ya(jj,i),T(jj,i),x(jj,i),y(jj,i),Peq(jj,i),Peqy(jj,i),Cp(jj,i)]=newconads(s.dt,As,s.k
,T(jj-1,i-1),T(jj,i-1)...
```

```
                    ,T(jj+1,i-1),tlad,s.h,dH,s.R,dS,Pd(i-1),xamax,xa(jj,i-1),ya(jj,i-
1),s.Ax,s.Ay,s.Namm,N0,mlad,CpC,Cpeng,Cpg,...
                    Tc(i),x(jj,i-
1),x(jj,1),msys,Mg,Tgbv(i),Vtc,Vpw,Vbv,no,i,jj,dHy,dSy,s.Nammy,y(jj,i-
1),y(jj,1),s.n,s.rt,x(jj,end),y(jj,end),mxi);   % returns new modelled
advancement,tempareture,equilibrium pressure and concentration for sythesis
reaction
            end
            Pd(i)=
newP1(N0,Mg,s.n,xa(:,i),s.Namm,s.Nammy,ya(:,i),msys,s.R,Tgbv(i),Tcell(i),Vbv,Vt
c,Vpw,s.rt);     % returns new modelled pressure
        end
    end
        end
end
for i=2:s.li
   Pe(i)=  abs((Pe(i)-Pe(1))/(Pe(end)-Pe(1)));      %normalise measured pressure
end
Pe(1)=0;

for i=1:s.li;
   Teq(i)=Tequilibrium(Pe(i),dH,dS,s.R);              %obtain equilibrium temperatures
end

%% bring results back to experimental time steps
switch (nnz(N>1))
   case 0
      xdpersecond=zeros(round(s.dt*ttotal),length(mx));
   case 1
      xdppersecond=zeros(round(s.dt*ttotal),(length(mx)*length(Axd)));
end
Tpersecond=zeros(round(s.dt*ttotal),no);
xapersecond=zeros(round(s.dt*ttotal),no);
xpersecond=zeros(round(s.dt*ttotal),no);

for i=1:ttotal
   if (i-1)*s.dt == round((i-1)*s.dt)
      switch (nnz(N>1))
         case 0
            xdppersecond(1+round((i-1)*s.dt))=xdp(1:(length(mx)),i);
         case 1
            xdppersecond(1+round((i-
1)*s.dt),1:(length(mx)*length(Axd)))=xdp(1:(length(mx)*length(Axd)),i);
      end
      Tpersecond(1+round((i-1)*s.dt),1:no)=T(1:no,i);
      xapersecond(1+round((i-1)*s.dt),1:no)=xa(1:no,i);
      xpersecond(1+round((i-1)*s.dt),1:no)=x(1:no,i);
   end
end
```

```
%************find root mean square
error**********************************
for z=1:1:length(Axd)*length(mx);
   zi=find(Pe>0.8,1,'first')
   ze=find(Pe>0.1,1,'first')
   zx=find(xdppersecond(:,z)>0.1,1,'first');
   zp=find(xdppersecond(:,z)>0.8,1,'first');
   zzz(z)=zx;
   zz(z)=zp;
   rmsd(z)=sqrt(sum(((xdppersecond((zx:(zx+zi-ze)),z)-
Pe(ze:zi)).^2))/(length(Pe(ze:zi))));
   figure(1)
   switch z
      case 1
         plot(xdppersecond((zx:end),z),'-.m','linewidth',1.5)
      case 2
         plot(xdppersecond((zx:end),z),'-.r','linewidth',1.5)
      case 3
         plot(xdppersecond((zx:end),z),'-.k','linewidth',1.5)
      case 4
         plot(xdppersecond((zx:end),z),':m','linewidth',1.5)
      case 5
         plot(xdppersecond((zx:end),z),':r','linewidth',1.5)
      case 6
         plot(xdppersecond((zx:end),z),':k','linewidth',1.5)
      case 7
         plot(xdppersecond((zx:end),z),'m','linewidth',1.5)
      case 8
         plot(xdppersecond((zx:end),z),'r','linewidth',1.5)
      case 9
         plot(xdppersecond((zx:end),z),'k','linewidth',1.5)
   end
   hold on
end
plot(Pe(ze:end),'linewidth',1.5);
legend('Cp=1500J/kgK','Cp=3000J/kgK','Cp=6000J/kgK','measured
advancement','yo=0.7,A=0.00002','yo=0.7,A=0.00003','yo=0.8,A=0.00001','yo=0.8,
A=0.00002','yo=0.8,A=0.00003','measured advancement')
figure(2)
plot(Pe(ze:zi),'linewidth',1.5)
hold on
plot(xdppersecond((zzz(2):zz(2)),2),'r','linewidth',1.5)
hold on
plot(xdppersecond((zzz(1):zz(1)),1),'k','linewidth',1.5)
hold on
legend('measured advancement', 'yo=0.72,A=0.000056 (reaction best fit)',
'yo=0.68,A=0.00004 (experiment best fit)')

%************************************************************************
********
```

```
%****plot graphs*****
switch nnz(N>1)
   case 0
      figure(1)
      plot(Pdpersecond,'b','linewidth',1.5)
      hold on
      plot(Pe,'k','linewidth',1.5)
      xlabel('time(s)')
      ylabel('pressure(bar)')
      legend('modeled pressure','measured pressure')
   case 1
      F1=num2str(F);
      figure(1)
      plot(Pdapersecond,'linewidth',1.5)
      for l=1:length(V)
         V1=num2str(V(l));
         legendinfo{l}=[(F1),  (V1)];
      end
      xlabel('time(s)')
      ylabel('pressure(bar)')
      hold on
      plot(Pe,'k','linewidth',1.5)
      legendinfo{length(V)+1}=('measured pressure')
      legend(legendinfo)
end
figure(2)
plot(Tpersecond,'linewidth',1.5)
if (rea>0)
   hold on
   plot(Teqy,'k','linewidth',1.5)
   legend('imposed  tempereture','layer 1','layer 2','layer 3','layer 4','layer
5','MgCl2(4-8)NH3 equilibrium temperature'),
else
   hold on
   plot(Teq,'k','linewidth',1.5)
   legend('imposed  tempereture','layer 1','layer 2','layer 3','layer 4','layer
5','MgCl2(4-8)NH3 equilibrium temperature'),
end
xlabel('time(s)')
ylabel('temperature (K)')
figure(3)
plot(yapersecond(:,2:s.n+1),'linewidth',1.5)
xlabel('time(s)')
switch (s.rt)
   case {1,2}
      ylabel('advancement(4-2) (-)')
   case {3,4}
      ylabel('advancement(2-4) (-)')
end
figure(4)
```

```
plot(xapersecond(:,2:s.n+1),'linewidth',1.5)
xlabel('time(s)')
switch (s.rt)
   case {1,2}
      ylabel('advancement(8-4) (-)')
   case {3,4}
      ylabel('advancement(4-8) (-)')
end
figure(5)
plot(ypersecond(:,2:s.n+1),'linewidth',1.5)
xlabel('time(s)')
switch (s.rt)
   case {1,2}
      ylabel('concentration(4-2) (-)')
   case {3,4}
      ylabel('concentration(2-4) (-)')
end
figure(6)
plot(xpersecond(:,2:s.n+1),'linewidth',1.5)
xlabel('time(s)')
switch (s.rt)
   case {1,2}
      ylabel('concentration(8-4) (-)')
   case {3,4}
      ylabel('concentration(4-8) (-)')
end
figure(7)
plot(Tpersecond((1:s.li-1),6),'linewidth',1.5)
hold on
plot(testcell,'r','linewidth',1.5)
legend('circulating bath water temperature', 'temperature of gas above sample')
xlabel('time(s)')
ylabel('temperature (K)')

figure(8)
tada=0:s.tad/s.n:s.tad;          % array of distances from test cell base

if (rea>0)
   rni=find(yapersecond(:,6)>0.99,1); % time for last layer to reach 0.99/1
completion
   plot(tada,Tpersecond(20,1:6),'-b*','linewidth',1.5, 'markersize',10);
   hold on
   plot(tada,Tpersecond(30,1:6),'-b+','linewidth',1.5, 'markersize',10);
   hold on
   plot(tada,Tpersecond(40,1:6),'-bo','linewidth',1.5, 'markersize',10);
   hold on
   plot(tada,Tpersecond(50,1:6),'-b*','linewidth',1.5, 'markersize',10);
   hold on
   plot(tada,Tpersecond(70,1:6),'-bx','linewidth',1.5, 'markersize',10);
   hold on
```

```
    plot(tada,Tpersecond(100,1:6),'-b>','linewidth',1.5, 'markersize',10);
    legend('t=20s','t=30s','t=40s','t=50s','t=70s','t=100s' )
    xlabel('distance from testcell base(m)')
    ylabel('temperature (K)')
else
    rni=find(xapersecond(:,10)>0.99,1)
    plot(tada,Tpersecond(20,1:10),'-b*','linewidth',1.5, 'markersize',10);
    hold on
    plot(tada,Tpersecond(30,1:10),'-b+','linewidth',1.5, 'markersize',10);
    hold on
    plot(tada,Tpersecond(40,1:10),'-bo','linewidth',1.5, 'markersize',10);
    hold on
    plot(tada,Tpersecond(50,1:10),'-b*','linewidth',1.5, 'markersize',10);
    hold on
    plot(tada,Tpersecond(70,1:10),'-bx','linewidth',1.5, 'markersize',10);
    hold on
    plot(tada,Tpersecond(100,1:10),'-b>','linewidth',1.5, 'markersize',10);
    legend('t=20s','t=30s','t=40s','t=50s','t=70s','t=100s' )
    xlabel('distance from testcell base(m)')
    ylabel('temperature (K)')
end

figure(9)
tada=s.tad/s.n:s.tad/s.n:s.tad;          % array of distances from test cell base
plot(tada,xapersecond(1,2:6),'-b*','linewidth',1.5, 'markersize',10);
hold on
plot(tada,xapersecond(30,2:6),'-b+','linewidth',1.5, 'markersize',10);
hold on
plot(tada,xapersecond(40,2:6),'-bo','linewidth',1.5, 'markersize',10);
hold on
plot(tada,xapersecond(60,2:6),'-b*','linewidth',1.5, 'markersize',10);
hold on
plot(tada,xapersecond(90,2:6),'-bx','linewidth',1.5, 'markersize',10);
hold on
plot(tada,xapersecond(100,2:6),'-b>','linewidth',1.5, 'markersize',10);
hold on
plot(tada,xapersecond(120,2:6),'-bp','linewidth',1.5, 'markersize',10);
hold on
plot(tada,xapersecond(150,2:6),'-bh','linewidth',1.5, 'markersize',10);
legend('t=1s','t=30s','t=40s','t=60s','t=90s','t=100s','t=120s','t=150s' )
xlabel('distance from testcell base(m)')
switch s.rt
   case(1)
      ylabel('advanacement(8-4)')
   case(3)
      ylabel('advanacement(4-8)')
end

figure(10)
tada=s.tad/s.n:s.tad/s.n:s.tad;          % array of distances from test cell base
```

```
plot(tada,yapersecond(1,2:6),'-b*','linewidth',1.5, 'markersize',10);
hold on
plot(tada,yapersecond(30,2:6),'-b+','linewidth',1.5, 'markersize',10);
hold on
plot(tada,yapersecond(40,2:6),'-bo','linewidth',1.5, 'markersize',10);
hold on
plot(tada,yapersecond(60,2:6),'-b*','linewidth',1.5, 'markersize',10);
hold on
plot(tada,yapersecond(90,2:6),'-bx','linewidth',1.5, 'markersize',10);
hold on
plot(tada,yapersecond(100,2:6),'-b>','linewidth',1.5, 'markersize',10);
hold on
plot(tada,yapersecond(120,2:6),'-bp','linewidth',1.5, 'markersize',10);
hold on
plot(tada,yapersecond(150,2:6),'-bh','linewidth',1.5, 'markersize',10);
legend('t=1s','t=100s','t=200s','t=300s','t=400s','t=500s' )
xlabel('distance from testcell base(m)')
switch s.rt
   case(1)
      ylabel('advanacement(4-2)')
   case(3)
      ylabel('advanacement(2-4)')
end

figure(11)
tada=s.tad/s.n:s.tad/s.n:s.tad;            % array of distances from test cell base
plot(tada,xpersecond(1,2:6),'-b*','linewidth',1.5, 'markersize',10);
hold on
plot(tada,xpersecond(100,2:6),'-b+','linewidth',1.5, 'markersize',10);
hold on
plot(tada,xpersecond(200,2:6),'-bo','linewidth',1.5, 'markersize',10);
hold on
plot(tada,xpersecond(300,2:6),'-b*','linewidth',1.5, 'markersize',10);
hold on
plot(tada,xpersecond(400,2:6),'-bx','linewidth',1.5, 'markersize',10);
hold on
plot(tada,xpersecond(500,2:6),'-b>','linewidth',1.5, 'markersize',10);
legend('t=1s','t=100s','t=200s','t=300s','t=400s','t=500s' )
xlabel('distance from testcell base(m)')
switch s.rt
   case(1)
      ylabel('concentration(8-4)')
   case(3)
      ylabel('concentration(4-8)')
end

figure(12)
tada=s.tad/s.n:s.tad/s.n:s.tad;            % array of distances from test cell base
plot(tada,ypersecond(1,2:6),'-b*','linewidth',1.5, 'markersize',10);
hold on
```

```
plot(tada,ypersecond(100,2:6),'-b+','linewidth',1.5, 'markersize',10);
hold on
plot(tada,ypersecond(200,2:6),'-bo','linewidth',1.5, 'markersize',10);
hold on
plot(tada,ypersecond(300,2:6),'-b*','linewidth',1.5, 'markersize',10);
hold on
plot(tada,ypersecond(400,2:6),'-bx','linewidth',1.5, 'markersize',10);
hold on
plot(tada,ypersecond(500,2:6),'-b>','linewidth',1.5, 'markersize',10);
legend('t=1s','t=100s','t=200s','t=300s','t=400s','t=500s' )
xlabel('distance from testcell base(m)')
switch s.rt
   case(1)
      ylabel('concentration(4-2)')
   case(3)
      ylabel('concentration(2-4)')
end
figure(13)
tada=s.tad/s.n:s.tad/s.n:s.tad;            % array of distances from test cell base
if (rea>0)
   plot(tada(1),find(yapersecond(:,2)>0.99,1),'-b*','linewidth',1.5, 'markersize',10);
   hold on
   plot(tada(2),find(yapersecond(:,3)>0.99,1),'-b+','linewidth',1.5, 'markersize',10);
   hold on
   plot(tada(3),find(yapersecond(:,4)>0.99,1),'-bo','linewidth',1.5, 'markersize',10);
   hold on
   plot(tada(4),find(yapersecond(:,5)>0.99,1),'-b*','linewidth',1.5, 'markersize',10);
   hold on
   plot(tada(5),find(yapersecond(:,6)>0.99,1),'-bx','linewidth',1.5, 'markersize',10);
   legend('t=1s','t=100s','t=200s','t=300s','t=400s','t=500s' )
   xlabel('distance from testcell base(m)')
   ylabel('temperature (K)')
else
   plot(tada(1),find(xapersecond(:,2)>0.99,1),'-b*','linewidth',1.5, 'markersize',10);
   hold on
   plot(tada(2),find(xapersecond(:,3)>0.99,1),'-b+','linewidth',1.5, 'markersize',10);
   hold on
   plot(tada(3),find(xapersecond(:,4)>0.99,1),'-bo','linewidth',1.5, 'markersize',10);
   hold on
   plot(tada(4),find(xapersecond(:,5)>0.99,1),'-b*','linewidth',1.5, 'markersize',10);
   hold on
   plot(tada(5),find(xapersecond(:,6)>0.99,1),'-bx','linewidth',1.5, 'markersize',10);
   legend('1st layer advanacement=0.99','2nd layer advanacement=0.99','3rd layer
advanacement=0.99','layer advanacement=0.99','1st layer advanacement=0.99')
   xlabel('distance from testcell base(m)')
   ylabel('time(s)')
end
```

Other Functions

Newcon

```
function [xa,T,x,Peq,Cps]= newcon
(dt,As,Kad,Tbb,Tnb,Tfb,tlad,h,dH,R,dS,Pdb,xamax,xanb,Ax,Namm,N0,mlad,CpC,C
peng,Cpg,Tcn,xnb,xn1,Msys,...
   Mg,Tgbv,Vtc,Vpw,Vbv,no,i,jj,n,yr,xads,mx)
%returns modelled advancement,concentration,temperature for each time step

%********************heat conducted through the
sample**********************
switch jj
   case no
      dQdot = ((Kad*As*(Tbb-Tnb))/tlad)*dt;              % heat conducted for last
node
   case 2
      dQdot = (((Tbb-Tnb)/((1/(h*As) + ((0.5*tlad)/(Kad*As)))))+((Tfb-
Tnb)/(tlad/(Kad*As))))*dt;% heat conducted for second node
   otherwise
      dQdot = ((Tbb+Tfb-(2*Tnb))/((1/(h*As)) + (tlad/(Kad*As))))*dt; % heat
conducted (J) for nodes 3 up to second to the last node
end
%*****************************************************************
********
%********************advancement*********************************
*******
Peq=exp(-dH/(R*Tnb)+dS/R);            % returns equilibrium pressure for given
node temperature (bar)
if Pdb>Peq                            % equilibrium pressure not reached
   da=0;
else
   da=dt*(((xamax-xanb)^mx)*Ax*((Peq-Pdb)/(Pdb)));  % change in advancement
for first reaction (8-4)
end
if xanb+da < xamax
   xa = xanb+da;                      % new advancement
else
   xa = xamax;
end

%*****************************************************************
********
%*********************new temperature*********************************
Cps=Cpeng+CpC+(Cpg*(xnb));            % specific heat and salt, binder and gas
dTx=(dQdot-(Namm*N0*dH*da))/((mlad*Cps));   % change in temperature of each
node for first reaction
dT = dTx;              % change in temperature as a result of both reactions
T = Tnb + dT;
%     if dT>0.01
```

```
%           disp('Warning! significant negative temperature development, reduce
timesteps!');
%     end;
%*************************************************************************
********
%********************new
concentration*************************************
x=xn1*(xamax-xa);            % new refrigerant concentration
%*************************************************************************
********
end
```

Newconads

```
function [xa,T,x,Peq,Cps]= newconads
(dt,As,Kad,Tbb,Tnb,Tfb,tlad,h,dH,R,dS,Pdb,xamax,xanb,Ax,Namm,N0,mlad,CpC,C
peng,Cpg,Tcn,xnb,xn1,Msys,...
    Mg,Tgbv,Vtc,Vpw,Vbv,no,i,jj,n,yr,xnend,mx)
%returns modelled pressure for each time step
%********************heat conducted through the
sample************************
switch jj
    case no
        dQdot = ((Kad*As*(Tbb-Tnb))/tlad)*dt;              % heat conducted for last
node
    case 2
        dQdot = (((Tbb-Tnb)/((1/(h*As) + ((0.5*tlad)/(Kad*As)))))+((Tfb-
Tnb)/(tlad/(Kad*As))))*dt;% heat conducted for second node
    otherwise
        dQdot = ((Tbb+Tfb-(2*Tnb))/((1/(h*As)) + (tlad/(Kad*As))))*dt; % heat
conducted (J) for nodes 3 up to second to the last node
end
%*************************************************************************
********
%********************advancement*************************************
********
Peq=exp(-dH/(R*Tnb)+dS/R);                % returns equilibrium pressure for given
node temperature for second reaction (bar)
if Pdb<Peq                                % equilibrium pressure not reached
    da = 0;
else
    da=dt*(((xamax-xanb)^mx)*Ax*(Pdb-Peq)/(Pdb));   % change in advancement
for first reaction (4-8)
end

if da+xanb>xamax
    xa=xamax;
else
    xa=xanb+da;                    % advanacement
end
```

```
%*****************************************************************
********
%*******************new temperature*********************************
Cps=Cpeng+CpC+(Cpg*(xnb));          % specific heat and salt, binder and gas
dTx=(dQdot+(Namm*N0*dH*da))/((mlad*Cps)/dt);   % change in temperature of
each node

dT = dTx ;                    % change in temperature as a result of both reactions
T = Tnb + dT;
% if dT>0.01
%       disp('Warning! significant negative temperature development, reduce
timesteps!');
% end;
%*****************************************************************
********
%*******************new
concentration*************************************
x=xnend*(xa);          % new refrigerant concentration first reaction
%*****************************************************************
********
end
```

NewP1

```
function [P]= newP1 (N0,Mg,n,xaan,Namm,msys,R,Tgbvn,Tgtcn,Vbv,Vtc,Vpw,yr)
switch yr
   case(1)
      madsorbed = N0*Mg*(n-sum(xaan));
   case(3)
      madsorbed = N0*Mg*(n-sum(xaan));
end
P=(((msys-
madsorbed)*R*Tgbvn*Tgtcn)/(Mg*((Vbv*Tgtcn)+(Tgbvn*(Vpw+Vtc)))))/1e5;  %
new pressure
%*****************************************************************
********
end
```

Samplechar

```
function [ no,tlad,ms,mlad,N0,As ] = samplechar( n,dia,tad,mc,Ms,persalt )
%calculates other physical characteristics of the sample
no=n+1;              % no of nodes

tlad=tad/n;          % thickness of single sample layer (m)
ms=mc*(persalt/100);    % mass of reactive salt (kg)
mlad=ms/n;           % mass of one layer of salt
N0=mlad/Ms;          % no of salt moles per layer (moles)
As=(pi*dia^2)/4;       % contact area of sample (sq.m)
end
```

Appendix 10: Matlab Model for the Simulation of the Entire Heat Pump

Main Script

```
clear all;  %clears all
clc;        %clears command page
close all;  %closes all previously opened graphs

%*********refrigerant properties***************
monh3=0.017;    %molar mass of Ammonia
cpl=4734;    %specific heat of liquid ammonia (J/kg/K)
Cpeng=890;  % Cp of expanded natural graphite
R=8.3145;     % gas constant (J/mol.K)

%*******temperature of heat transfer fluid********
s.Thm=240+273.15;   %heating temperature of MgCl htf
s.Tcm=150+273.15;    %cooling temperature of mgcl2 htf
s.Thc=120+273.15;   %heating temperature of MgCl htf
s.Tcc=45+273.15;    %cooling temperature of mgcl2 htf
s.Tcco=[40+273.15, 60+273.15];     %cooling temperature of cacl2 htf


%*heat transfer, physical and geometric properties in the reactor*********
km=4.12;    %thermal conductivity (W/mK)
kc=4.82;    %thermal conductivity of cacl2+ENG (W/mK)
kt=30;    %thermal conductivity of reactor tubes (W/mK)
dth=0.0254;  %diameter of htf tube (m)
do=0.09;  %diameter of entire reactor (m)
mm=1;   %mass of pure mgcl2 (kg)
nmamm=4;    %no of moles of nh3 reacted with mgcl2
ncamm=4;    %total no of moles of nh3 reacted with cacl2
ncamm1=2;    %total no of moles of nh3 reacted with cacl2 reaction 2
mom=0.095211;    %molar mass of magnesium chloride
mmamm=(nmamm*mm*monh3)/mom; %mass of nh3 to be reacted
pem=0.43;    %percentage of mgcl2 in mgcl2+ENG
mmp=mm+(((1-pem)*mm)/pem);   %mass of magnesium chloride (43%)+ENG ,
(kg)
rhom=205;   %density of mgcl2/cacl2+ENG (kg/m3)
tt=0.001;   %thickness of htf tube (m)
ts=(do-(dth+2*tt))/2;   %thickness of mgcl2+ENG chunk(m)
lem=(4*mmp)/(pi*rhom*(do^2-(dth+tt)^2));     %length of htf tube (m) mgcl2
%length of the CaCl2 reactor to be calculated later on based on heat from
%mgcl2+NH3
fp=2.5;    %heat transfer fluid pressure (bar)
s.mf=1;  %mass flow rate of htf (kg/s)
miu=XSteam('my_pT',fp,s.Thm);    %dynamic visocity of htf (Ns/m2)
kf=XSteam('tc_pT',fp,s.Thm);      %thermal conductivity of htf (W/mK)
cf=XSteam('Cp_pT',fp,s.Thm)*1e3;    %isobaric specific heat of htf (J/kg/K)
re=(4*s.mf*dth)/(miu*pi*dth^2); %reynolds number of htf flow
```

```
pr=(cf*miu)/kf;   %Prandtl number of htf flow
Nuh=0.023*(re^0.8)*(pr^0.4);    %nusselt number for heating (decomposition)
Nuc=0.023*(re^0.8)*(pr^0.3);    %nusselt number for heating (synthesis)
hfwh=20000000;%(Nuh*kf)/lem;   %heat transfer coefficient between heat transfer
fluid and reactor tube walls (decomposition) (W/m^2K)
hfwc=(Nuc*kf)/lem;   %heat transfer coefficient between heat transfer fluid and
reactor tube walls (synthesis) (W/m^2K)
hws=20000000;   %heat transfer coefficient between reactor tube and salt
(MgCl2/CaCl2) (W/m^2K)
n=5;   %total no of layers (salt, tube and fluid)
no=n+1; %no of nodes (salt, tube and fluid)
ns=n-1; %no of salt layers
tsl=ts/ns;   %thickness of a single mgc2l layer
afm=pi*dth*lem;    %contact area of fluid for mgcl2
mst=1;  %total mass of steel in a reactor
mrat=mst/mm;    %ratio of mass of steel to mass of mgcl2
vm=(pi*lem*(do^2-(dth+tt)^2))/4;  %volume of mgcl2 reactor
cpmg=746.7;%specific heat of pure magnesium chloride (J/kg/K)
cpca=656.8; %specific heat of pure calcium chloride (J/kg/K)
cpeng=890;  %specific heat of expanded graphite (J/kg/K)
cpt=510;    %specific heat of stainless steel tube (J/kgK)


%******the reactions************************
nnh3m=4;    %no of moles to be reacted with magnesium chloride
mom=0.095211;    %molar mass of magnesium chloride
moc=0.11098;    %molar mass of magnesium chloride
mnh3m=(nnh3m*mm*monh3)/mom; %mass of nh3 to be reacted with mgcl2
%mass of the nh3 to be reacted CaCl2 reactor to be calculated later on based on heat
from
%mgcl2+NH3
xamax=1;    %maximum reaction advancement
dhm=60456;  %heat of reaction mgcl2(6-2)nh3 (J/mol) (P in bar)
dsm=145.06; %entropy change mgcl2(6-2)nh3 (J/mol.K) (P in bar)
dhms=46677; %heat of reaction mgcl2(2-6)nh3 (J/mol) (P in bar)
dsms=118.53;    %entropy change mgcl2(2-6)nh3 (J/mol.K) (P in bar)
dhc=41413;  %heat of reaction cacl2(8-4-8)nh3 (J/mol) (P in Pa)
dsc=231.2;  %entropy change cacl2(8-4-8)nh3 (J/mol.K) (P in Pa)
dhc1=42268; %heat of reaction cacl2(4-2-4)nh3 (J/mol) (P in Pa)
dsc1=231;   % entropy change cacl2(4-2-4)nh3 (J/mol.K) (P in Pa)
am=0.03;   % A value for mgcl2(6-2)nh3 reaction
ym=0.7;     % yo value for mgcl2(6-2)nh3 reaction
ams=0.03;  % A value for mgcl2(2-6)nh3 reaction
yms=0.7;     % yo value for mgcl2(2-6)nh3 reaction
ac=0.02;   % A value for cacl2(8-4)nh3 reaction
yc=0.7;    % yo value for cacl2(8-4)nh3 reaction
acs=0.01;  % A value for cacl2(4-8)nh3 reaction
ycs=0.7;   % yo value for cacl2(4-8)nh3 reaction
ac1=0.02;   % A value for cacl2(4-2)nh3 reaction
yc1=0.7;    % yo value for cacl2(4-2)nh3 reaction
```

```
acs1=0.01;  % A value for cacl2(2-4)nh3 reaction
ycs1=0.7;   % yo value for cacl2(2-4)nh3 reaction



%********the condenser**********************
s.Tcon=323;   %condensing temperature (50degC)
Pcon=psatamm(s.Tcon);  %condensing pressure

%********the evaporator**********************
s.Tev=263;   %condensing temperature (50degC)
Pev=psatamm(s.Tev);  %evaporating pressure

%*******others*****************************
dt=0.01;  %time step (s)
nc=6;    %no of cycles to stabilise
s.ht=1500;   %half of the cycles time (s)
tto=round((s.ht*2)/dt);  %no of points

%******************make initial
matrices**********************************
Tm=zeros(no,tto);              % an initial matrix of zeros for temperature of all nodes
mgcl2
Tc=zeros(no,tto);             % an initial matrix of zeros for temperature of all nodes
cacl2
xm=zeros(no,tto);              % an initial matrix of zeros for refigerant concentration
in each layer mgcl2
xc=zeros(no,tto);              % an initial matrix of zeros for refigerant concentration
in each layer cacl2
xam=zeros(no,tto);             % an initial matrix of zeros for local advancement in
each layer mgcl2
xac=zeros(no,tto);             % an initial matrix of zeros for local advancement in
each layer cacl2
xacy=zeros(no,tto);            % an initial matrix of zeros for local advancement in
each layer cacl2 second reaction
yc=zeros(no,tto);              % an initial matrix of zeros for refigerant concentration
in each layer for second reaction in cacl2
yac=zeros(no,tto);             % an initial matrix of zeros for local advancement in
each layer
pqm=zeros(no,tto);             % an initial row vector of zeros for equilibrium
pressure of equal layer mgcl2
pqc=zeros(no,tto);             % an initial row vector of zeros for equilibrium pressure
of equal layer cacl2
pqc1=zeros(no,tto);            % an initial row vector of zeros for equilibrium
pressure of equal layer cacl2 r2
pqcy=zeros(no,tto);            % an initial row vector of zeros for equilibrium
pressure of equal layer cacl2 (second reaction)
pdm=zeros(1,tto);              % an initial row vector of zeros for modelled pressure
mgcl2
```

```
pdc=zeros(1,tto);              % an initial row vector of zeros for modelled pressure
cacl2
cpm=zeros(no,tto);             % an initial matrix of zeros for specific heat of each
layer mgcl2
cpc=zeros(no,tto);             % an initial matrix of zeros for specific heat of each
layer cacl2
mrgm=zeros(no,tto);            % an initial matrix of zeros for the mass of nh3
reacted with mgcl2
Pm=zeros(1,tto);               % an initial matrix of zeros for the pressure in the
mgcl2 reactor
mgm=zeros(1,tto);              % an initial matrix of zeros for the mass of nh3 in
mgcl2 reactor
mrgc=zeros(no,tto);            % an initial matrix of zeros for the mass of nh3
reacted with cacl2
mgtm=zeros(1,tto);             % an initial matrix of zeros for the total mass of nh3
(gas and reacted) in the mgcl2 reactor
Pc=zeros(1,tto);               % an initial matrix of zeros for the pressure in the cacl2
reactor
mgc=zeros(1,tto);              % an initial matrix of zeros for the mass of nh3 in cacl2
reactor
mgtc=zeros(1,tto);             % an initial matrix of zeros for the total mass of nh3
(gas and reacted) in the cacl2 reactor
SHP=zeros(1,tto);              % an initial matrix of zeros for the SHP
Qdm=zeros(1,tto);              % an initial matrix of zeros for the heat into mgcl2
bed
Qdc=zeros(1,tto);              % an initial matrix of zeros for the heat into cacl2 bed
Qsm=zeros(1,tto);              % an initial matrix of zeros for the heat out of mgcl2
bed
Qsc=zeros(1,tto);              % an initial matrix of zeros for the heat out of mgcl2
bed
% Qcon=zeros(1,tto);           % an initial matrix of zeros for condenoation heat
% Qev=zeros(1,tto);            % an initial matrix of zeros for evaporation heat

N= structfun(@numel,s);        % number of element each user input parameter has
if (nnz(N>1)==1);              % if one of the parameters has elements greater than one
or has been varied
   C=fieldnames(s);            % declares the names of all the user input parameters
   F=C{N>1};                   % declares the name of the parameter with more than one
element
   V=s.(F);                    % stores the value of the parameter above as variable V

%*****************************************************************
********
   for l=1:length(V),

      s.(F)=V(l);              % declare the values for parameter that was varied
      Tm(:,1)=s.Tcm;    %initial temperature of all mgcl2 layers
      xm(3:no,1)=mmamm/mm;  %initial concentration through all the layers
      pqm(3:no,1)=Pequilibrium(dhm,dsm,R,s.Tcm); %equilibrium pressure at initial
temperaturee (bar)
```

```
      cpm(3:no,1)=cpmg+cpeng+(cpl*(xm(1,1)));    %specific heat at initial
concentration (J/kg/K)
      Pm(1)=psatamm(s.Tev);  %starting pressure in the reactor mgcl2
      Pc(1)=psatamm(s.Tev);  %starting pressure in the reactor cacl2
      mrgm(3:no,1)=mmamm/ns;   %initial mass of reacted nh3 in every layer
      mgm(1)=(Pm(1)*1e5*monh3*vm)/(R*Tm(1,1));   %initial mass of gas in
mgcl2 reactorm
      mgtm(1)=mgm(1)+(sum(mrgm(1:no,1)));  %sum of total initial nh3 (gas and
reacted) in the mgcl2 reactor

      for ncr=1;
         Qconm=0; %condensation heat
         %***here we use only mgcl2 so we can calculate how much cacl2 we need
later on*****
         %**********initial conditions*******************
         Tm(1,2:tto/2)=s.Thm;    %fluid temperature of mgcl2 set (K)


         for i=2:(tto/2)-1; %decomposition phase

            for jj=2:no

               %********************heat conduction through the nodes
(watts)***********************
               switch jj
                  case(2)    %steel tube node
                     qdot=((Tm(jj-1,i-1)-Tm(jj,i-
1))/((1/(hfwh*pi*dth*lem))+((log((dth+tt)/dth))/(2*pi*kt*lem))))+...
                        ((Tm(jj+1,i-1)-Tm(jj,i-
1))/((1/(hws*pi*(dth+(2*tt))*lem))+(((log((dth+(2*tt))/(dth+tt))+log((dth+(2*tt)+(0.
5*tsl))/(dth+(2*tt))))/(2*pi*kt*lem)))));
                  case (3)    %first mgcl2 node
                     qdot=((Tm(jj-1,i-1)-Tm(jj,i-
1))/((1/(hws*pi*(dth+(2*tt))*lem))+(((log((dth+(2*tt))/(dth+tt))+log((dth+(2*tt)+(0.
5*tsl))/(dth+(2*tt))))/(2*pi*kt*lem)))))...
                        +((Tm(jj+1,i-1)-Tm(jj,i-1))/(((log((dth+(2*tt)+((jj-
1.5)*tsl))/(dth+(2*tt)+((jj-2.5)*tsl)))/(2*pi*km*lem)))));
                  case (no)   %last mgcl2 node
                     qdot=((Tm(jj-1,i-1)-Tm(jj,i-1))/(((log((dth+(2*tt)+((no-
2.5)*tsl))/(dth+(2*tt)+((no-3.5)*tsl)))/(2*pi*km*lem)))));
                  otherwise   %middle mgcl2 nodes
                     qdot=((Tm(jj-1,i-1)-Tm(jj,i-1))/(((log((dth+(2*tt)+((jj-
2.5)*tsl))/(dth+(2*tt)+((jj-3.5)*tsl)))/(2*pi*km*lem)))))+...
                        ((Tm(jj+1,i-1)-Tm(jj,i-1))/(((log((dth+(2*tt)+((jj-
1.5)*tsl))/(dth+(2*tt)+((jj-2.5)*tsl)))/(2*pi*km*lem)))));
               end
               %**********************reaction advanacements
****************************
               pqm(jj,i)=Pequilibrium(dhm,dsm,R,Tm(jj,i-1)); %equilibrium pressure
at initial temperaturee (bar)
```

```
            if Pm(i-1)>pqm(jj,i)                    % equilibrium pressure not
reached
                da=0;
            else
                da=dt*(((xamax-xam(jj,i-1))^ym)*am*((pqm(jj,i)-Pm(i-1))/(Pm(i-
1))));  % change in advancement for first reaction (8-4)
            end
            if xam(jj,i-1)+da < xamax
                xam(jj,i)= xam(jj,i-1)+da;              % new advancement
            else
                xam(jj,i)= xamax;
            end
            %*******************new
concentration*************************************
            xm(jj,i)=xm(jj,i-1)*(xamax-xam(jj,i));      % new refrigerant
concentration
            mrgm(jj,i)=xm(jj,i)*mm/ns;    %mass of reacted nh3 in the mgcl2
recator

            %*******************new
temperature*********************************
            switch jj
                case(2)
                    dTst=(qdot*dt)/(mst*cpt);  %change in steel tube temperature
                    Tm(jj,i)=Tm(jj,i-1)+dTst;
                    pqm(jj,i)=0;
                    xm(jj,i)=0;
                    xam(jj,i)=0;
                    mrgm(jj,i)=0;
                otherwise
                    cpm(jj,i)=cpmg+cpeng+(cpl*(xm(jj,i)));      % specific heat
and salt, binder and gas
                    dTm=(qdot-
(nmamm*(mm/(mom*ns))*dhm*da))*((dt*ns)/((mmp+(mm*xm(jj,i)))*cpm(jj,i)));
% change in temperature of each node for first reaction
                    Tm(jj,i)=Tm(jj,i-1)+dTm;

            end

        end

        if Pm(i-1)<Pcon %reactor pressure is less than condensation pressure so
constant mass desorption
            mgtm(i)=mgtm(i-1);   %total mass of nh3 in the reactor stays constant
            mgm(i)=mgtm(i)-sum(mrgm(:,i)); %mass of nh3 gas in the system
            Pm(i)=((mgm(i)*R*mean(Tm(3:no,i)))/(monh3*vm))/1e5; % the new
pressure
        else    %mgcl2 reactor has now reached condenser pressure and there is
constant pressure desorption
            Pm(i)=Pcon;
```

```
            mgm(i)=(Pm(i)*1e5*monh3*vm)/(R*mean(Tm(3:no,i)));   %initial
mass of gas in mgcl2 reactorm
            mgtm(i)=mgm(i)+sum(mrgm(:,i)); %total amount of nh3 in mgcl2
reactor
        end

        Qdm(i)=((Tm(1,i)-
Tm(2,i))/((1/(hfwh*pi*dth*lem))+((log((dth+tt)/dth))/(2*pi*kt*lem))))*dt;
        Qconm=Qconm-(mgtm(i)-mgtm(i-1))*(hsupamm(s.Tcon-
273.15,Tm(no,i)-273.15)-hfamm(s.Tcon-273));

    end
    Tm(1,(tto/2):tto)=s.Tcm;    %fluid temperature of mgcl2 set (K) for synthesis
stage
    xam(3:no,i)=0;  %initial concentration through all the layers
    %          mgm(i)=((Pm(1)*1e5*monh3*vm)/(R*Tm(1,1)))+((xamax-
mean(xam(3:no,i)))*sum(mrgm(:,1)));%mass of nh3 gas in the system
    %                Pm(i)=(mgm(i)*R*mean(Tm(3:no,i))/(monh3*vm))/1e5; %
the new pressure
    for i=tto/2:tto %synthesis phase

        for jj=2:no

            %********************heat conduction through the nodes
(watts)**********************
            switch jj
                case(2)    %steel tube node
                    qdot=((Tm(jj-1,i-1)-Tm(jj,i-
1))/((1/(hfwh*pi*dth*lem))+((log((dth+tt)/dth))/(2*pi*kt*lem))))+...
                        ((Tm(jj+1,i-1)-Tm(jj,i-
1))/((1/(hws*pi*(dth+(2*tt))*lem))+(((log((dth+(2*tt))/(dth+tt))+log((dth+(2*tt)+(0.
5*tsl))/(dth+(2*tt))))/(2*pi*kt*lem)))));
                case (3)    %first mgcl2 node
                    qdot=((Tm(jj-1,i-1)-Tm(jj,i-
1))/((1/(hws*pi*(dth+(2*tt))*lem))+(((log((dth+(2*tt))/(dth+tt))+log((dth+(2*tt)+(0.
5*tsl))/(dth+(2*tt))))/(2*pi*kt*lem)))))...
                        +((Tm(jj+1,i-1)-Tm(jj,i-1))/(((log((dth+(2*tt)+((jj-
1.5)*tsl))/(dth+(2*tt)+((jj-2.5)*tsl)))/(2*pi*km*lem)))));
                case (no)   %last mgcl2 node
                    qdot=((Tm(jj-1,i-1)-Tm(jj,i-1))/(((log((dth+(2*tt)+((no-
2.5)*tsl))/(dth+(2*tt)+((no-3.5)*tsl)))/(2*pi*km*lem)))));
                otherwise   %middle mgcl2 nodes
                    qdot=((Tm(jj-1,i-1)-Tm(jj,i-1))/(((log((dth+(2*tt)+((jj-
2.5)*tsl))/(dth+(2*tt)+((jj-3.5)*tsl)))/(2*pi*km*lem)))))+...
                        ((Tm(jj+1,i-1)-Tm(jj,i-1))/(((log((dth+(2*tt)+((jj-
1.5)*tsl))/(dth+(2*tt)+((jj-2.5)*tsl)))/(2*pi*km*lem)))));
            end
            %**********************reaction advanacements
****************************
```

```
            pqm(jj,i)=Pequilibrium(dhms,dsms,R,Tm(jj,i-1)); %equilibrium
pressure at initial temperaturee (bar)
            if Pm(i-1)<pqm(jj,i)                    % equilibrium pressure not
reached
               da=0;
            else
               da=dt*(((xamax-xam(jj,i-1))^yms)*ams*((Pm(i-1)-pqm(jj,i))/(Pm(i-
1))));  % change in advancement for first reaction (8-4)
            end
            if xam(jj,i-1)+da < xamax
               xam(jj,i)= xam(jj,i-1)+da;              % new advancement
            else
               xam(jj,i)= xamax;
            end
            %********************new
concentration*************************************
            xm(jj,i)=xm(jj,1)*xam(jj,i);          % new refrigerant concentration
            mrgm(jj,i)=xm(jj,i)*mm/ns;    %mass of reacted nh3 in the mgcl2
recator

            %********************new
temperature*********************************
            switch jj
               case(2)
                  dTst=(qdot*dt)/(mst*cpt);  %change in steel tube temperature
                  Tm(jj,i)=Tm(jj,i-1)+dTst;
                  pqm(jj,i)=0;
                  xm(jj,i)=0;
                  xam(jj,i)=0;
                  mrgm(jj,i)=0;
               otherwise
                  cpm(jj,i)=cpmg+cpeng+(cpl*(xm(jj,i)));          % specific heat
and salt, binder and gas

dTm=(qdot+(nmamm*(mm/(mom*ns))*dhms*da))*((dt*ns)/((mmp+(mm*xm(jj,i)))
*cpm(jj,i)));   % change in temperature of each node for first reaction
                  %-((mrgm(jj,i)-mrgm(jj,i-1)*cpl*(Tm(jj,i)-s.Tev)))
                  Tm(jj,i)=Tm(jj,i-1)+dTm;

            end
         end

         if Pm(i-1)>Pev %reactor pressure is higher than evaporation pressure so
constant mass synthesis
            mgtm(i)=mgtm(i-1);   %mass of gas in the reactor stays constant
            mgm(i)=mgtm(i)-sum(mrgm(:,i)); %mass of nh3 gas in the system
            Pm(i)=(mgm(i)*R*mean(Tm(3:no,i))/(monh3*vm))/1e5; % the new
pressure
         else    %mgcl2 reactor has now reached condenoer pressure and there is
constant pressure desorption
```

```
            Pm(i)=Pev;
            mgm(i)=(Pm(i)*1e5*monh3*vm)/(R*mean(Tm(3:no,i)));   %initial
mass of gas in mgcl2 reactorm
            mgtm(i)=mgm(i)+sum(mrgm(:,i)); %total amount of nh3 in mgcl2
reactor
          end
            Qsm(i)=((Tm(2,i)-
Tm(1,i))/((1/(hfwh*pi*dth*lem))+((log((dth+tt)/dth))/(2*pi*kt*lem))))*dt;
            Qev=(mgtm(i)-mgtm(i-1))*(hsupamm(s.Tev-273.15,Tm(no,i)-273.15)-
hfamm(s.Tev-273));
        end

        COPh(ncr)=(Qconm+sum(Qsm))/sum(Qdm); %heat pump COP for MgCl2
only run
        SHPh(ncr)=(Qconm+sum(Qsm))/(s.ht*2*mm); % Heating power W/kg
mgcl2
        xm((3:no),1)=xm((3:no),i);
        xam((3:no),1)=0;
        Pm(1)=Pm(i);
        mgm(1)=(Pm(1)*1e5*monh3*vm)/(R*Tm(1,1));
        mrgm((3:no),1)=xm((3:no),i)*mm/ns;

        mgtm(1)=mgtm(i);
    end
    %find mass of cacl2 required bassed on synthesis heat from mgcl2
    %reaction
    mcp=sum(Qsm)/((cpca+cpeng+(cpl*0.6))*(s.Thc-s.Tcc));  %mass of calcium
chloride +ENG that heat from mgcl2 can heat up
    lec=(4*mcp)/(pi*rhom*(do^2-(dth+tt)^2));     %length of htf tube (m) cacl2
    vc=(pi*lec*(do^2-(dth+tt)^2))/4;  %volume of cacl2 reactor
    mc=0.43*mcp;    %mass of calcium chloride
    for ncr=2
        Tm(:,1)=s.Tcm;    %initial temperature of all mgcl2 layers
        Tc(:,1)=s.Thc;      %initial temperature of all cacl2 layers
        xm(3:no,1)=mmamm/mm;  %initial concentration through all the layers
mgcl2
        pqm(3:no,1)=Pequilibrium(dhm,dsm,R,s.Tcm); %equilibrium pressure at
initial temperaturee (bar) mgcl2
        pqc(3:no,1)=Pequilibrium(dhc,dsc,R,s.Thc)/1e5; %equilibrium pressure at
initial temperaturee (bar) cacl2
        pqc1(3:no,1)=Pequilibrium(dhc1,dsc1,R,s.Thc)/1e5; %equilibrium pressure
at initial temperaturee (bar) cacl2
        cpm(3:no,1)=cpmg+cpeng+(cpl*(xm(1,1)));    %specific heat at initial
concentration (J/kg/K) mgcl2
        cpc(3:no,1)=cpca+cpeng+(cpl*(xc(1,1)));    %specific heat at initial
concentration (J/kg/K) cacl2
        Pm(1)=psatamm(s.Tev);  %starting pressure in the reactor mgcl2
        Pc(1)=psatamm(s.Tcon);  %starting pressure in the reactor cacl2
        mrgm(3:no,1)=mmamm/ns;   %initial mass of reacted nh3 in every layer
```

```
        mgm(1)=(Pm(1)*1e5*monh3*vm)/(R*Tm(1,1));   %initial mass of gas in
mgcl2 reactor
        mgc(1)=(Pc(1)*1e5*monh3*vc)/(R*Tc(1,1));   %initial mass of gas in cacl2
reactor
        mgtm(1)=mgm(1)+(sum(mrgm(1:no,1)));  %sum of total initial nh3 (gas and
reacted) in the mgcl2 reactor
        mgtc(1)=mgc(1)+(sum(mrgc(1:no,1)));  %sum of total initial nh3 (gas and
reacted) in the cacl2 reactor
        Qconm=0; %condensation heat mgcl2 desorption
        Qconc=0; %condensation heat cacl2 desorption
        Qevc=0;%condensation heat cacl2 desorption
        Qevm=0;%condensation heat mgcl2 desorption
        xac(3:no,1)=1;%starting condition for advanacement of first reaction in cacl2
        xcmax=(ncamm*monh3)/moc;    %maximum concentration of first reaction
cacl2
        ycmax=(ncamm1*monh3)/moc;   %maximum concentration of second
reaction cacl2




        for i=2:(tto/2)-1; %decomposition phase
           Tm(1,2:tto/2)=s.Thm;    %fluid temperature of mgcl2 set (K)
           Tc(1,2:tto/2)=s.Tcc;    %fluid temperature of cacl2 set (K) for synthesis
stage

           for jj=2:no

              %********************heat conduction through the nodes
(watts)**********************
              switch jj
                 case(2)    %steel tube node
                    qdot=((Tm(jj-1,i-1)-Tm(jj,i-
1))/((1/(hfwh*pi*dth*lem))+((log((dth+tt)/dth))/(2*pi*kt*lem))))+...
                       ((Tm(jj+1,i-1)-Tm(jj,i-
1))/((1/(hws*pi*(dth+(2*tt))*lem))+(((log((dth+(2*tt))/(dth+tt))+log((dth+(2*tt)+(0.
5*tsl))/(dth+(2*tt))))/(2*pi*kt*lem)))));
                    qdotc=((Tc(jj-1,i-1)-Tc(jj,i-
1))/((1/(hfwh*pi*dth*lec))+((log((dth+tt)/dth))/(2*pi*kt*lec))))+...
                       ((Tc(jj+1,i-1)-Tc(jj,i-
1))/((1/(hws*pi*(dth+(2*tt))*lec))+(((log((dth+(2*tt))/(dth+tt))+log((dth+(2*tt)+(0.5
*tsl))/(dth+(2*tt))))/(2*pi*kt*lec)))));
                 case (3)    %first mgcl2 node
                    qdot=((Tm(jj-1,i-1)-Tm(jj,i-
1))/((1/(hws*pi*(dth+(2*tt))*lem))+(((log((dth+(2*tt))/(dth+tt))+log((dth+(2*tt)+(0.
5*tsl))/(dth+(2*tt))))/(2*pi*kt*lem)))))...
                       +((Tm(jj+1,i-1)-Tm(jj,i-1))/(((log((dth+(2*tt)+((jj-
1.5)*tsl))/(dth+(2*tt)+((jj-2.5)*tsl)))/(2*pi*km*lem)))));
```

```
                qdotc=((Tc(jj-1,i-1)-Tc(jj,i-
1))/((1/(hws*pi*(dth+(2*tt))*lec))+(((log((dth+(2*tt))/(dth+tt))+log((dth+(2*tt)+(0.5
*tsl))/(dth+(2*tt))))/(2*pi*kt*lec)))))...
                    +((Tc(jj+1,i-1)-Tc(jj,i-1))/(((log((dth+(2*tt)+((jj-
1.5)*tsl))/(dth+(2*tt)+((jj-2.5)*tsl)))/(2*pi*kc*lec)))));
            case (no)   %last mgcl2 node
                qdot=((Tm(jj-1,i-1)-Tm(jj,i-1))/(((log((dth+(2*tt)+((no-
2.5)*tsl))/(dth+(2*tt)+((no-3.5)*tsl)))/(2*pi*km*lem)))));
                qdotc=((Tc(jj-1,i-1)-Tc(jj,i-1))/(((log((dth+(2*tt)+((no-
2.5)*tsl))/(dth+(2*tt)+((no-3.5)*tsl)))/(2*pi*kc*lec)))));
            otherwise   %middle mgcl2 nodes
                qdot=((Tm(jj-1,i-1)-Tm(jj,i-1))/(((log((dth+(2*tt)+((jj-
2.5)*tsl))/(dth+(2*tt)+((jj-3.5)*tsl)))/(2*pi*km*lem)))))+...
                    ((Tm(jj+1,i-1)-Tm(jj,i-1))/(((log((dth+(2*tt)+((jj-
1.5)*tsl))/(dth+(2*tt)+((jj-2.5)*tsl)))/(2*pi*km*lem)))));
                qdotc=((Tc(jj-1,i-1)-Tc(jj,i-1))/(((log((dth+(2*tt)+((jj-
2.5)*tsl))/(dth+(2*tt)+((jj-3.5)*tsl)))/(2*pi*kc*lec)))))+...
                    ((Tc(jj+1,i-1)-Tc(jj,i-1))/(((log((dth+(2*tt)+((jj-
1.5)*tsl))/(dth+(2*tt)+((jj-2.5)*tsl)))/(2*pi*kc*lec)))));
            end
            %**********************reaction advanacements
*****************************
            pqm(jj,i)=Pequilibrium(dhm,dsm,R,Tm(jj,i-1)); %equilibrium pressure
at initial temperaturee (bar) mgcl2 reaction
            pqc(jj,i)=Pequilibrium(dhc,dsc,R,Tc(jj,i-1))/1e5; %equilibrium pressure
at initial temperaturee (bar)cacl2 first reaction
            pqc1(jj,i)=Pequilibrium(dhc1,dsc1,R,Tc(jj,i-1))/1e5; %equilibrium
pressure at initial temperaturee (bar)cacl2 second reaction
            if Pm(i-1)>pqm(jj,i)                    % equilibrium pressure not
reached
                da=0;
            else
                da=dt*(((xamax-xam(jj,i-1))^ym)*am*((pqm(jj,i)-Pm(i-1))/(Pm(i-
1))));  % change in advancement for first reaction (8-4)
            end
            if xam(jj,i-1)+da < xamax
                xam(jj,i)= xam(jj,i-1)+da;              % new advancement
            else
                xam(jj,i)= xamax;
            end
            if Pc(i-1)<pqc1(jj,i)                   % equilibrium pressure not
reached
                dac1=0;
            else
                dac1=dt*(((xamax-yac(jj,i-1))^ycs1)*acs1*((Pc(i-1)-pqc1(jj,i))/(Pc(i-
1))));  % change in advancement for first reaction (8-4)
            end
            if yac(jj,i-1)+dac1 < xamax
                yac(jj,i)= yac(jj,i-1)+dac1;            % new advancement
            else
```

```
            yac(jj,i)= xamax;
        end
        if Pc(i-1)<pqc(jj,i)                    % equilibrium pressure not
reached
            dac=0;
        else
            dac=dt*(((xamax-xac(jj,i-1))^ycs)*acs*((Pc(i-1)-pqc(jj,i))/(Pc(i-1))));
% change in advancement for first reaction (4-8)
        end
        if dac-dac1+xac(jj,i-1)<0                % no second reaction
            xac(jj,i)=0;
        else
            if dac-dac1+xac(jj,i-1)>xamax
                xac(jj,i)=xamax;
            else
                xac(jj,i)=xac(jj,i-1)+dac-dac1;          % advanacement
            end
        end
        %********************new
concentration*************************************
        xm(jj,i)=xm(jj,i-1)*(xamax-xam(jj,i));      % new refrigerant
concentration
        if (i==2)
            xc(jj,i)=xc(jj,i-1);
        elseif xac(jj,i-1)>xac(jj,i-2)
            xc(jj,i)=xcmax*xac(jj,i);
        else
            xc(jj,i)=0;
        end

        yc(jj,i)=ycmax*yac(jj,i);
        mrgm(jj,i)=xm(jj,i)*mm/ns;    %mass of reacted nh3 in the mgcl2
recator
        mrgc(jj,i)=(xc(jj,i)+yc(jj,i))*mc/ns;    %mass of reacted nh3 in the
mgcl2 recator

        %********************new
temperature*********************************
        switch jj
            case(2)
                dTst=(qdot*dt)/(mst*cpt);  %change in steel tube temperature
                dTstc=(qdotc*dt)/((mcp/mmp)*mst*cpt);  %change in steel tube
temperature cacl2
                Tm(jj,i)=Tm(jj,i-1)+dTst;
                Tc(jj,i)=Tc(jj,i-1)+dTstc;
                pqm(jj,i)=0;
                xm(jj,i)=0;
                xam(jj,i)=0;
                mrgm(jj,i)=0;
                pqc(jj,i)=0;
```

```
                    pqc1(jj,i)=0;
                    xc(jj,i)=0;
                    yc(jj,i)=0;
                    xac(jj,i)=0;
                    yac(jj,i)=0;
                    mrgc(jj,i)=0;
                otherwise
                    cpm(jj,i)=cpmg+cpeng+(cpl*(xm(jj,i)));          % specific heat
and salt, binder and gas
                    cpc(jj,i)=cpca+cpeng+(cpl*(xc(jj,i)));          % specific heat and
salt, binder and gas
                    dTm=(qdot-
(nmamm*(mm/(mom*ns))*dhm*da))*((dt*ns)/((mmp+(mm*xm(jj,i)))*cpm(jj,i)));
% change in temperature of each node for first reaction
                    %%%%%start here

dTc=(qdotc+(ncamm*(mc/(moc*ns))*dhc*dac)+(ncamm1*(mc/(moc*ns))*dhc1*da
c1))*((dt*ns)/((mcp+(mc*xc(jj,i)))*cpc(jj,i)));
                    Tm(jj,i)=Tm(jj,i-1)+dTm;
                    Tc(jj,i)=Tc(jj,i-1)+dTc;

            end

        end

        if Pm(i-1)<Pcon %reactor pressure is less than condensation pressure so
constant mass desorption
            mgtm(i)=mgtm(i-1);   %total mass of nh3 in the reactor stays constant
            mgm(i)=mgtm(i)-sum(mrgm(:,i)); %mass of nh3 gas in the system
            Pm(i)=((mgm(i)*R*mean(Tm(3:no,i)))/(monh3*vm))/1e5; % the new
pressure
        else    %mgcl2 reactor has now reached condenser pressure and there is
constant pressure desorption
            Pm(i)=Pcon;
            mgm(i)=(Pm(i)*1e5*monh3*vm)/(R*mean(Tm(3:no,i)));   %initial
mass of gas in mgcl2 reactorm
            mgtm(i)=mgm(i)+sum(mrgm(:,i)); %total amount of nh3 in mgcl2
reactor
        end
        if Pc(i-1)>Pev %reactor pressure is higher than evaporation pressure so
constant mass synthesis
            mgtc(i)=mgtc(i-1);   %mass of gas in the reactor stays constant
            mgc(i)=mgtc(i)-sum(mrgc(:,i)); %mass of nh3 gas in the system
            Pc(i)=(mgc(i)*R*mean(Tc(3:no,i))/(monh3*vc))/1e5; % the new
pressure
        else    %mgcl2 reactor has now reached condenoer pressure and there is
constant pressure desorption
            Pc(i)=Pev;
            mgc(i)=(Pc(i)*1e5*monh3*vc)/(R*mean(Tc(3:no,i)));   %initial mass of
gas in mgcl2 reactorm
```

```
            mgtc(i)=mgc(i)+sum(mrgc(:,i)); %total amount of nh3 in mgcl2 reactor
        end

        Qdm(i)=((Tm(1,i)-
Tm(2,i))/((1/(hfwh*pi*dth*lem))+((log((dth+tt)/dth))/(2*pi*kt*lem))))*dt;
        Qconm=Qconm-(mgtm(i)-mgtm(i-1))*(hsupamm(s.Tcon-
273.15,Tm(no,i)-273.15)-hfamm(s.Tcon-273));
        Qsc(i)=((Tc(2,i)-
Tc(1,i))/((1/(hfwh*pi*dth*lec))+((log((dth+tt)/dth))/(2*pi*kt*lec))))*dt;
        Qevc=(mgtc(i)-mgtc(i-1))*(hsupamm(s.Tev-273.15,Tc(no,i)-273.15)-
hfamm(s.Tev-273));

    end
    Tm(1,(tto/2):tto)=s.Tcm;    %fluid temperature of mgcl2 set (K) for synthesis
stage
    xam(3:no,i)=0;  %initial concentration through all the layers
    xac(3:no,i)=0;  %initial concentration through all the layers
    yac(3:no,i)=1;  %initial concentration through all the layers

    for i=tto/2:tto %synthesis phase for mgcl2 and decomposition phase for cacl2

        for jj=2:no

            %********************heat conduction through the nodes
(watts)**********************
            switch jj
                case(2)    %steel tube node
                    qdot=((Tm(jj-1,i-1)-Tm(jj,i-
1))/((1/(hfwh*pi*dth*lem))+((log((dth+tt)/dth))/(2*pi*kt*lem))))+...
                        ((Tm(jj+1,i-1)-Tm(jj,i-
1))/((1/(hws*pi*(dth+(2*tt))*lem))+(((log((dth+(2*tt))/(dth+tt))+log((dth+(2*tt)+(0.
5*tsl))/(dth+(2*tt))))/(2*pi*kt*lem)))));
                case (3)    %first mgcl2 node
                    qdot=((Tm(jj-1,i-1)-Tm(jj,i-
1))/((1/(hws*pi*(dth+(2*tt))*lem))+(((log((dth+(2*tt))/(dth+tt))+log((dth+(2*tt)+(0.
5*tsl))/(dth+(2*tt))))/(2*pi*kt*lem)))))...
                        +((Tm(jj+1,i-1)-Tm(jj,i-1))/(((log((dth+(2*tt)+((jj-
1.5)*tsl))/(dth+(2*tt)+((jj-2.5)*tsl)))/(2*pi*km*lem)))));
                case (no)   %last mgcl2 node
                    qdot=((Tm(jj-1,i-1)-Tm(jj,i-1))/(((log((dth+(2*tt)+((no-
2.5)*tsl))/(dth+(2*tt)+((no-3.5)*tsl)))/(2*pi*km*lem)))));
                otherwise   %middle mgcl2 nodes
                    qdot=((Tm(jj-1,i-1)-Tm(jj,i-1))/(((log((dth+(2*tt)+((jj-
2.5)*tsl))/(dth+(2*tt)+((jj-3.5)*tsl)))/(2*pi*km*lem)))))+...
                        ((Tm(jj+1,i-1)-Tm(jj,i-1))/(((log((dth+(2*tt)+((jj-
1.5)*tsl))/(dth+(2*tt)+((jj-2.5)*tsl)))/(2*pi*km*lem)))));
            end
            %**********************reaction advanacements
****************************
```

```
            pqm(jj,i)=Pequilibrium(dhms,dsms,R,Tm(jj,i-1)); %equilibrium
pressure at initial temperaturee (bar)
            if Pm(i-1)<pqm(jj,i)                    % equilibrium pressure not
reached
               da=0;
            else
               da=dt*(((xamax-xam(jj,i-1))^yms)*ams*((Pm(i-1)-pqm(jj,i))/(Pm(i-
1))));  % change in advancement for first reaction (8-4)
            end
            if xam(jj,i-1)+da < xamax
               xam(jj,i)= xam(jj,i-1)+da;              % new advancement
            else
               xam(jj,i)= xamax;
            end
            %*******************new
concentration*************************************
            xm(jj,i)=xm(jj,1)*xam(jj,i);          % new refrigerant concentration
            mrgm(jj,i)=xm(jj,i)*mm/ns;    %mass of reacted nh3 in the mgcl2
recator

            %*******************new
temperature*********************************
            switch jj
               case(2)
                  dTstm=(qdot*dt)/(mst*cpt);  %change in steel tube temperature
cacl2

                  Tm(jj,i)=Tm(jj,i-1)+dTstm;
                  xc(jj,i)=0;
                  yc(jj,i)=0;
                  xac(jj,i)=0;
                  yac(jj,i)=0;
                  pqm(jj,i)=0;
                  xm(jj,i)=0;
                  xam(jj,i)=0;
                  mrgm(jj,i)=0;

               otherwise
                  cpm(jj,i)=cpmg+cpeng+(cpl*(xm(jj,i)));          % specific heat
and salt, binder and gas

dTm=(qdot+(nmamm*(mm/(mom*ns))*dhms*da))*((dt*ns)/((mmp+(mm*xm(jj,i)))
*cpm(jj,i)));   % change in temperature of each node for first reaction
                  %-((mrgm(jj,i)-mrgm(jj,i-1)*cpl*(Tm(jj,i)-s.Tev)))
                  Tm(jj,i)=Tm(jj,i-1)+dTm;

            end
         end
         Tc(1,i)=((((Tm(2,i)-
Tm(1,i))/((1/(hfwh*pi*dth*lem))+((log((dth+tt)/dth))/(2*pi*kt*lem)))))...
```

```
*(((1/(hfwh*pi*dth*lem))+((log((dth+tt)/dth))/(2*pi*kt*lem)))+((1/(hfwh*pi*dth*le
c))+...
            ((log((dth+tt)/dth))/(2*pi*kt*lec)))))-Tm(2,i)+Tm(1,i)+Tc(2,i-1); %fluid
temeperature of cacl2 based on heat recovered from mgcl2
        for jj=2:no

            switch jj
               case(2)    %steel tube node
                  qdotc=((Tc(jj-1,i-1)-Tc(jj,i-
1))/((1/(hfwh*pi*dth*lec))+((log((dth+tt)/dth))/(2*pi*kt*lec))))+...
                     ((Tc(jj+1,i-1)-Tc(jj,i-
1))/((1/(hws*pi*(dth+(2*tt))*lec))+(((log((dth+(2*tt))/(dth+tt))+log((dth+(2*tt)+(0.5
*tsl))/(dth+(2*tt))))/(2*pi*kt*lec)))));
               case (3)    %first mgcl2 node
                  qdotc=((Tc(jj-1,i-1)-Tc(jj,i-
1))/((1/(hws*pi*(dth+(2*tt))*lec))+(((log((dth+(2*tt))/(dth+tt))+log((dth+(2*tt)+(0.5
*tsl))/(dth+(2*tt))))/(2*pi*kt*lec)))))...
                     +((Tc(jj+1,i-1)-Tc(jj,i-1))/(((log((dth+(2*tt)+((jj-
1.5)*tsl))/(dth+(2*tt)+((jj-2.5)*tsl)))/(2*pi*kc*lec)))));
               case (no)   %last mgcl2 node
                  qdotc=((Tc(jj-1,i-1)-Tc(jj,i-1))/(((log((dth+(2*tt)+((no-
2.5)*tsl))/(dth+(2*tt)+((no-3.5)*tsl)))/(2*pi*kc*lec)))));
               otherwise   %middle mgcl2 nodes
                  qdotc=((Tc(jj-1,i-1)-Tc(jj,i-1))/(((log((dth+(2*tt)+((jj-
2.5)*tsl))/(dth+(2*tt)+((jj-3.5)*tsl)))/(2*pi*kc*lec)))))+...
                     ((Tc(jj+1,i-1)-Tc(jj,i-1))/(((log((dth+(2*tt)+((jj-
1.5)*tsl))/(dth+(2*tt)+((jj-2.5)*tsl)))/(2*pi*kc*lec)))));
            end
            pqc(jj,i)=Pequilibrium(dhc,dsc,R,Tc(jj,i-1))/1e5; %equilibrium pressure
at initial temperaturee (bar)cacl2 first reaction
            pqc1(jj,i)=Pequilibrium(dhc1,dsc1,R,Tc(jj,i-1))/1e5; %equilibrium
pressure at initial temperaturee (bar)cacl2 second reaction
            if Pc(i-1)>pqc(jj,i)                    % equilibrium pressure not
reached
               dac=0;
            else
               dac=dt*(((xamax-xac(jj,i-1))^ycs)*acs*((pqc(jj,i)-Pc(i-1))/(Pc(i-1))));
% change in advancement for first reaction (8-4)
            end
            if xac(jj,i-1)+dac < xamax
               xac(jj,i) = xac(jj,i-1)+dac;              % new advancement
            else
               xac(jj,i) = xamax;
            end

            if Pc(i-1)>pqc1(jj,i)                    % equilibrium pressure not
reached
               dac1 = 0;
            else
```

```
                dac1=dt*(((xamax-yac(jj,i-1))^ycs1)*acs1*(pqc1(jj,i)-Pc(i-1))/(Pc(i-
1))); % change in advancement for second reaction (4-2)
            end
            if dac1-dac+yac(jj,i-1)<0                    % no second reaction change
in advancement
                yac(jj,i)=0;
            else
                if dac1-dac+yac(jj,i)>xamax              % second reaction change in
advancement
                    yac(jj,i)=xamax;
                else
                    yac(jj,i)=yac(jj,i-1)+dac1-dac;      % new second reaction
advancement
                end
            end
            xc(jj,i)=xc(jj,i-1)*(xamax-xac(jj,i));       % new refrigerant
concentration
            if i==(tto/2)+1||i==(tto/2)+2||i==(tto/2)+3||i==(tto/2)+4
                xc(jj,i)=xc(jj,i-1);
            elseif xac(jj,i-1)>xac(jj,i-4)
                xc(jj,i)=xc(jj,i-1)*(xamax-xac(jj,i));
            else
                xc(jj,i)=0;
            end

            yc(jj,i)=ycmax*yac(jj,i);
            mrgm(jj,i)=xm(jj,i)*mm/ns;    %mass of reacted nh3 in the mgcl2
recator
            mrgc(jj,i)=(xc(jj,i)+yc(jj,i))*mc/ns;    %mass of reacted nh3 in the
mgcl2 recator
            switch jj
                case(2)
                    dTstc=(qdotc*dt)/((mcp/mmp)*mst*cpt);  %change in steel tube
temperature  cacl2
                    Tc(jj,i)=Tc(jj,i-1)+dTstc;
                    pqc(jj,i)=0;
                    pqc1(jj,i)=0;
                    xc(jj,i)=0;
                    xac(jj,i)=0;
                    yc(jj,i)=0;
                    yac(jj,i)=0;
                    mrgc(jj,i)=0;

                otherwise
                    cpc(jj,i)=cpca+cpeng+(cpl*(xc(jj,i)));          % specific heat and
salt, binder and gas
                    dTc=(qdotc-
(ncamm*(mc/(moc*ns))*dhc*dac)+(ncamm1*(mc/(moc*ns))*dhc1*dac1))*((dt*ns)/
((mcp+(mc*xc(jj,i)))*cpc(jj,i)));
                    Tc(jj,i)=Tc(jj,i-1)+dTc;
```

```
            end
        end

        if Pm(i-1)>Pev %reactor pressure is higher than evaporation pressure so
constant mass synthesis
            mgtm(i)=mgtm(i-1);   %mass of gas in the reactor stays constant
            mgm(i)=mgtm(i)-sum(mrgm(:,i)); %mass of nh3 gas in the system
            Pm(i)=(mgm(i)*R*mean(Tm(3:no,i))/(monh3*vm))/1e5; % the new
pressure
        else    %mgcl2 reactor has now reached condenoer pressure and there is
constant pressure desorption
            Pm(i)=Pev;
            mgm(i)=(Pm(i)*1e5*monh3*vm)/(R*mean(Tm(3:no,i)));   %initial
mass of gas in mgcl2 reactorm
            mgtm(i)=mgm(i)+sum(mrgm(:,i)); %total amount of nh3 in mgcl2
reactor
        end
        if Pc(i-1)<Pcon %reactor pressure is less than condensation pressure so
constant mass desorption
            mgtc(i)=mgtc(i-1);   %total mass of nh3 in the reactor stays constant
            mgc(i)=mgtc(i)-sum(mrgc(:,i)); %mass of nh3 gas in the system
            Pc(i)=((mgc(i)*R*mean(Tc(3:no,i)))/(monh3*vc))/1e5; % the new
pressure
        else    %mgcl2 reactor has now reached condenser pressure and there is
constant pressure desorption
            Pc(i)=Pcon;
            mgc(i)=(Pc(i)*1e5*monh3*vc)/(R*mean(Tc(3:no,i)));   %initial mass of
gas in mgcl2 reactorm
            mgtc(i)=mgc(i)+sum(mrgc(:,i)); %total amount of nh3 in mgcl2 reactor
        end
        Qsm(i)=((Tm(2,i)-
Tm(1,i))/((1/(hfwh*pi*dth*lem))+((log((dth+tt)/dth))/(2*pi*kt*lem))))*dt;
        Qev=(mgtm(i)-mgtm(i-1))*(hsupamm(s.Tev-273.15,Tm(no,i)-273.15)-
hfamm(s.Tev-273));
        Qdc(i)=((Tc(1,i)-
Tc(2,i))/((1/(hfwh*pi*dth*lec))+((log((dth+tt)/dth))/(2*pi*kt*lec))))*dt;
        Qconc=Qconc-(mgtc(i)-mgtc(i-1))*(hsupamm(s.Tcon-273.15,Tc(no,i)-
273.15)-hfamm(s.Tcon-273));
    end

    COPh(ncr)=(Qconm+Qconc+sum(Qsc))/sum(Qdm); %heat pump COP for
MgCl2 only run
    SHPh(ncr)=(Qconm+Qconc+sum(Qsc))/(s.ht*2*(mm+mc)); % Heating
power W/kg mgcl2 and cacl2
    xm((3:no),1)=xm((3:no),i);
    xam((3:no),1)=0;
    Pm(1)=Pm(i);
    mgm(1)=(Pm(1)*1e5*monh3*vm)/(R*Tm(1,1));
    mrgm((3:no),1)=xm((3:no),i)*mm/ns;
    mgtm(1)=mgtm(i);
```

```
            xac(3:no,1)=1;  %initial concentration through all the layers
            yac(3:no,1)=0;  %initial concentration through all the layers

        end
    end
else
    x=1
end
```